

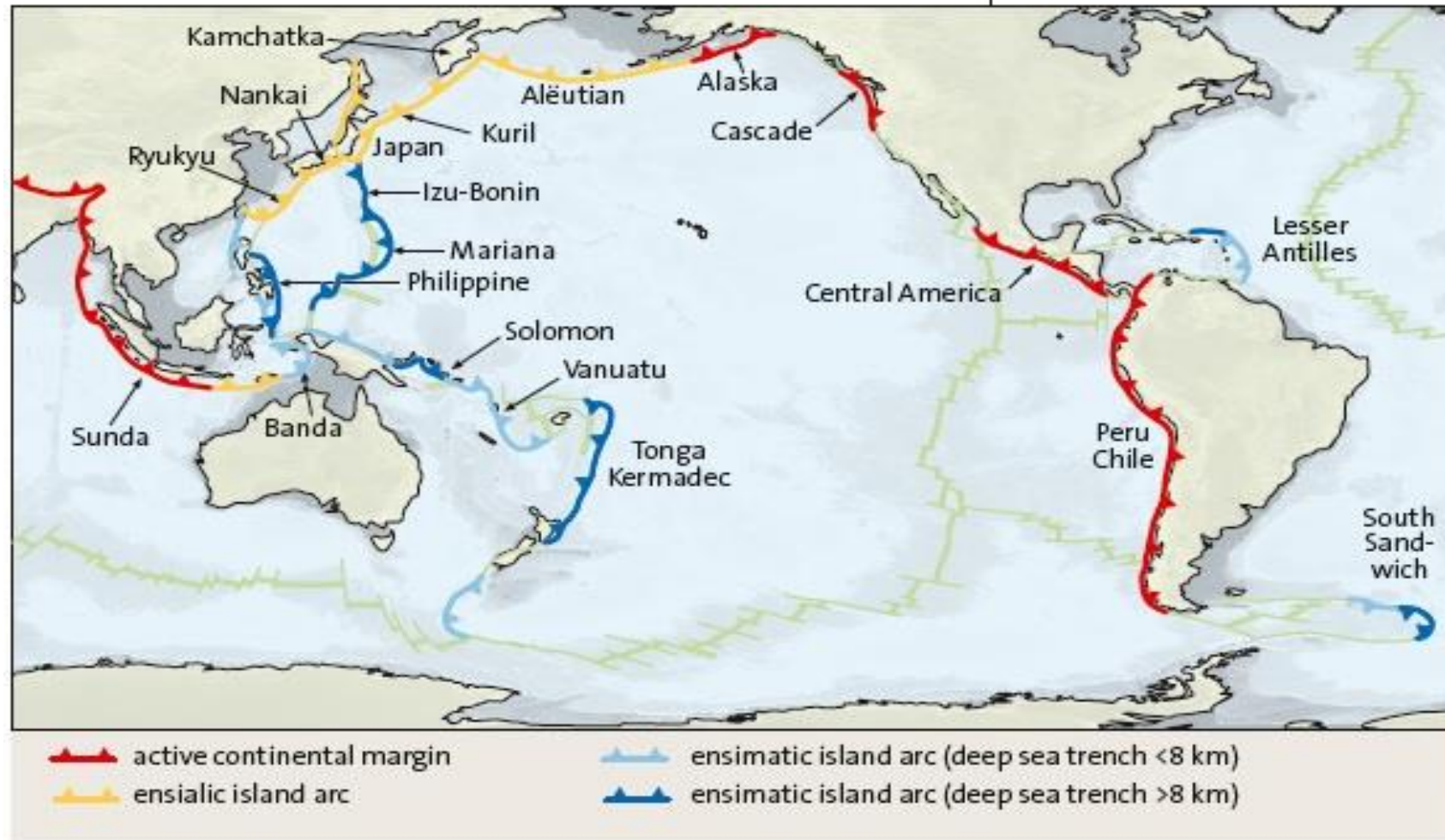
Course of Geodynamics

Dr. Magdala Tesauro

Course Outline:

1. Thermo-physical structure of the continental and oceanic crust
2. Thermo-physical structure of the continental lithosphere
3. Thermo-physical structure of the oceanic lithosphere and oceanic ridges
4. Rheology and mechanics of the lithosphere
5. Plate tectonics and boundary forces
6. Hot spots, plumes, and convection
- 7. Subduction zones systems**
8. Orogens formation and evolution
9. Sedimentary basins formation and evolution

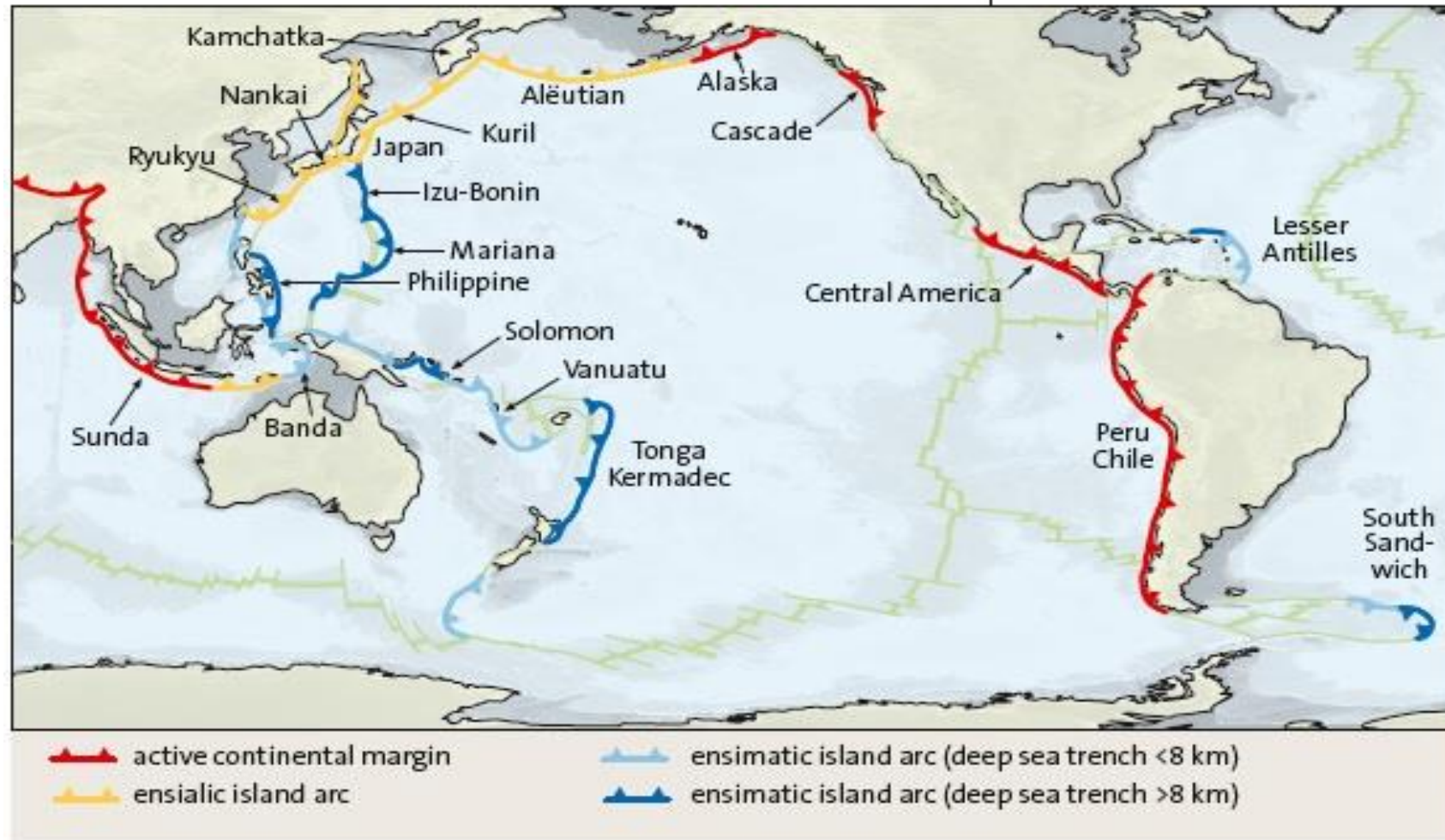
Convergent plate margins of the Earth



Global subduction zones sums to more than 55,000 km

- The total length of these subduction zones amounts to some 48,800 km, while the total length of incipient subduction zones amounts to some 10,550 km.
- Most collision zones are found along the Alpine–Himalayan chain and the total length of these collision zones amounts to some 23,000 km. This results in a total of 82,350 km of convergent plate boundaries on Earth.

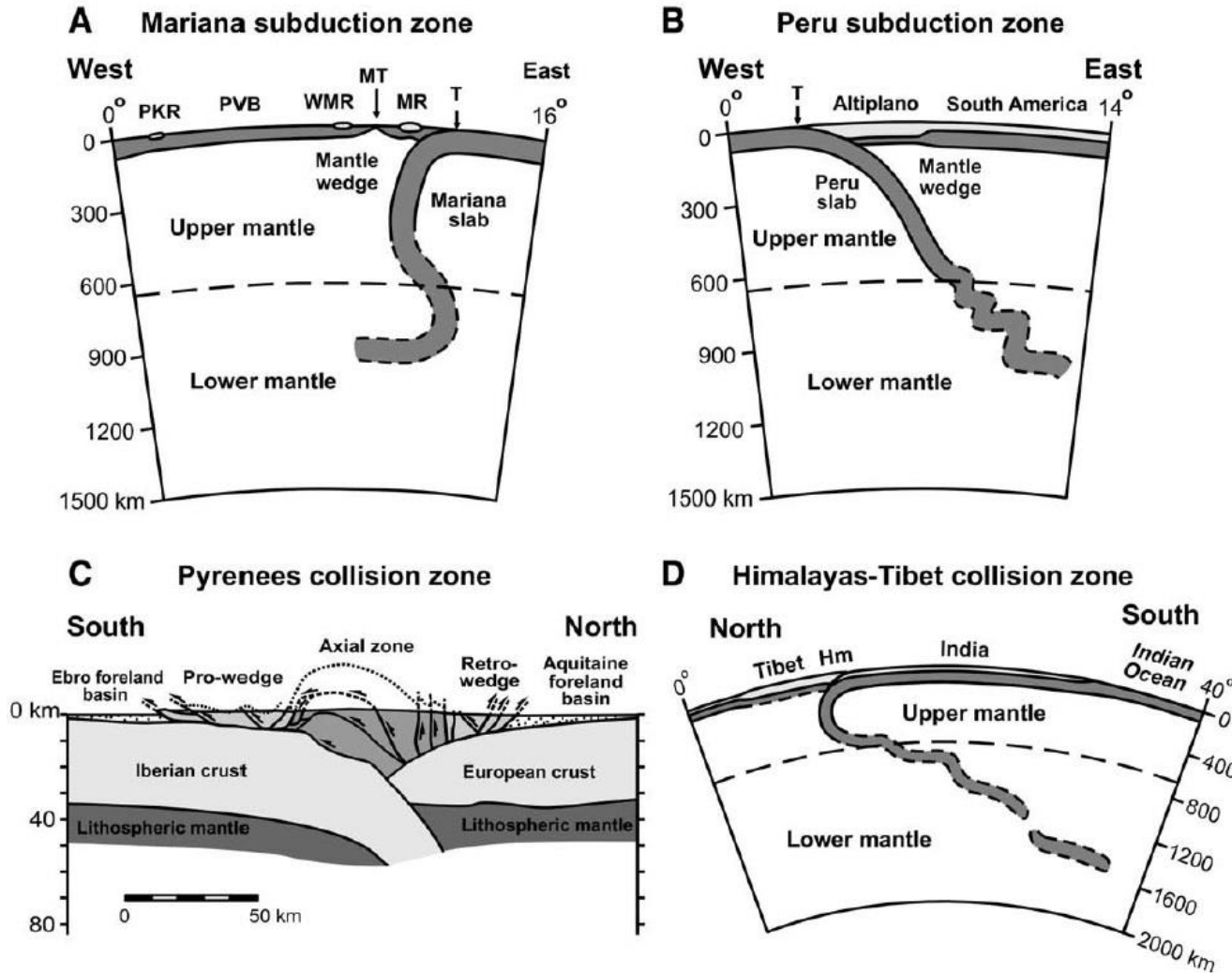
Convergent plate margins of the Earth



- **Ensimatic island arc:** it refers to a volcanic island arc system built on oceanic crust (ocean lithosphere is subducted below other ocean lithosphere).
- **Ensialic island arc:** it refers to an island arc underlain by continental crust (oceanic lithosphere is subducted beneath continental lithosphere).
- **The arc is built directly on the adjacent continent:** There is an active continental margins where oceanic lithosphere is subducted beneath continental lithosphere without a marine basin behind the volcanic arc.

Convergent Plate Margins

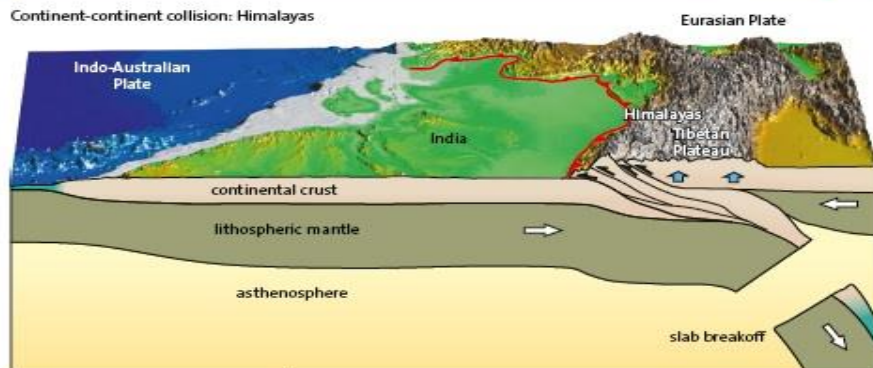
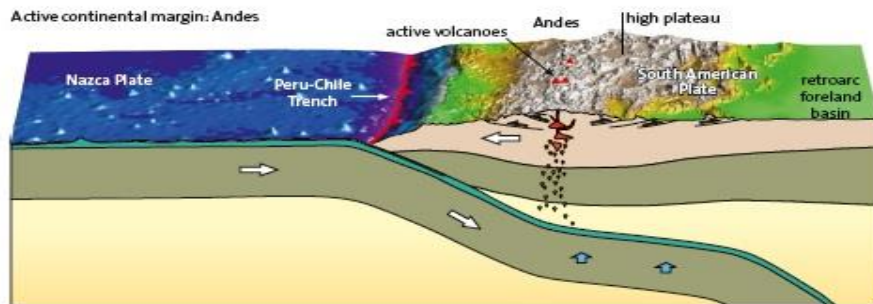
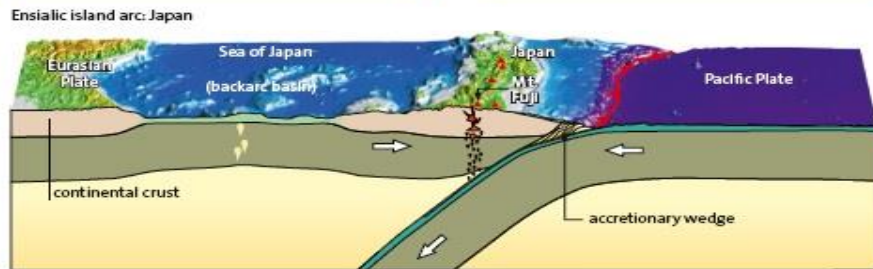
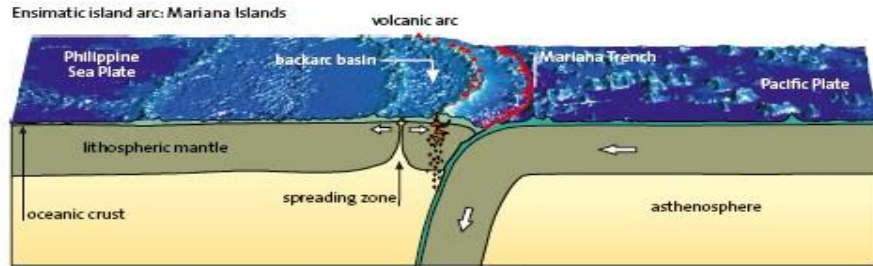
Two types of convergent plate margins: subduction zones (A and B) and collision zones (C and D)



- (A) The Mariana subduction zone as an example of an ocean–ocean subduction zone with an oceanic overriding (upper) plate (Philippine plate) and an oceanic subducting (lower) plate (Pacific plate).
- (B) The Peru subduction zone: ocean–continent subduction zone with a continental overriding (upper) plate (South American plate) and an oceanic subducting (lower) plate (Nazca plate).
- (C) The Pyrenees mountain belt: continent–continent collision zone, with two converging continental plates (Iberian plate and Eurasian plate).
- (D) The Himalayas–Tibet mountain belt: continent–continent collision zone between the Indian plate and the Eurasian plate with apparent penetration of Indian lithosphere into the sub-lithospheric mantle down to >600 km.

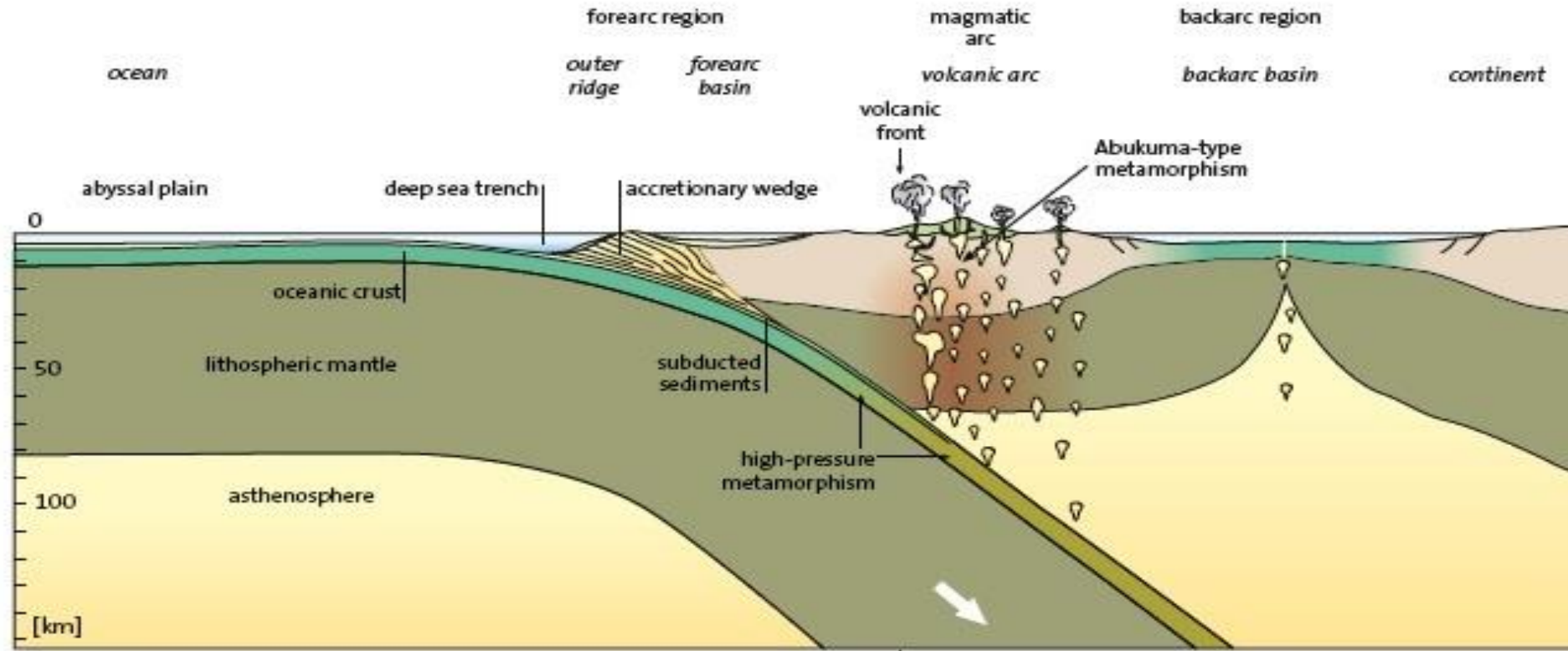
Slab geometry reconstructed from seismic tomography

Types of plate margins with subduction zones



1. Intraoceanic subduction zone, ensimatic island arc (Mariana Islands).
2. Oceanic lithosphere is subducted beneath continental lithosphere, with a marine basin behind the ensialic island arc (Japanese Islands and the eastern Sunda Arc).
3. Oceanic lithosphere is subducted beneath continental lithosphere without a marine basin behind the ensialic island arc built directly on the adjacent continent (Andes, SE Alaska).
4. Zones of continent-continent collision resulting in «slab breakoff» of the oceanic part of the subducting plate and in formation of mountain ranges (e.g., the Himalayas or the Alps).

Structure of a subduction system



Oceanic trenches:

Are direct manifestation of underthrusting lithosphere. Trenches depth (up to 10-11 km) is controlled by the age of the oceanic lithosphere. Sediment fill of trenches vary greatly depending on proximity of continental areas.

Forarc basin:

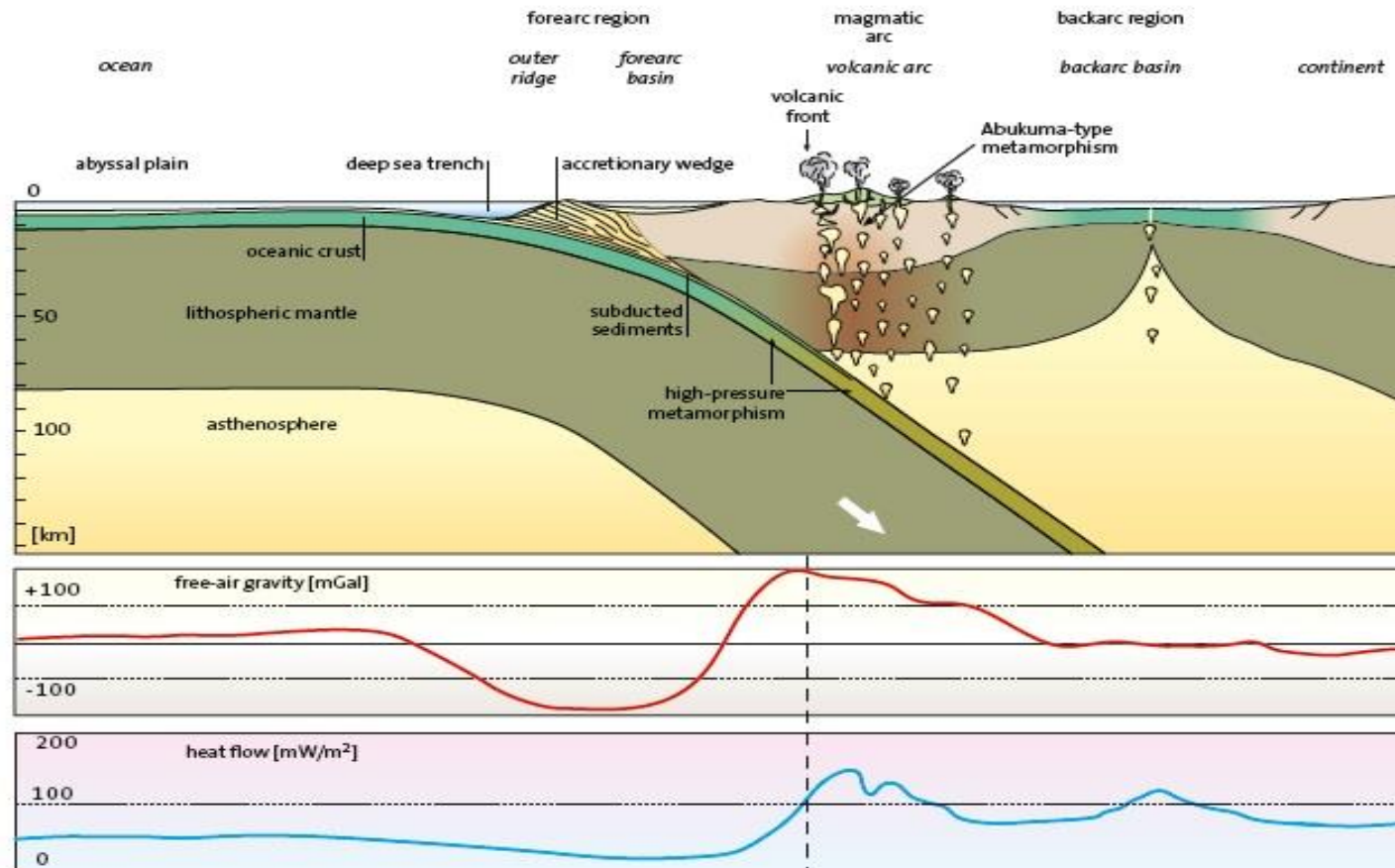
Underlain by thinned continental and oceanic crust, contain a variable thickness of sediments marine and derived from volcanic arc.

Volcanic arc:

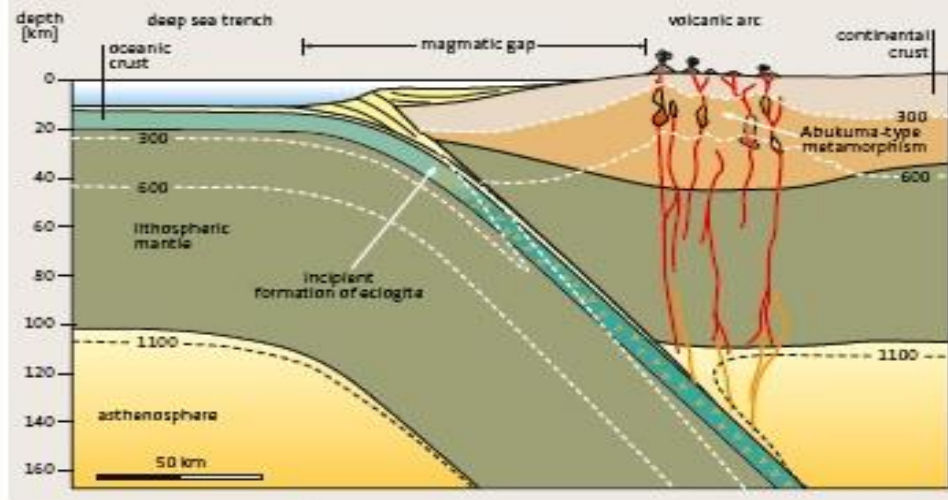
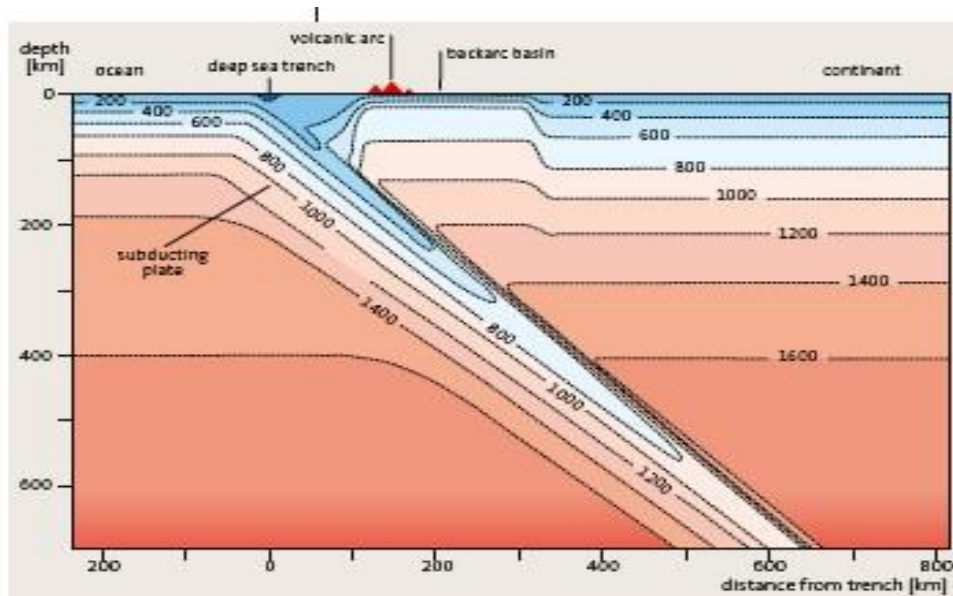
It is located 100-150 km far from the trench, has an average width of 100 km, and is the central part of the island arc or the active continental margin.

Gravity and heat flow in the subduction zones

- The forearc area shows a negative gravity anomaly (due to the bending of the subducting plate resulting in a trench filled with water and water-saturated sediments) and adjacent positive anomaly (due to the dense subducting plate and overthrusting upper plate).
- Volcanic front shows also a positive gravity anomaly which gradually decreases to normal gravity values towards the backarc basin (due to the contribution of the lighter asthenosphere).
- Heat flow increases abruptly in the magmatic arc and back-arc basin from 50 mW/m² to 80–150 mW/m²

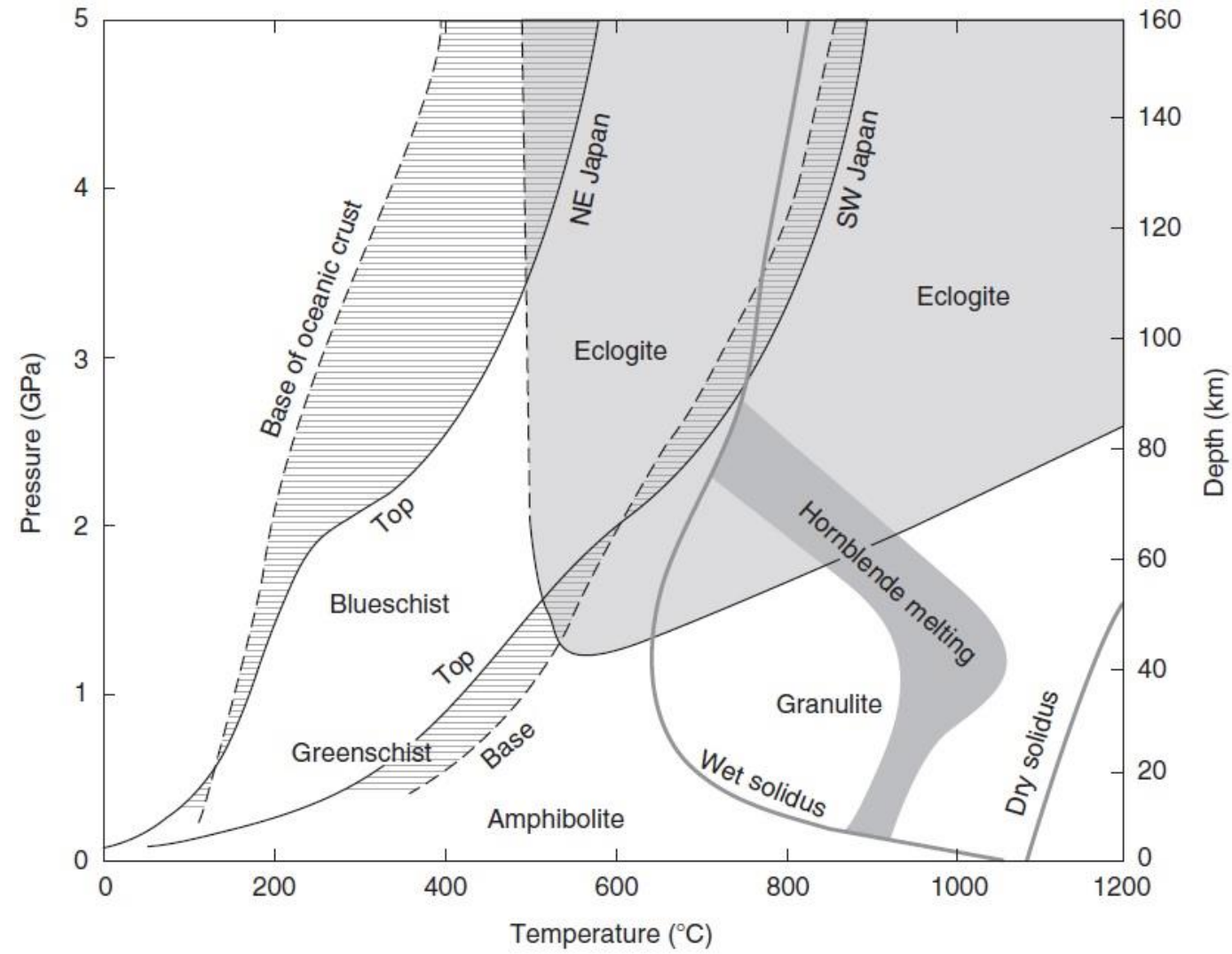


Thermal conditions of a subduction zone system



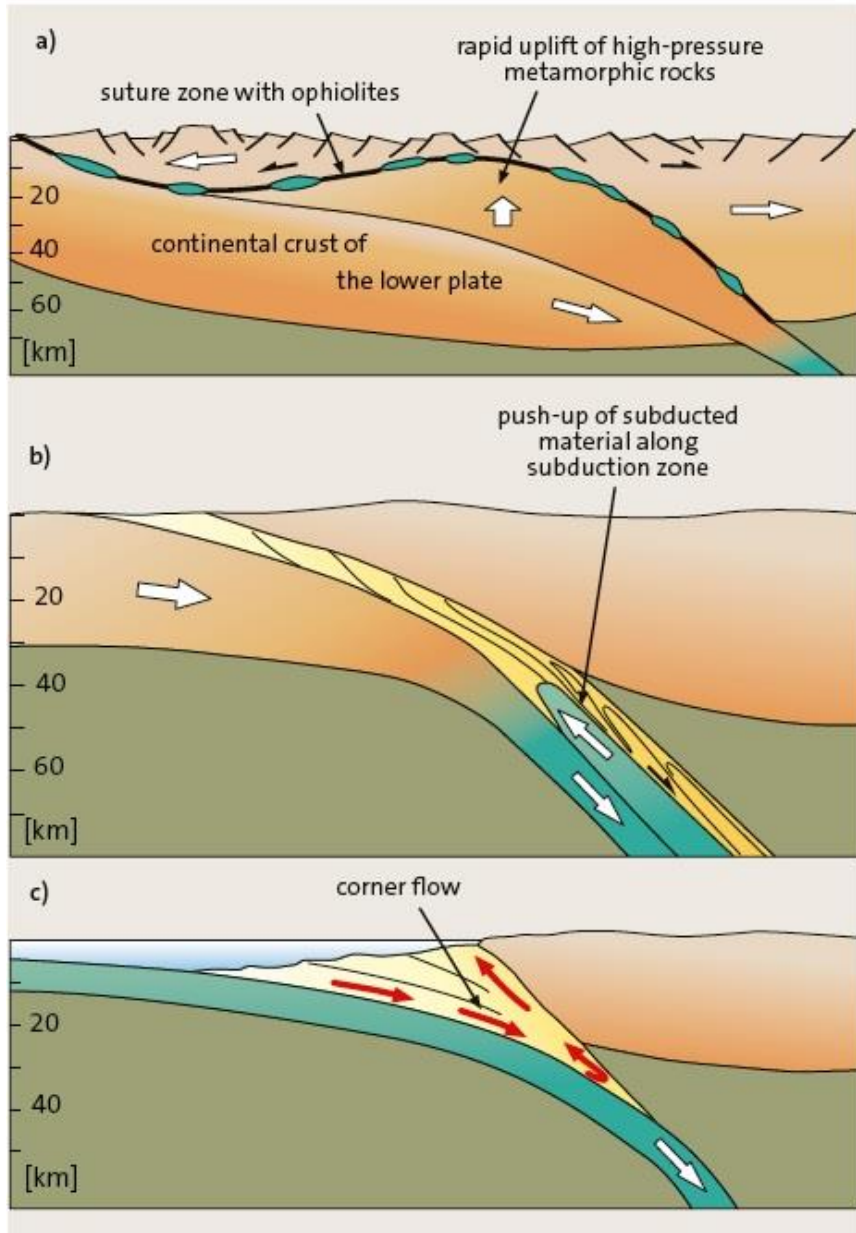
- Rate of subduction.
- Age and thickness of descending slab.
- Frictional heating of the upper and lower slab surfaces (product of the shear stress and the convergence velocity).
- Conduction of heat into the slab from the asthenosphere.
- Adiabatic heating associated with slab compression.
- Heat derived from radioactive decay of minerals in the oceanic lithosphere.
- Latent heat associated with phase transitions of minerals (olivine-spinel transition, exothermic; spinel-oxide transitions, endothermic).

Metamorphism in the subduction zones



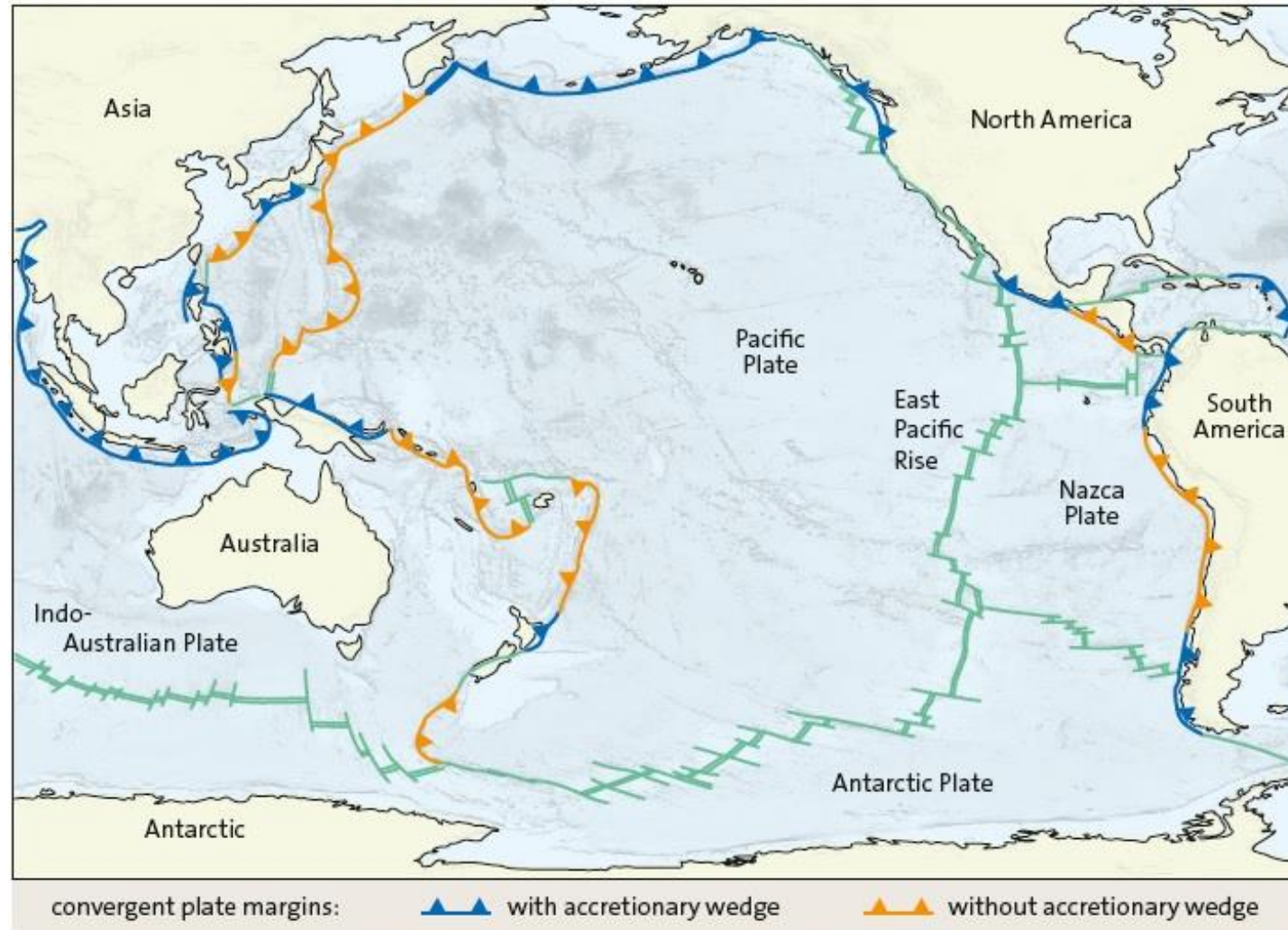
- The most common groups of metamorphic rocks in the subduction zones are blueschist (MP-HP and LT), greenschist (MP and MT), amphibolite (MP and MT-HT), and the granulite facies (MP-HP and HT), depending on the initial composition of the crust, ambient pressure, temperature and fluid conditions.
- The transition of basalts in amphibolite occurs at $T > 500^{\circ}\text{C}$, while at $T > 650^{\circ}\text{C}$ amphibolite transforms into granulite, which are usually characterized by the presence of anhydrous mineral assemblages (OPX, CPX, and plagioclase).

Uplift of high-pressure metamorphic rocks



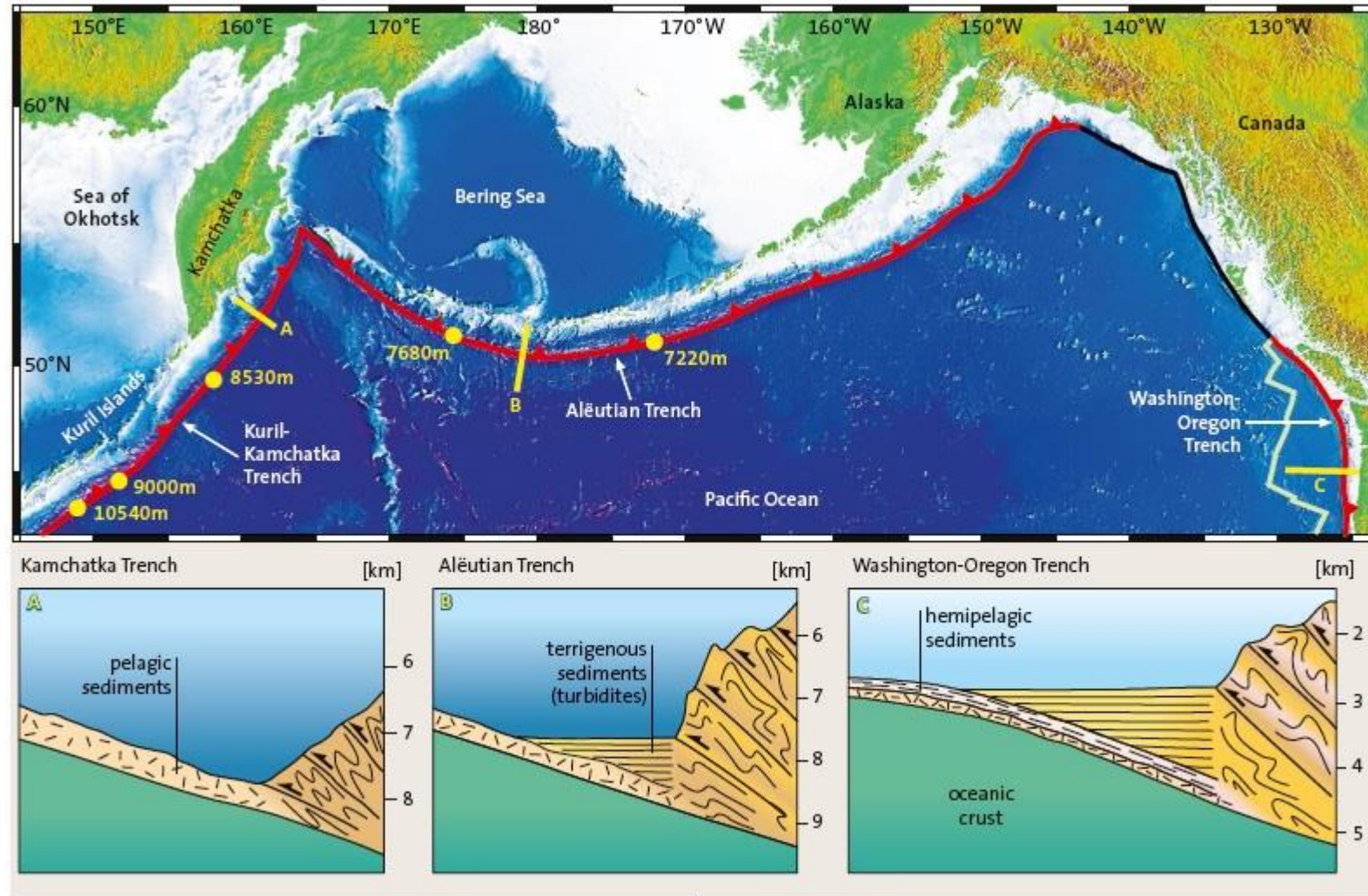
- a) Crust that is thickened by underplating during the subduction process is gravitationally unstable, a condition that initiates crustal extension by an orogenic collapse: The rocks are removed by rapid horizontal displacement during orogenic collapse of the orogen (metamorphic core complexes).
- b) High-pressure sequences can be pressed in reverse upwards along subduction zones even during continuous subduction and compression.
- c) Corner flow can rapidly uplift high-pressure metamorphic rocks: The wedge consists of scraped-off sediments that becomes narrower at depth and thus the subducted and metamorphosed rocks from the lower part of the wedge are returned towards the surface along the frontal part of the upper plate.

Accretionary Prisms



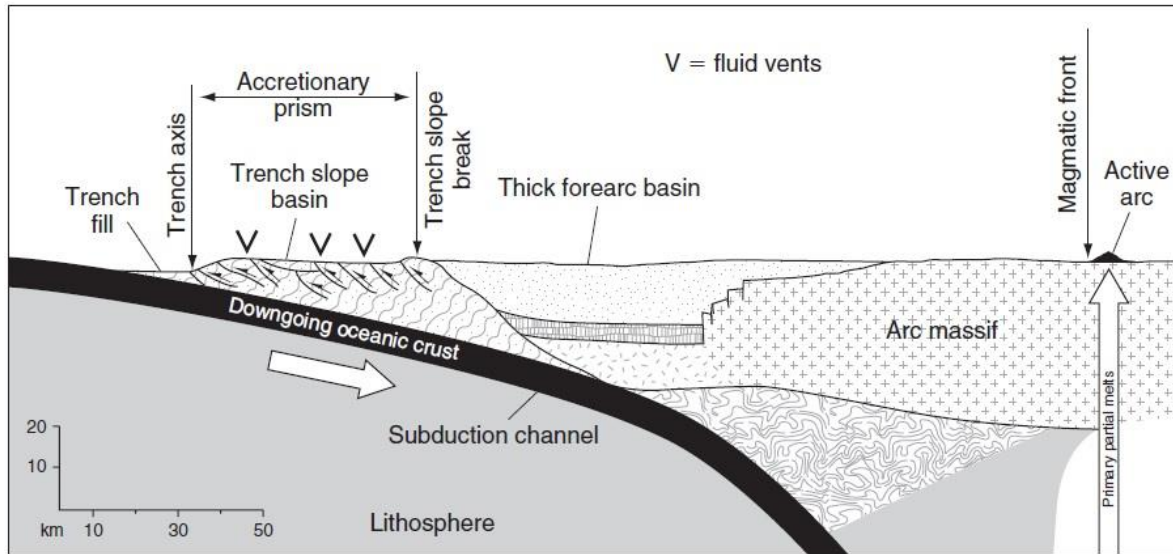
- Sedimentary accretionary wedges occur in many subduction zones including large portions of the Gulf of Oman, Sumatra, SW Japan, and in smaller areas of western North America and the Lesser Antilles.
- Other subduction zones are characterized by subduction erosion, during which rock material is scraped-off from the bottom of the upper plate and transported downward with the subducting plate (Tonga Islands, Costa Rica and Chile).

Accretionary Prisms



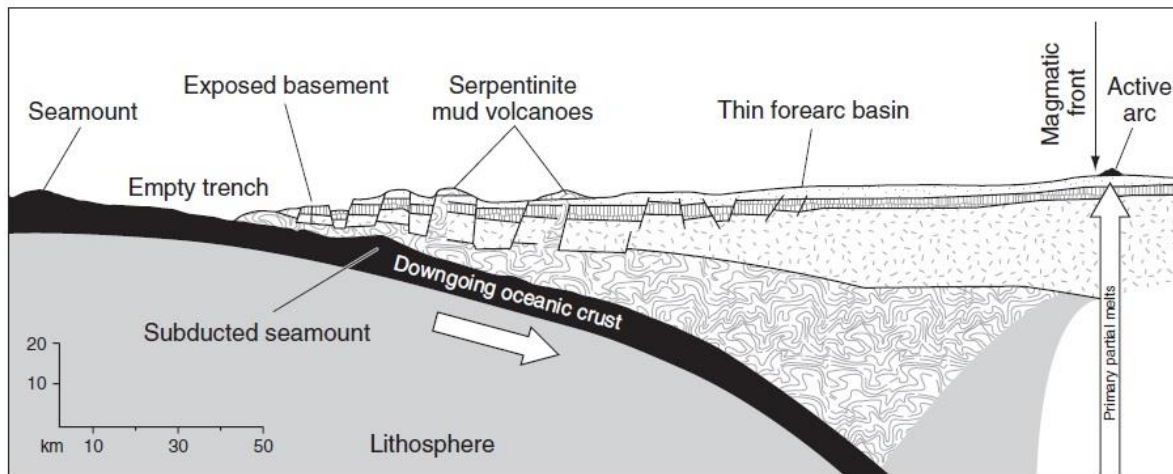
- Most trenches have a mixture of pelagic and terrigenous deposits as well as sediments and sedimentary rocks transported into the trench on the subducting lower plate.
- The amount of sediment in a trench is related to the balance between the sediment supply and the slow tectonic removal of trench fill.
- Thick trench deposits are generally favored by a low subduction rate and accompanying slow tectonic removal of trench-fill material.

Accretionary Prisms

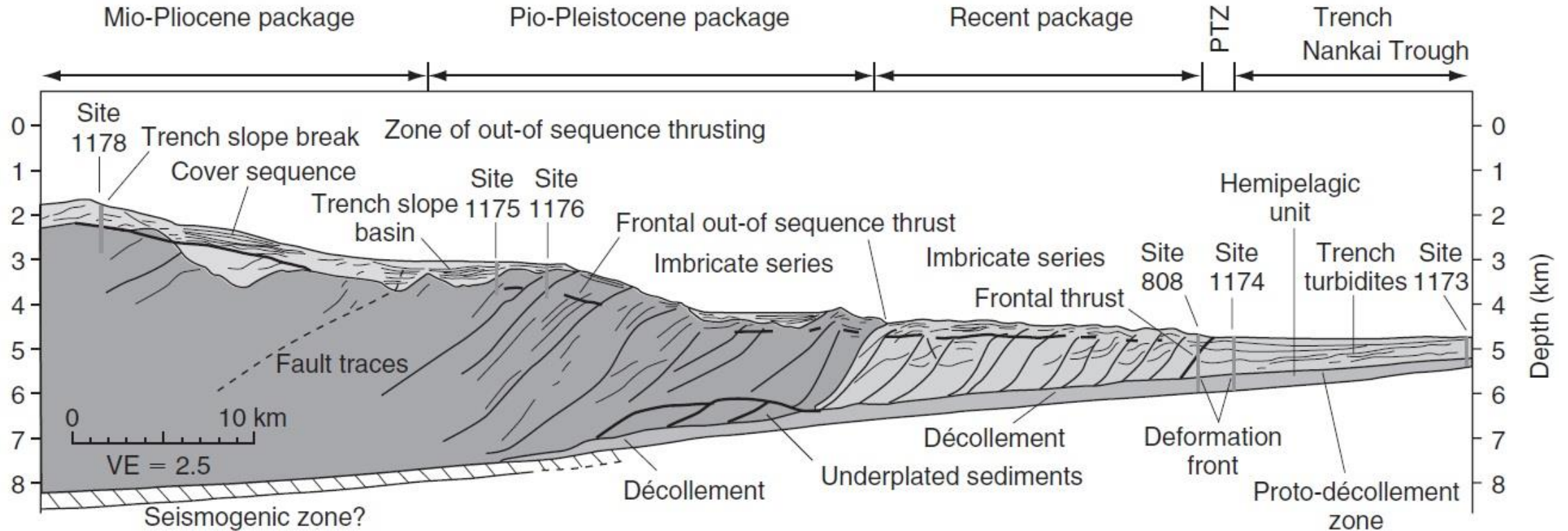


- Accretionary prisms grow from below, developing where trench-fill turbidites (flysch), and some pelagic sediments, are scraped-off the descending oceanic plate by the leading edge of the overriding plate, to which they become accreted.
- 80% of pelagic sediments entering the trench is subducted (only when the sedimentary thickness exceeds 400-1000 m it is scraped off).
- Off-scraped material first moves down toward the base of the prism and then moves back toward the surface, creating a chaotic mixture of igneous, sedimentary and metamorphic rock types called a *mélange*.
- Over time, erosion, deformation, and sedimentary recycling result in a long-term circulation of material within the wedge.

Non-accretionary forearc

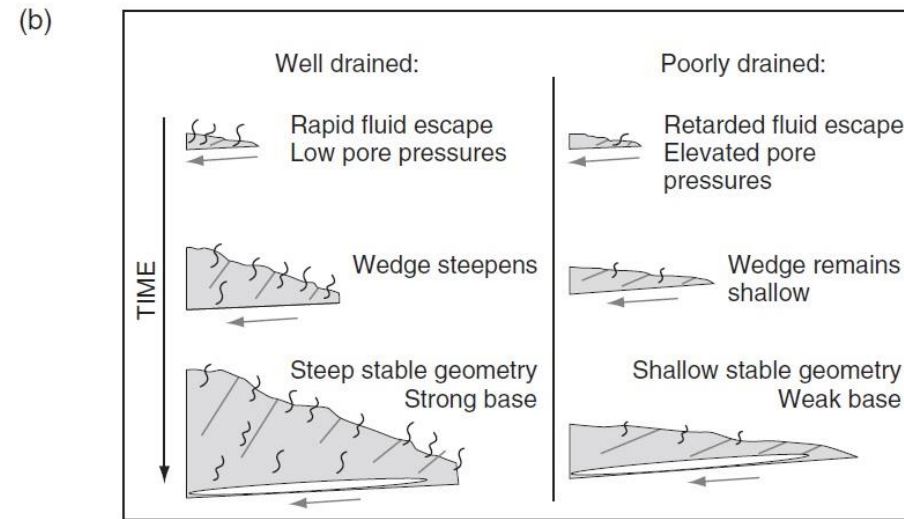
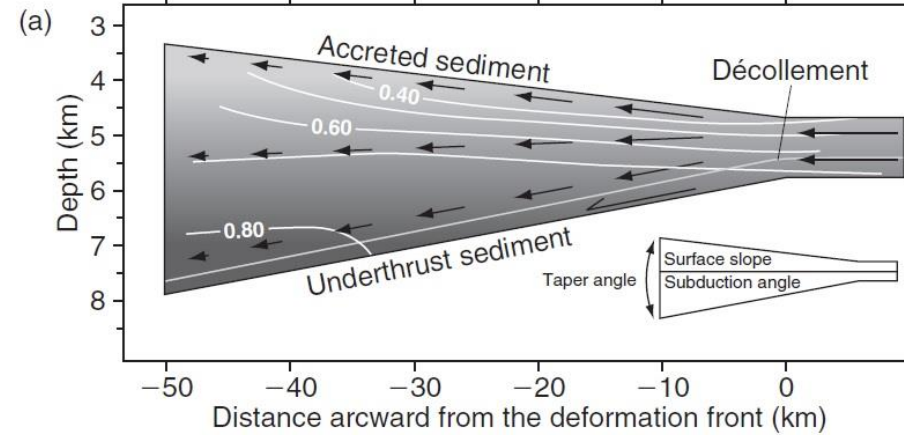
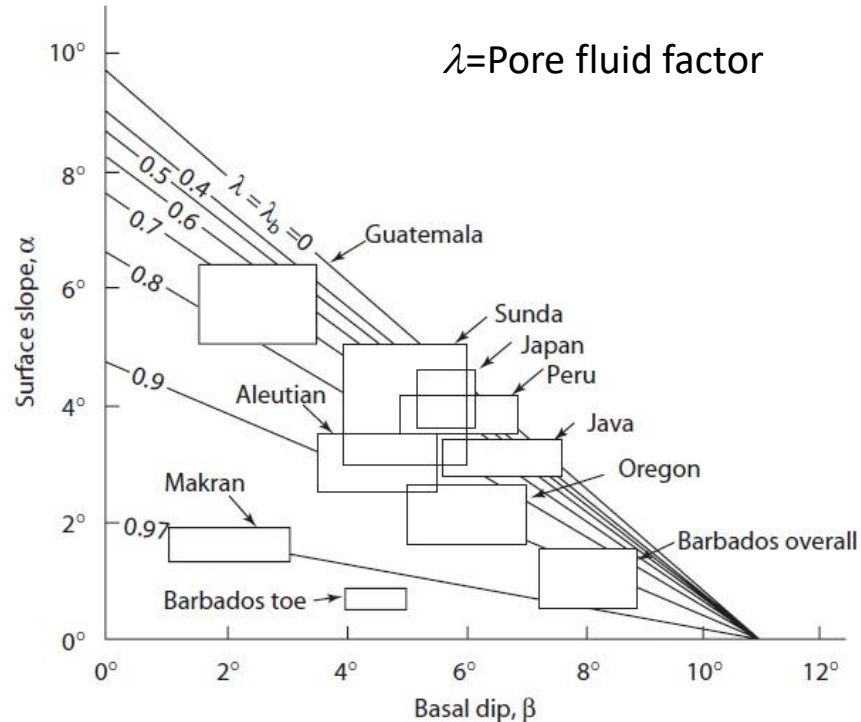
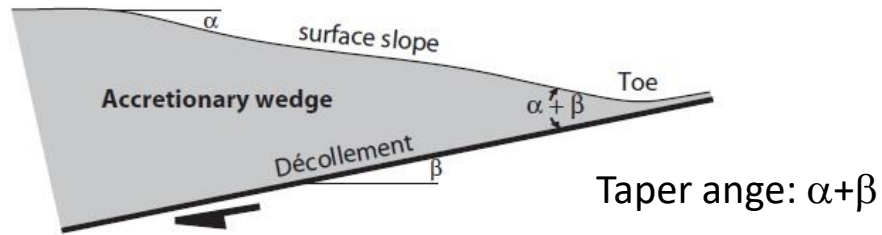


Accretionary Prisms



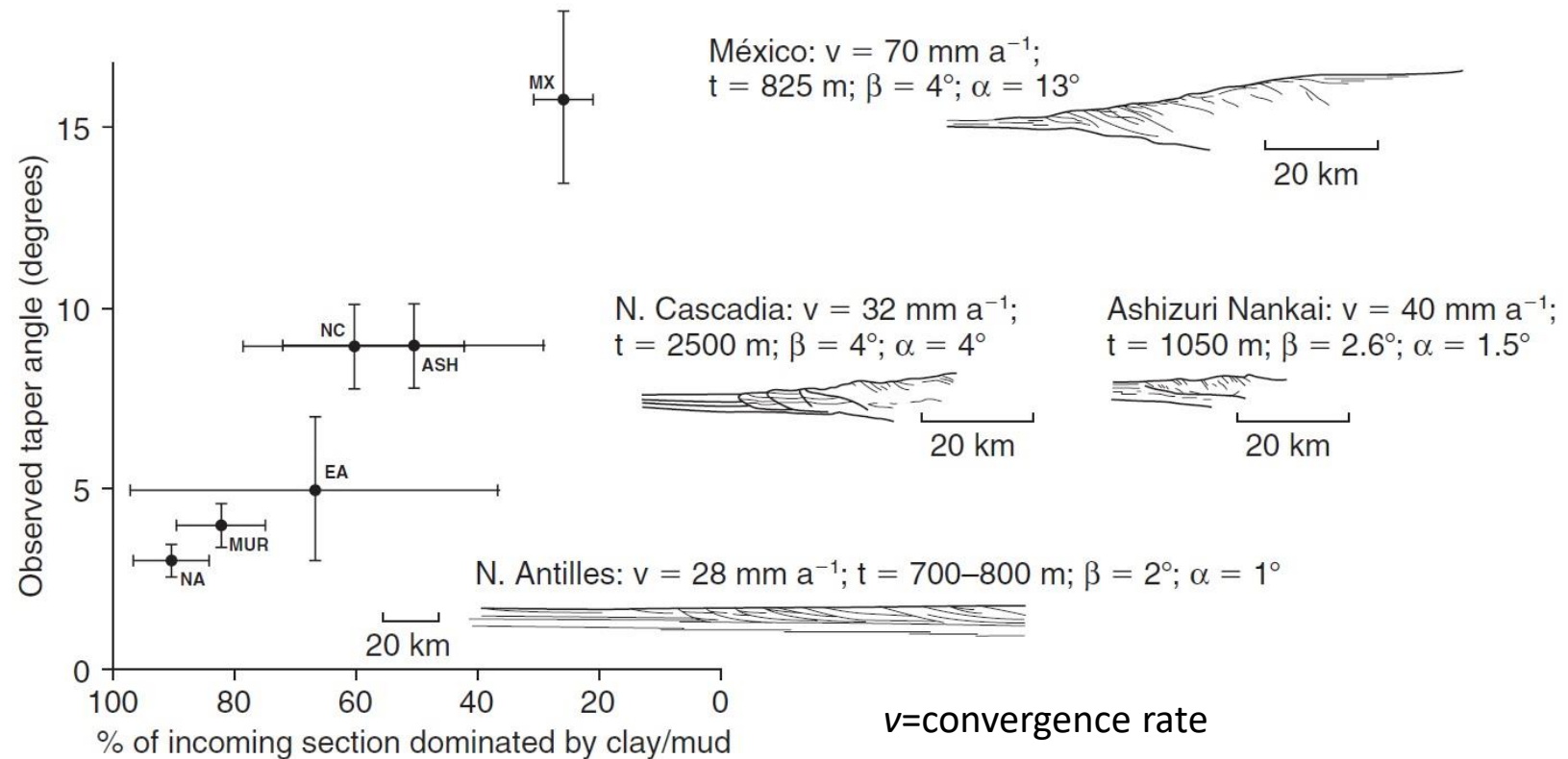
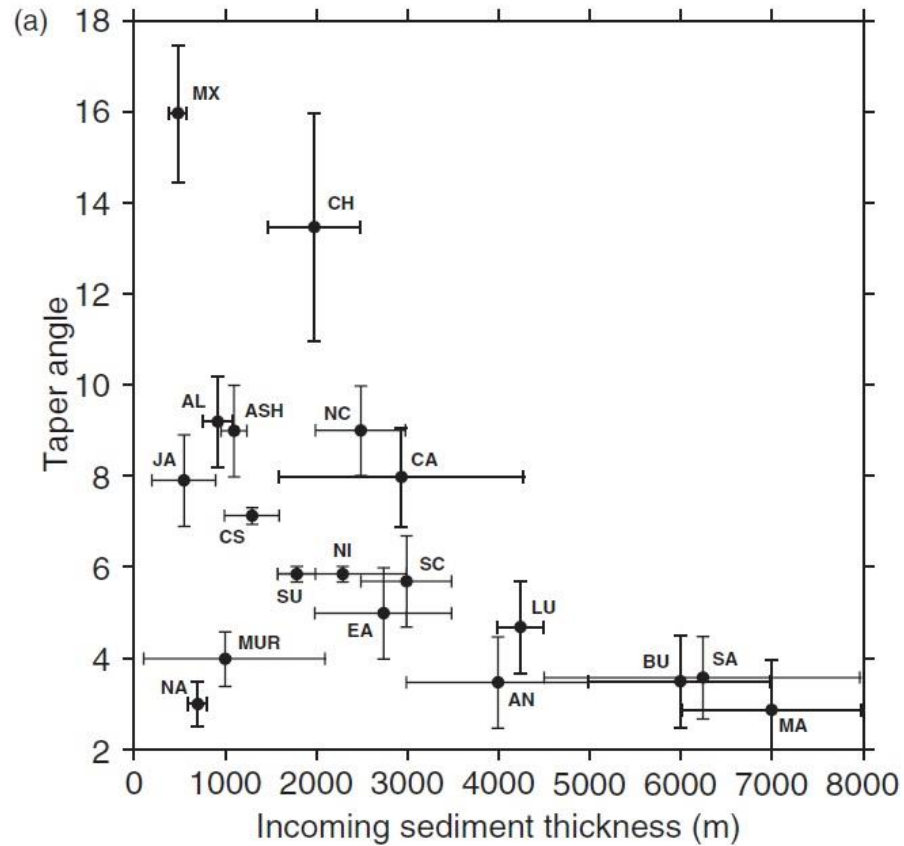
- Beneath the prism, the plate boundary is defined by a 20-30-m-thick, gently dipping fault or shear zone that separates a deformed sedimentary wedge above from a little-deformed section of subducted trench sediment, volcanoclastic rock, and basaltic crust below.
- This boundary, or *décollement*, develops in a weak sedimentary layer (hemipelagic mud) underlying stronger trench turbidites. Above the *décollement* is a *fold and thrust belt* composed of listric thrust ramps that rise through the stratigraphic section forming imbricated arrays.
- The top of an accretionary prism is defined by a relatively abrupt decrease in slope called the *trench slope break*. Between this break and the island arc, a forearc basin may develop, which is then filled with sediments derived from erosion of the volcanic arc and its substrate.

Accretionary Prisms



- The overall shape of accretionary prisms in profile approximates that of a tapered wedge, where the upper surface slopes in a direction opposite to that of the underlying décollement.
- The surface slope (α) is determined by the interplay between resistance to sliding on the décollement and the strength of the rock in the thrust wedge, which are strongly influenced by the pore fluid factor (λ), the dip of the basal décollement (β), and the weight of the overlying rock.

Accretionary Prisms

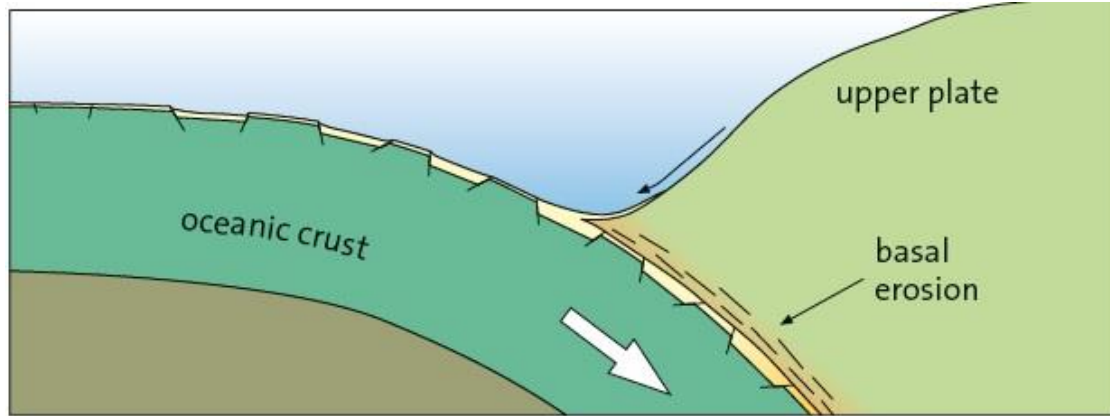


NA, northern Antilles; SA, southern Antilles; MUR, Nankai Muroto; AL, eastern Aleutians (160°W); EA, eastern Aleutians ($148\text{--}150^\circ\text{W}$); CA, central Aleutians ($172\text{--}176^\circ\text{W}$); NC, north Cascadia; SC, southern Cascadia; ASH, Nankai Ashizuri; MX, Mexico; JA, Java; CS, central Sumatra; SU, Sunda; CH, Chile; NI, Nicobar; AN, Andaman; LU, Luzon; BU, Burma; MA, Makran.

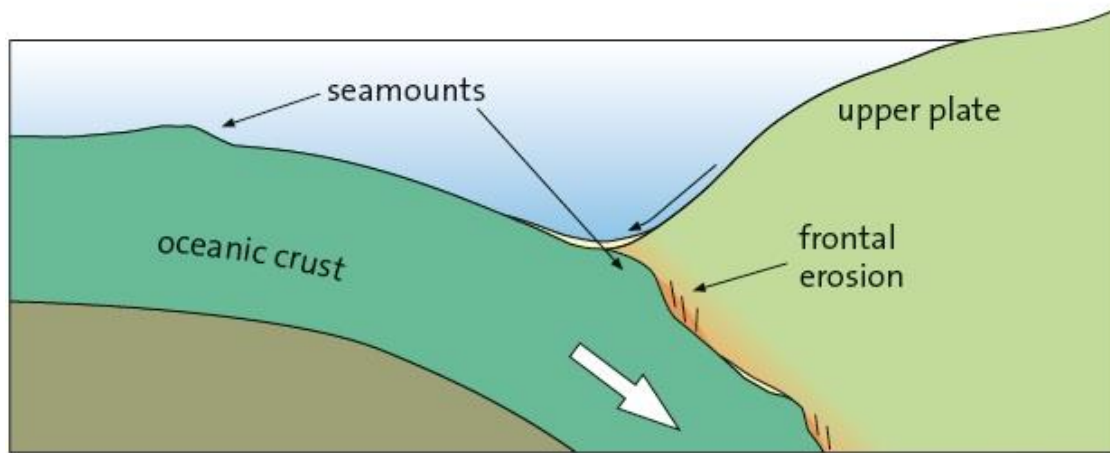
- Thick sedimentary sections produce large prisms that are able to sustain high pore fluid pressures and low stable taper angles.
- Prisms composed mostly of low permeability fine-grained sediments (e.g., northern Antilles), exhibit thin taper angles and those characterized by a high proportion of high permeability turbidites (eg., Cascadia, Chile, and México), have steep taper angles.

Erosion of accretionary prisms

Marianna Subduction Zone



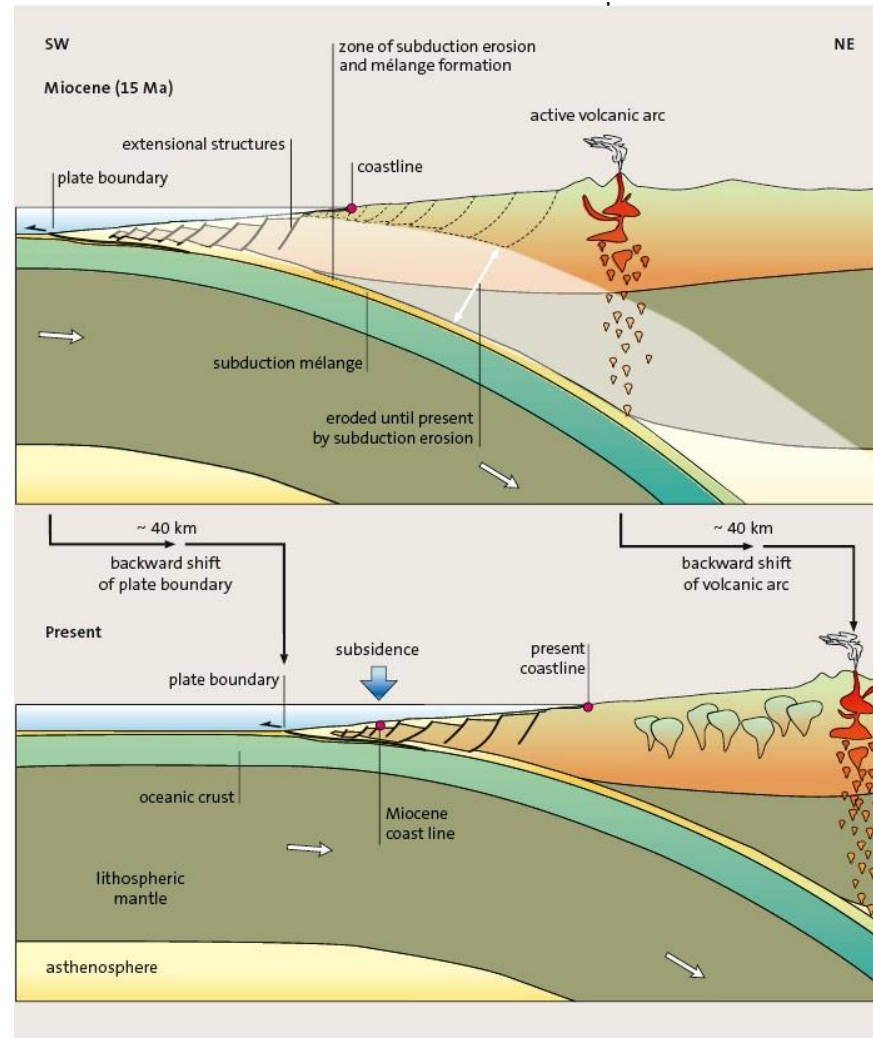
Costa Rica Subduction Zone



- Subduction erosion is particularly effective when the lower plate has a roughly textured surface and is only covered by a thin sedimentary layer.
- As the lower plate enters the subduction zone and is bent, the upper part of the plate is extended and form a series of horst and graben, favoring the removal of the sediments.
- Seamounts on the subducting plate create a somewhat different kind of subduction erosion: Single seamounts scrape material from the frontal tip of the accretionary wedge along the upper plate and carry it into the subduction zone (frontal erosion).
- Subduction erosion can occur both where the subduction zone angle is relatively low and there is a strong coupling between the two plates (Chile type) and where the subduction angle is high and subduction roll-back occurs (Mariana type).
- Pore fluids in the high-stress zone along the plate boundary decollement actually increase mobility and slippage in this zone by acting as a lubricant.

Erosion of accretionary prisms

Costa Rica Subduction Zone



- Erosion of the accretionary prism on the upper plate causes the plate boundary to migrate towards the arc, which itself is moving backward in response to the migrating subduction zone (Costa Rica).
- The Cocos Plate is being subducted beneath the Caribbean Plate with a velocity of about 9 cm yr^{-1} . The volcanic front has shifted 40 km backwards (towards the Caribbean plate) during the last 15 million years.

Sediment thickness controls geometry of convergent margin, max M and type of seismicity

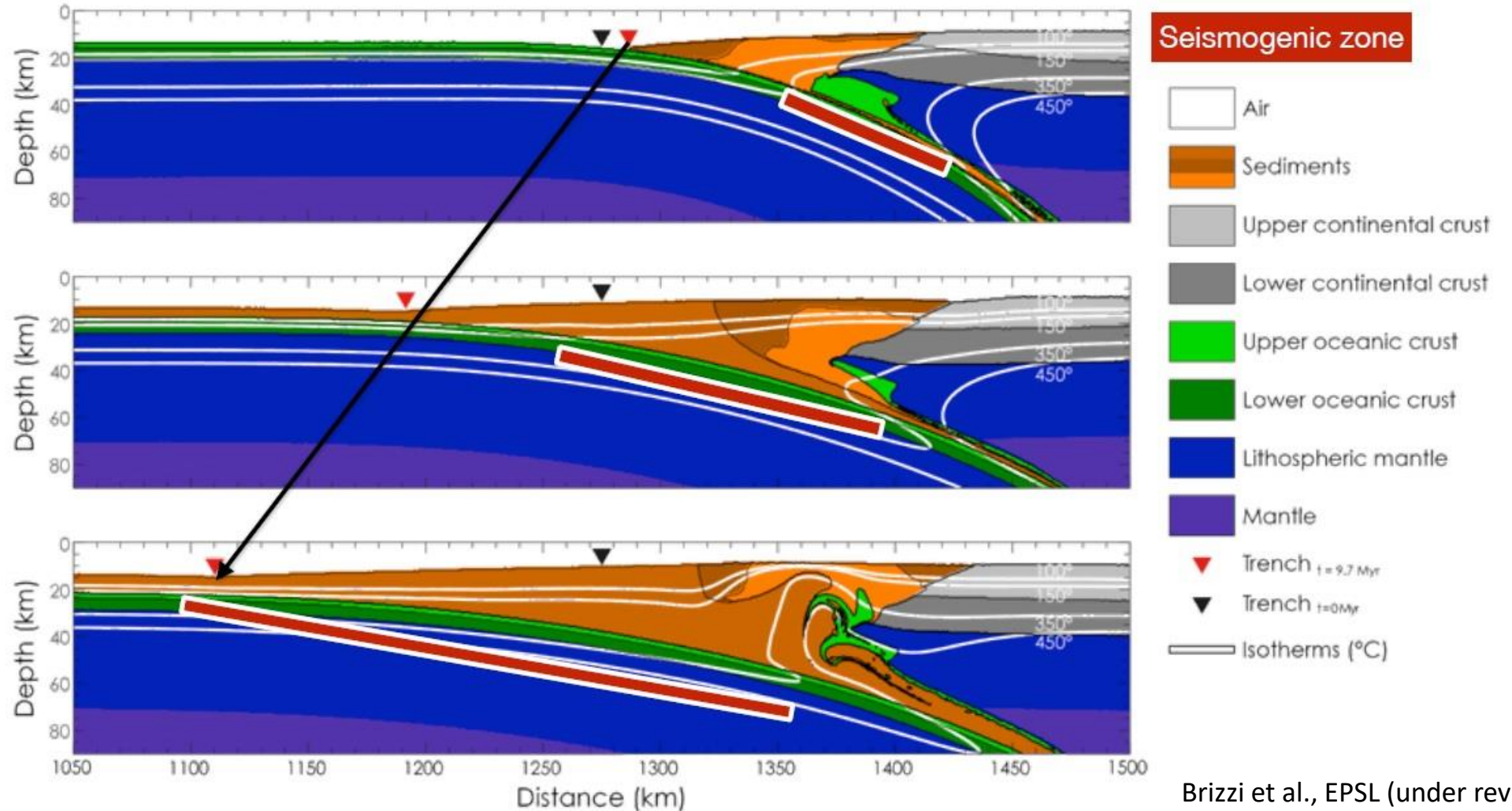
- More sediments → seaward growth wedge → trench retreat and unbending → shallower dip → wider seismogenic zone
- More sediments → less mechanical coupling → more slab retreat → shallower dip → wider seismogenic zone

Sediment thickness:

0 km

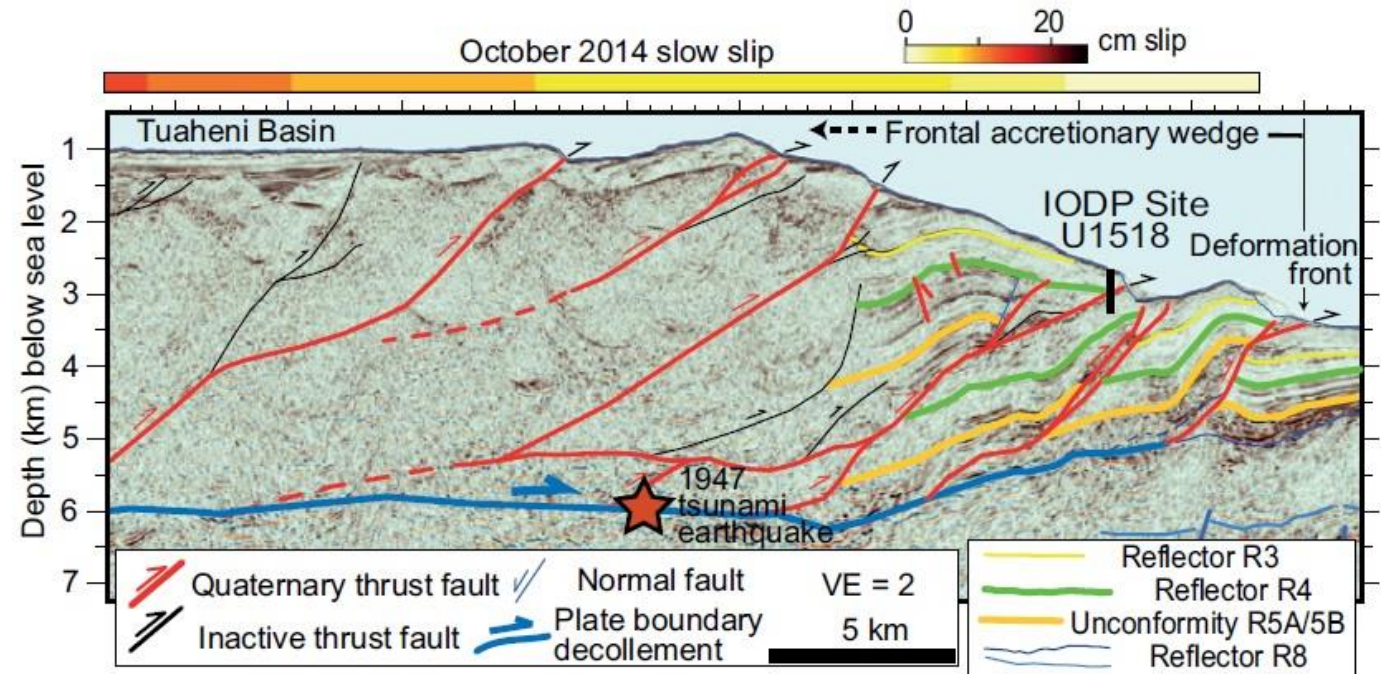
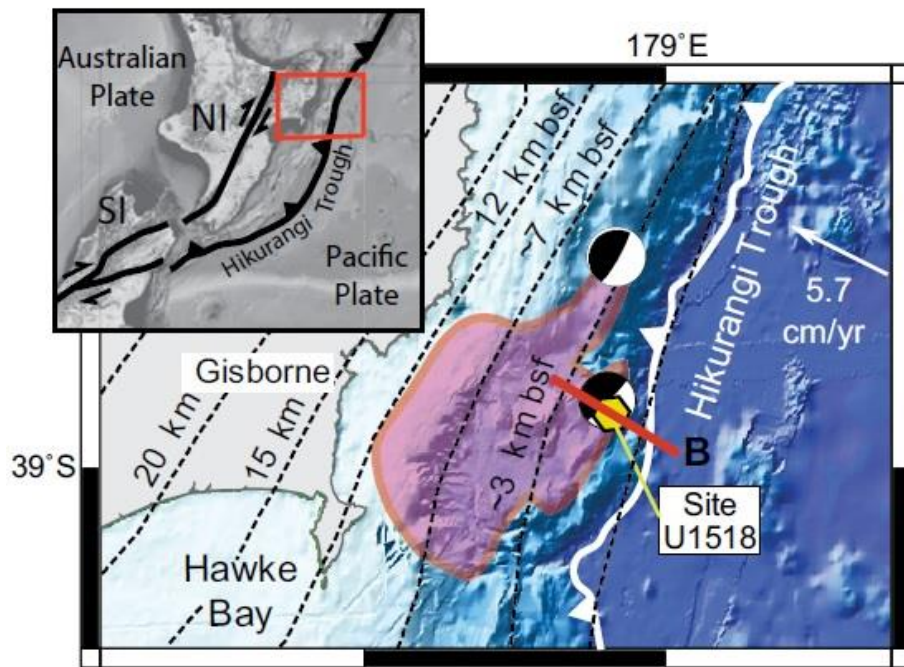
4 km

8 km



Mixed Deformation Style in Subduction Zones

Hikurangi subduction margin

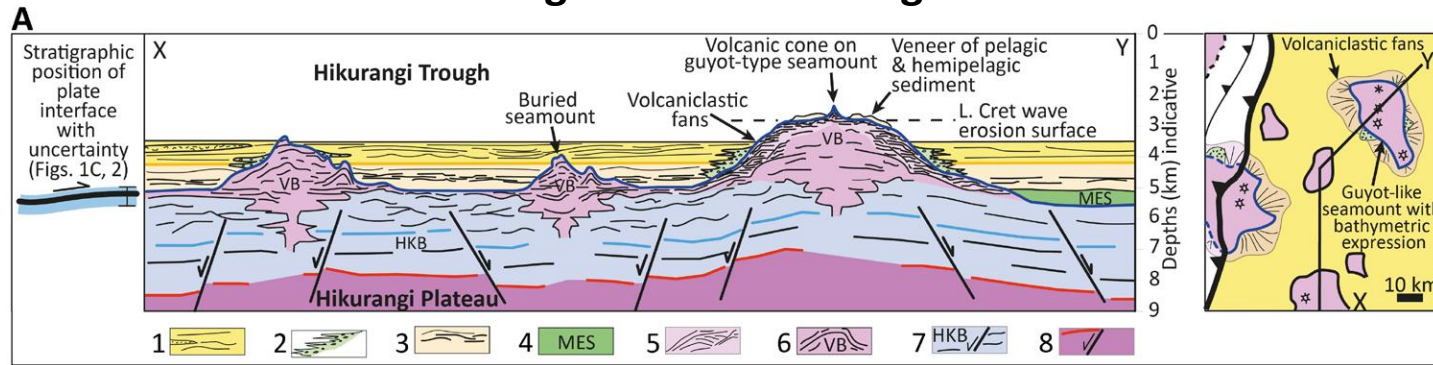


Fagereng et al., 2019, *Geology*, 47.

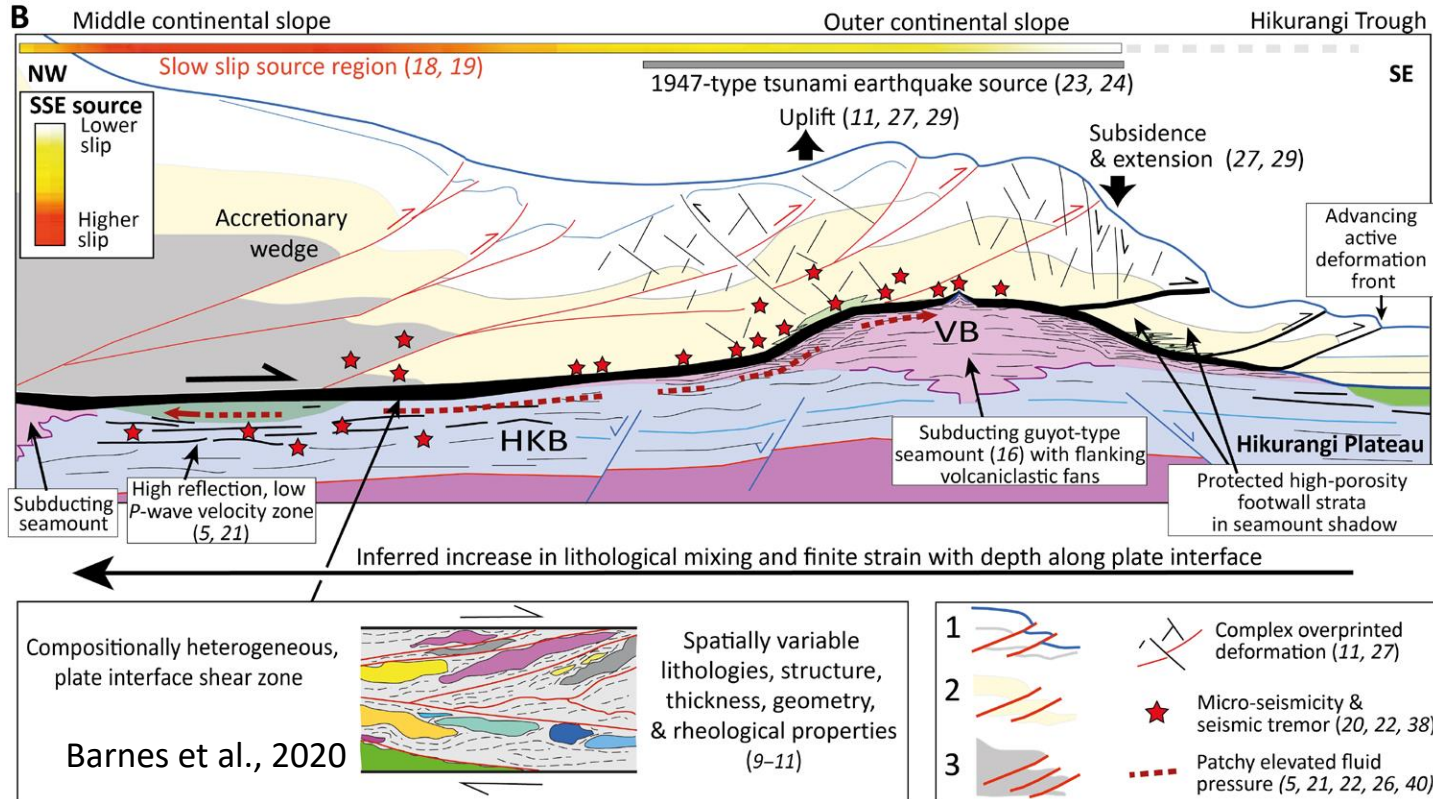
- The fault zone contains brittle and ductile features in Pleistocene hemipelagic sediments. The deformation and brittle modes were coeval, since flow bands are preserved between intensely brecciated intervals, without being affected by this brittle deformation.
- There is a lithological heterogeneity that are not the main reason for mixed brittle-ductile deformation within the Pāpaku fault, since they are restricted to cm-scale variations.
- The structures indicative of fluidization are locally present and suggest that local and transient increases in pore fluid pressure can modulate slip mode.
- The Pāpaku fault has experienced mixed styles of slip as a function of loading rate and/or pore fluid pressure.

Mixed Deformation Style in Subduction Zones

Hikurangi subduction margin



1, siliciclastic sediments; 2, mass transport deposits; 3, pelagic sediments (chalk, marl, calcareous mudstone, nannofossil ooze) and volcanic tuff; 4, inferred siliciclastics; 5, volcanic conglomerate/breccia, minor marl, and volcaniclastic sandstones; 6, basaltic volcanics and volcaniclastic sediments; 7, volcaniclastic sediments, siltstone, silty claystone, limestone, and basalt; 8, Hikurangi Plateau basaltic basement.

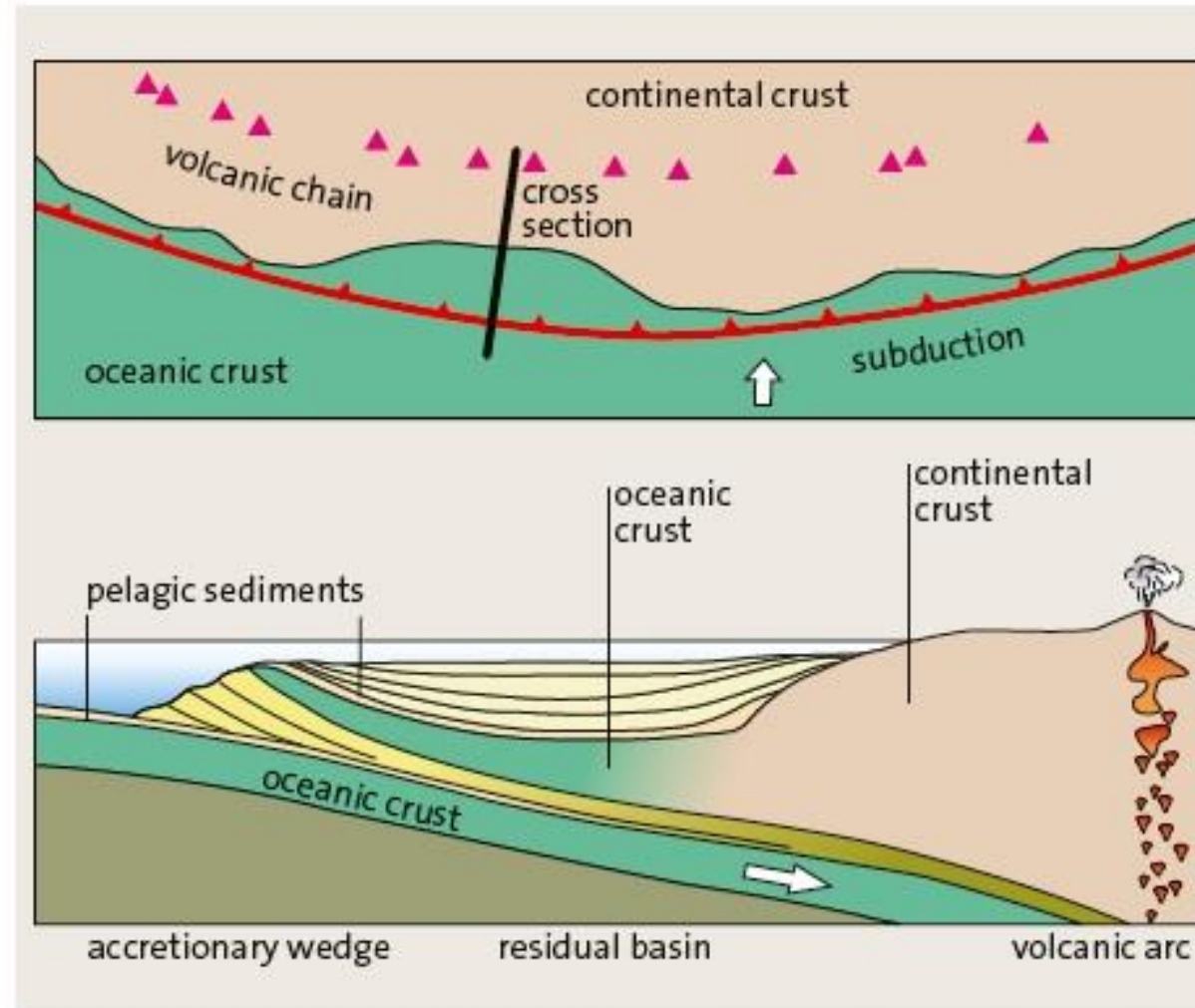


- Combination of compaction-driven mechanical fluid pressurisation and thermal pressurisation, enhanced by low permeability of the host rocks, contribute largely to the weakening and propagation of earthquake at shallow depths during tsunamigenic earthquakes.
- Fluid pressurisation in impermeable clay-rich sediments is likely to be active and promote propagation of earthquake at shallow depth in clay-dominated subduction zones worldwide.
- The lower permeability of the clay-rich faults promotes more rapid pore fluid pressure increase, faster dynamic fault weakening, and lower breakdown work, promoting rupture propagation and tsunamigenic earthquakes.

- Shallow slow slip transients can arise from lithological, geometric, and rheological heterogeneity along the plate boundary megathrust.

Forearc Basin

- Forearc basins are zones of crustal subsidence that lie between the outer ridge and the volcanic arc, underlain by either thinned continental or normal oceanic crust.
- They are generally dominated by great thicknesses of marine sediment and derived from the adjacent volcanic arc.



Volcanic Arc

- Volcanic Arc develops 150-200 km from the trench axis
- Depth of the lithospheric slab beneath the volcanic arc is in a range of 65-130 km, depending on the vertical rate of descent of the slab: high descent rate increases the rate of flow in the mantle wedge, causing higher temperature and melting at shallower depth.

Thickness of the arc crust reflects both the age of the system and type of the arc

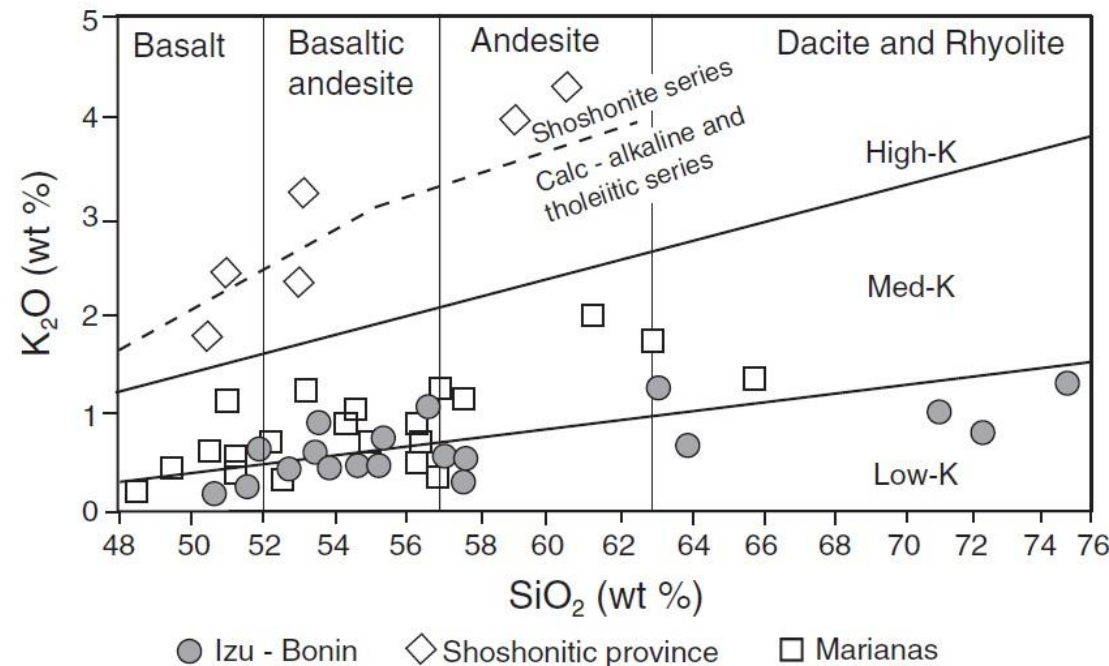
Oceanic Arc: volcanic rocks have 53-55% SiO_2

Marianna volcanic arc (3-4 My): crustal thickness 20 km

Japanese Arc (Neogene): crustal thickness 30-50 km

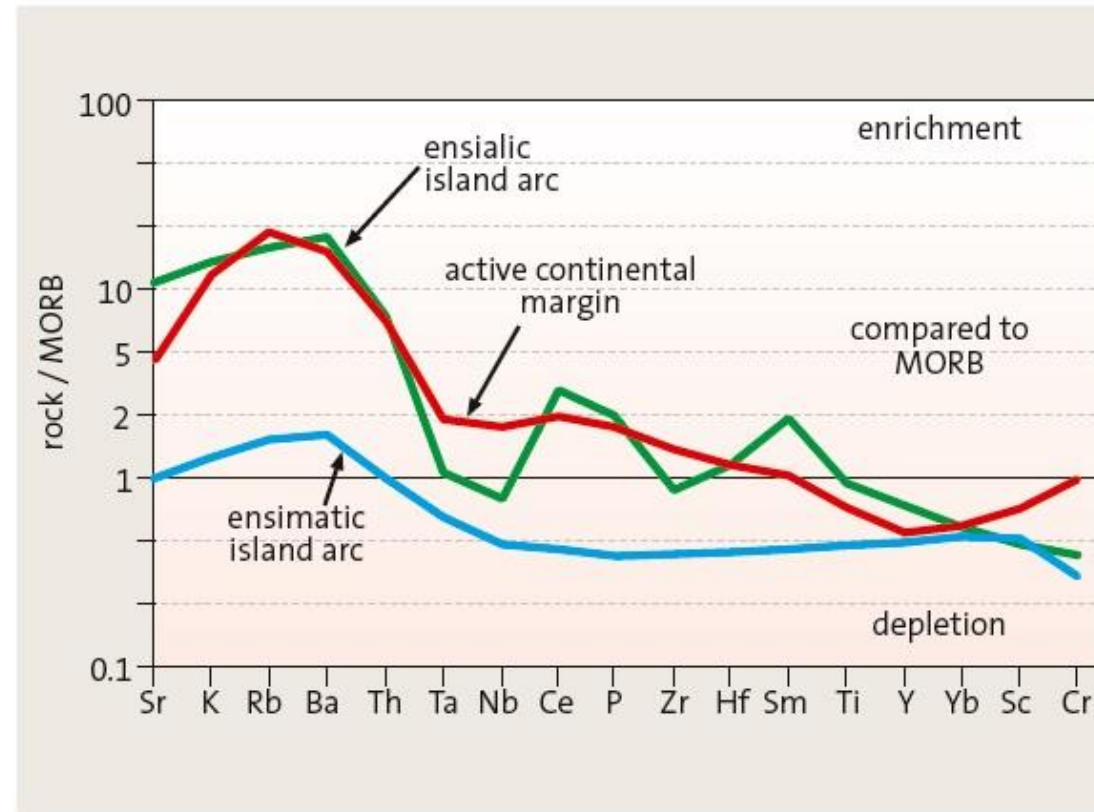
Continental Arc: volcanic rocks have 63% SiO_2

Andes and Cascades volcanic Arc: crustal thickness up to 60-70 km.



Volcanic Arc

Calc-alkaline basalts



Spatial patterns of volcanic series (Japanese island arc): It reflects decreasing magma generation from the subducted rocks with increasing depth of the subduction zone.

- Low potassium tholeiitic series: basaltic lavas
- Calc-alkaline series: andeites moderately enriched in potassium, aluminium (up to 20%) and lithophile elements, such as strontium, barium, thorium, and uranium and poor in «immobile elements», such as niobium and tantalum.
- Alkaline series: alkaline basalts and high-potassium (i.e., shoshonitic) lavas.

Deviations from the spatial patterns (Marianna arc produces tholeiitic basalts and boninites, derived from melted harzburgites of the lithospheric mantle) are due to variations in the depth and degree of partial melts and other processes (e.g., assimilation, magma mixing)

Backarc Basins

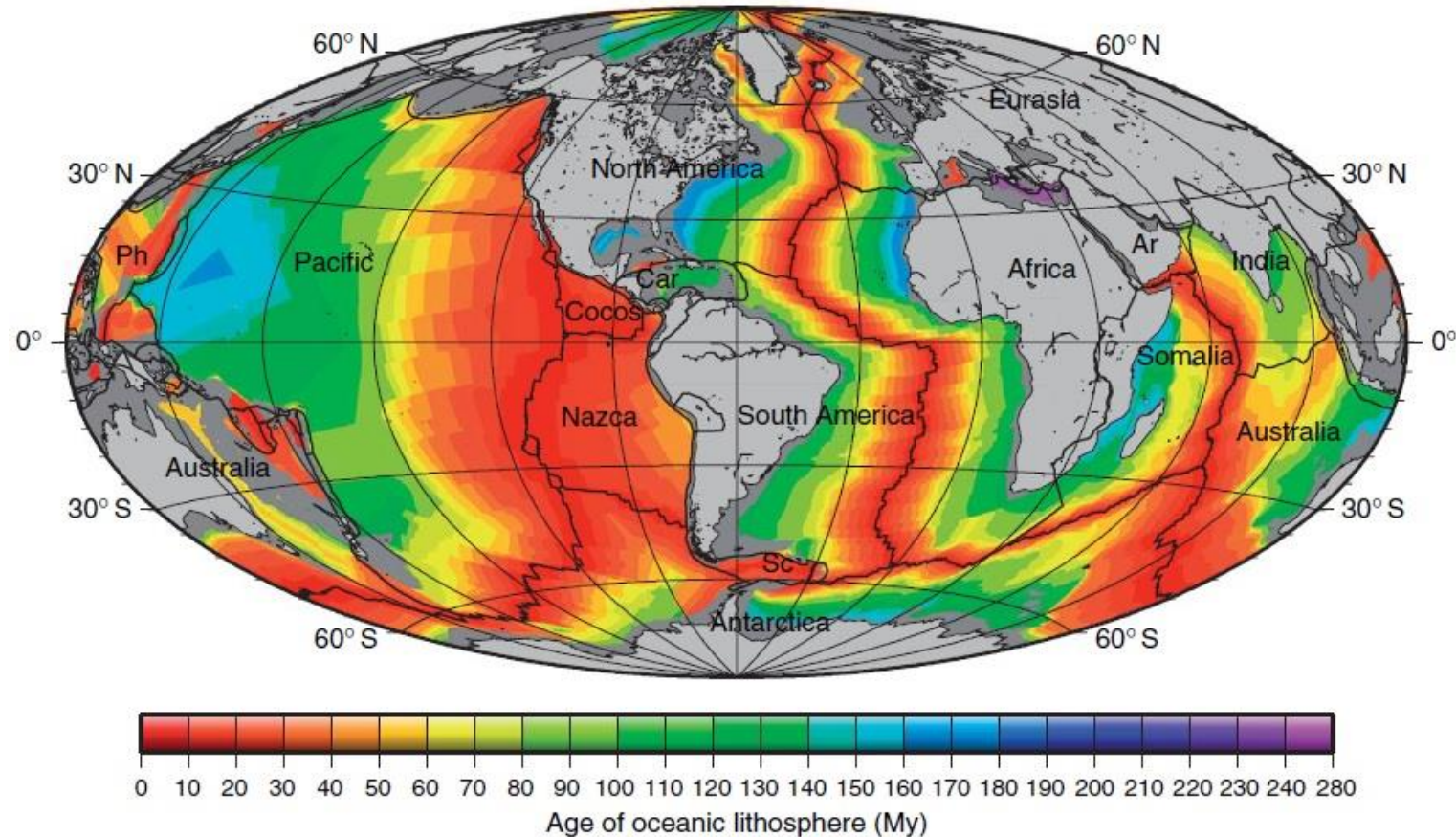
Backarc basins are small basins of either oceanic or continental affinity that form behind the volcanic arc in the overriding plate of a subduction zone.

- Crust composition and accretion rate is similar to that of the oceanic basins (variable spreading velocity: 16 cm yr⁻¹ in the backarc basin of Tonga Island to 2-4 cm yr⁻¹ in the backarc basin of the Marianna).
- Crustal accretion, magmatic activity, and thickness of the backarc basins are influenced by processes related to subduction (dynamics of flow of the upper mantle wedge), which cause a main difference in the geochemistry (similar to that of the adjacent volcanic arc, usually including higher water content).
- Sediments deposited in backarc basins consist of arc-derived volcanoclastics and volcanic ashes, sand and mud eroded from the continent, and marine carbonates.
- Magnetic anomalies are present, but not so well developed as in the oceanic basins.

Origin of the back-arc basin, extension induced by:

- Slab roll-back
- Convection of the upper mantle wedge induced by the subducting slab or an increase in the angle of subduction with depth.

Subduction conditions



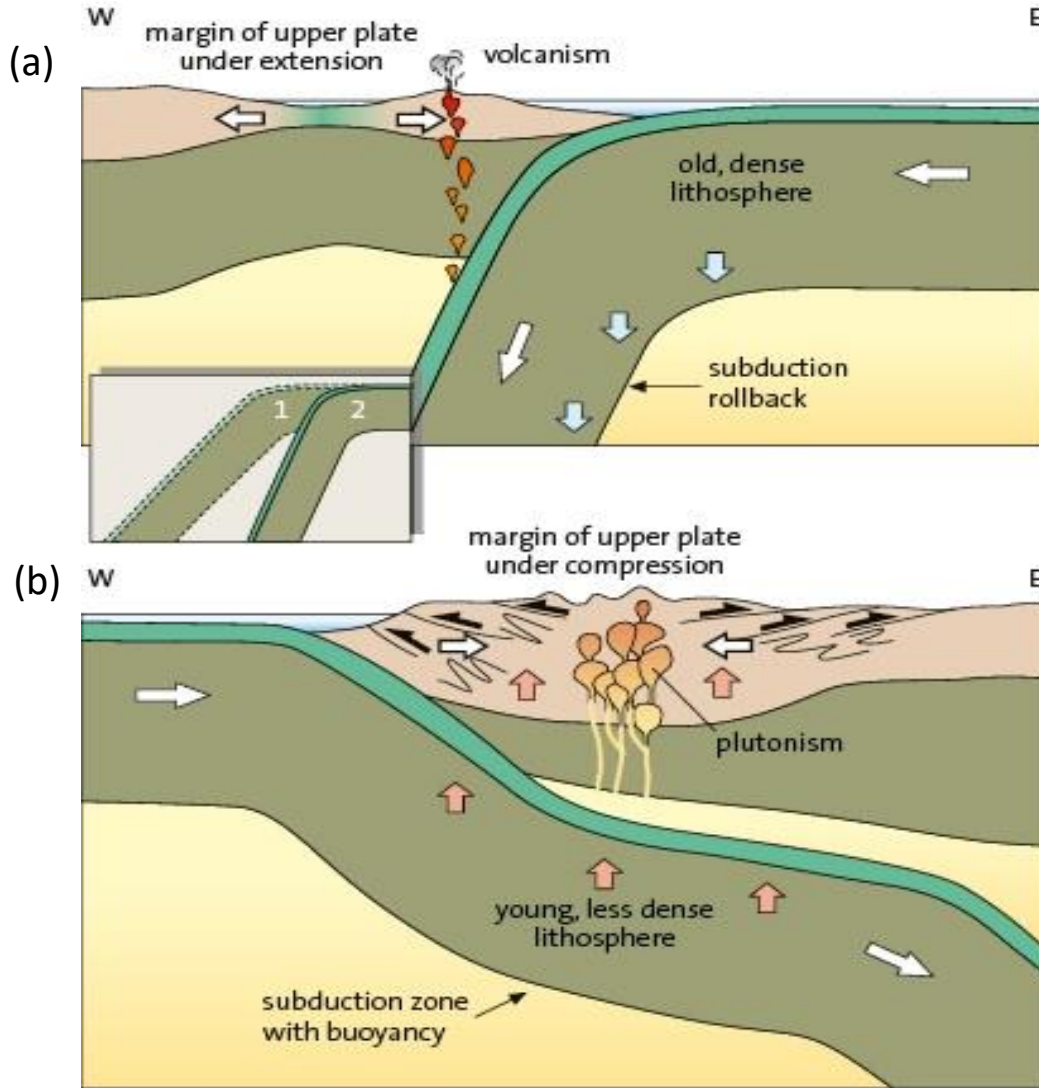
Favour subduction

- Excess of density is necessary to create the vertical forces that are capable of initiating spontaneous subduction (western rim of the Pacific plate, age > 100 Myr).
- Young oceanic lithosphere (eastern margin of the Pacific plate < 50 Myr) forced to subduction by compressional forces.

Against subduction

- Forces exerted on the subducting slab by the flow of the asthenosphere (causing uplift).

Dip of the slab and type of subduction



(a) Spontaneous subduction: extensive decoupling, strong slab pull with consequent roll-back of the subduction zone, extensional structures in the upper plate (backarc basin, new oceanic crust formation), deep trenches, high elevation of volcanic arc (i.e., **Marianna-type subduction**).

(b) Forced subduction: shallow subduction and a strong coupling with the upper plate (compressional forces are transferred to the upper plate), back-arc compression, thickening of the upper plate, shallow trenches, high elevation of volcanic arc, larger compressional earthquakes (25-100 km), flow of the asthenosphere restricted to mantle wedge (i.e., **Chilean-type subduction**)

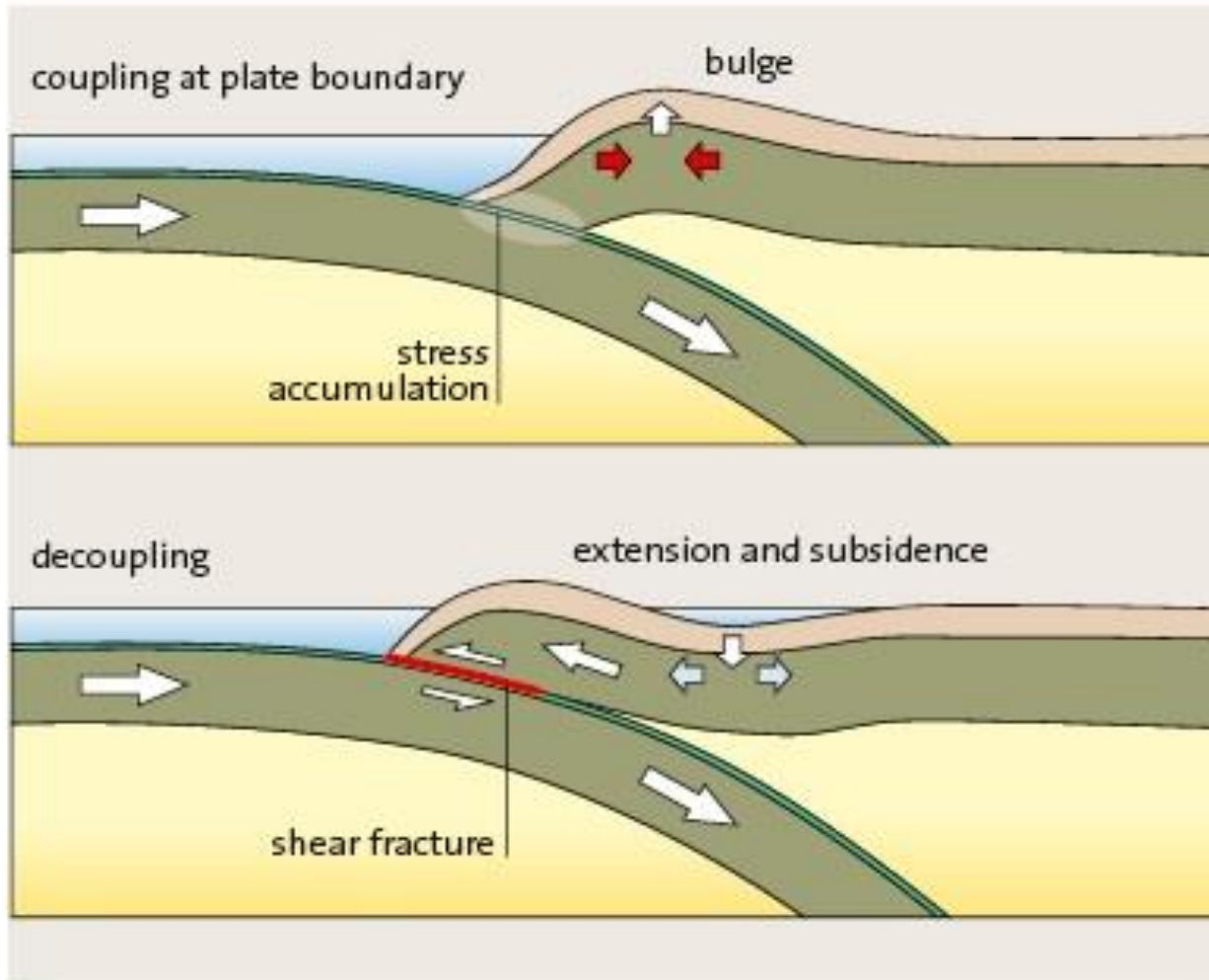
Factors influencing the dip:

- Slab age (if > 30 Myr the slab can subduct spontaneously at high angle)
- High rate of underthrusting enhance uplift
- Absolute motion of the overriding plate
- Slab width (enhances trench suction which favors the uplift of the slab)

- Forced subduction may evolve from spontaneous subduction as increasingly younger portions of the downgoing plate.

Mariana-type and Chile-type subduction zones

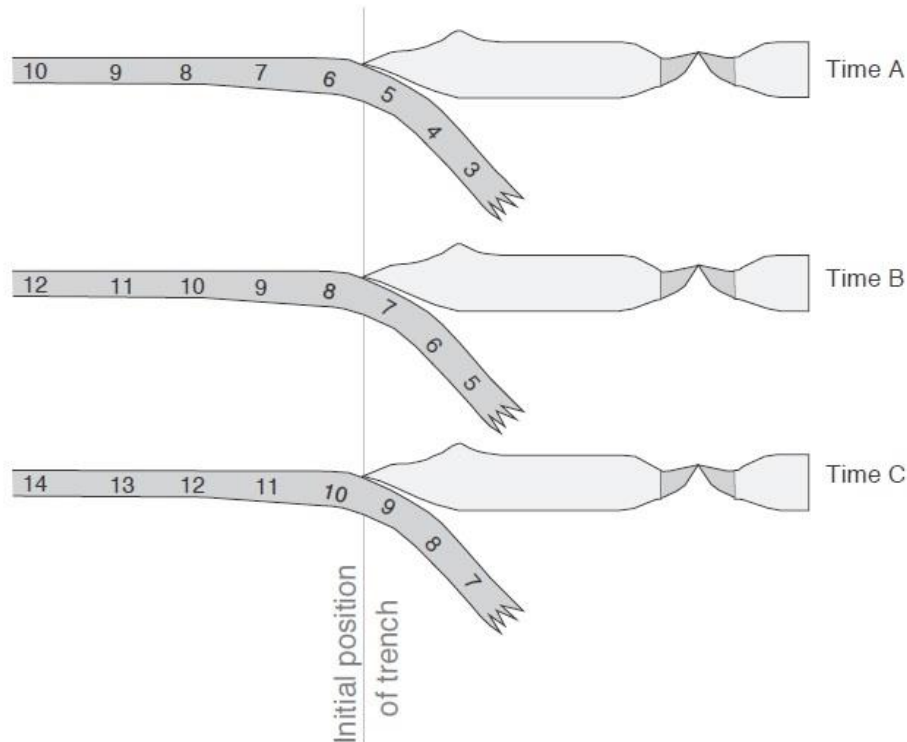
The transfer of forces at convergent plate boundaries can vary with time



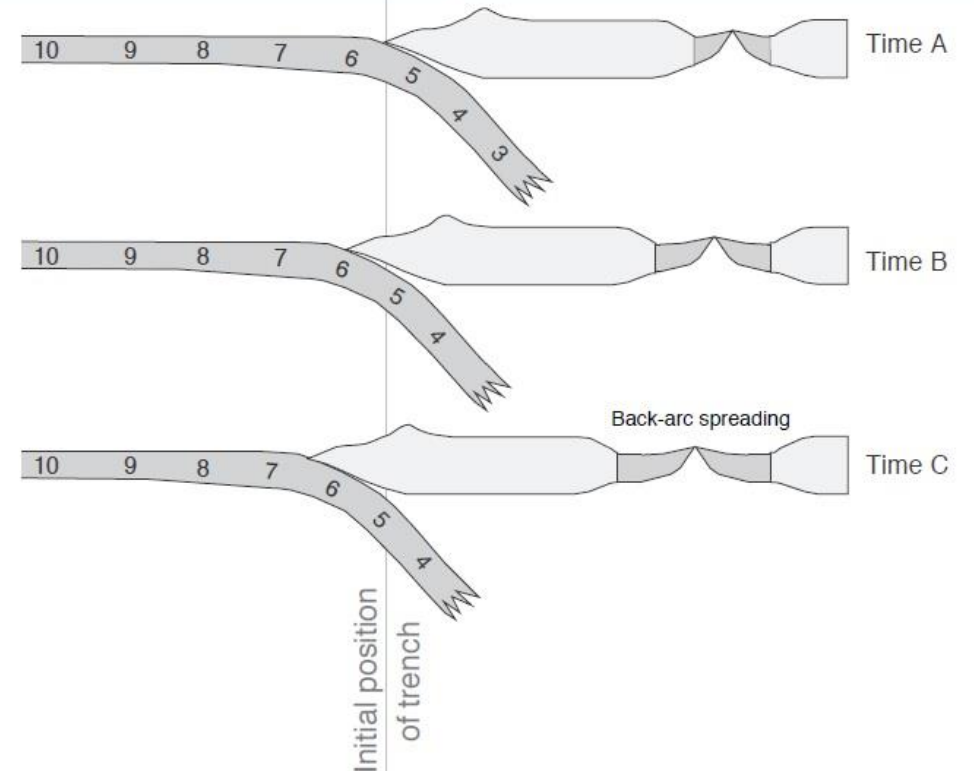
- Phases of compression that reflect coupling of forces between both plates may be followed by extensional phases during which decoupling occurs.
- During periods of plate coupling, the edge of the upper plate is vaulted until there is a spontaneous decoupling because of the high accumulation of energy. As a result, the upper plate abruptly steps forward towards the subducting plate and its margin is accompanied by subsidence.

Subducting Slab Age

Subduction due to convergence

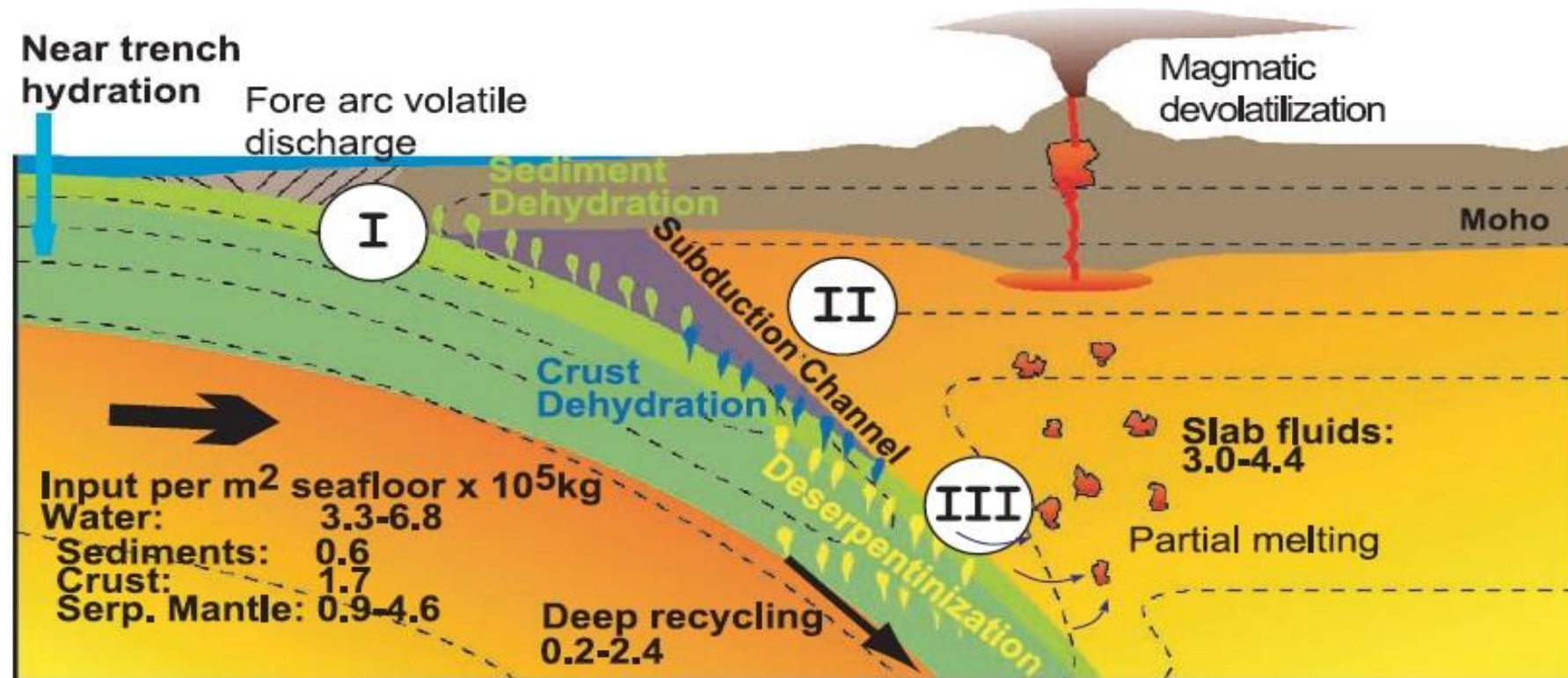


Subduction by slab roll-back



- **Forced Subduction (in case of convergence):** at the initial trench position the age of the slab is progressively older.
- **Subduction characterized by slab roll-back:** at the initial trench position the age of the slab is progressively younger.
- Slab roll back is mainly induced by the increase of age of the subducting slab, causing the increase of density and inclination (in order to not create voids, the slab must retreat) and causes extension (back-arc basins).

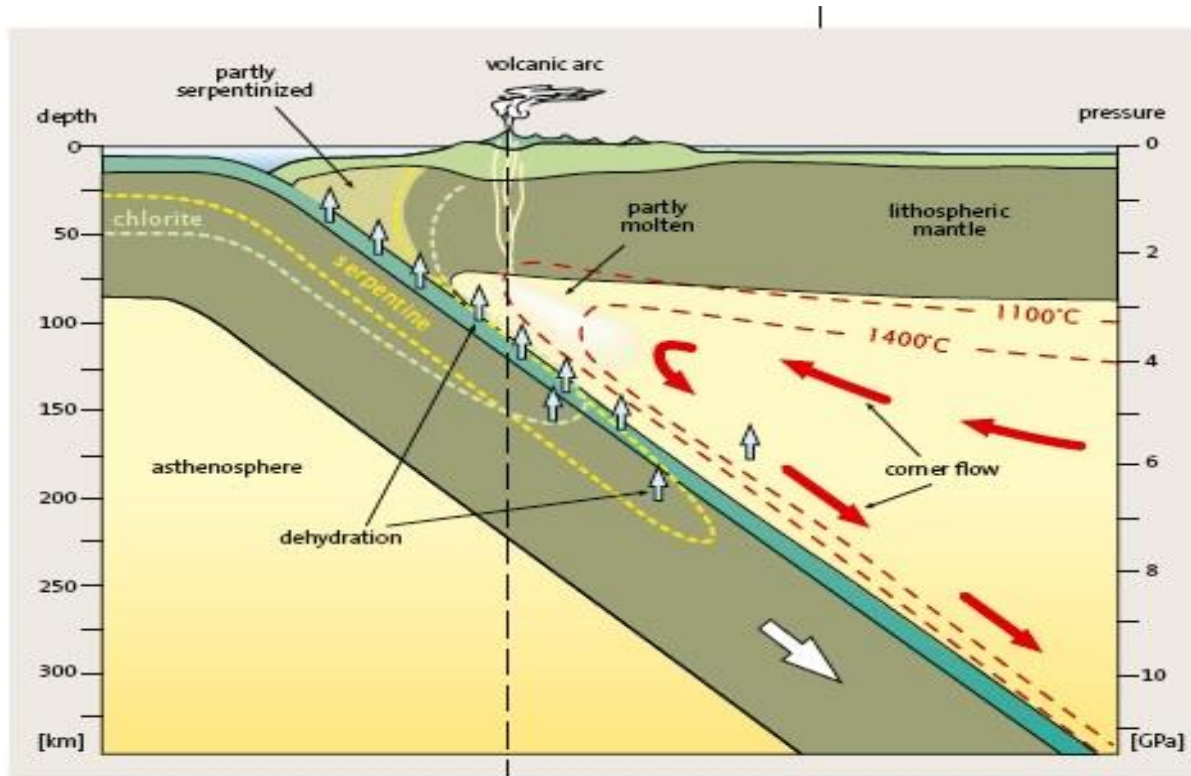
Serpentinite in subduction zone systems



Rupke et al., 2004, EPSL, 223

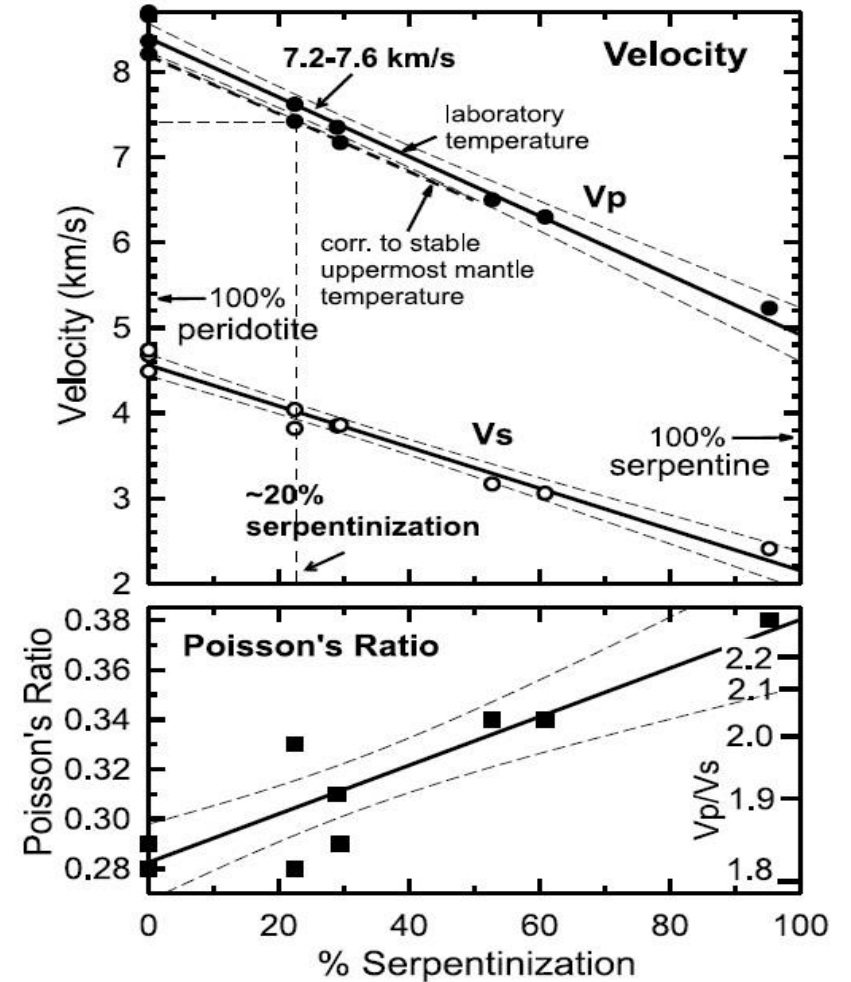
- I shallow fluid release occurs at depths < 20 km from subducting sediments
- II Intermediate depth (20– 100 km) water release from sediments and ocean crust
- III Deep fluid release (>100 km) from oceanic crust and deserpentinizing mantle triggers arc melting

Physical parameters of the serpentinite



Magmatic rocks formed above the subduction zones ($9 \text{ km}^3 \text{ yr}^{-1}$) have several % of water (up to 6 % H_2O)

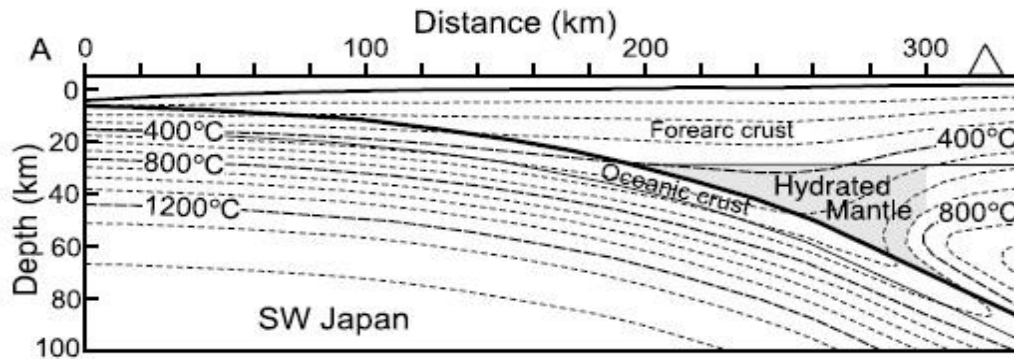
Serpentine: a magnesium silicate mineral ($\text{Mg}_6[\text{Si}_4\text{O}_{10}(\text{OH})_8]$) with a high water-content 13 weight-%)



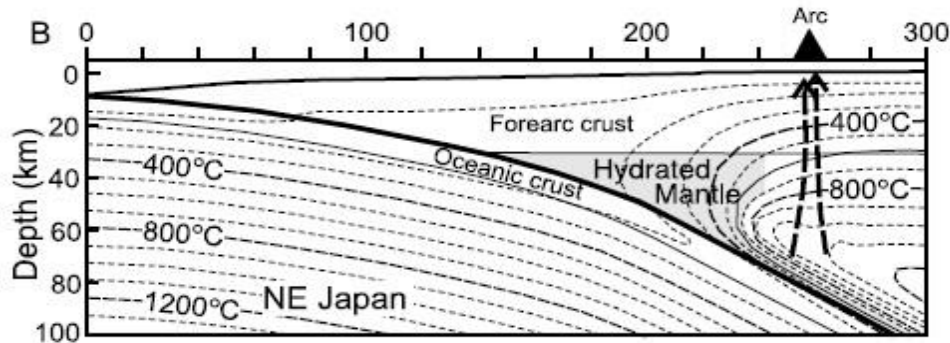
Hyndman and Peacock, 2013, EPSL, 212

- Serpentinite: low V_p and V_s velocity, low density, and high V_p/V_s ratio and σ
- Serpentinization may generate seismic reflectivity, an increase in magnetization, an increase in electrical conductivity, and a reduction in mechanical strength.

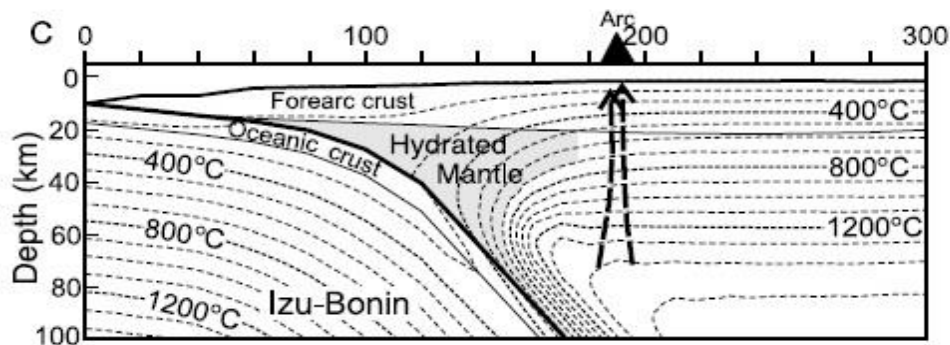
Serpentinized forearc mantle



Warm continental subduction zone: Calculated forearc temperatures are 400-600°C. This results in less extended zone of serpentinized forearc mantle, shallow metamorphic transformation from blueschist facies to eclogite (50 km).

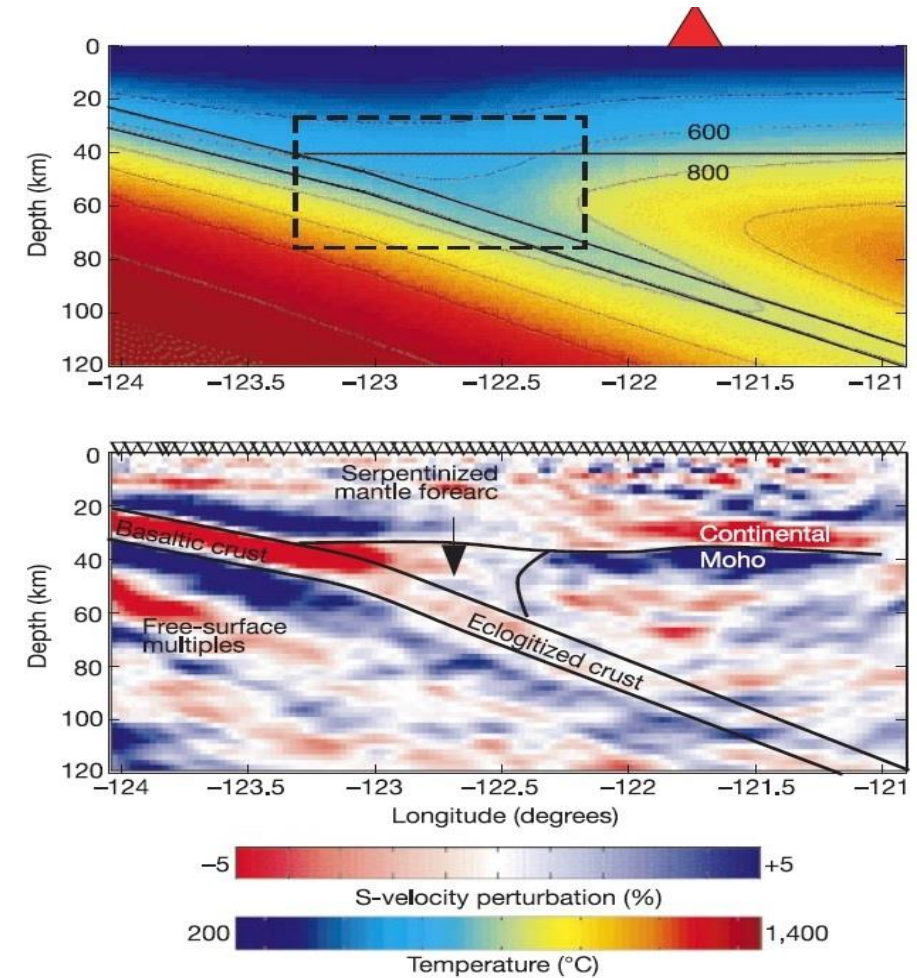
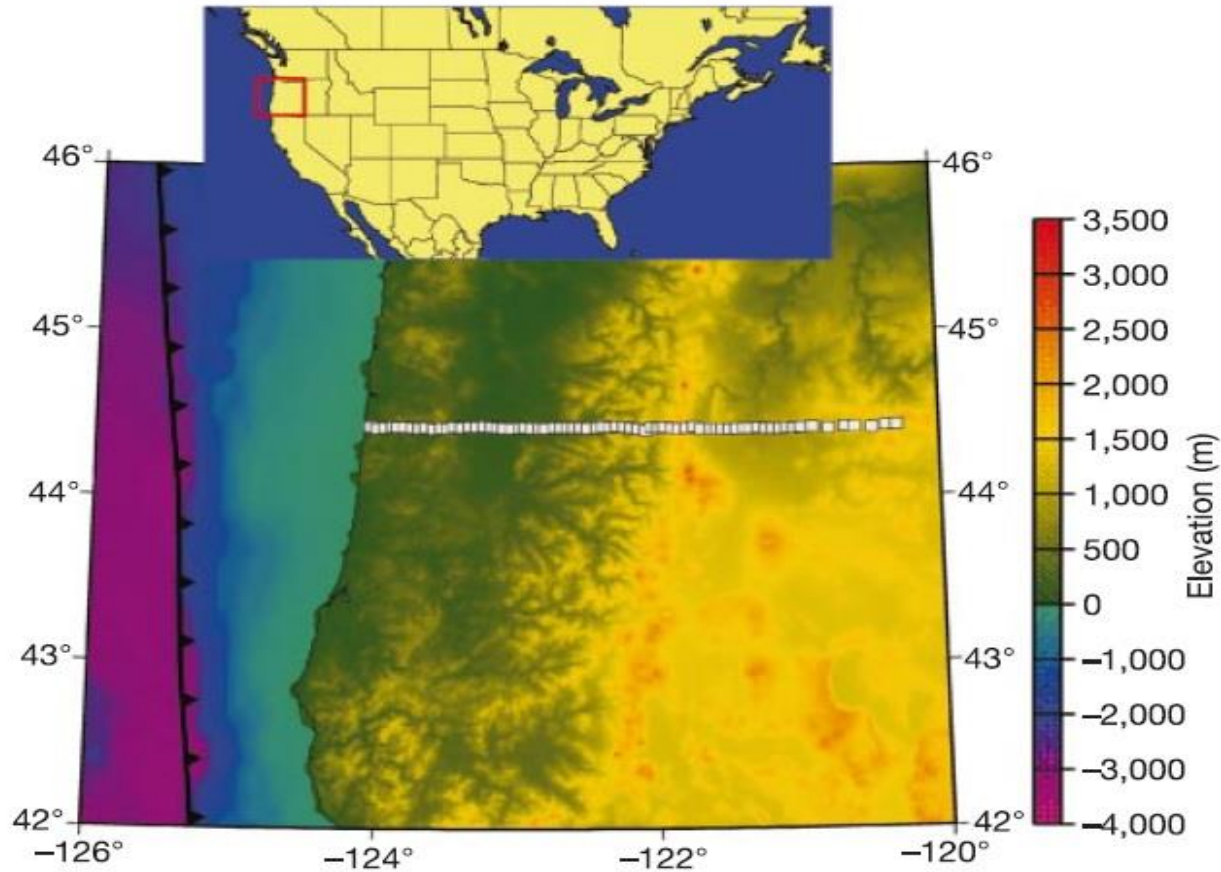


Cool continental subduction zone: The subducting slab intersects the forearc Moho at 30-50 km depth, the calculated temperatures in the uppermost forearc mantle are 150-250°C.



Cold oceanic subduction zone: Uppermost forearc mantle temperatures are especially low for island arcs with thin forearc crust (10-15 km), where the T in the mantle wedge corner are $\sim 100^\circ\text{C}$. This results in more extended zone of serpentinized forearc mantle, deep metamorphic transformation from blueschist facies to eclogite (100 km).

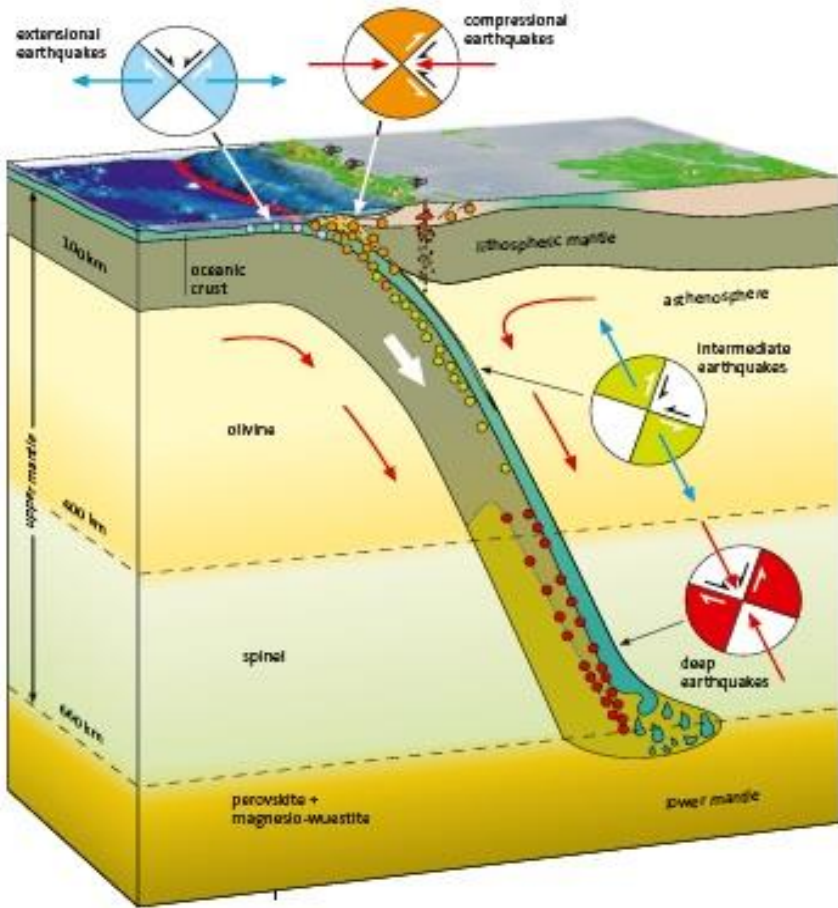
Cascadia Subduction Zone



Bostock et al., 2002, Nature, 417

The degree of hydration diminishes eastwards, producing an inverted continental Moho (high-velocity crust on low-velocity mantle), reduced velocity contrast, disappearance of the inverted Moho, and restoration to a normal polarity crust–mantle boundary 40 km west of the arc.

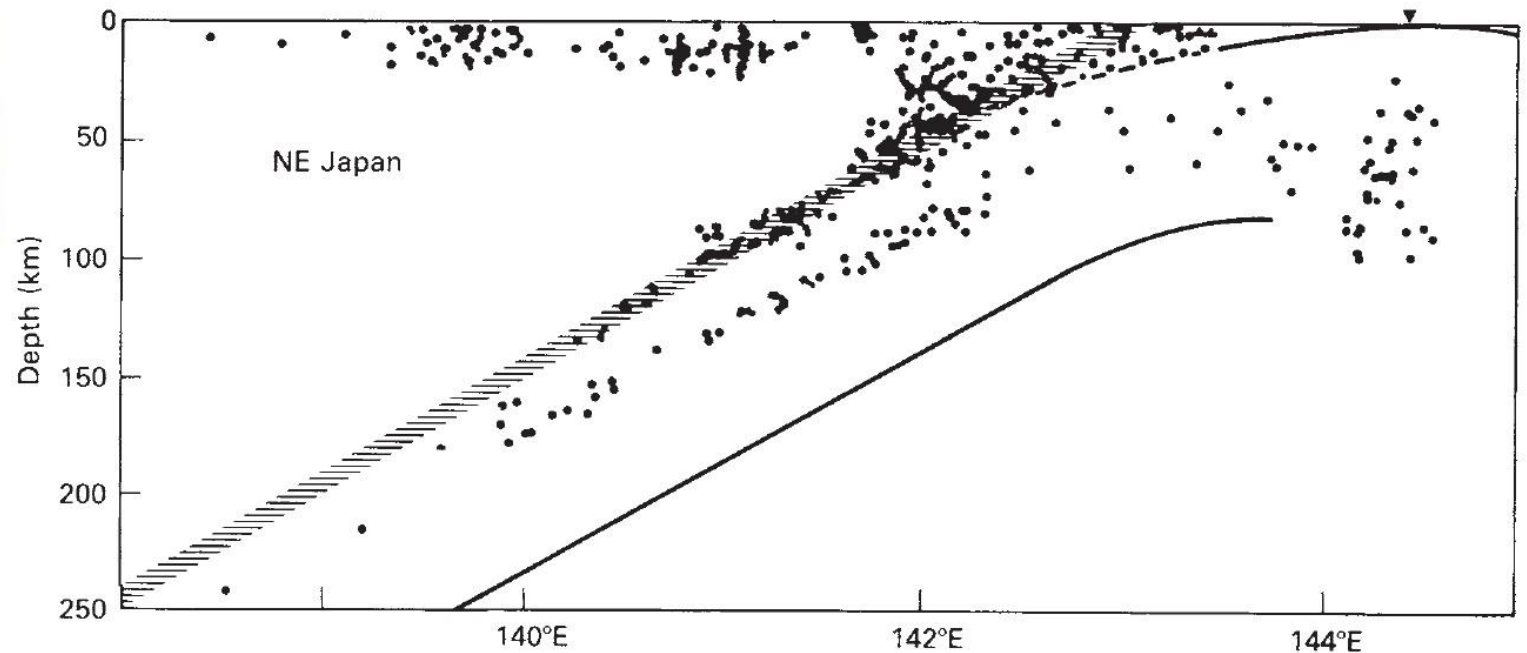
Stress conditions and seismicity in the subducting slab



Shallow earthquakes

Depth < 25km: Earthquakes are generated in response to bending of the lithosphere, which puts the upper surface of the plate into tension (normal faults).

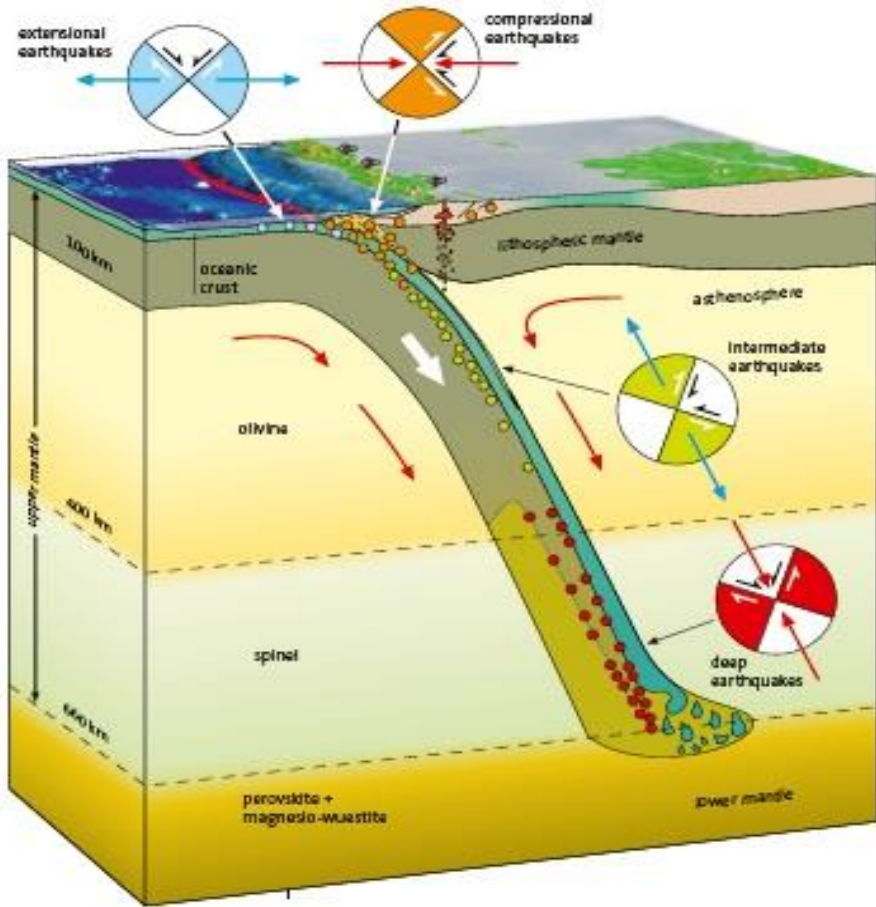
Depth >25km <70-100 km (90 % of total seismicity energy): Earthquakes are generated from thrust faulting along the contact between the overriding and underthrusting plates (horizontal compression and friction of between the two plates), e.g., Alaska 1964, Chile 1960 and 2010 ($M_0 > 9.0$), Sumatra 2004. Other earthquakes sources: dewatering of serpentinized mantle and eclogitization.



Upper zone: eclogite formation

Lower zone: dehydration of serpentinite

Stress conditions and seismicity in the subducting slab



Intermediate earthquakes (20%)

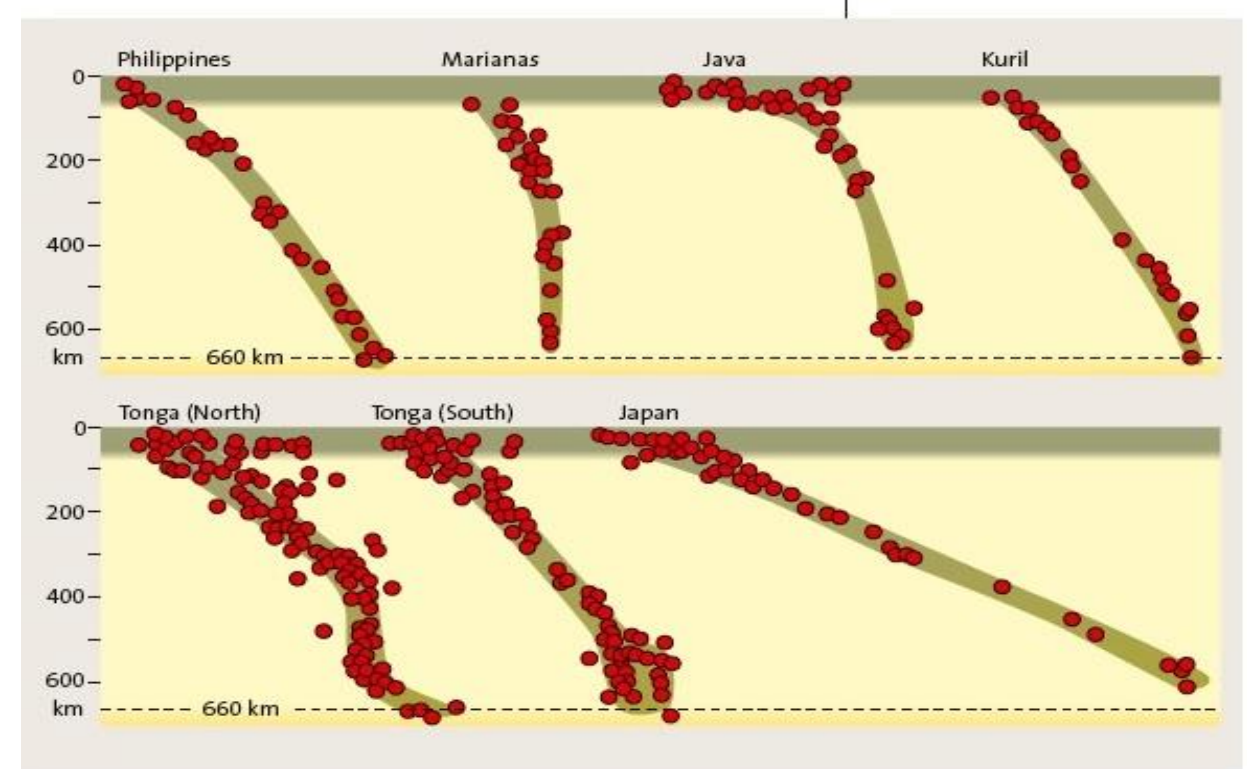
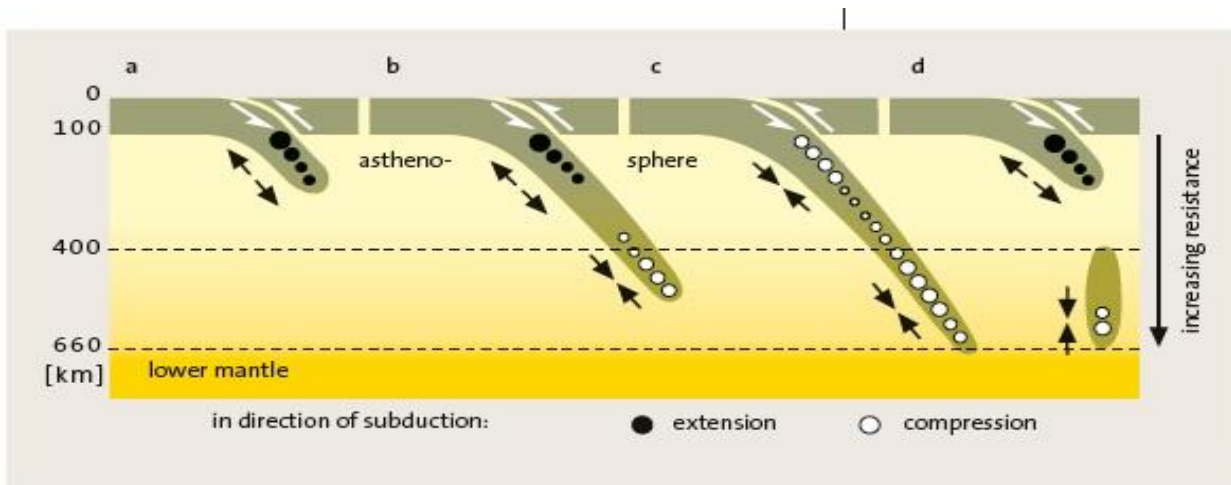
Depth larger than the thickness of the lithosphere of the overriding plate (> 70-100 km < 350 km): Earthquakes are the result of the internal deformation of the descending slab (tensional stress no resistance from the asthenosphere) and metamorphic reactions involving dehydration of serpentinized mantle and eclogitization.

Deep earthquakes (8%)

Depth > 350 km: Earthquakes are the result of the high resistance of the mantle to slab penetration (becoming more dense because of mineral phase transitions), which generate compressive stress in the subducting slab. Olivine-spinel phase transition occurs within the cold subducting slab between 350 and 700 km (olivine is in metastable conditions).

- The phase changes that occur in the slab at a depth of approximately 700 km likely produce fine-grained materials that behave in a superplastic manner and thus cannot generate earthquakes.

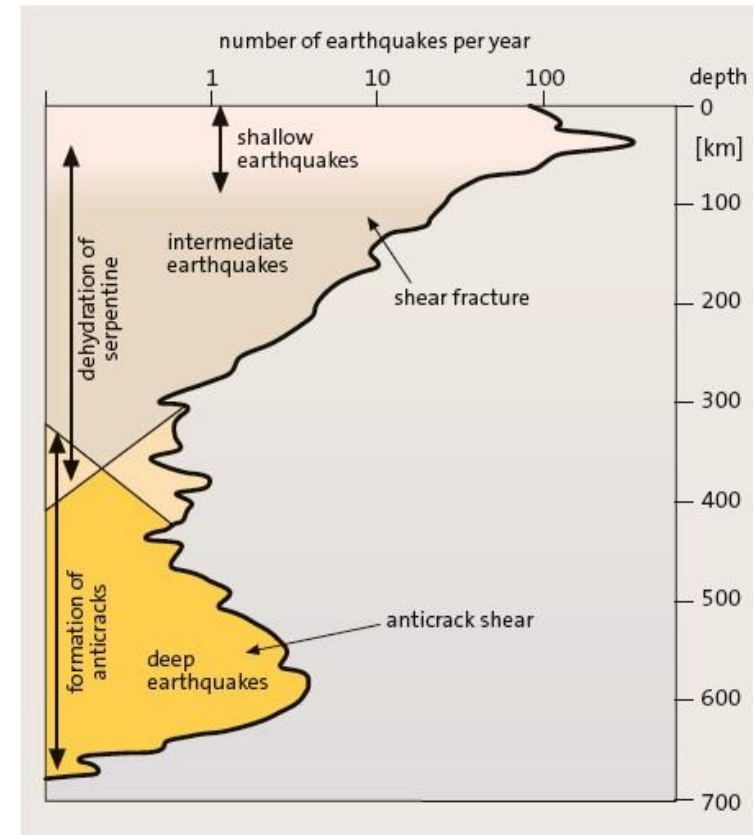
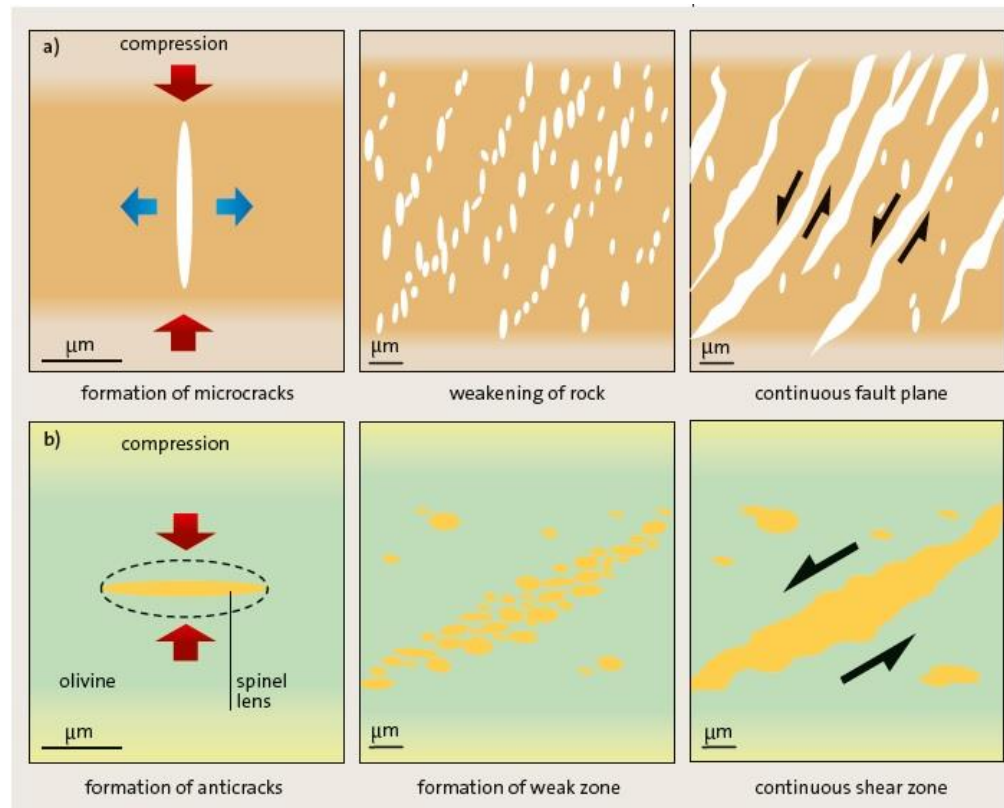
Deep stress and seismicity in the subducting slab



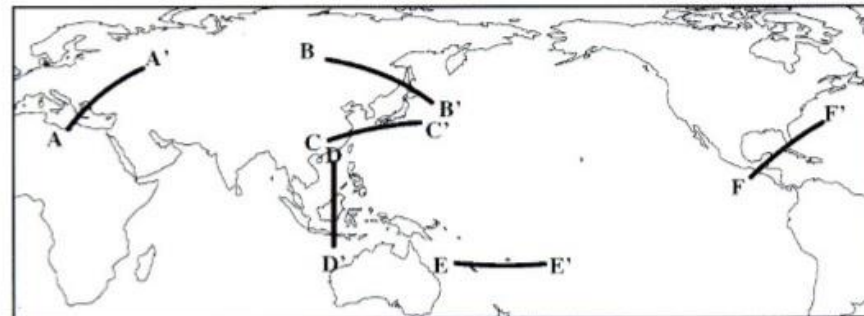
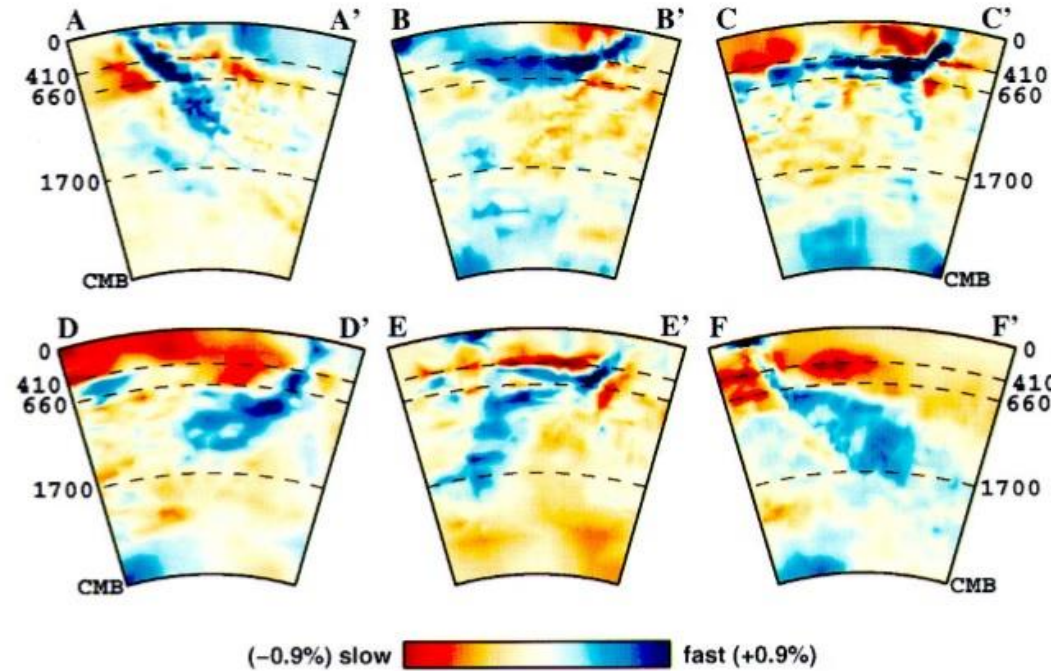
- When the slab reaches the bottom of the transition zone, compressive stress is transferred upwards.
- In case of slab-breakoff no stress transfer, the slab remains in state of tensional stress.

Origin of the earthquakes in the subduction zone

- **Origin of shallow earthquakes (25-70 km):** In compressional conditions, numerous microcracks develop parallel oriented to the direction of maximum compressional stress. This lead to weakening of the rocks, followed by failure and shear planes oblique to the main direction of pressure that join the existing microfractures.
- **Origin of intermediate earthquakes (70-350 km):** Dewatering processes with increasing depth of serpentine, which is accompanied by a substantial decrease of volume and consequent microfracturing and weakening of the the rock.
- **Origin of deep earthquakes (> 350 km):** The mineral phase transition of olivine to spinel (occurring with volume reduction): Small lenses of spinel within the peridotite are aligned perpendicular to the maximum compressional stress and interpreted as “anticracks”, since they are rotated 90° compared with normal microcracks. If enough anticracks are formed, the rock becomes weakened, the anticracks are joined and an instantaneous shear movement of the rock develops, through a pocess called ‘superplasticity’ (favored by high T and fine grains).

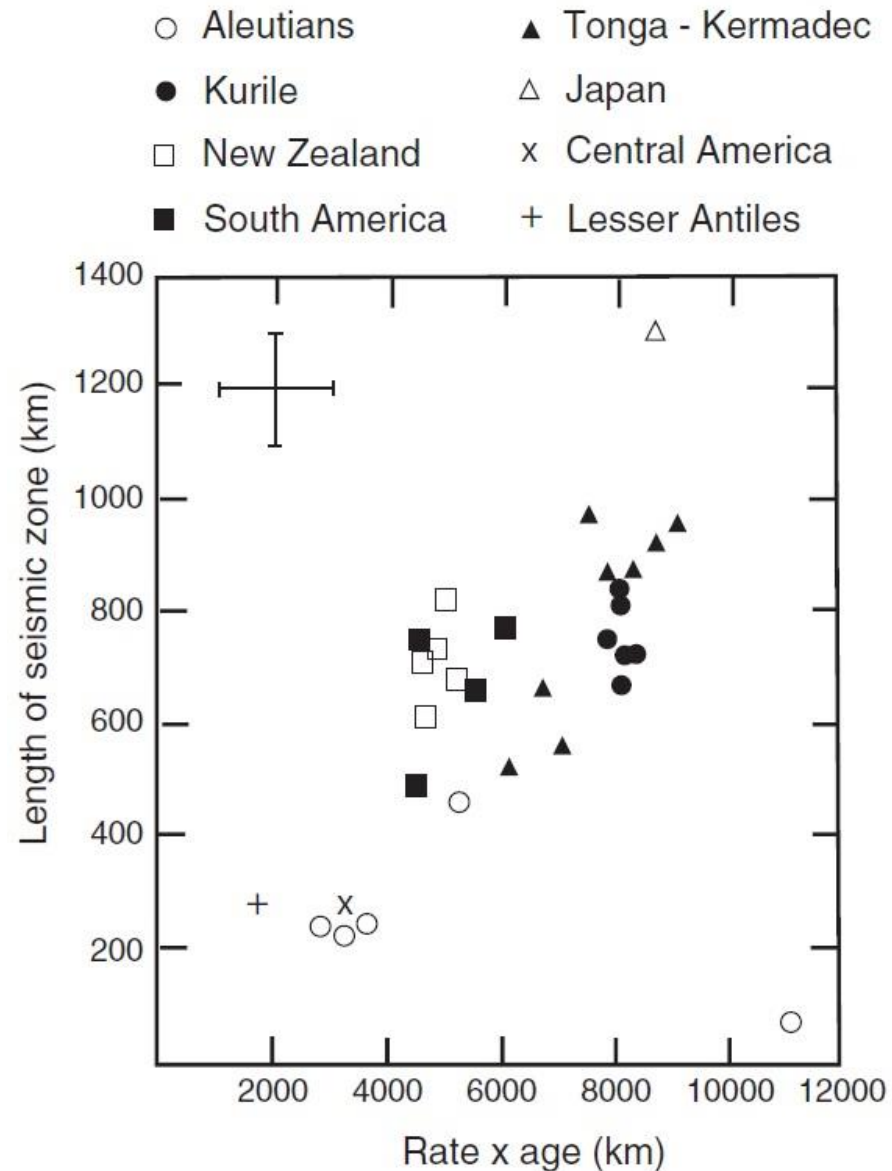


Slab depth penetration



- No direct relationship between age of a subducting slab and depth penetration (transition zone or lower mantle), there is an interaction among different factors.
- The depth extent of seismicity is linked to how deep the slab core remains cooler than a potential temperature of 600–800°C (many slabs extend beyond their Benioff zones).

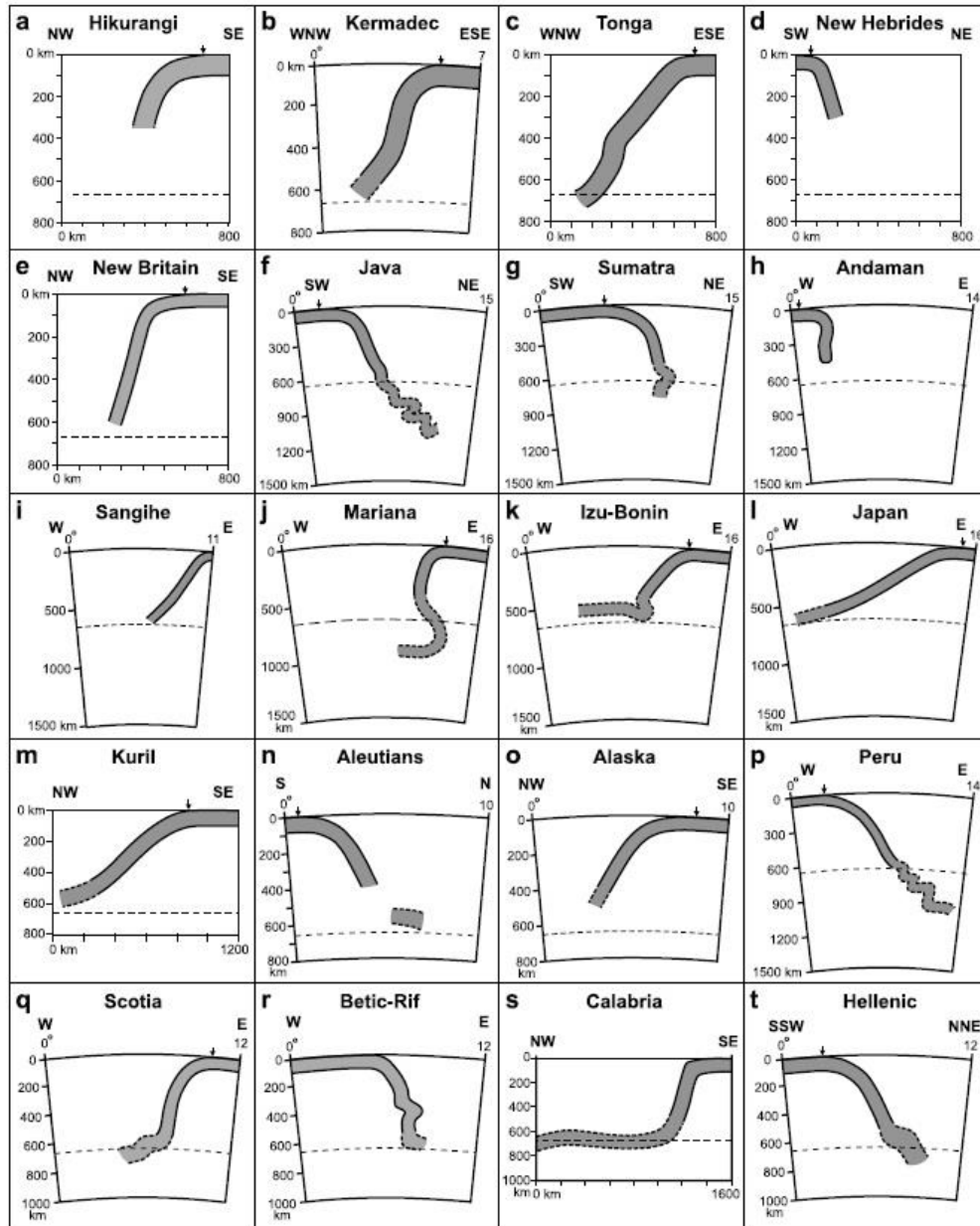
Length of Benioff Zone



Length of the seismic zone is proportional to the product between the convergence rate and age (the slab should preserve a strong core):

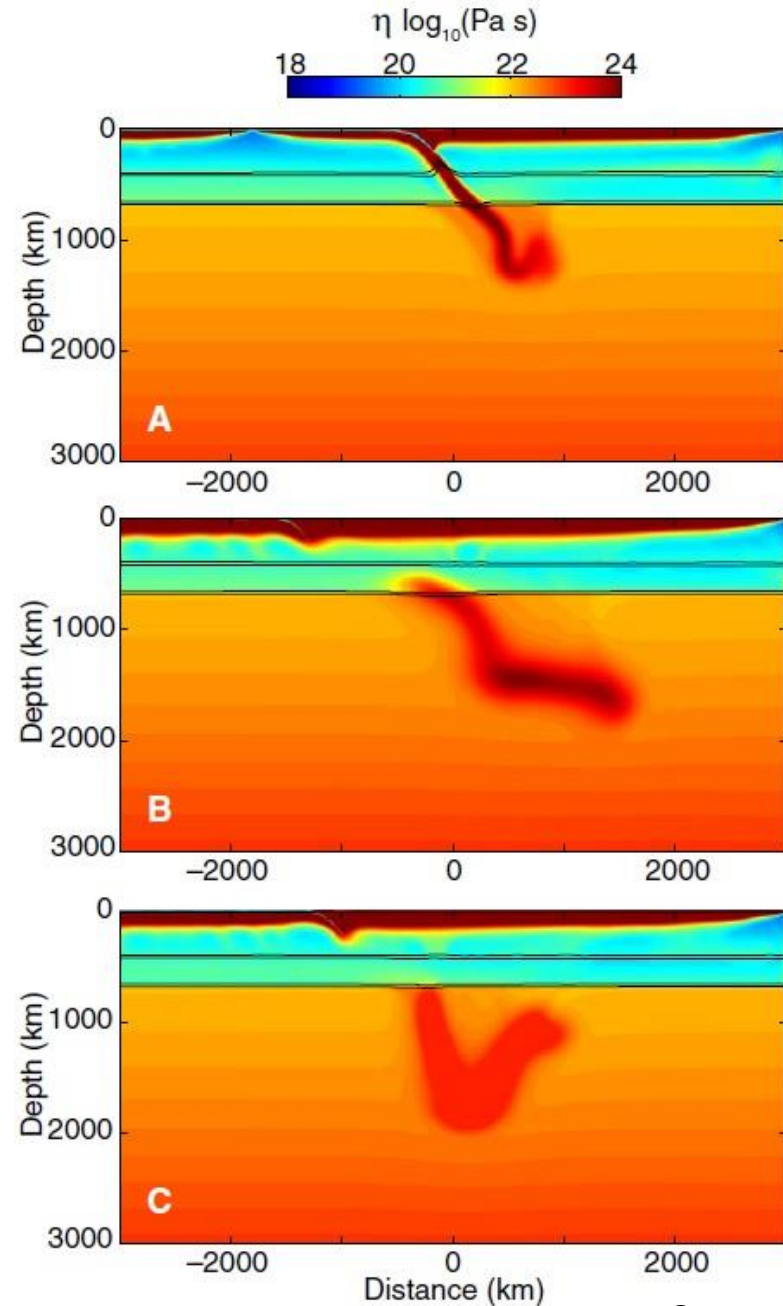
Downward deflection of the lithosphere (length of the seismic zone) proportional to both rate of subduction and age (square of the lithospheric thickness).

Slab Shape and Geometry



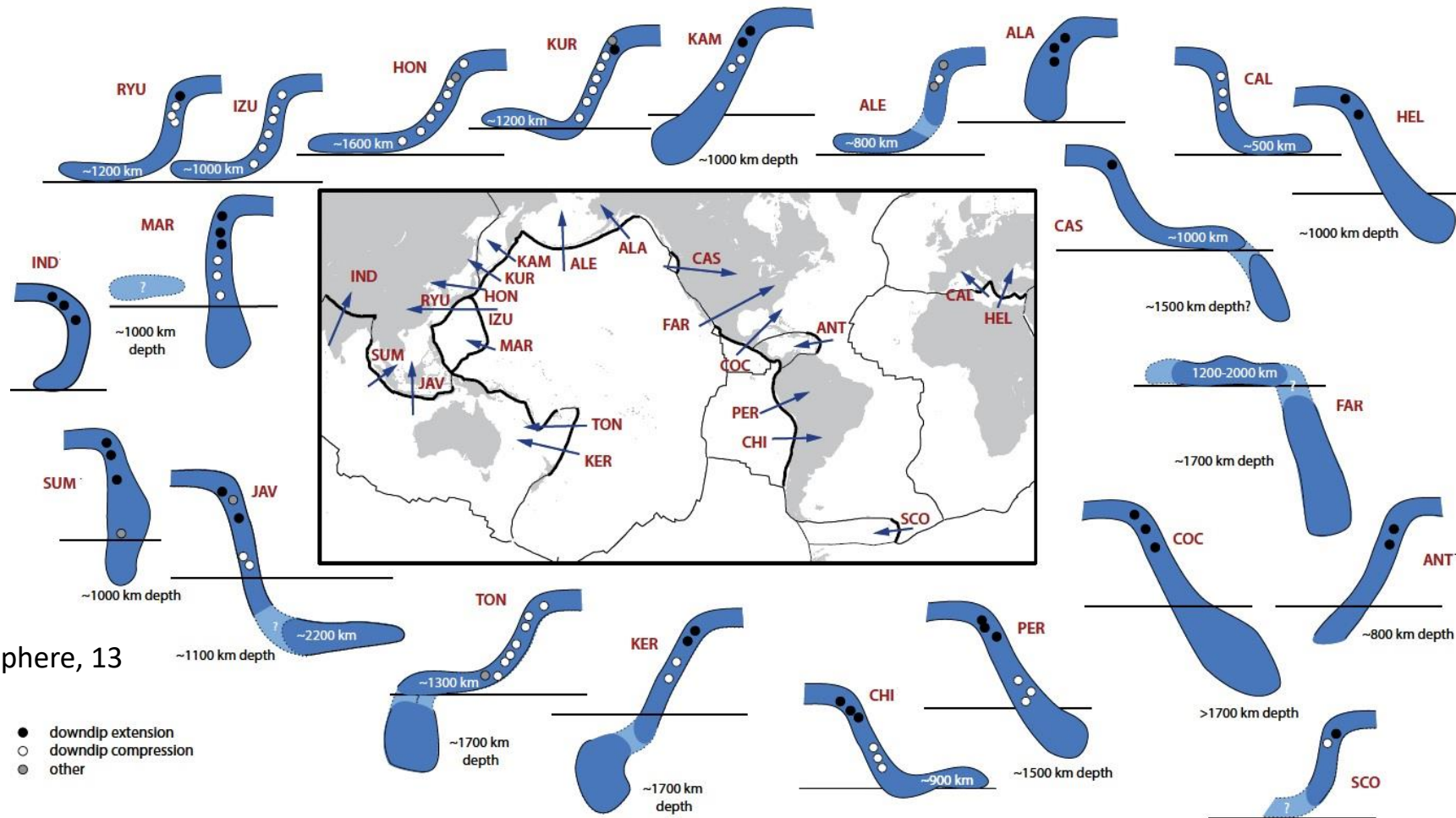
- All slabs show that in the uppermost 300–500 km, the slab is convex upward.
- Slabs that do not reach the upper-lower mantle discontinuity at 660 km are convex upward throughout (e.g., Hikurangi, New Hebrides, Andaman, Alaska).
- Those that do reach the discontinuity can be relatively straight below ~400 km depth (e.g., New Britain, Sangihe), or show indications of kinking (e.g., Kermadec, Tonga) or folding (e.g., Java, Sumatra, Mariana, Peru, Betic- Rif) or have a concave upward bend near the transition zone with a horizontally deflected slab geometry (e.g., Calabria, Scotia, Kuril, Japan).
- All slabs also show that their downdip curvature changes considerably with depth.
- Some slabs, e.g., the Cocos, Java, and Hellenic slabs, thicken by a factor of 4–5 upon entering into the lower mantle, to widths of ~400 km or more. Such strong thickening has commonly been attributed to slab buckling that starts in the transition zone.
- Slabs stagnating in the transition zone generally correspond to subduction of the past 15-60 Myr, while earlier subducted slabs have sunk into the lower mantle.

Slab Shape and Geometry



- Upon sinking, all slabs will develop a more rounded form because they try to achieve a shape that sinks more efficiently than the planar geometry they start subducting with.
- Thermo-mechanical subduction models demonstrate that a combination of buckling, folding, rounding, and diffusive widening leads to a significant change in slab shape as they sink through the lower mantle.
- Models and observations suggest that the sinking of previously stagnant slabs leads to large increases in subducting-plate velocities up to a factor of 2. However, periods of much higher subduction velocities are likely the result of different mechanisms (e.g., deep subduction in conjunction with plumes).

Slab Shape and Geometry

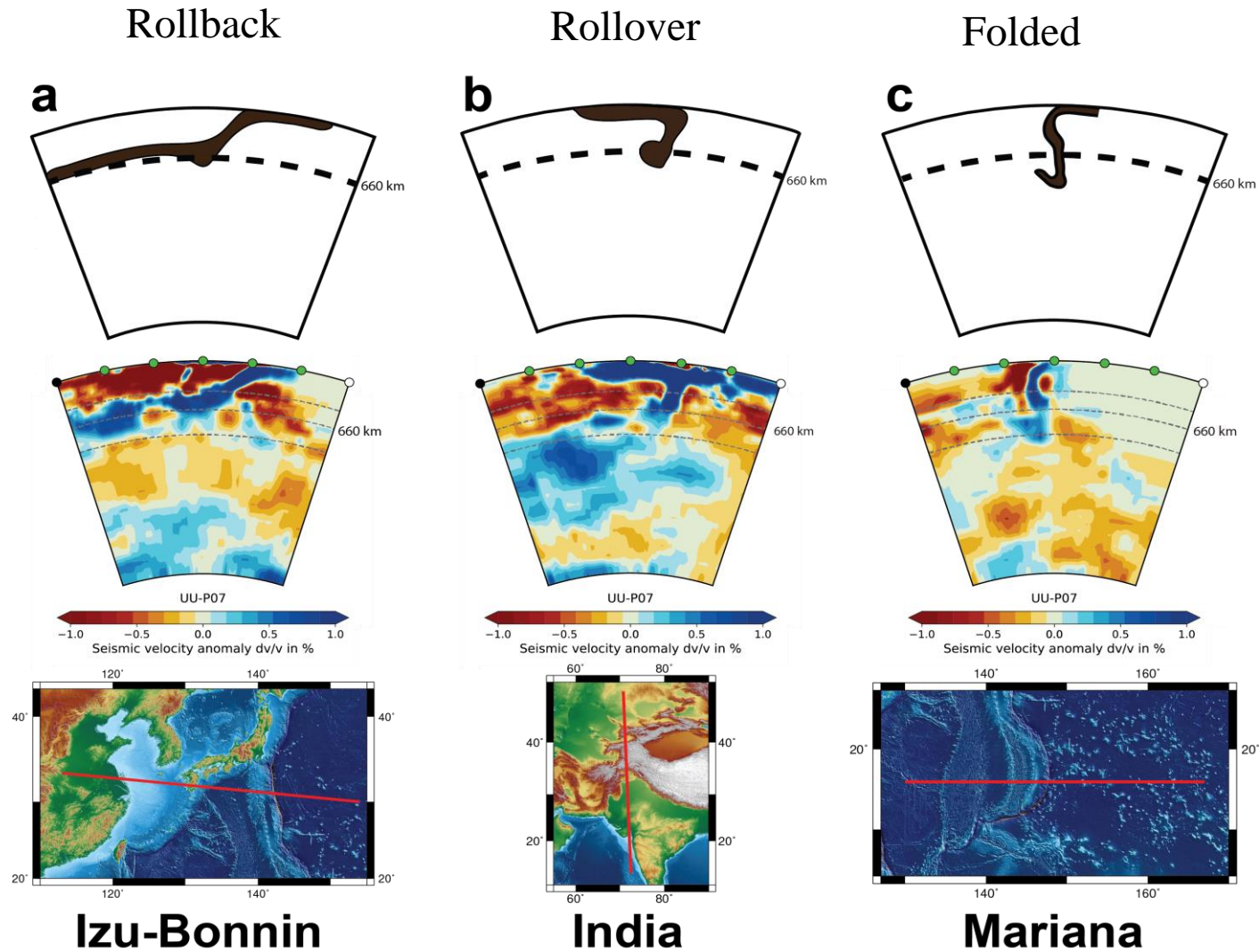


Goes et al., 2017, Geosphere, 13

RYU—Ryukyu, **IZU**—Izu, **HON**—Honshu, **KUR**—Kuriles, **KAM**—Kamchatka, **ALE**—Aleutians, **ALA**—Alaska, **CAL**—Calabria, **HEL**—Hellenic, **IND**—India, **MAR**—Marianas, **CAS**—Cascadia, **FAR**—Farallon, **SUM**—Sumatra, **JAV**—Java, **COC**—Cocos, **ANT**—Antilles, **TON**—Tonga, **KER**—Kermadec, **CHI**—Chile, **PER**—Peru, **SCO**—Scotia.

- Lengths of the flat slabs in the transition zone range from several hundred km (below Calabria) to up to 2000 km (below North America).
- **Comparison of tomography with plate reconstructions has estimated accumulation times (stagnation times) of few tens of Myr:** 20-30 Myr for the ~1000-km flat Izu-Bonin slab, 30-40 Myr for the ~1300 km Tonga flat segment and 8-10 Myr for the ~500-km-long, Calabrian flat slab.
- Material subducted in the early Cenozoic and Mesozoic has apparently sunk into the deeper mantle because of its thermal re-equilibration.

Slab Shape and Geometry

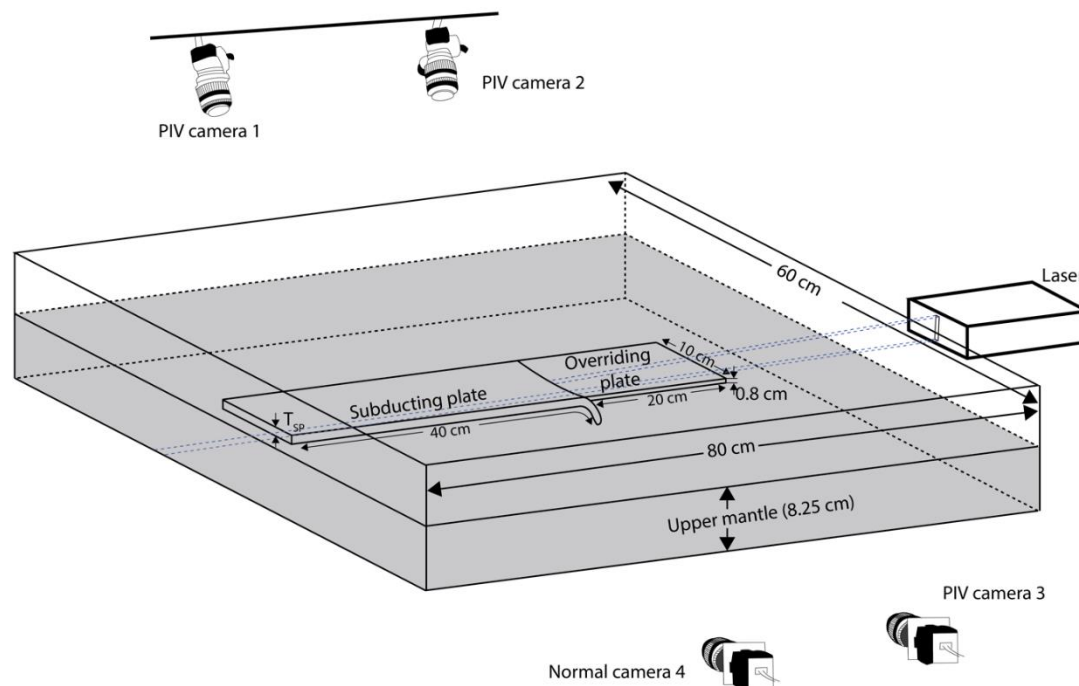


Three types of slab geometry

Slab Shape and Geometry

- 3D fully dynamic upper mantle analog models
- Particle image velocimetry (PIV) system
- Two parameters varied: Subducting plate thickness (T_{SP}) and η_{OP}/η_{UM}

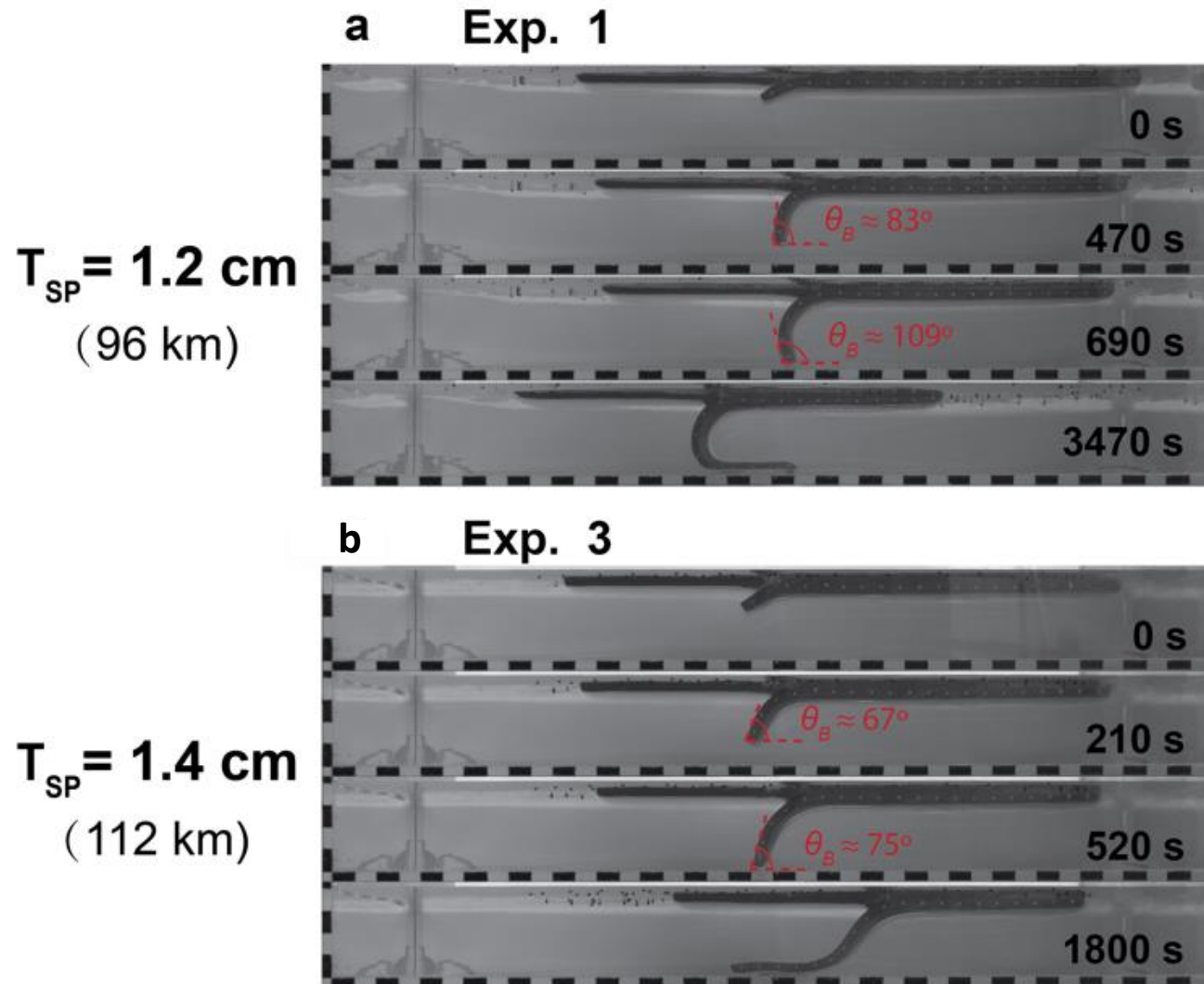
Model setup



Experiment number	SP thickness (cm)	η_{OP}/η_{UM}	Slab geometry
Exp. 1	1.2 (96 km)	~650	Slab rollover
Exp. 2	1.2 (96 km)	~1300	Slab rollover
Exp. 3	1.4 (112 km)	~650	Slab rollback
Exp. 4	1.4 (112 km)	~1300	Slab rollback

Slab Shape and Geometry

Subduction evolution

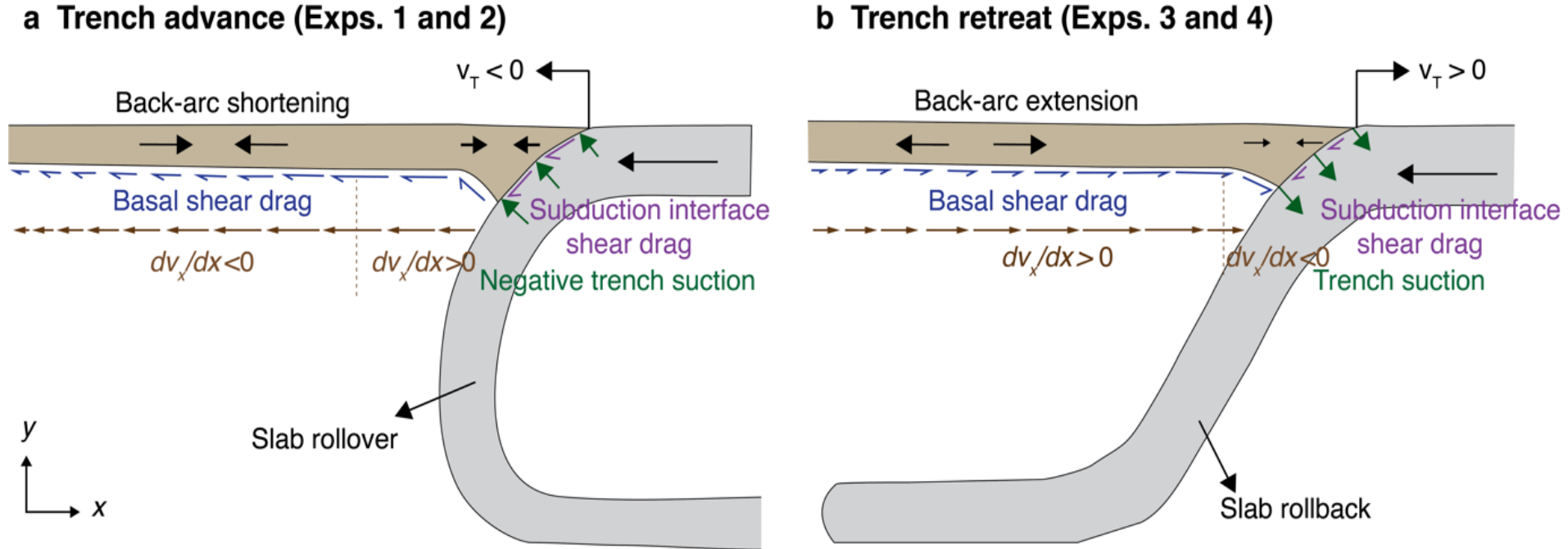


Progressive subduction evolution. θ_B : slab tip dip angle

Slab Shape and Geometry

Overall overriding plate deformation

- Basal shear drag (F_D) induced by horizontal mantle flow at the base of the OP.
- dv_x/dx controls the horizontal trench-normal gradient in F_D .



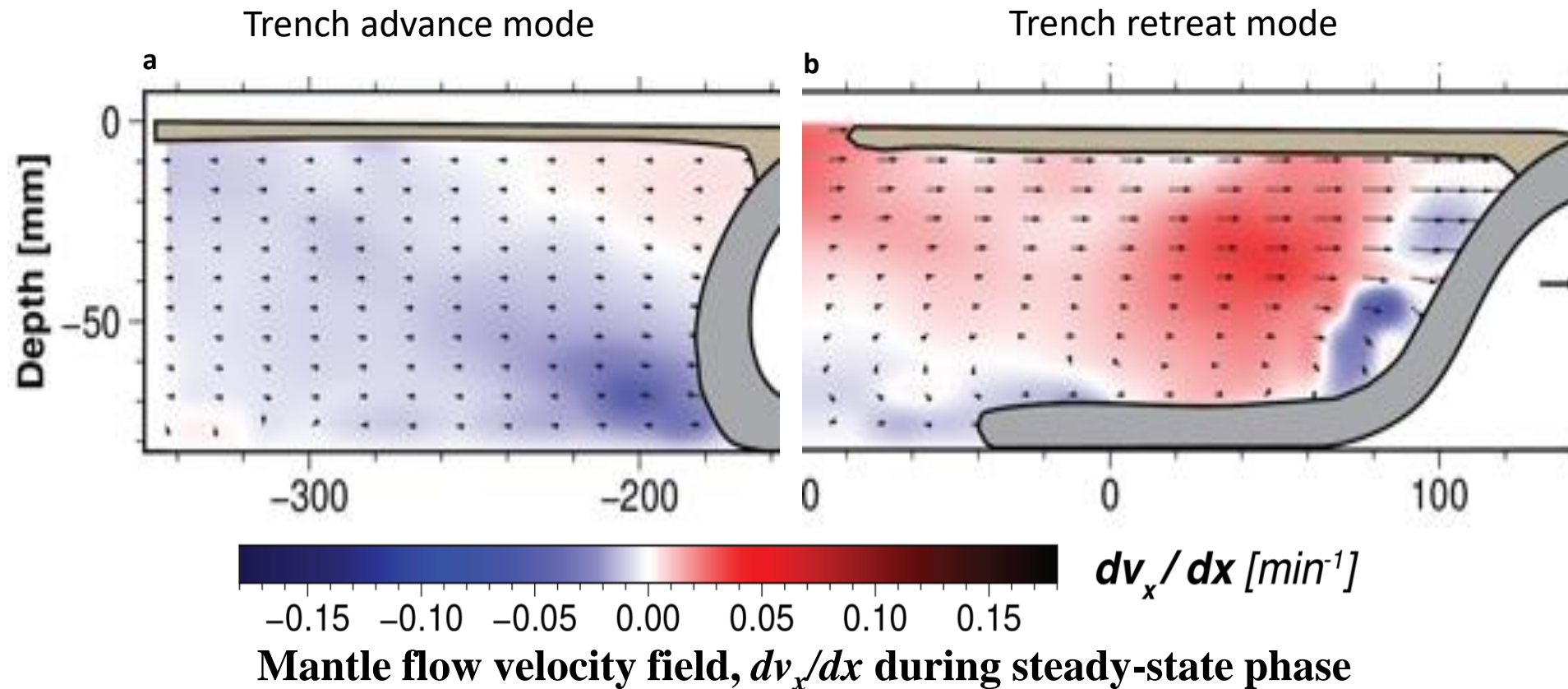
Xue et al., 2020, JGR, 125

Forces and horizontal velocity gradients for two different subduction modes

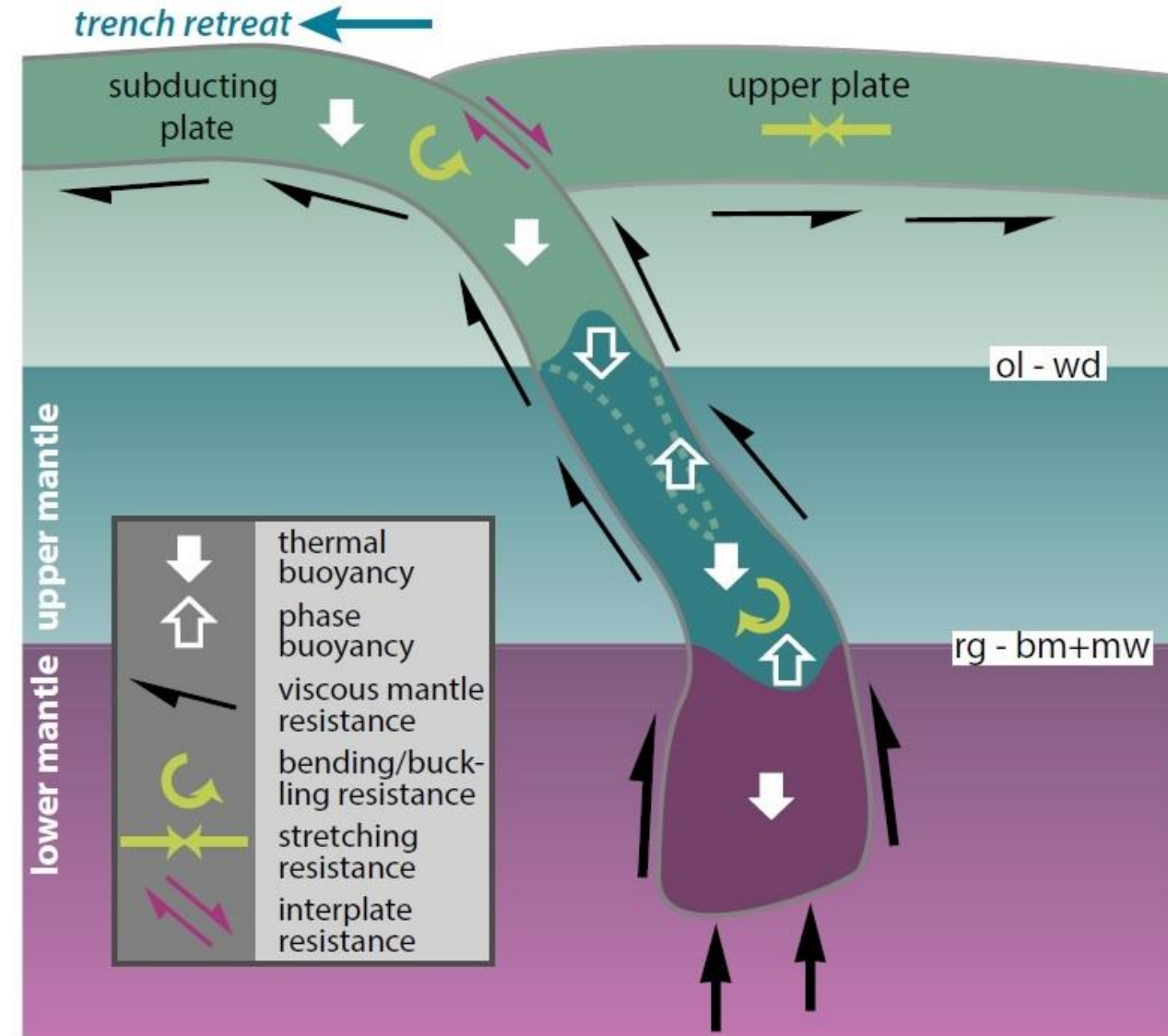
Slab Shape and Geometry

Dynamic topography

- Large-scale landward mantle flow (with an upward velocity component) (Fig. 8a.)
- Large-scale trenchward mantle flow (with a downward velocity component) (Fig. 8b.)

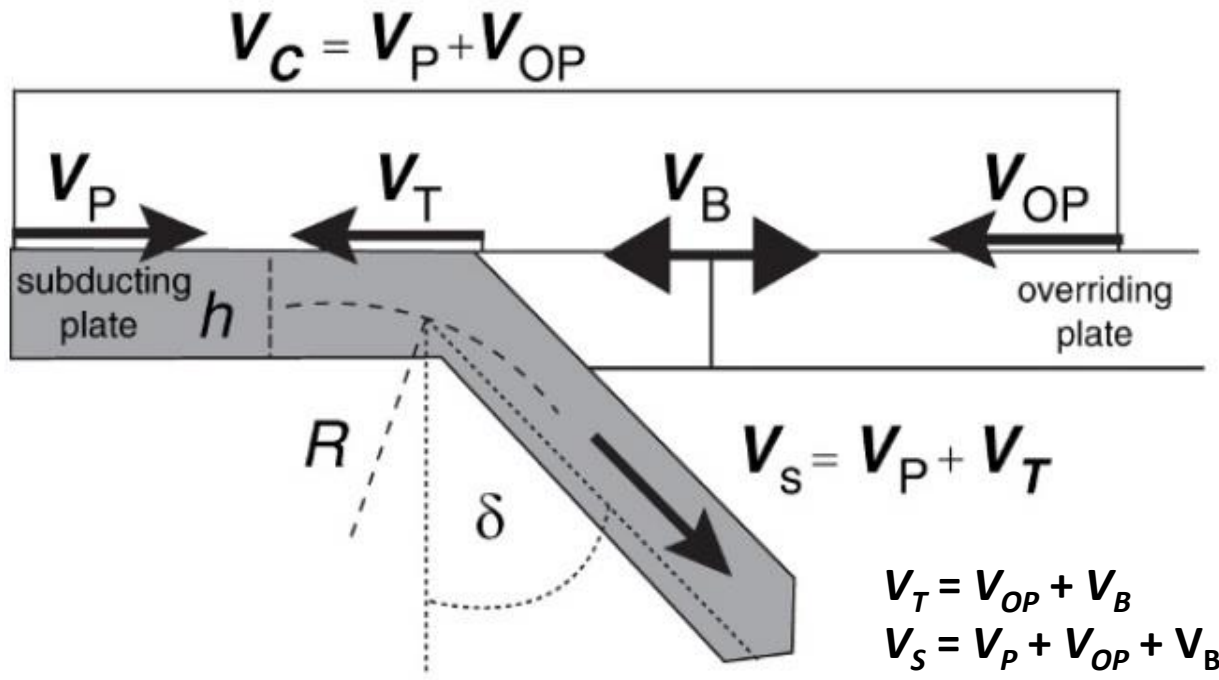


Forces acting on the subducting slab



- The slab sinks is driven by its negative thermal buoyancy: Sinking is resisted by viscous drag in the mantle and the frictional/viscous coupling between the subducting and upper plate, while the slab bending is resisted by slab strength.
- At the transition from ringwoodite to the postspinel phases of bridgmanite and magnesiowüstite ($rg - bm + mw$), the slab's further sinking is hampered by increased viscous resistance as well as the deepening of the endothermic phase transition in the cold slab, which adds positive buoyancy to the slab.
- The shallowing of exothermic phase transition from olivine to wadsleyite ($ol-wd$) adds an additional driving force, unless it is kinetically delayed in the cold core of the slab (dashed green line), in which case it diminishes the driving force (reduces the negative buoyancy, favoring slab stagnation). Pyroxene to garnet transitions may also be kinetically inhibited in the cold slabs aiding their stagnation in the transition zones.
- Tomographic evidences show that slabs experience significant resistance at the base of the transition zone leading to their flattening, buckling, and thickening.

Slab geometry parameters



V_b = back-arc deformation rate (positive for extension)

V_c = convergence rate

V_s = sinking velocity of the subducting plate

V_p = plate velocity

V_T = trench velocity (positive for rollback)

V_{OP} = overriding plate velocity (positive toward the trench)

h = width of the slab and plate

R = approximate bending radius at the trench

δ = slab dip angle

Becker and Faccenna, 2009

- Any trench migration has important consequences for tectonics such as backarc spreading, but also for large-scale upper mantle dynamics. The migration of the slab inside the mantle induces a toroidal component of flow, with significant effects on back-arc temperatures, volcanism, and the interpretations of seismic anisotropy observations.
- V_T can be estimated by subtracting the back-arc deformation rate, V_B from the velocity of the upper plate, V_{OP} , assuming that erosion and accretion at trenches are negligible. Trench migration rates are typically not more than 50% of the convergence rates.
- Trenches are often found to retreat toward the subducting plate with respect to the lower mantle ($V_T > 0$).
- In several regions, e.g. Marianas-Izu Bonin, trenches also appear to advance toward the subducting plates in all reference frames ($V_T < 0$).
- If the sinking rate is larger than the rifting rate, the trench moves away from the upper plate (slab roll-back).
- If the rifting rate at the mid-oceanic ridge exceeds the sinking rate of the subducting slab, then the trench will move towards the upper plate.

Observations subducting plate velocity ($v_{SP\perp}$)

Subducting plates move trenchward ($v_{SP\perp} > 0$):

97% for Indo-Atlantic HS [O2005]

89% for Pacific HS [G&G2002]

95% for Pacific HS [W2006]

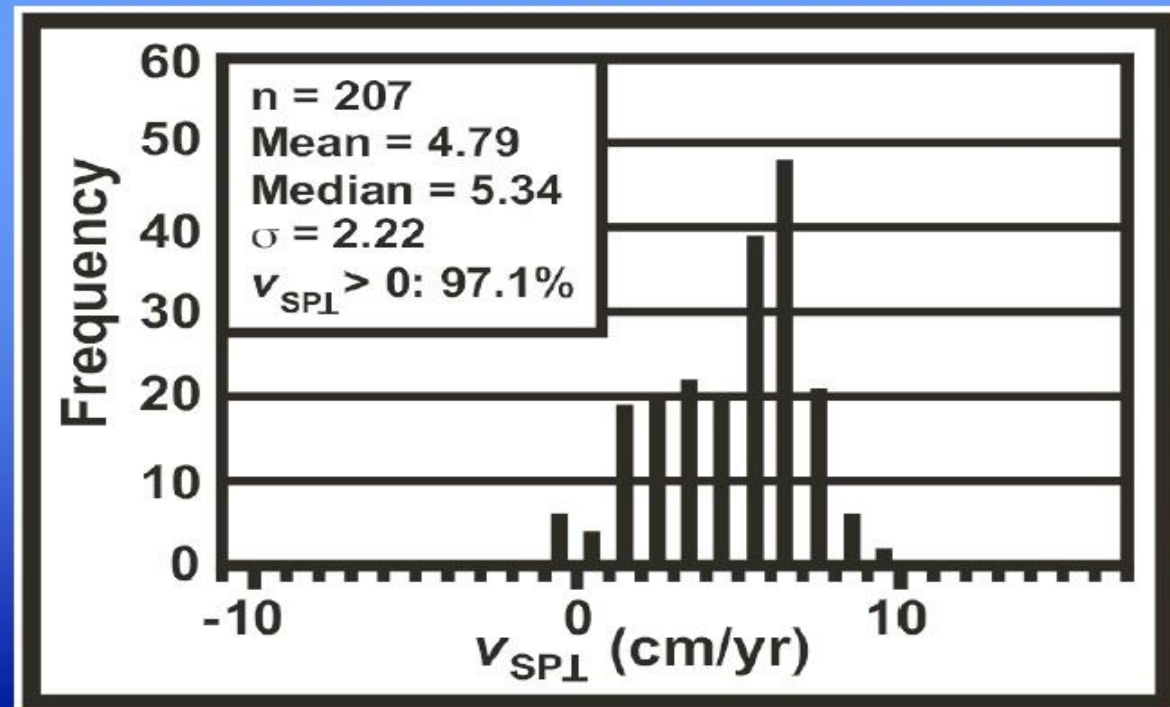
99% for global HS [G&J1986]

98% for NNR [K2003]

96% for NNR [A&G1991]

**maximum $v_{SP\perp}$ range
(all reference frames)
= -8 to 12 cm/yr**

Indo-Atlantic HS reference frame



Observations trench velocity ($v_{T\perp}$)

Trenches predominantly retreat ($v_{T\perp} > 0$) (i.e. rollback):

73% for Indo-Atlantic HS [O2005]

63% for Pacific HS [G&G2002]

73% for Pacific HS [W2006]

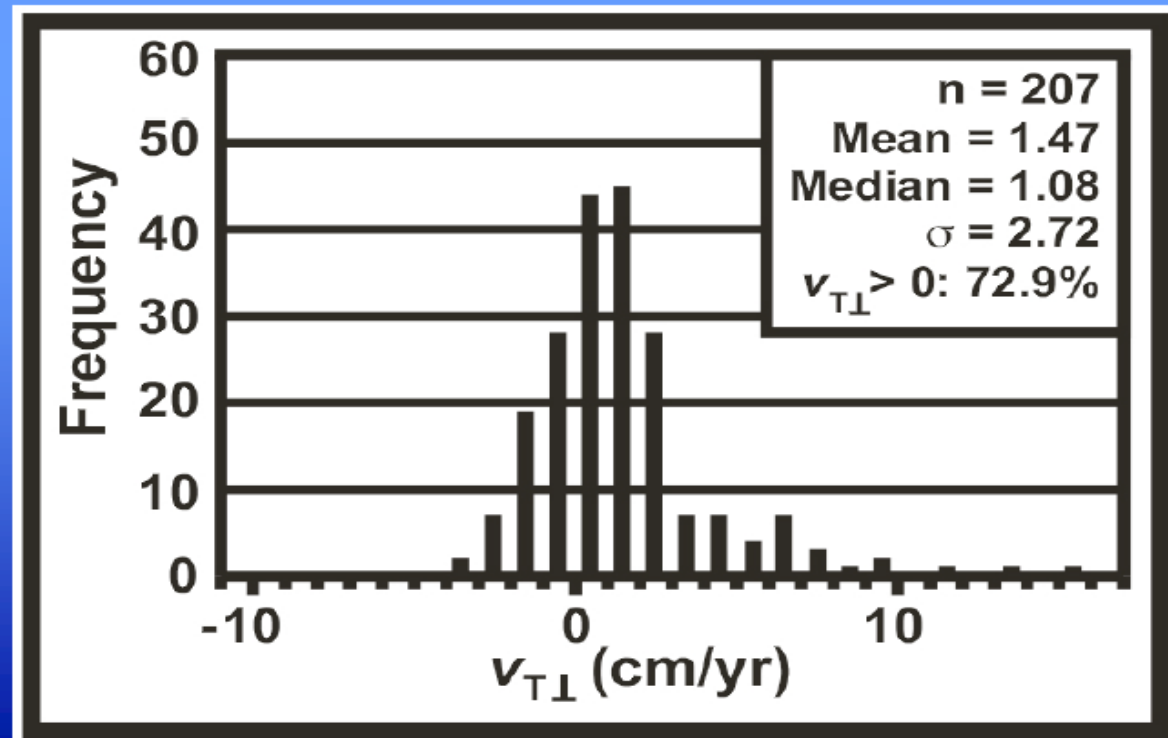
71% for global HS [G&J1986]

62% for NNR [K2003]

67% for NNR [A&G1991]

**maximum $v_{T\perp}$ range
(all reference frames)
= -6 to 17 cm/yr**

Indo-Atlantic HS reference frame



Observations subduction partitioning

Subduction rate dominated by $v_{SP\perp}$ ($v_{SP\perp}/v_{S\perp} > 0.5$):

81% for Indo-Atlantic HS [O2005]

62% for Pacific HS [G&G2002]

78% for Pacific HS [W2006]

80% for global HS [G&J1986]

79% for NNR [K2003]

79% for NNR [A&G1991]

$v_{SP\perp}/v_{S\perp}$ range = -1 to 2

Indo-Atlantic HS reference frame

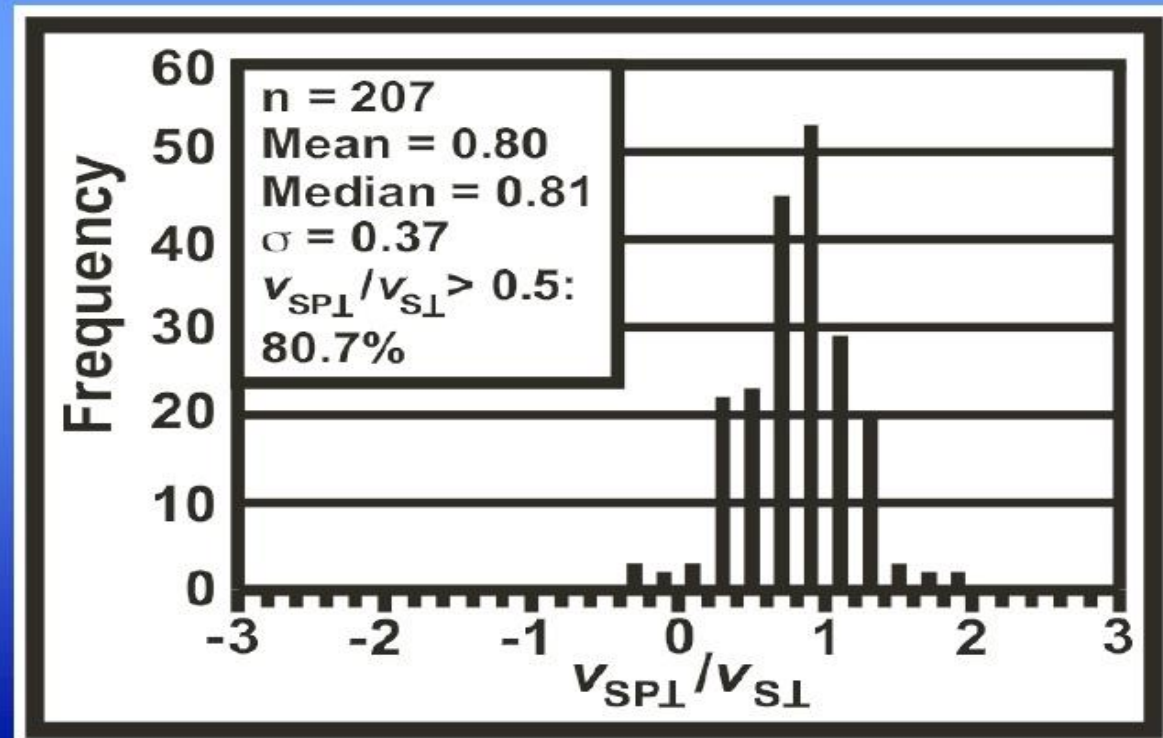
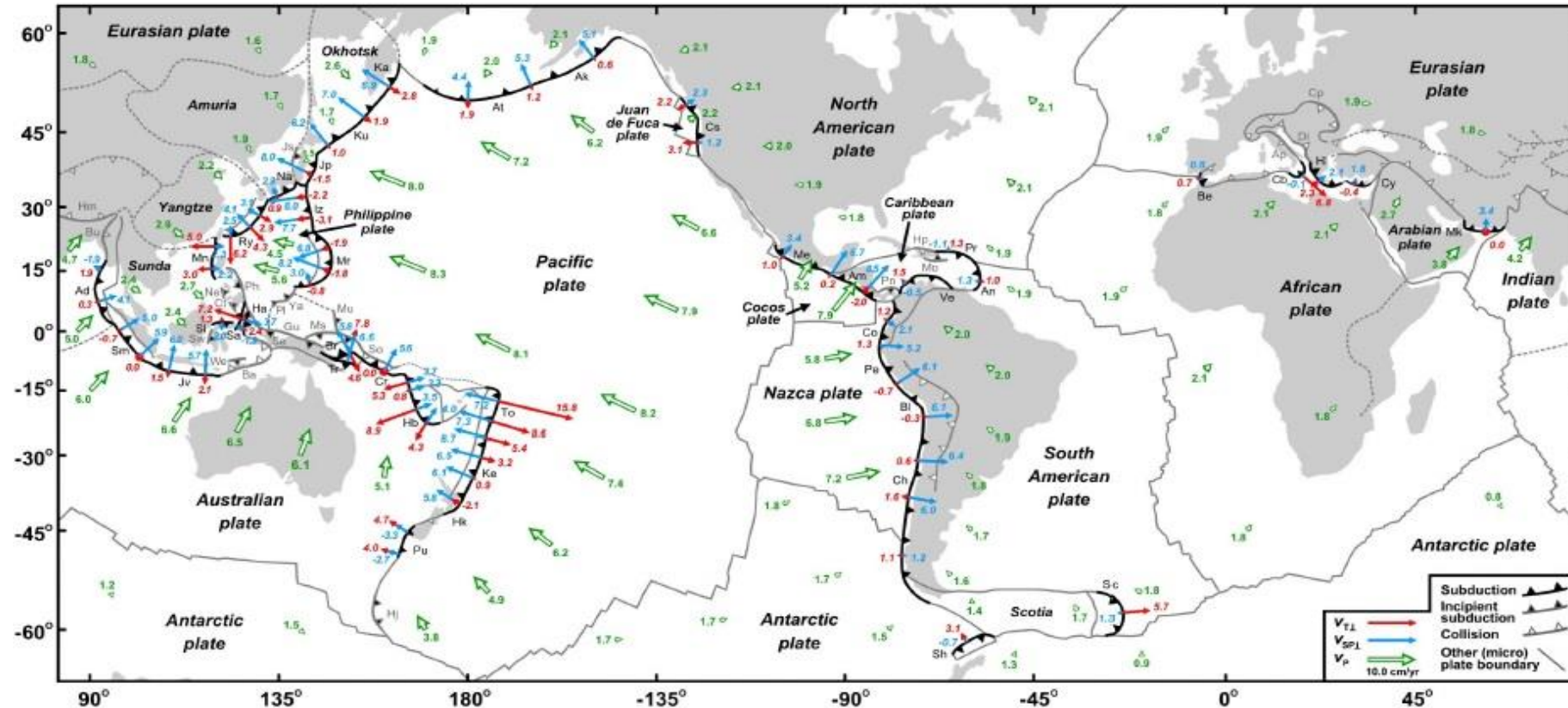


Plate boundary velocities [cm/yr]



Schellart et al., 2011, JGR

$$V_S = V_{SP} + V_T$$

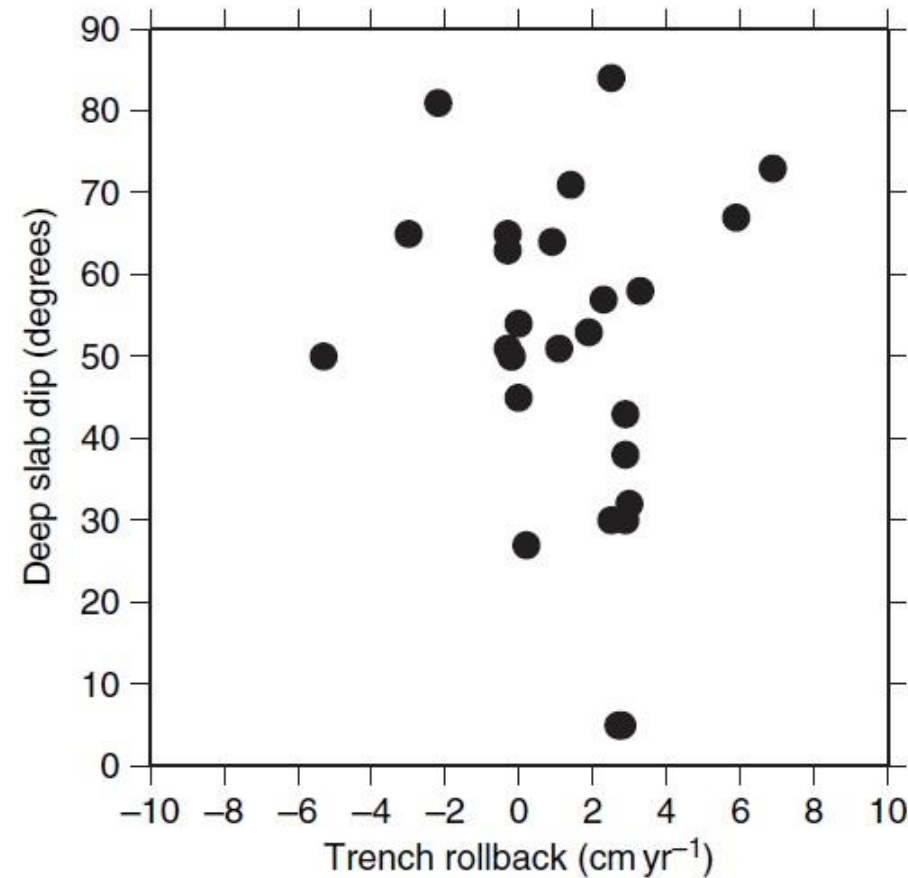
Major subduction zones on Earth, blue vectors: trench-normal subducting plate velocity (v_{SP}), red vectors: trench-normal trench migration velocity (v_T), large white vectors with green outline: plate velocity (v_P) for the major plates and some microplates, calculated in the Indo-Atlantic hot spot reference frame from O'Neill et al. (2005).

Numerical models demonstrated that the trench migration results predominantly from lateral migration of the slab, most likely driven by the negative buoyancy force of the slab itself, rather than from overriding plate motion.

- ❑ Rollback velocities and trench curvature in nature may be controlled by slab width.
- ❑ Narrow slabs (e.g., Scotia arc) show fast rollback, while wide slabs such as in the Chilean roll back slowly.

Trench rollback and slab geometry

- There is almost no correlation between the dip of a slab in the 100–400 km depth range and the rate of trench migration, reflecting that subduction is a time-dependent phenomenon and thus the shape of subducting slabs evolves with time.
- It is difficult to separate the effects of dip direction from the fact that most of the eastward-dipping slabs are being overridden by the North and South American Plates (i.e., continents) while many of the slabs in the Pacific are being overridden by island arcs or oceanic plates.



Subduction partitioning (v_{sp}/v_s) and slab width

- Subduction for narrow slab models (**W = 300–1500 km**) is characterized by rapid trench retreat, slow trenchward plate motion and low partitioning with $v_{sp}/v_s = 0.2\text{--}0.4$, except for the earliest subduction stage (before ~ 5 Myr). A progressive development of a curved slab and trench that are concave toward the mantle wedge is also observed.
 - Subduction for large slab models (**W = 7000 km**) is characterized by overall slow trench migration, rapid trenchward plate motion and high partitioning with $v_{sp}/v_s = 0.7\text{--}1.2$, except for the earliest stage (before ~ 7 Myr). A progressive development of a curved subduction zone that is overall convex toward the mantle wedge but concave edges are also observed.
 - Subduction for an intermediate slab width (**W = 2000–3000 km**) show intermediate behavior.
-
- ❑ **On a global scale subduction is dominated by trenchward subducting plate motion:** mean partitioning in nature is 0.80, while for 80.7% of the trench segments $v_{sp}/v_s > 0.5$.
 - ❑ Partitioning is always high far from slab edges ($D_{SE} > 2200$ km), with $0.76 \leq v_{sp}/v_s \leq 1.84$. Low partitioning ratios in nature ($v_{sp}/v_s < 0.39$) are only found close to lateral slab edges ($D_{SE} < 1000$ km).
 - ❑ In the numerical models, the lowest partitioning ratios are found for narrow slabs such as $W = 300$ km with $v_{sp}/v_s = 0.28\text{--}0.32$.

D_{SE} =horizontal distance from the slab edges

In Summary:

- Slab segments close to lateral slab edges (as well as narrow slabs) experience relatively minor resistance from the ambient mantle to migrate laterally, resulting in relatively fast v_T .
- Segments far from lateral slab edges will experience large resistance from the ambient mantle, resulting in relatively slow v_T .

Subduction kinematics and dynamics

- Data for subducting plate age shows negligible/minor correlation with $v_{sp\perp}$ and $v_T\perp$
- Data and numerical subduction models show significant correlation between slab width and $v_{sp\perp}$:
 - *Subducting plate velocity scales with $W^{2/3}$*
- Data and numerical subduction models show significant correlation between slab width and $v_T\perp$:
 - *Trench retreat velocity scales with $1/W$*
- $v_{sp\perp}$ is associated with poloidal flow, while $v_T\perp$ is associated with quasi-toroidal flow.
- Slab rollback induces a toroidal flow around the lateral slab edges from the sub-slab region towards the mantle wedge.
- The toroidal flow has a strong component of upwelling next to the slab edge, sub-slab region and mantle wedge.

Physical parameters affecting velocity of trench ($v_T \perp$), subducting plate ($v_{SP} \perp$), and overriding plate ($v_{OP} \perp$)

Physical parameters affecting $v_{SP} \perp$

- **% of plate circumference attached to a slab** (*Forsyth and Uyeda*, GJRS 1975; *Gripp and Gordon*, GJI 2002)

Physical parameters affecting $v_T \perp$

- **Upper plate velocity** (*Jarrard*, RG, 1986; *Heuret and Lallemand*, PEPI, 2005)
- **Trenchward subducting plate velocity** (*Schellart*, EPSL, 2005)

Physical parameters affecting $v_{SP} \perp$ and $v_T \perp$

- **Slab/mantle viscosity ratio** (*Di Giuseppe et al.*, G3, 2008; *Schellart*, G3, 2008; *Stegman et al.*, Tectonophysics 2010)
- **Mantle viscosity stratification** (*Kincaid and Olson*, JGR 1987; *Zhong and Gurnis* Science 1995)

Physical parameters affecting $v_{SP} \perp$, $v_T \perp$ and $v_{OP} \perp$

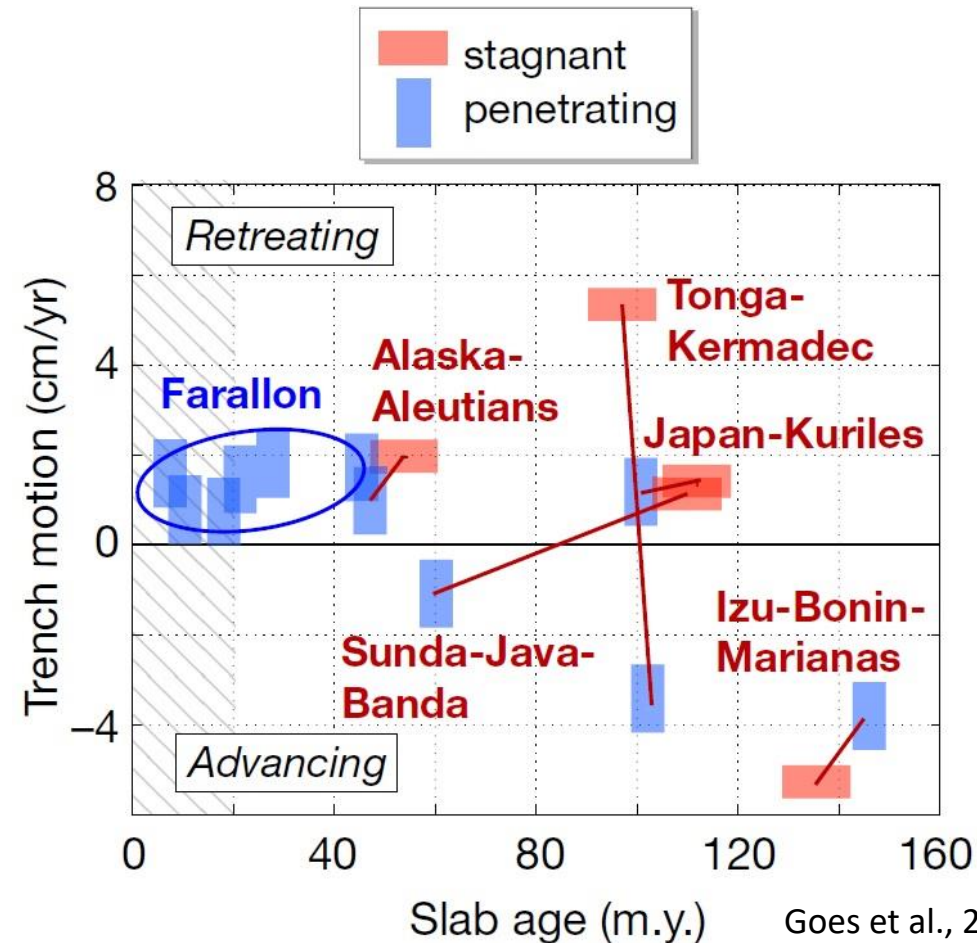
Subducting plate age (*Molnar and Atwater*, EPSL 1978; *Carlson et al*, GRL 1983; *Sdrolias & Muller*, G3 2006; *Capitanio et al*, EPSL 2007; *Goes et al*, Nature 2008):

Old slab \rightarrow dense \rightarrow rapid rollback, plate motion and extension

Young slab \rightarrow light \rightarrow no rollback, slow plate motion and shortening

- **Slab width** (*Dvorkin et al.*, Tectonophysics 1993; *Schellart*, JGR 2004; *Stegman et al.*, G3 2006; *Schellart et al.*, Nature 2007, Science 2010)

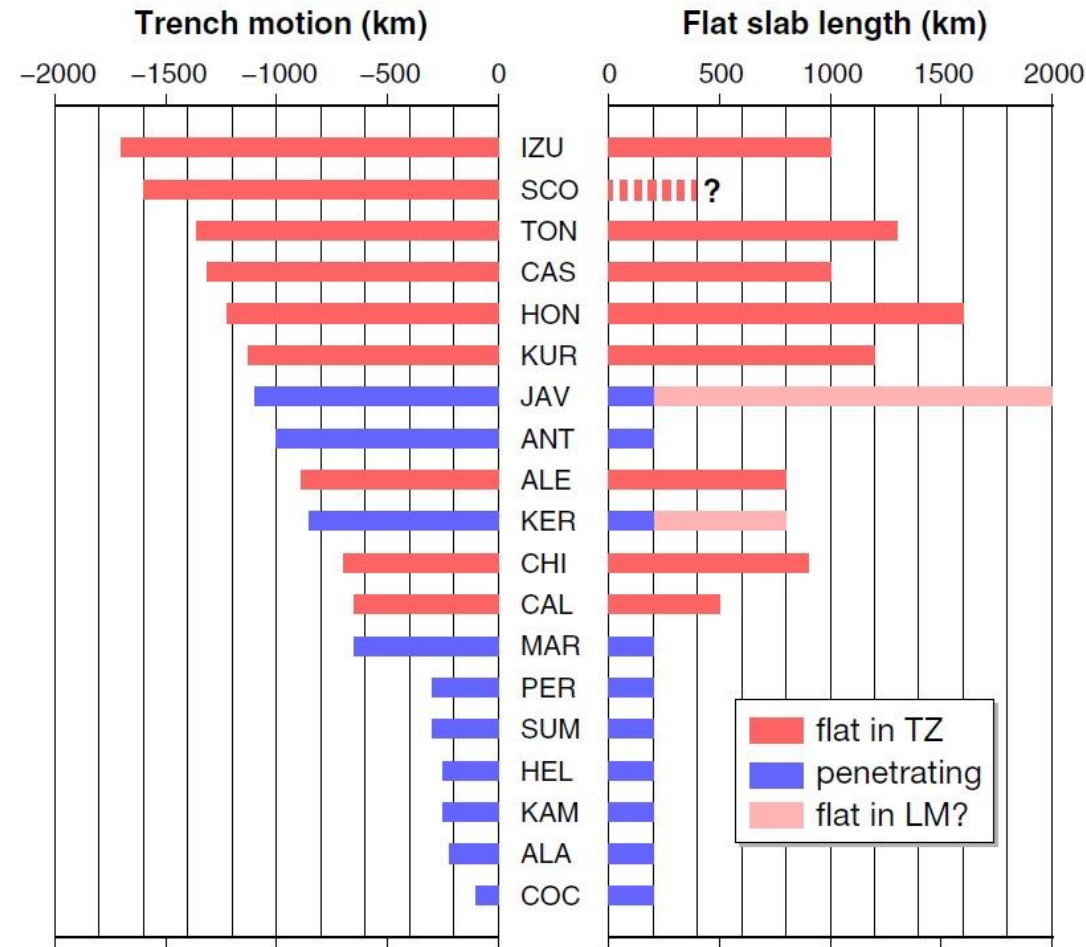
Plate boundary velocities, age, and slab morphology



Goes et al., 2017, Geosphere, 13

- There is a general correlation of increasing velocity with the age of the plate at the trench, which has been interpreted as an expression of upper-mantle slab pull as driving force of the plates.
- The action or interplay of different factors cause change of the subducting plate velocity during its history: such as for the Farallon slab, plate avalanching into the lower mantle, and for India, the push of the Reunion plume or a pull by double subduction or the removal of the Indian cratonic keel.
- There is no correlation between present-day trench motions and slab morphology or dip.

Trench Motion and Plate Morphology

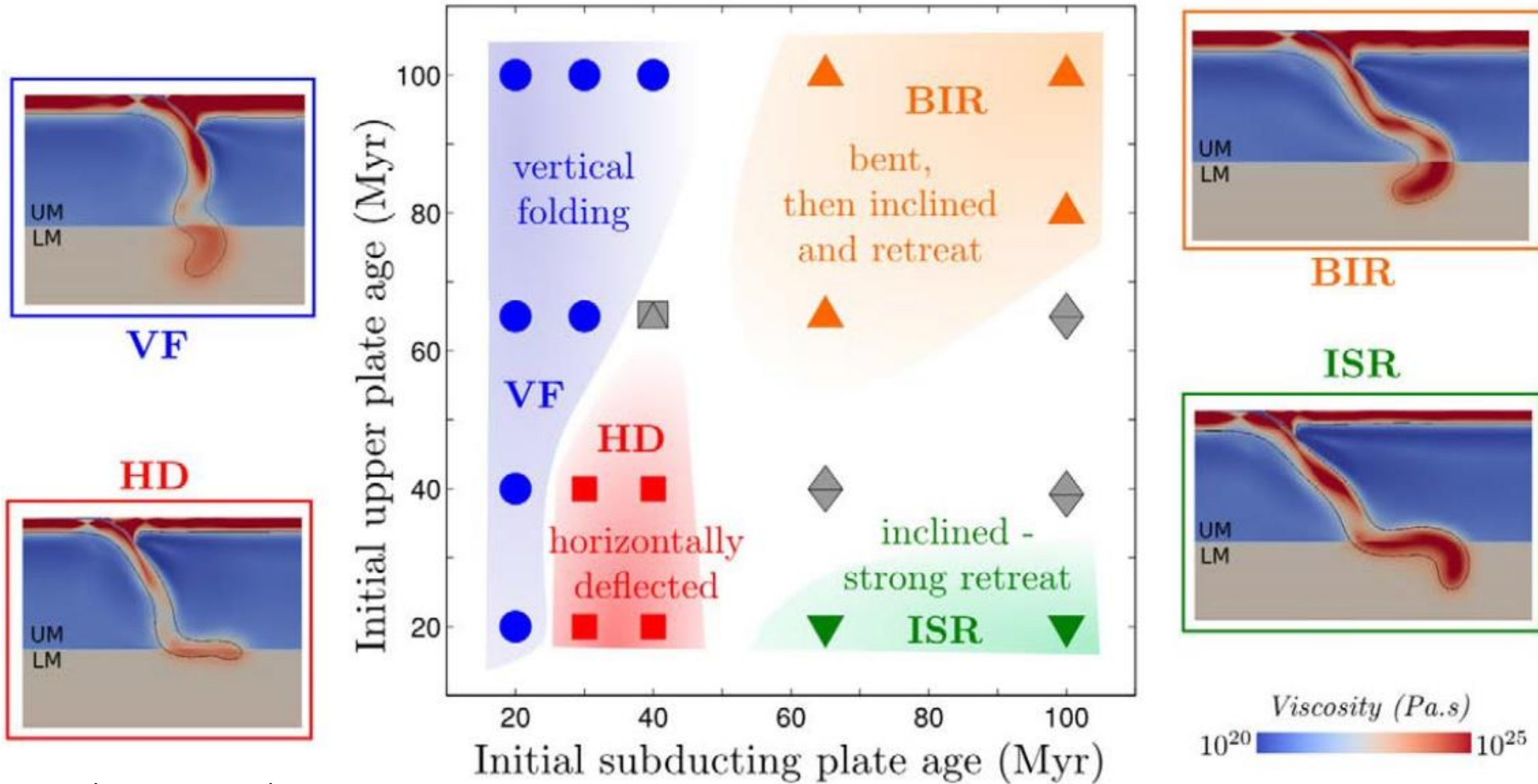


Goes et al., 2017, Geosphere, 13

Total trench retreat approximately perpendicular to the present-day trench during the past 50 Myr (the total trench motions were achieved in some cases in less than 50 Myr, e.g., Calabria in the last 15 Myr). IZU—Izu, HON—Honshu, KUR—Kuriles, KAM—Kamchatka, ALE—Aleutians, ALA—Alaska, CAL—Calabria, HEL—Hellenic, IND—India, MAR—Marianas, CAS—Cascadia, FAR—Farallon, SUM—Sumatra, JAV—Java, COC—Cocos, ANT—Antilles, TON—Tonga, KER—Kermadec, CHI—Chile, PER—Peru, SCO—Scotia.

There is a correlation between trench-motion history and plate morphology: most of the slab retreating are reclining, while those that penetrate into the lower mantle subducted at relatively stable trenches.

Slab Morphology vs Age

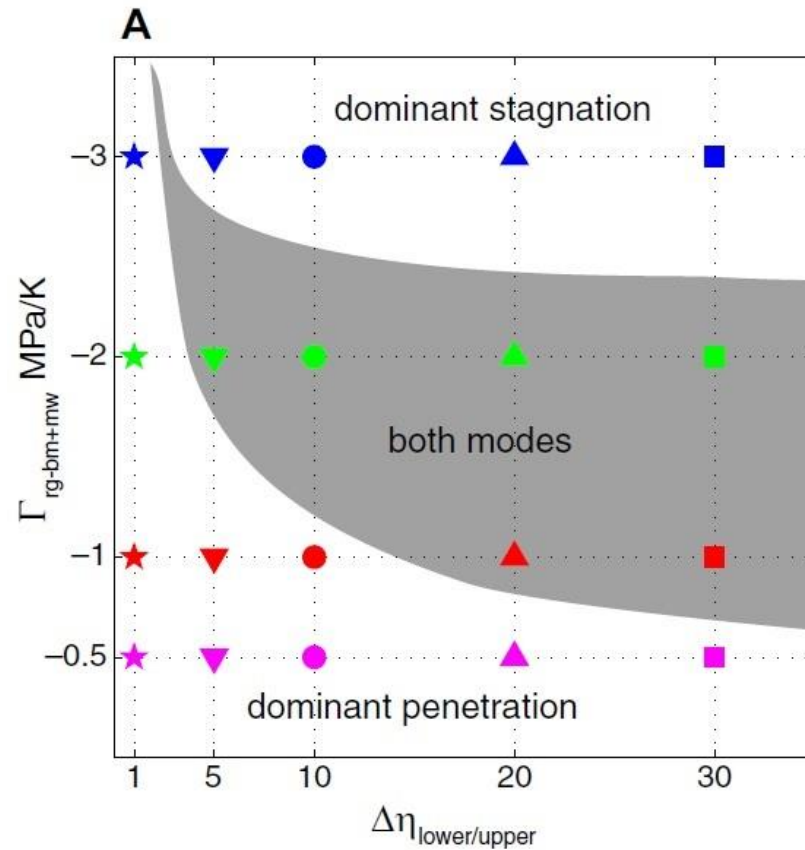


Goes et al., 2017, Geosphere, 13

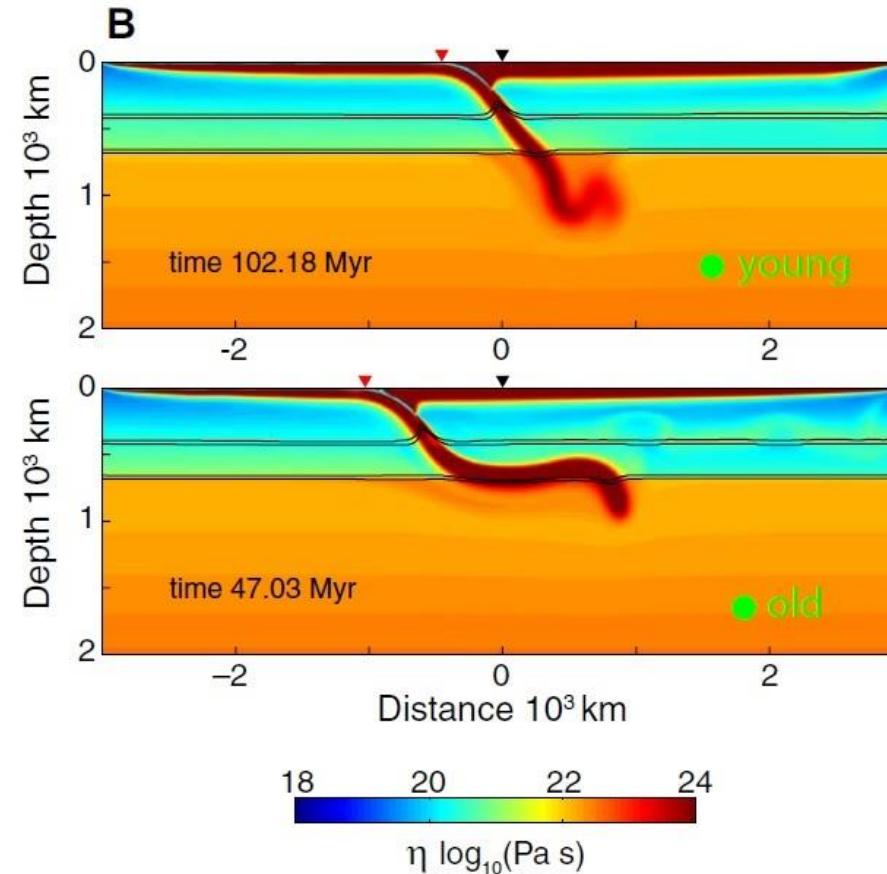
Viscosity jump of a factor of 30 is assumed between upper (UM) and lower mantle (LM)

- Different deformation modes are possible for subducting and upper plates of different initial ages

What does influence slab stagnation?



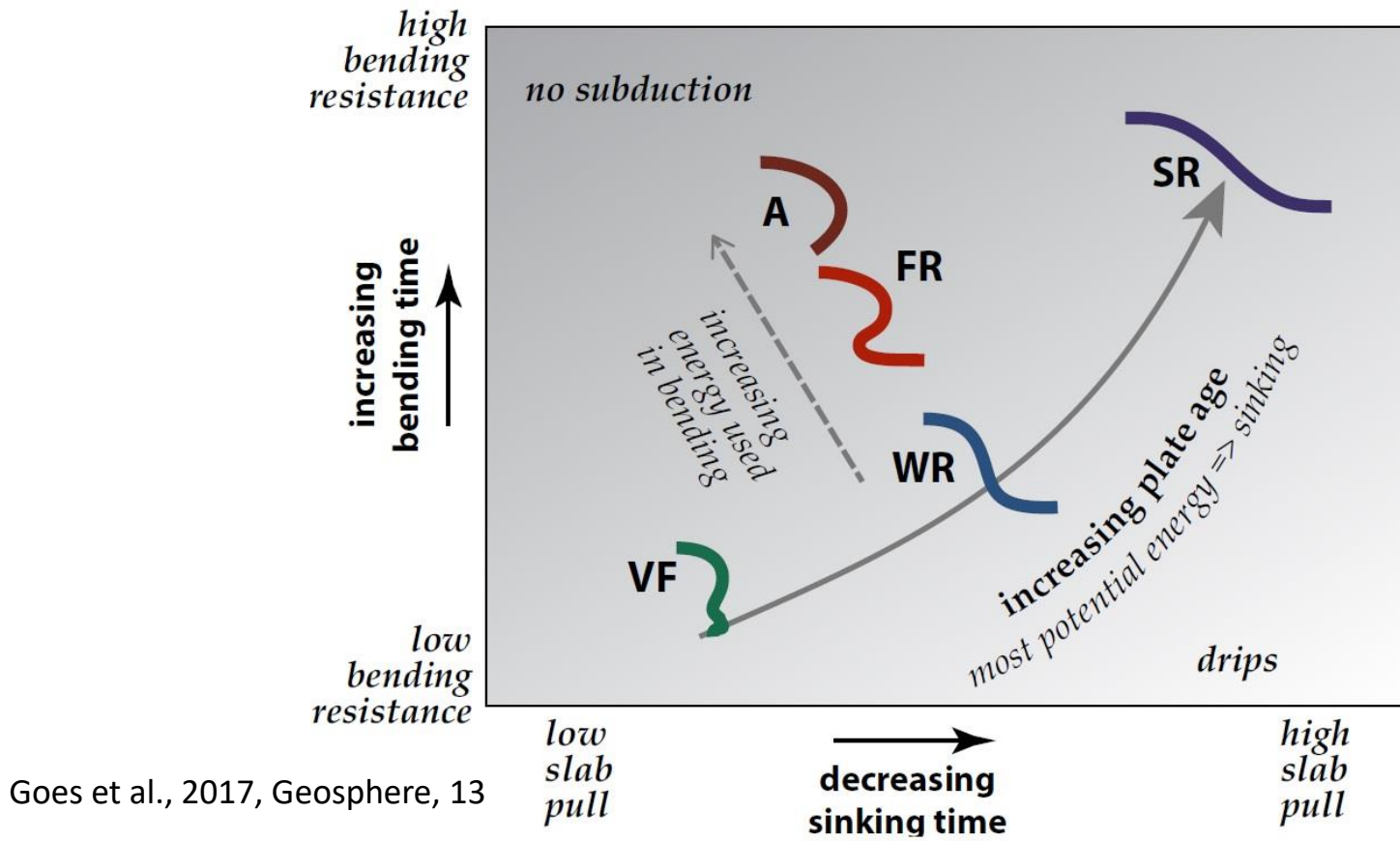
Goes et al., 2017, Geosphere, 13



Black and red triangles show the initial and current position of the trench

- Old and young slabs either both penetrate (“dominant penetration”), both stagnate (“dominant stagnation”), or old ones stagnate while young ones penetrate (“both modes”) as a function of upper-lower mantle viscosity jump and postspinel transition Clapeyron slope.
- Near 660 km depth, the effect of the ringwoodite to postspinel transition with a negative Clapeyron slope and the transition from garnet to bridgmanite, which occurs near this depth and has a strongly positive Clapeyron slope, may largely cancel out any dynamic effects.
- When trench retreat is possible, due to the slab’s negative buoyancy, partial stagnation can already occur at relatively low Clapeyron slopes.

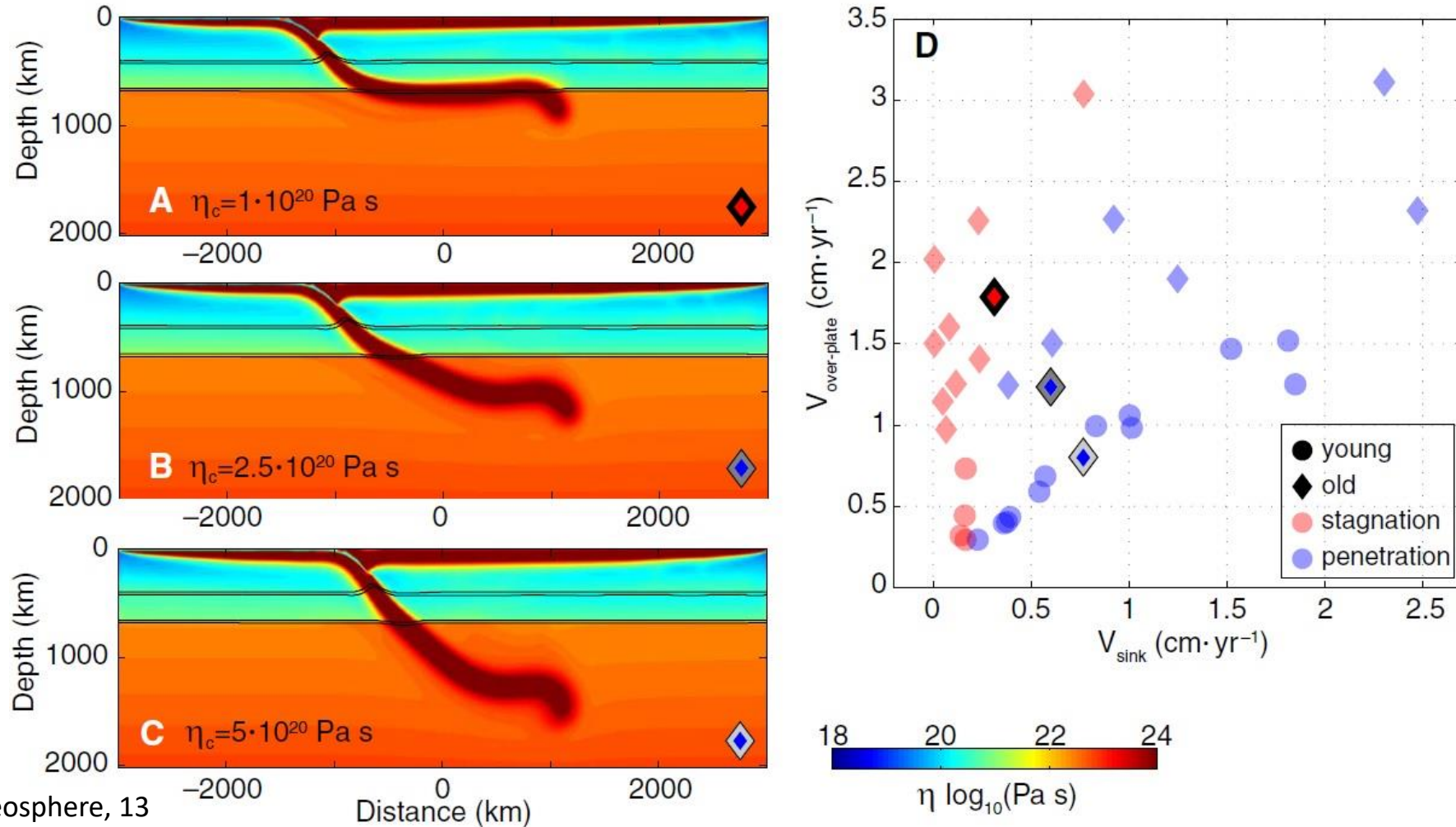
Trench retreat velocity



VF—vertical folding with little trench motion; WR—weak trench retreat; SR—strong trench retreat; A—advancing trench; FR—fold and retreat.

- **The speed of trench retreat is controlled by subducting-plate strength and buoyancy: the style of subduction is the result of a competition between the time required to bend the plate at the trench and the time available to achieve this bending.**
- Slabs with increasing age have higher density and larger strength and thus encourage trench retreat: The time that the plate has available to bend is controlled by its sinking rate, which again is governed by its density.
- If the sinking time is too short to allow the plate to bend, the trench will retreat while the slab sinks.
- Trench advance is the result of additional forcing either at the trailing end of the downgoing plate or from the upper plate or the arrival of buoyant features at the trench.

External Controls on Trench Motion



Goes et al., 2017, Geosphere, 13

η_c = viscosity of the crustal layer on top of the subducting plate (governing the coupling between the two plates.)

Old plate has a viscosity jump of 20 and a postspinel transition has a Clapeyron slope of -2 MPa/K

- Interplate coupling and upper-plate forcing provide resistance: Stronger plate coupling limits trench mobility and can even preclude subduction (thicker, more buoyant, and longer overriding plates provide more resistance to trench motion).

Subduction Styles

Subduction occurs via several different styles, characterized by a distinct type of slab geometry, generated by the associated subduction kinematics, in agreement with two controlling factors: **flexural stiffness** and **slab buoyancy**.

Subduction styles observed in analogue and numerical experiments: slabs retreating and plate advancing

Styles of subduction



Style I

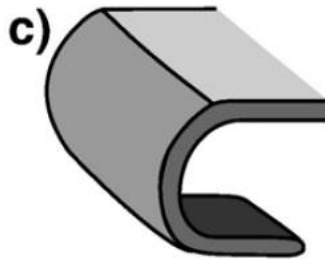
Stokes buoyancy (B_S, s^{-1}) is the ratio of volumetric potential energy ($\Delta\rho g h_{plate}$) to the upper mantle viscosity (η_{UM}):

$$B_S = \frac{\Delta\rho g h_{plate}}{\eta_{um}}$$

Models which accommodate subduction entirely through slab rollback and a retreating trench are those with $B_S > 10^{-11}$, while models in which plate advance is favored are those with $B_S < 10^{-11}$.



Style II



Style III

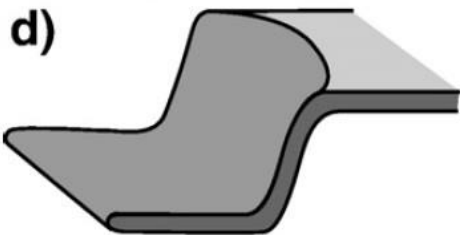
Flexural stiffness (D_{vis}, Nms) is similar to the elastic equivalent (flexural rigidity), depending on the cube of the plate thickness:

$$D_{vis} = \frac{\eta_{plate} h_{plate}^3}{3}$$

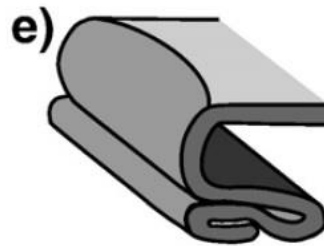
Effective flexural stiffness (D_{vis}^*):
$$D_{vis}^* = \frac{D_{vis}}{\frac{1}{3}\eta_{lum} H^3} = \frac{\eta_{plate}}{\eta_{lum}} \left(\frac{h_{plate}}{H} \right)^3$$

H=mantle thickness

Plate strength is described qualitatively as “strong” or “weak”, considering that a value of $\eta_{plate}/\eta_{um} \sim 500$ usually discriminates between the two.



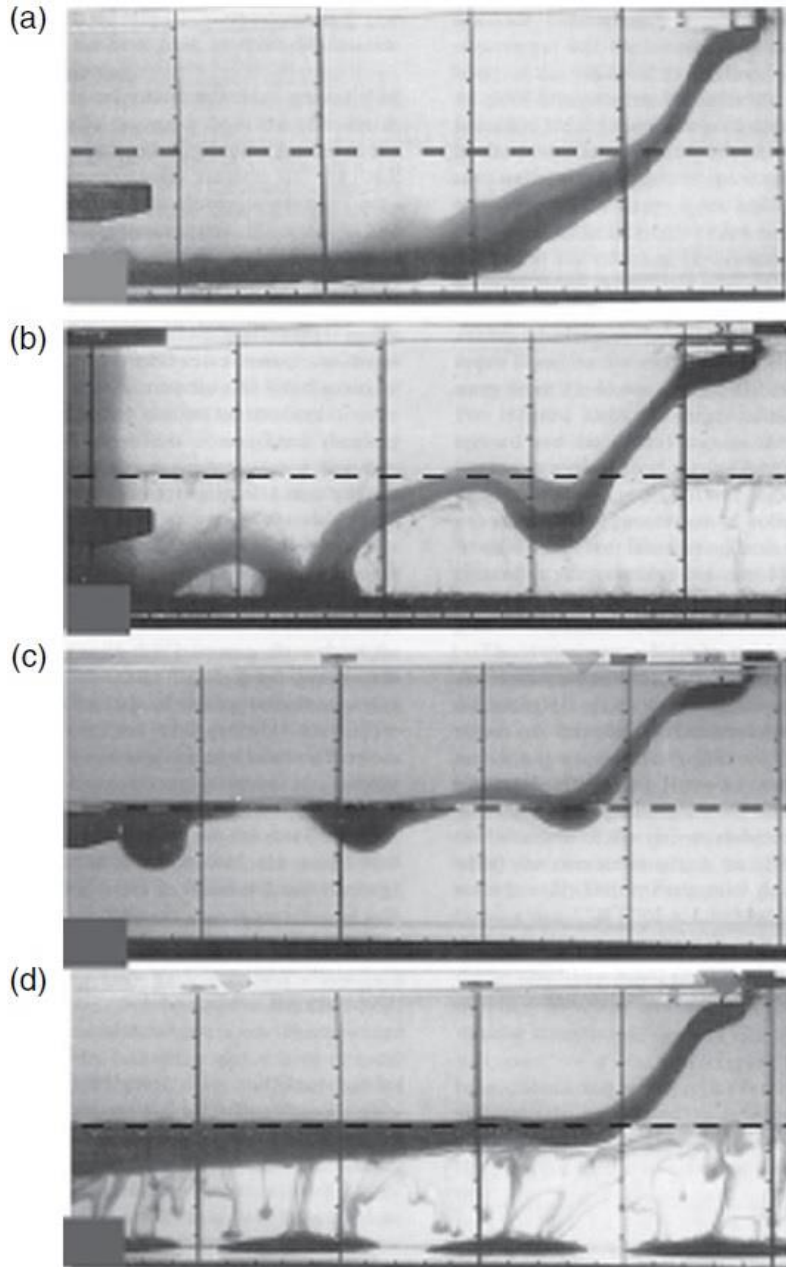
Style IV



Style V

- **The transition between strong slabs (Regimes I–III) and weak slabs (Regimes IV–V) is ($D_{vis}^* \sim 0.5$).**
- **The models in certain strong slab regimes exhibit advancing trenches.**
- **The models in the weak slab regimes exhibit features such as highly curved trench geometry.**
- **Slab piles occur in Earth as a result of weak slabs interacting with a partially stratified mantle.**
- **Slabs that are weak can be easily perturbed by a number of processes that occur in the Earth.**

Slab interaction with a viscosity/density interface (analogue experiments)

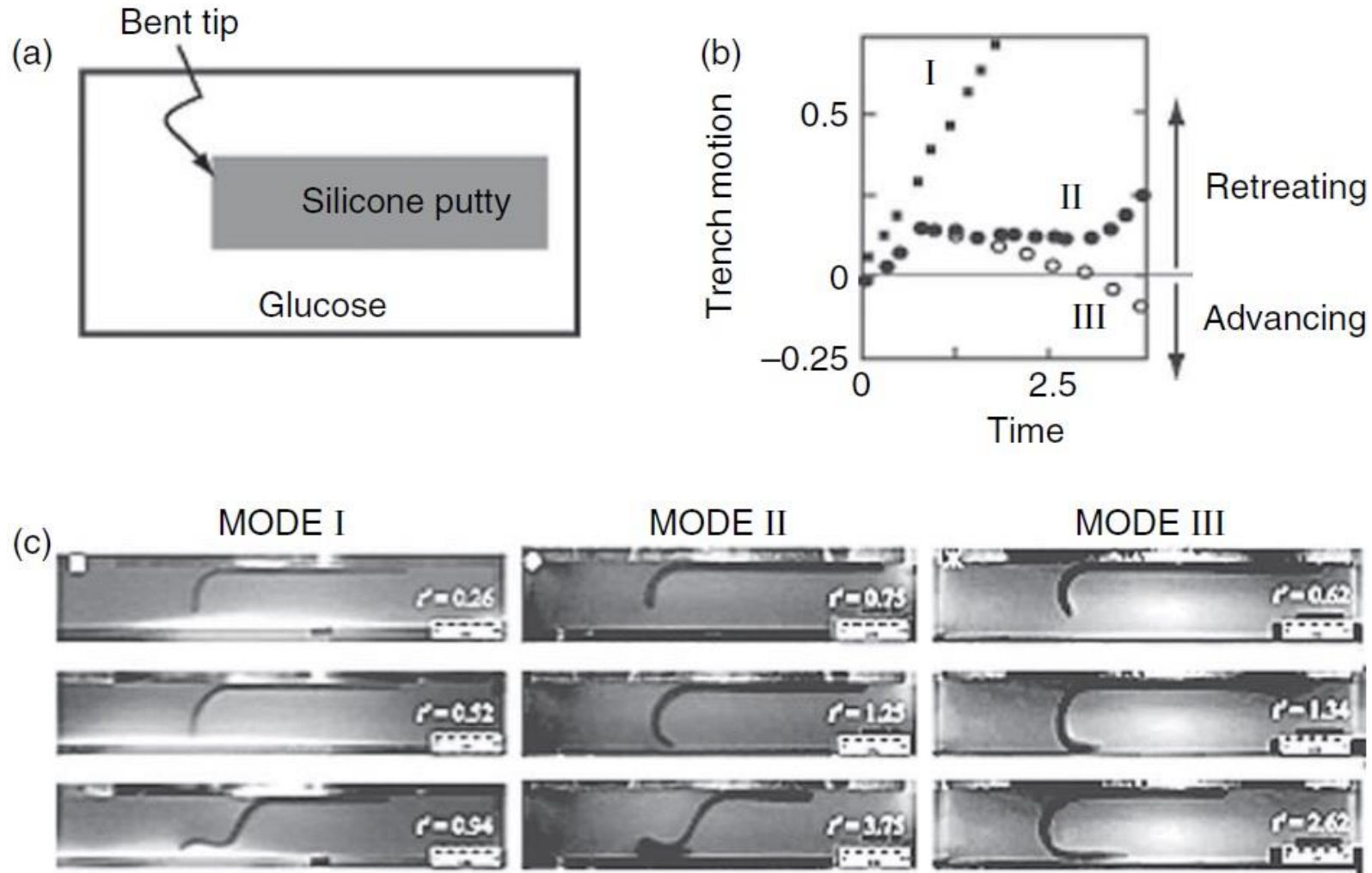


- Slab deformation modes therefore finally depend on three parameters: (1) the slab to mantle viscosity ratio, (2) the ratio of sinking velocities in the upper and lower mantle, and (3) the ratio of the slab's horizontal velocity to its vertical velocity.
- Increasing trench rollback (from **a** to **c**) enhances slab flattening on the interface, while increased resistance in the lower mantle promotes folds and piles.
- When the slab is not too viscous (**c**), Rayleigh Taylor instabilities have time to develop from the slab resting on the interface, and to sink into the lower mantle (**d**).

Different regimes of slab interaction with a viscosity/density interface for a slab which is between 3 and 50 times more viscous than the lower layer. The trench velocity increases from (a) to (c) and the viscosity contrast from (c) to (d).

Davaille and Limare, 2007, Treatise of Geophysics, vol 7

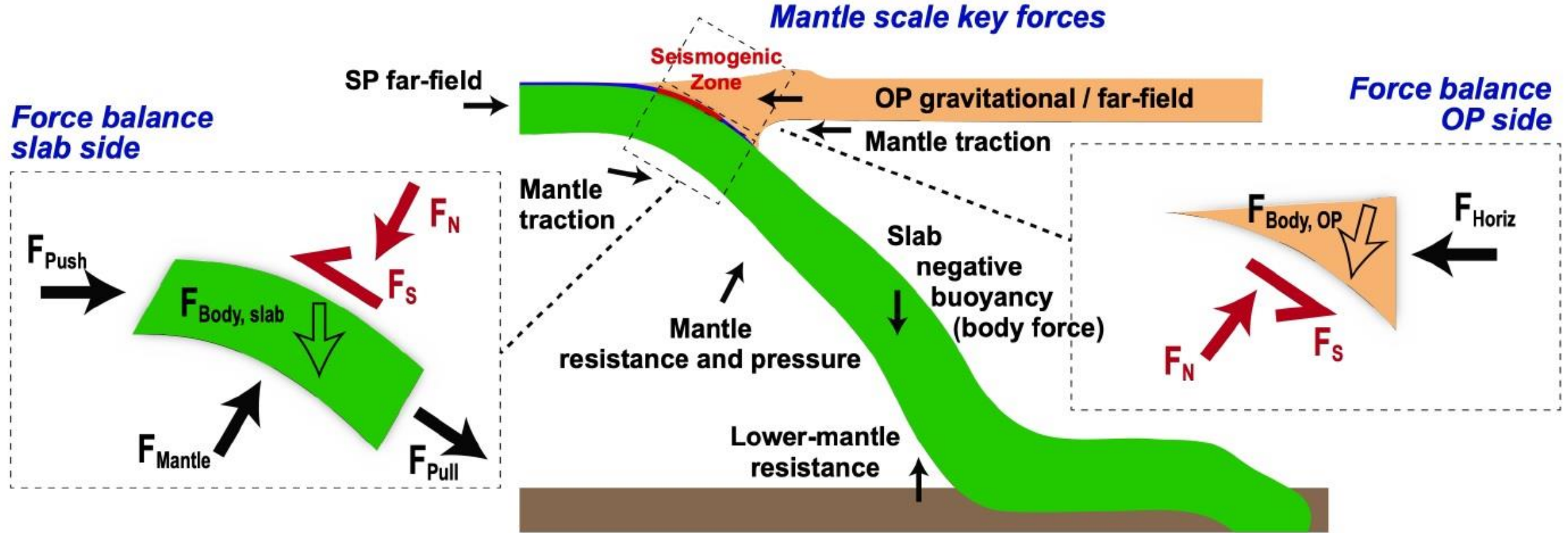
From slab retreating to slab advancing



Davaille and Limare, 2007, Treatise of Geophysics, vol 7

By varying the thickness, width, viscosity, and density of the slab and mantle, can vary the modes of subduction for a slab connected to a plate: a retreating trench mode (mode I), a retreating trench mode following a transient period of advancing trench (mode II), and an advancing trench mode (mode III).

Plate interface stress and geodynamic coupling



Beall et al., 2021, EGU

Plate interface stress largely depends on how effectively forces are transmitted across the plate interface (**geodynamic coupling**), which relates to how the forces driving subduction are balanced.

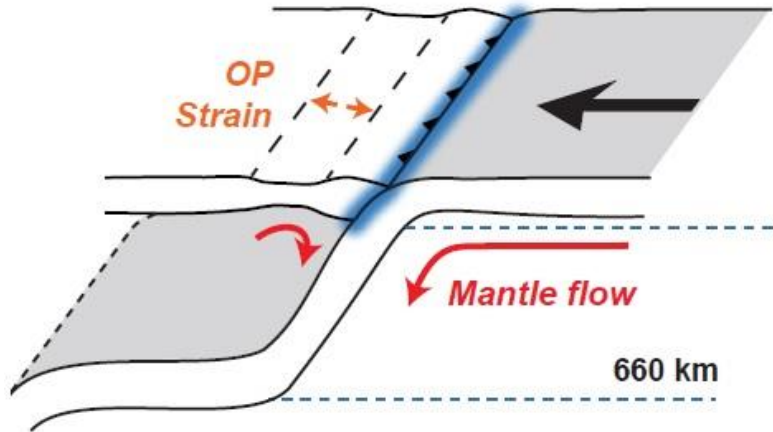
- **High geodynamic Coupling:** High OP forcing and Low mantle resistance (no rollback and short/torn slabs).
- **Low geodynamic Coupling:** Low OP forcing and High mantle resistance (significant rollback and long slabs).

Geodynamic coupling depends on whole-mantle flow and interaction between margin segments

Plate interface stress and geodynamic coupling

A) Free subduction by rollback

Low coupling

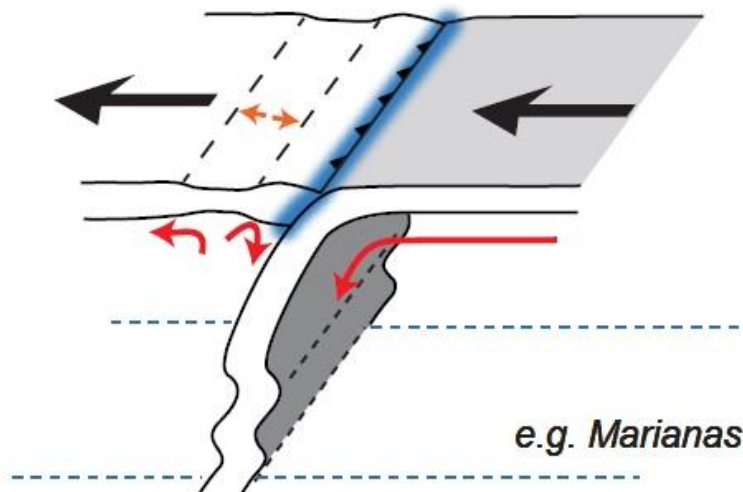


e.g. Tonga

- Subduction dominated by slab buoyancy and rollback, typically old sea-floor
- Slab rollback drives back-arc extension
- The slab stagnates at 660 km and mantle flow is asymmetric
- Examples: Tonga-Kermadec, Ryukyu — Izu-Bonin

B) Overriding plate retreat

Low coupling

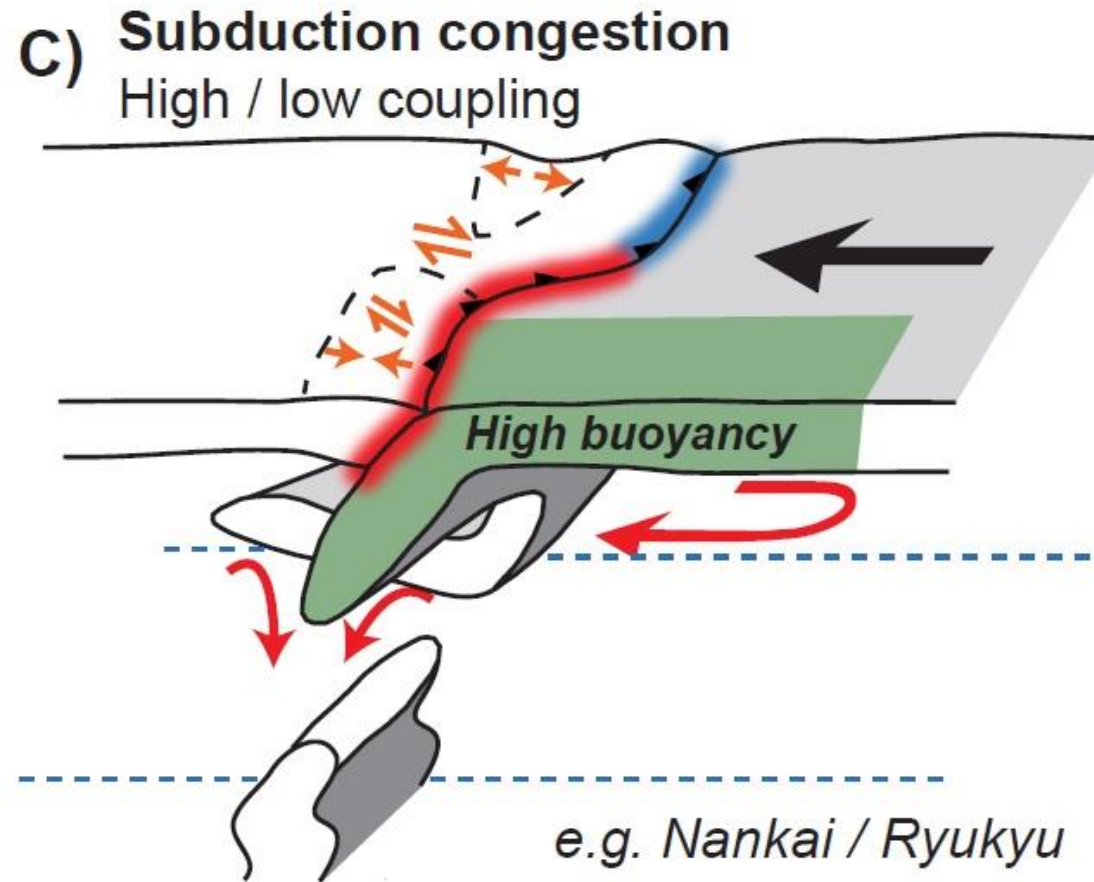


e.g. Marianas

OP is pulled away from the trench

- Convergent mantle flow towards the trench is low
- The slab can still penetrate the lower mantle and steepen
- Examples: Mariana — Izu-Bonin

Plate interface stress and geodynamic coupling

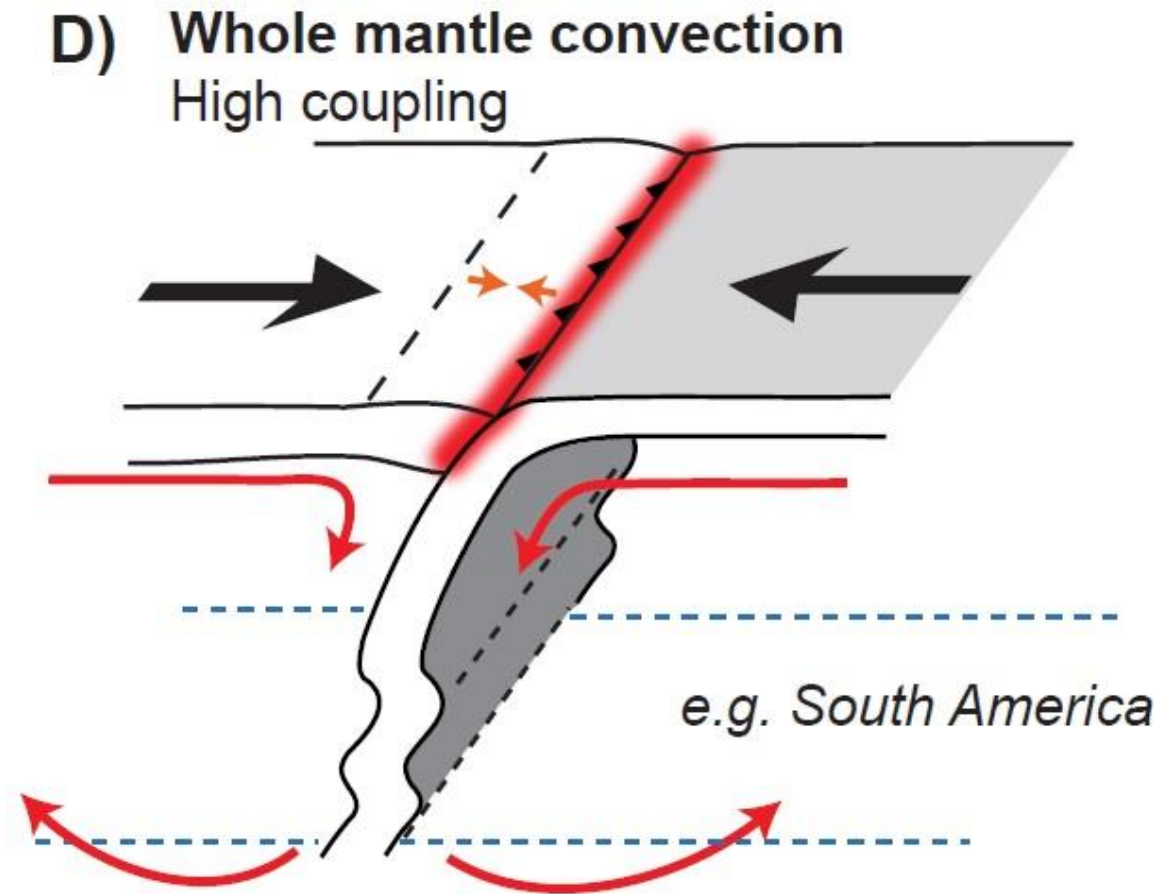


Beall et al., 2021, EGU

Subduction affected by collision of a buoyant oceanic plate segment (sufficient to cause margin rotation or convergence slow-down).

- Margin segments with buoyant material and/or rotated margin segments experience trench advance or minimal rollback.
- Margin segments away from buoyant material undergoes increased slab rollback.
- Examples: Nankai/Ryukyu (high/low geodynamic coupling), Solomon Islands / Vanuatu (high/low), southern/northern Hikurangi (high/low).

Plate interface stress and geodynamic coupling



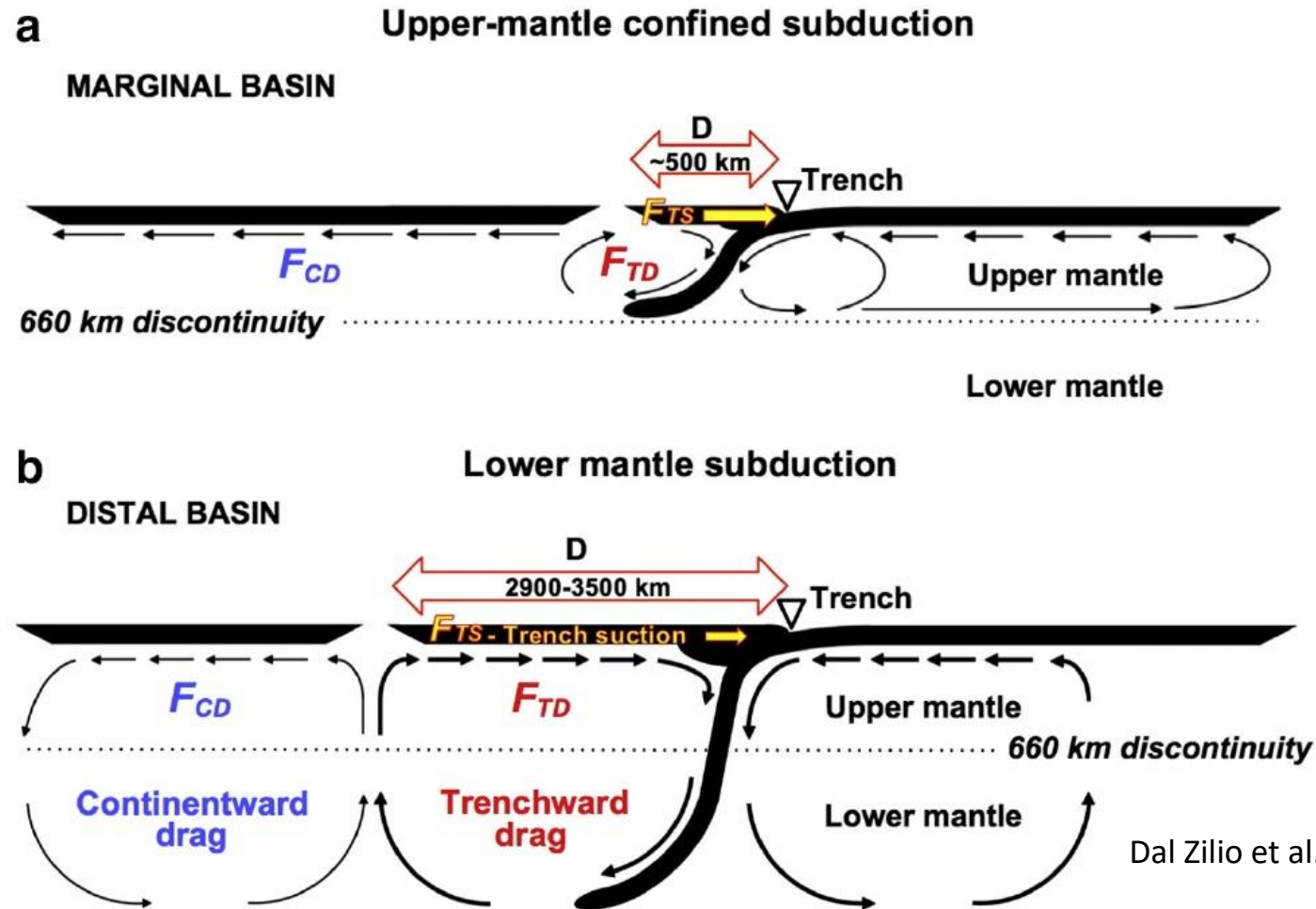
Beall et al., 2021, EGU

Whole mantle convection drives plates together

OP deformation: **back-arc shortening**

- Upper-plate advance
- Slab penetrates the mantle for 20-50 Myrs, driving lower mantle flow.
- Examples: South America — central/northern Japan, Sumatra/Java.

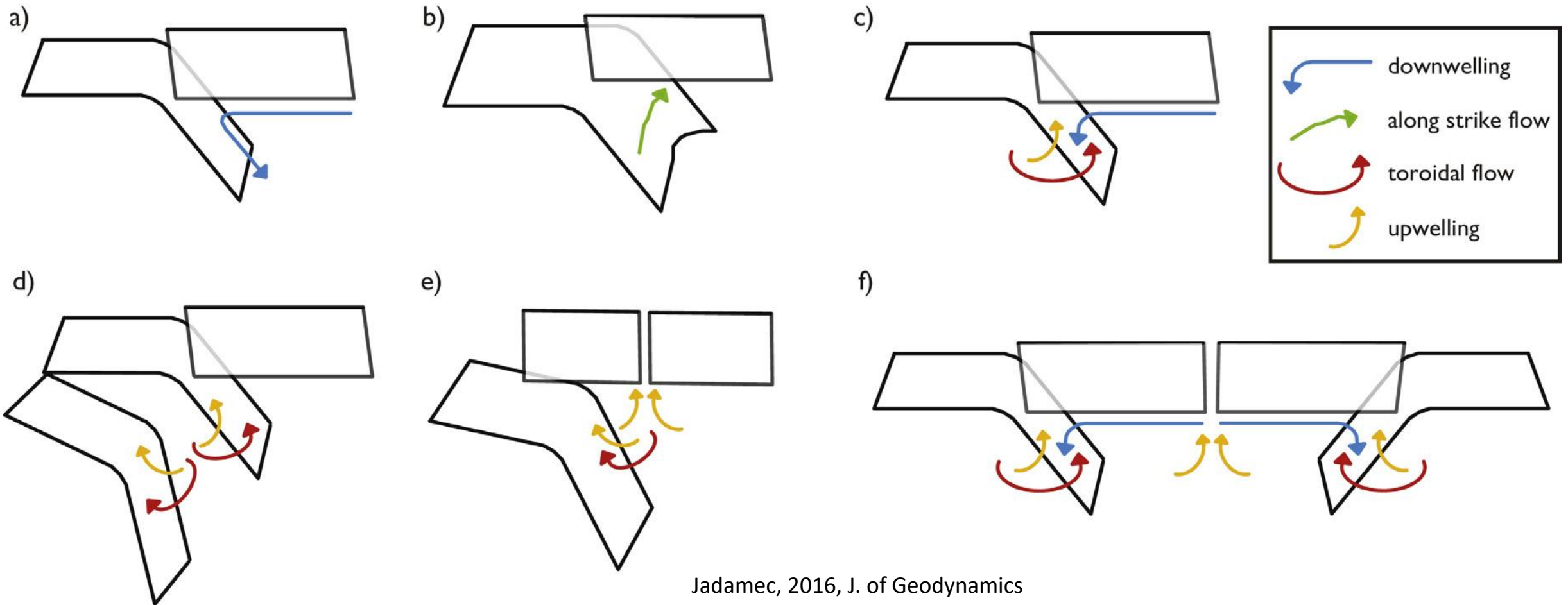
Effects of shallow and deep subduction on continental plate



Dal Zilio et al., 2018, Tectonophysics, 746

- More vigorous mantle flow and basal tractions in the deep subduction model: the perturbation of the lower mantle upon subduction reorganizes the flow in much larger convective cells. In this case, extensional tractions are propagated for much greater distances within continent interiors, comparable to the thickness of the whole mantle.
- Trench suction forces act within the upper plate in proximity of the trench and are stronger in upper-mantle confined subduction models.
- These processes have distinct durations: while breakup occurs within 10 Myr when subduction is confined in the upper mantle, a tensile regime can be sustained for ~ 40 Myr before breakup when subduction penetrates deeper.

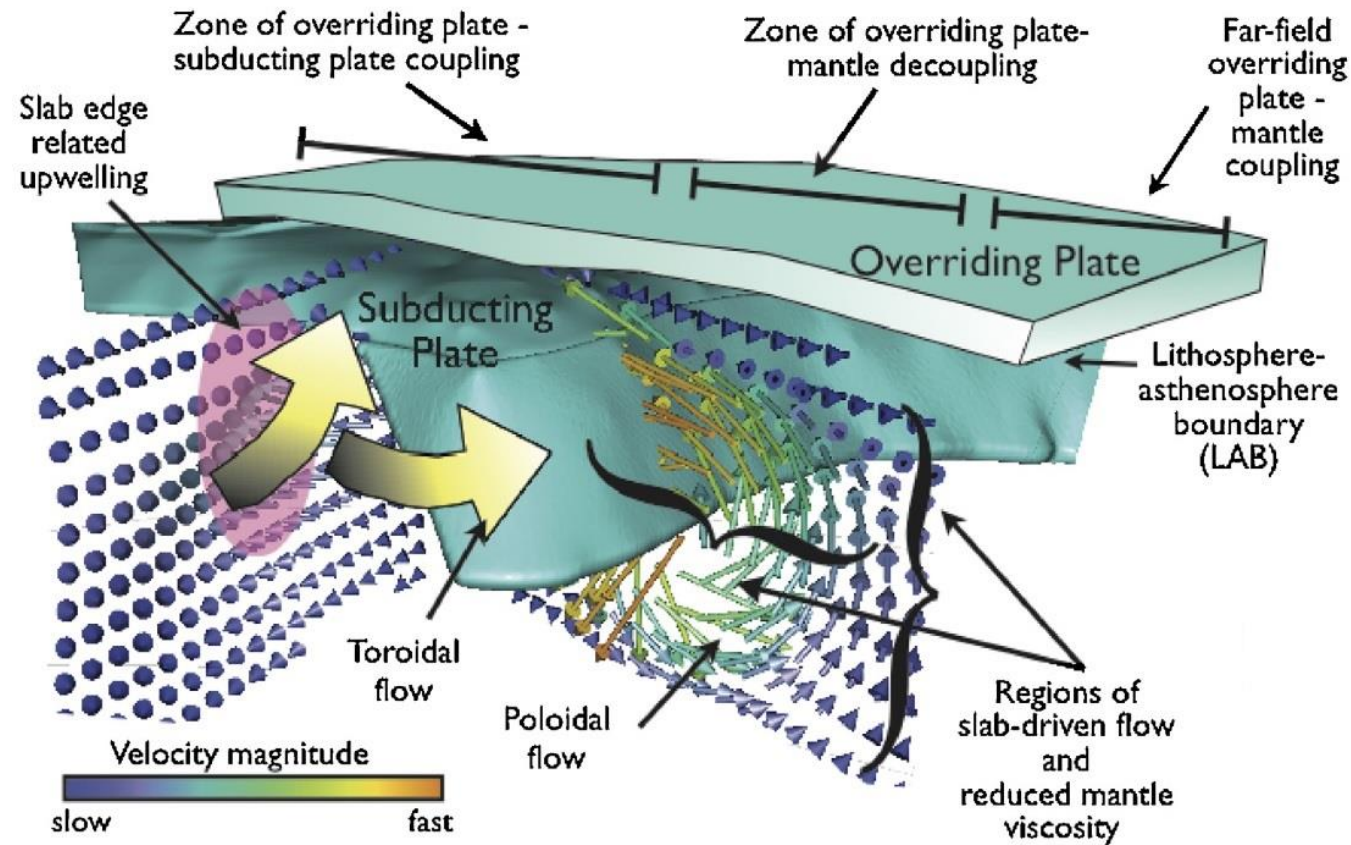
General patterns of slab-driven 3D mantle flow



Jadamec, 2016, J. of Geodynamics

- Lateral changes in the dip and buoyancy of the slab, as well as in the mantle wedge viscosity, can drive arc-parallel flow in the mantle wedge and in the subslab mantle, with mantle material moving perpendicular to the cross section plane (along strike flow).
- Tearing of a viscous slab can facilitate mantle upwelling through and along the slab tears.
- 3D mantle wedge flow can also occur due to structure in the mantle wedge, structure in the upper plate, or motions in the upper plate.

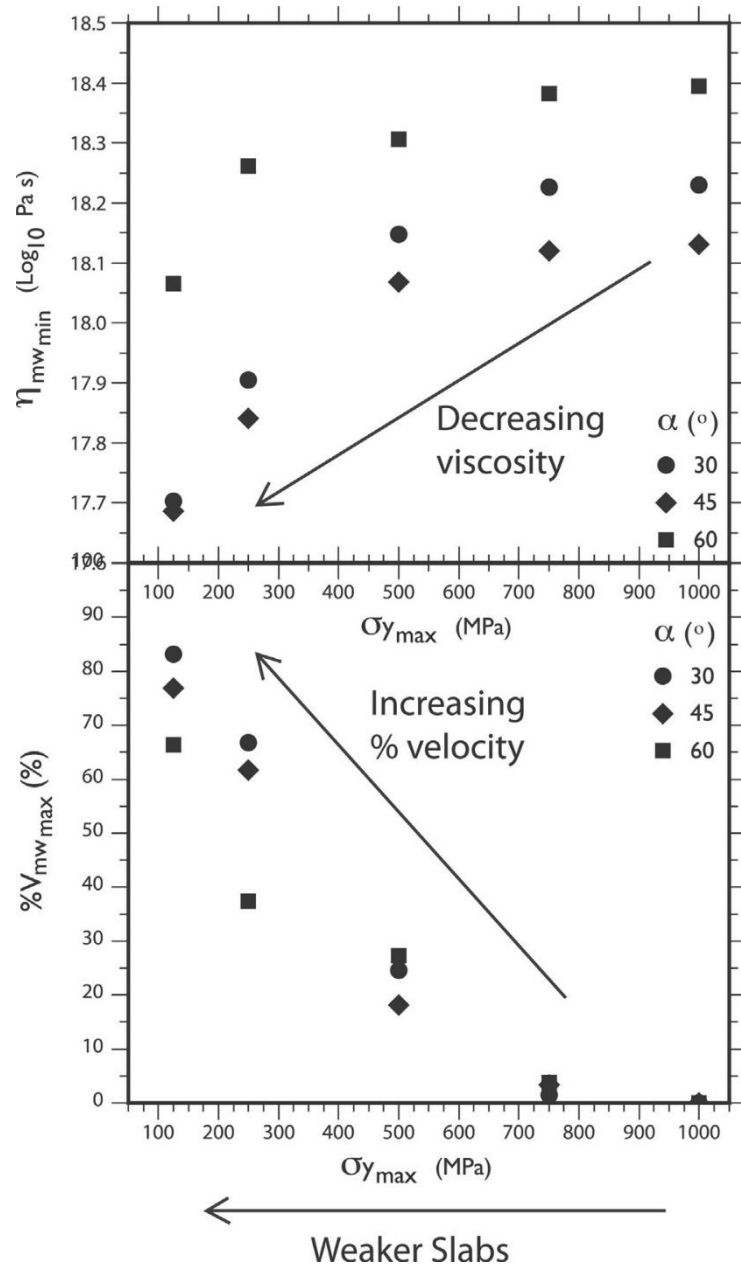
General patterns of slab-driven 3D mantle flow



Jadamec, 2016, J. of Geodynamics

- 3D models reveal the complex nature of slab-driven mantle flow, including trench parallel flow, toroidal flow around slab edges, mantle upwelling at lateral slab edges, small scale convection within the mantle wedge, and the effects of lateral gravitational instabilities above the mantle wedge.
- Associated with this toroidal flow, is an upwelling component in the mantle, such that, as the arcuate toroidal flow field moves material laterally around the slab edge, warm mantle is also transported from underneath the slab into the lower pressure mantle wedge in an upward and arcuate pattern around the edge.

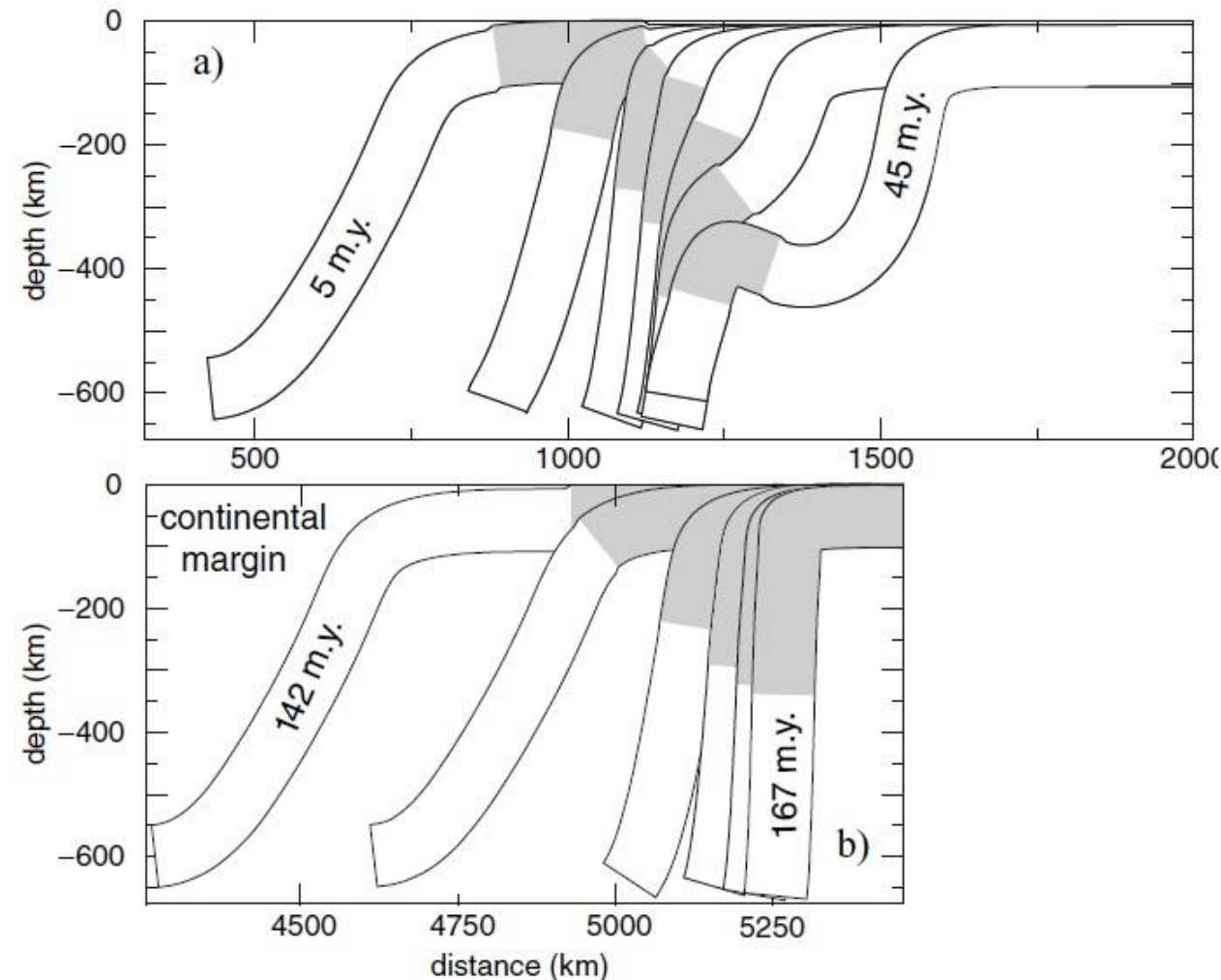
Mantle Flow Velocity and Slab Viscosity



- Reducing the viscous support of the slab, requires the slab to support more of its own weight which can lead to plastic failure in the slab hinge, allowing for slab steepening (local reduced resistance to subduction) and slab induced rapid mantle flow.
- Decreasing mantle viscosity increases mantle flow velocity in the mantle wedge, as a function on decreasing maximum yield stress (slab strength).
- Models with the shallower initial slab dips resulted in greater slab-induced mantle flow due to the tendency for the shallower slabs to steepen.
- The maximum flow velocities occur in models with a lower maximum yield stress and shallower slab dip, whereas, the slowest flow velocities occur in models with the largest maximum yield stress and steeper initial slab dip.
- However, if the slab becomes too shallow, less of the slab protrudes into the mantle and thus a smaller magnitude of flow is induced.
- The maximum velocities and the velocity gradients are larger for models including the non-Newtonian rheology because of the local reduction in mantle viscosity.

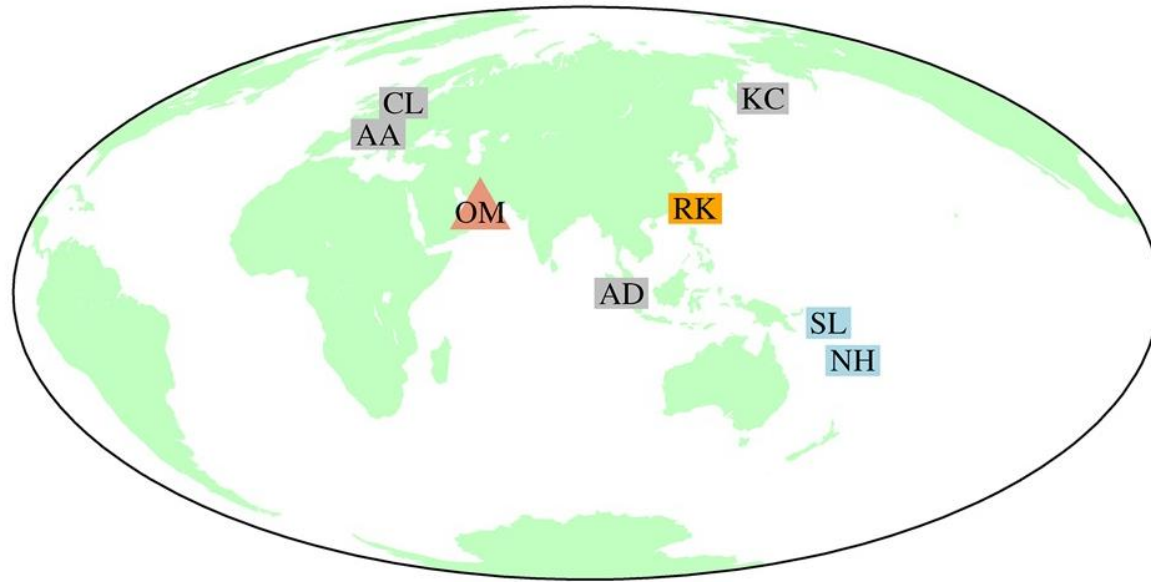
Subduction with variations in slab buoyancy





Subduction of the continental island and of continental margin



- Flattening of the shallow slab occurs when dense lithosphere follows buoyant lithosphere into the trench because the dense slab at shallow depth sinks more rapidly than the buoyant material at larger depth.
- There is a strong correlation between slab dip and trench migration rate: For narrow, highly buoyant slab segments, the dip of the slab may become inverted at depth, with a local depth-minimum coinciding with the buoyant slab segment.
- Rapid cessation of subduction is due to the creation of a shortcut for mantle flow that is critical in enabling rapid steepening of the slab into its final, stationary position.
- When subduction terminates, the viscous stresses on the slab disappear and the stresses on the slab arise only from its buoyancy.
- In these conditions, the extensional stress within the subducted slab is greatest at the former ocean-continent transition and increases upwards to the point where the density of the slab is less than the density of the surrounding mantle. This may induce possible slab detachment at this site.

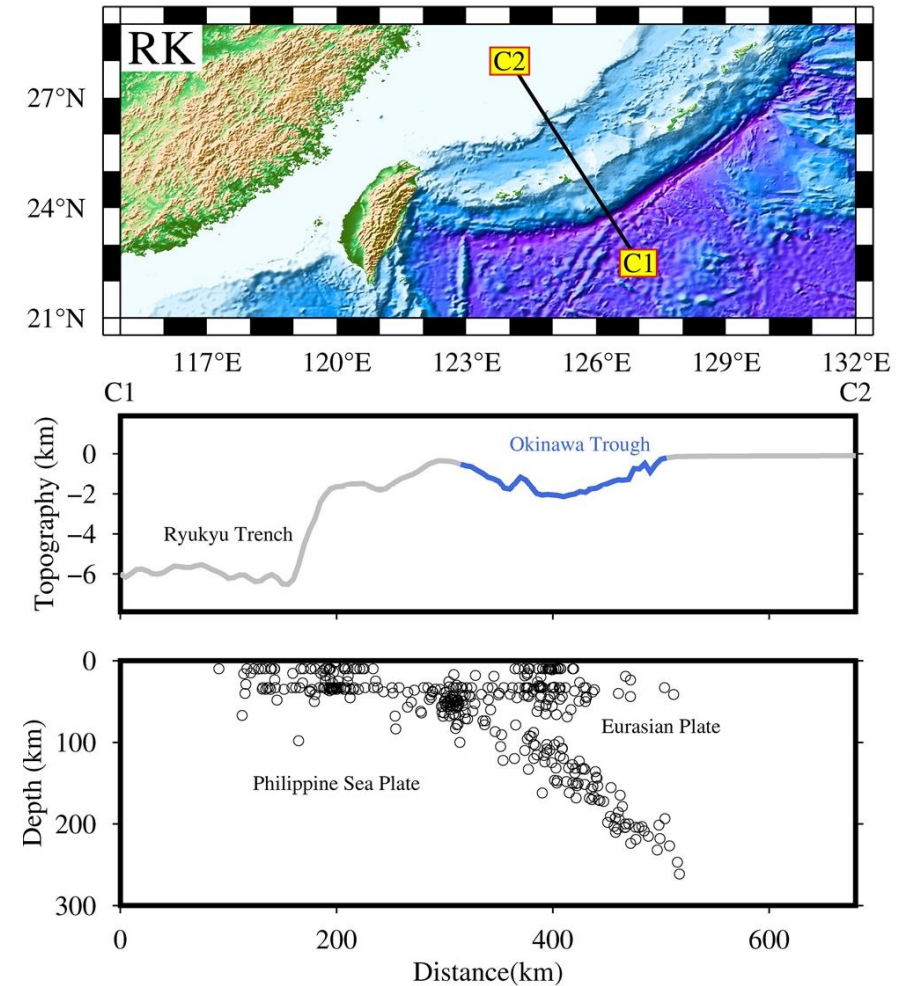
Subduction Polarity Reversal (SPR)



- | | |
|--|--|
|  Historical obduction event |  Historical SPR event |
|  Controversial SPR event |  Ongoing SPR event |

- Subduction polarity reversal (SPR), which always follows a prior intra-oceanic subduction, is a typical compression-induced subduction in response to the arc-continent collision.

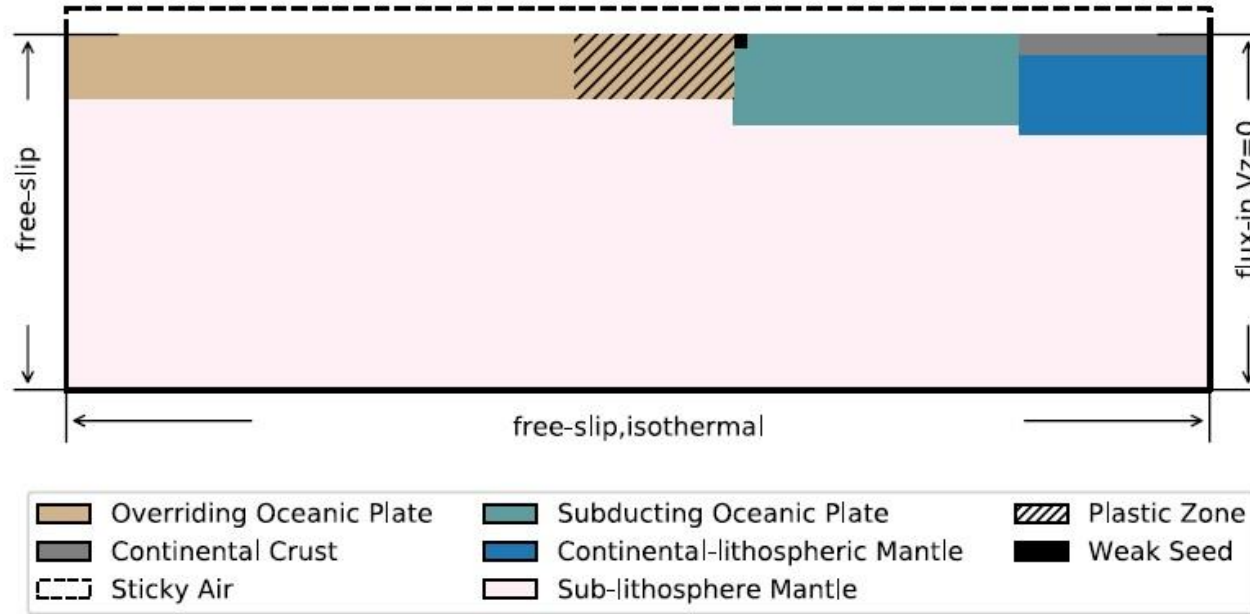
Zhang et al., 2021, GRL, 48



OM, Oman; RK, Ryukyu; SL, Solomon; NH, New Hebrides; KC, Kamchatka; AD, Andaman; AA, Alpine-Apennines; CL, Caledonides.

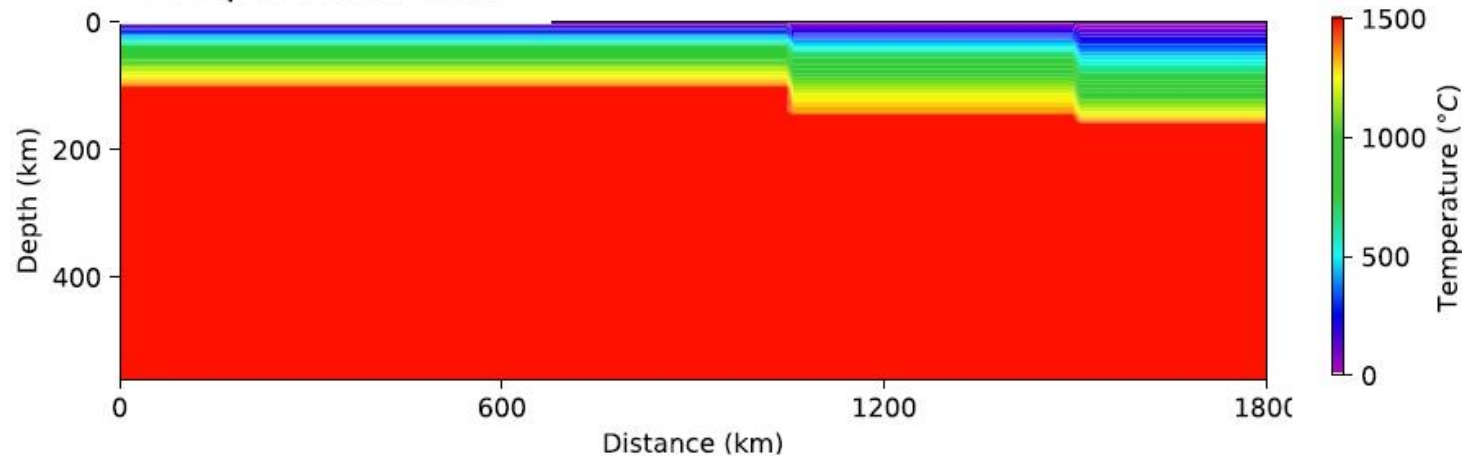
Subduction Polarity Reversal (SPR)

Material field



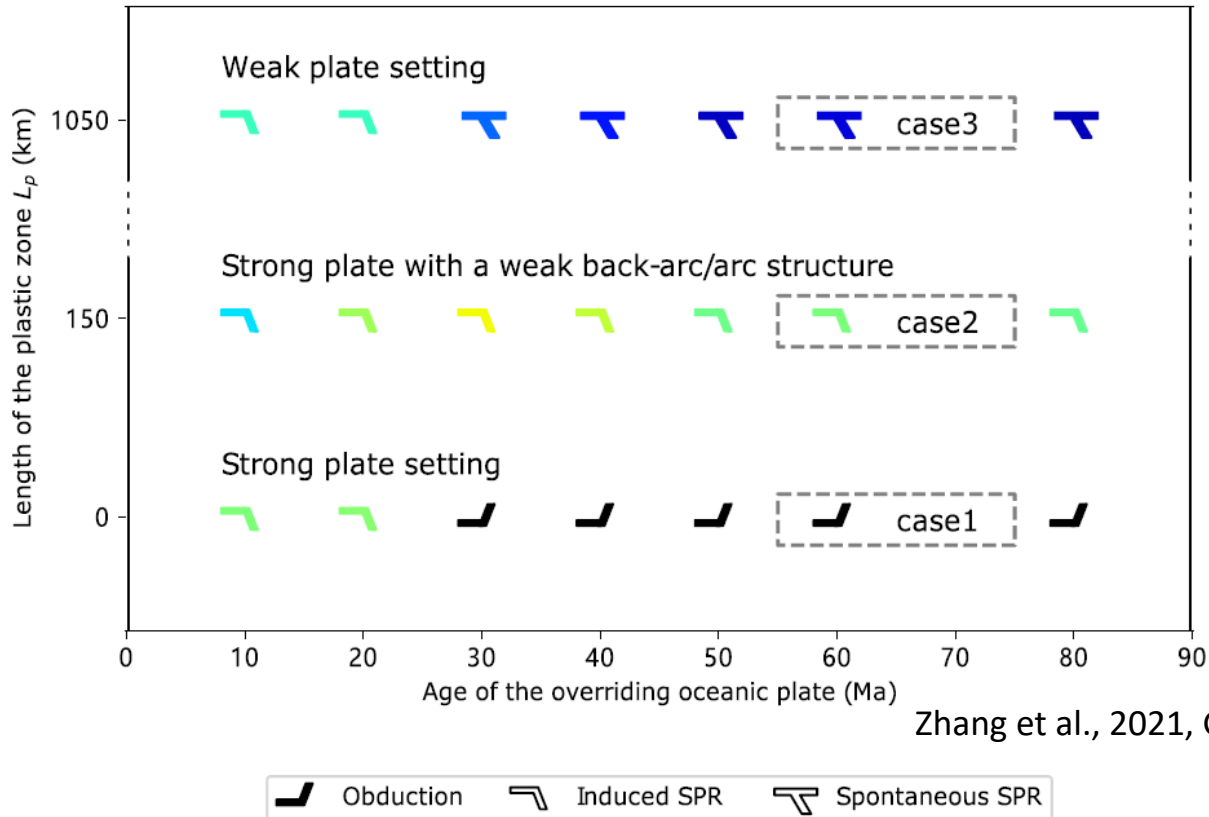
- By changing the length of the plastic zone, we obtain three typical tectonic settings in nature: (1) The strong overriding plate setting ($L_p = 0$ km), (2) the strong overriding plate with a weak back-arc/arc structure ($L_p = 150$ km), (3) the weak overriding plate setting ($L_p = 1050$ km).

Temperature field

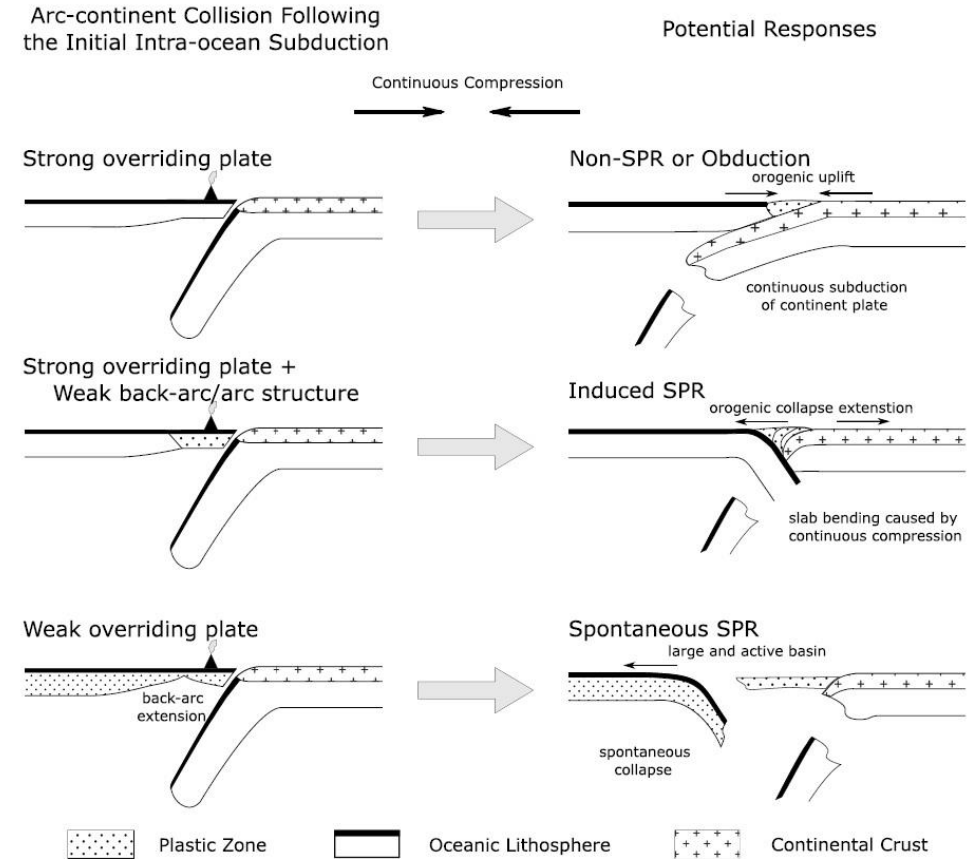


Subduction Polarity Reversal (SPR)

Simulation results

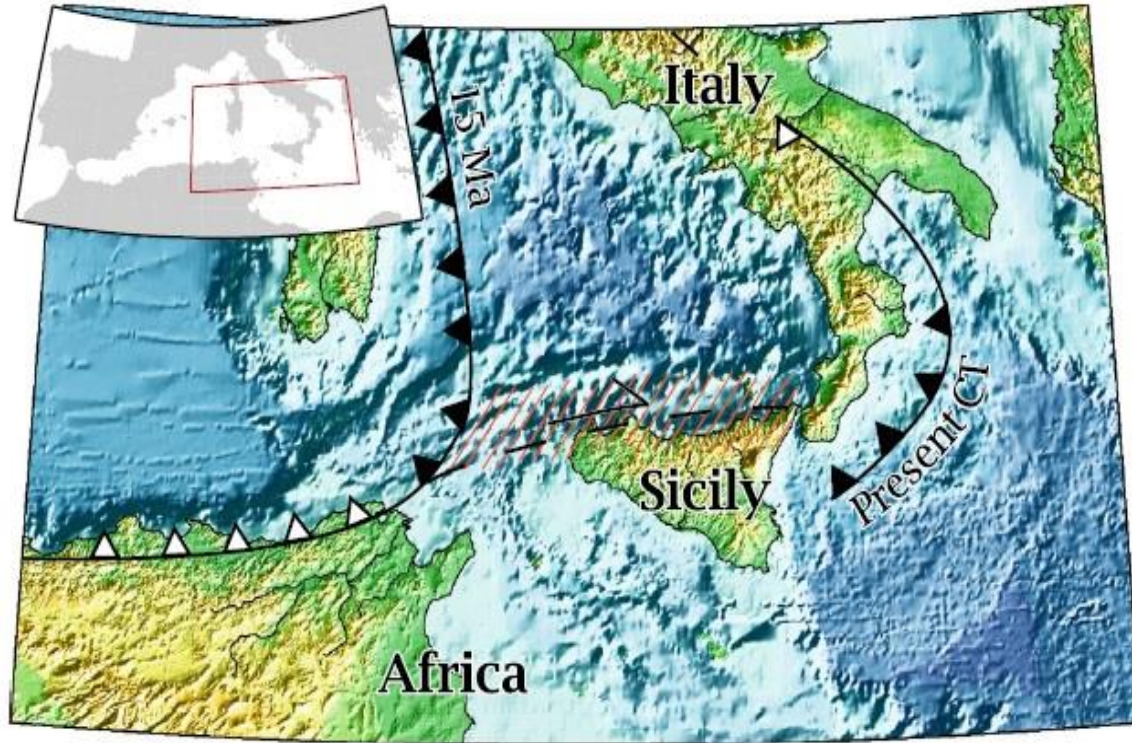


Zhang et al., 2021, GRL, 48



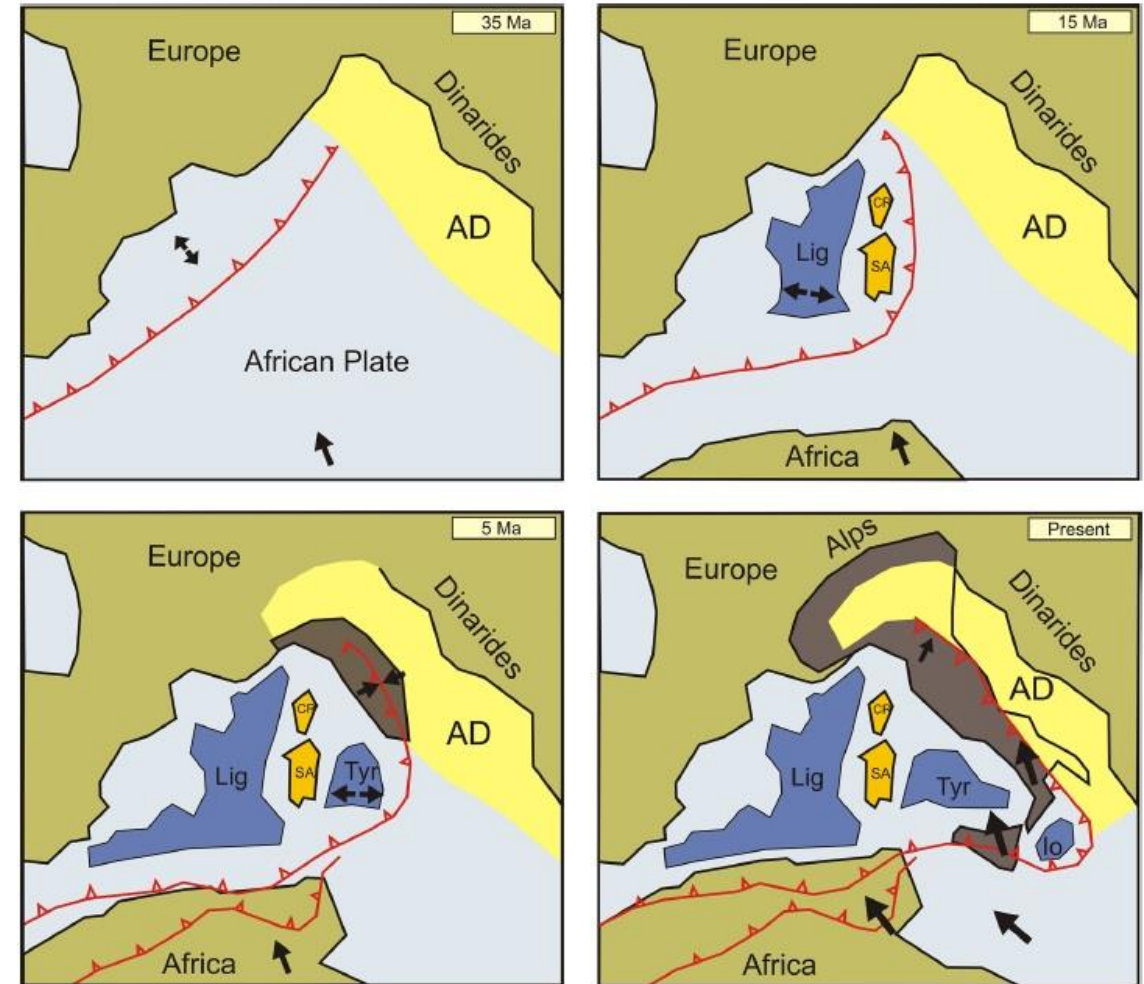
- Without the plastic zone, the SPR does not occur as long as the overriding oceanic plate is older than 20 Ma. The continuous continent subduction follows the precedent intra-oceanic subduction (obduction).
- A limited weak back-arc/arc structure greatly promotes the initiation of the SPR. The continuous compression shortens the fore-arc structure and results in the bending of the original overriding plate. After starting the new subduction, a small-scale extensional basin appears in the back-arc area, because of the unloading of the compression.
- When the plastic zone is long enough, the vigorous wedge flow generated by the initial subduction will pull the overriding plate apart. The extensional force from this active extension center also forms a young and thin oceanic basin.

Continental collision due to convergent plate boundaries in the Western Mediterranean



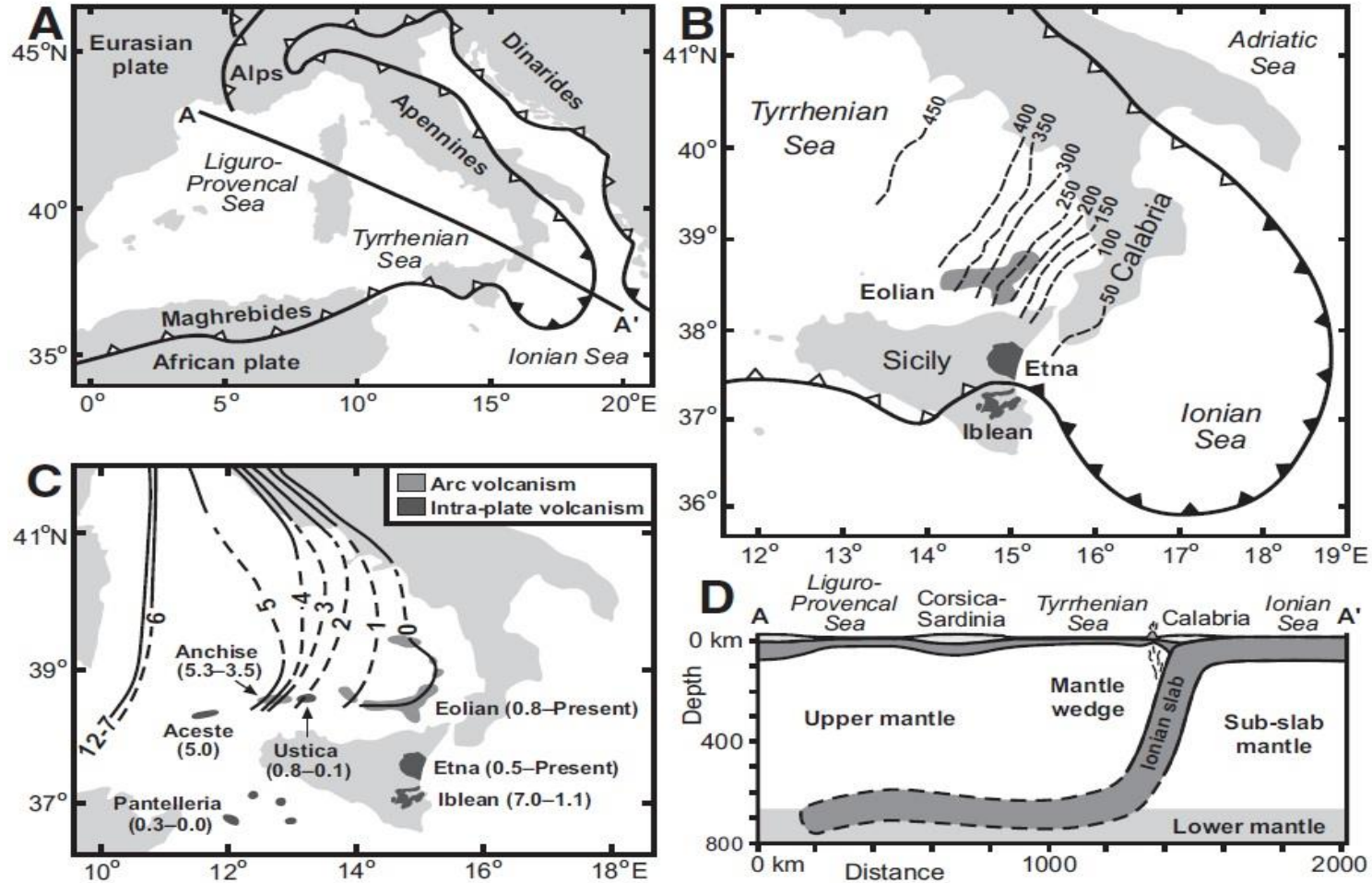
White dents = detachment of subducted slab
black dents = continuous slabs.

- In the Late Oligocene arc migration started from a location along the eastern margin of Iberia and southern France. The migrating trench system made contact with the north African continental margin in the Langhian (~15 Ma).
- In a second episode of extension starting at about 10 Ma, the extension continued with an eastward shift of activity, towards the Tyrrhenian realm.



Lig – Ligurian Sea, CR – Corsica, SA – Sardinia, Tyr – Tyrrhenian Sea, Io – Ionian Sea, AD – Adriatic Sea.

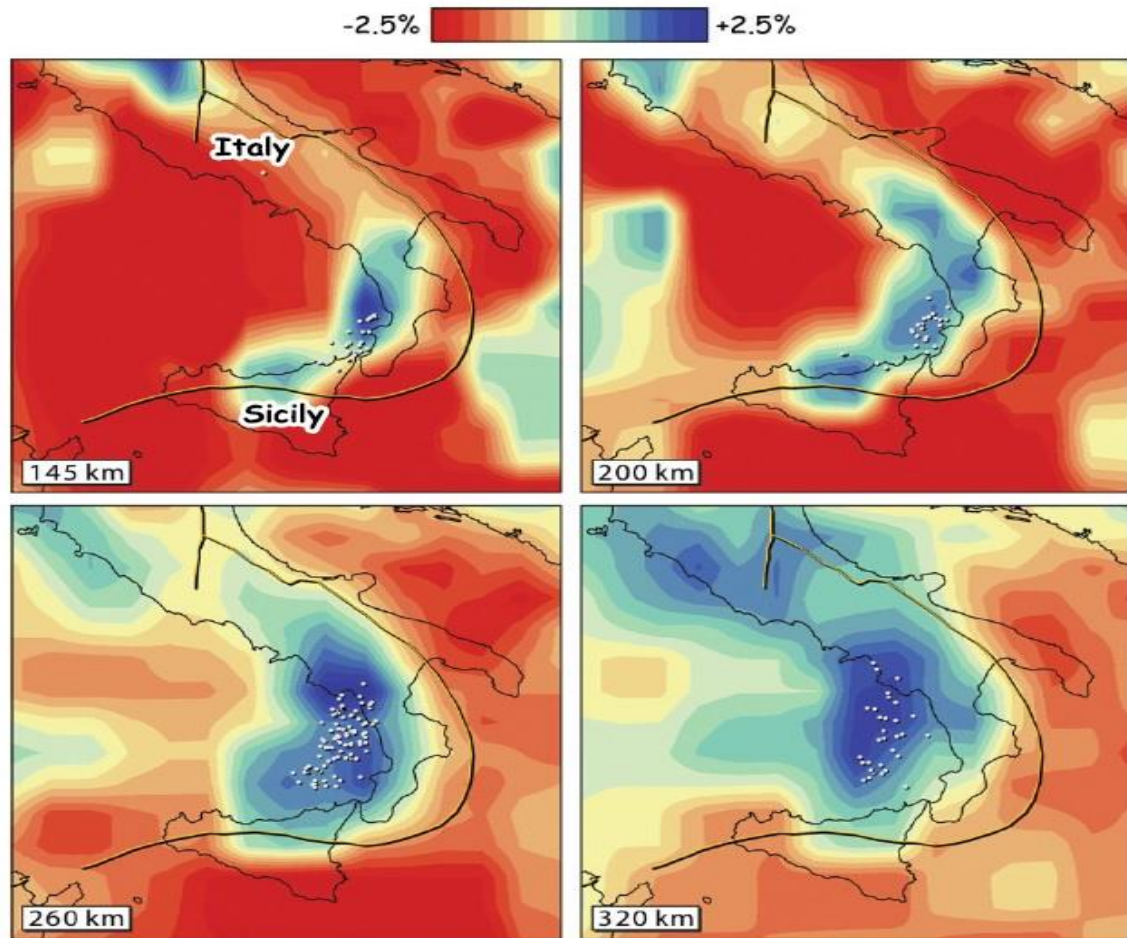
Mediterranean Tectonics



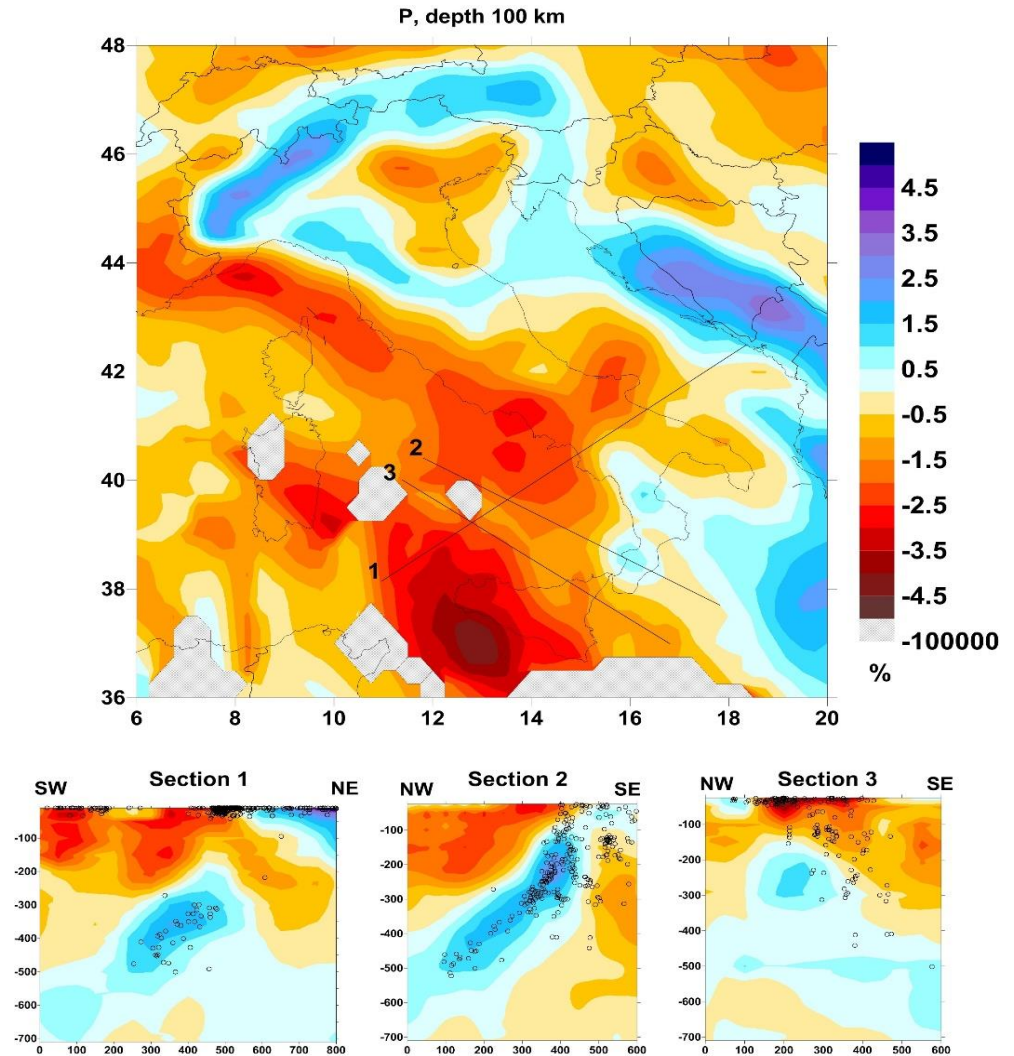
Schellart, 2010, GSA

- Reconstruction of the southern Apennines suggests a Late Miocene subduction rate of $\sim 30\text{--}50$ mm/year or perhaps higher.
- In Pliocene time, the southern Apennine trench encountered the continental Adriatic lithosphere and subduction ended by Quaternary time.
- Then, there was a rapid termination of subduction in the latter stages of continental margin subduction, which can be ascribed to slab break-off (e.g., slab delamination, slab tearing).
- The subduction remained limited to a narrow area (Ionian slab), whose east-directed fast rollback caused the opening of the Tyrrhenian and migration of magmatic arc with progressive time.

Slab subduction and back-arc basin in the Tyrrhenian domain



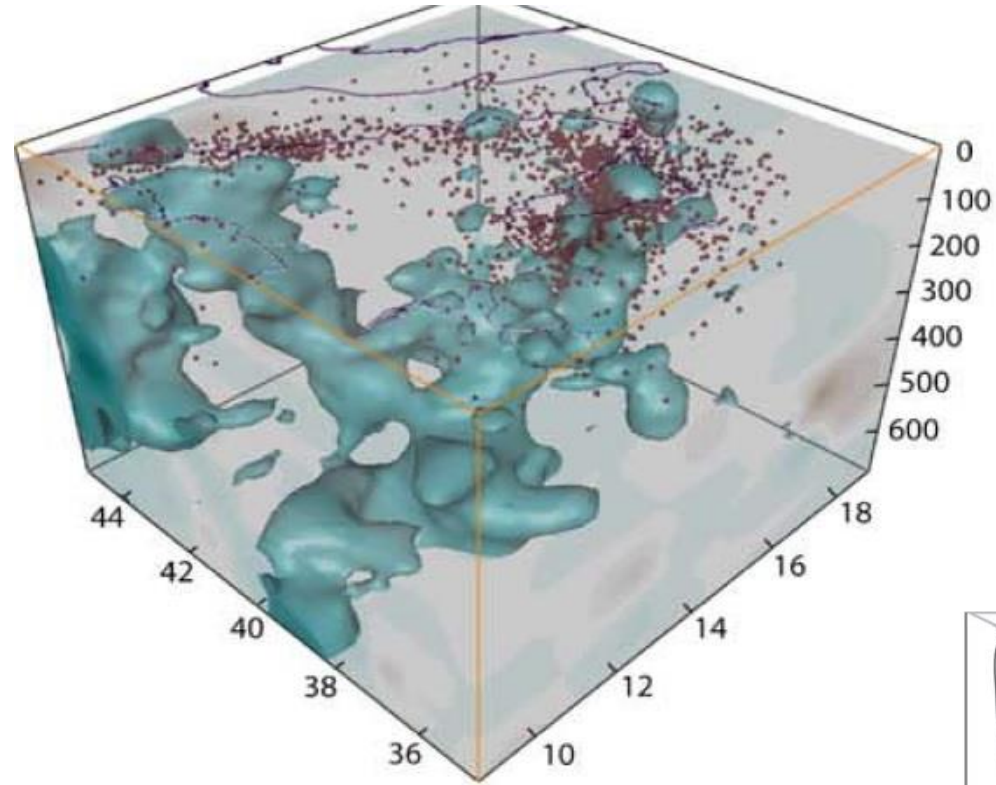
Bijwaard and Spakman, 2000, JGR



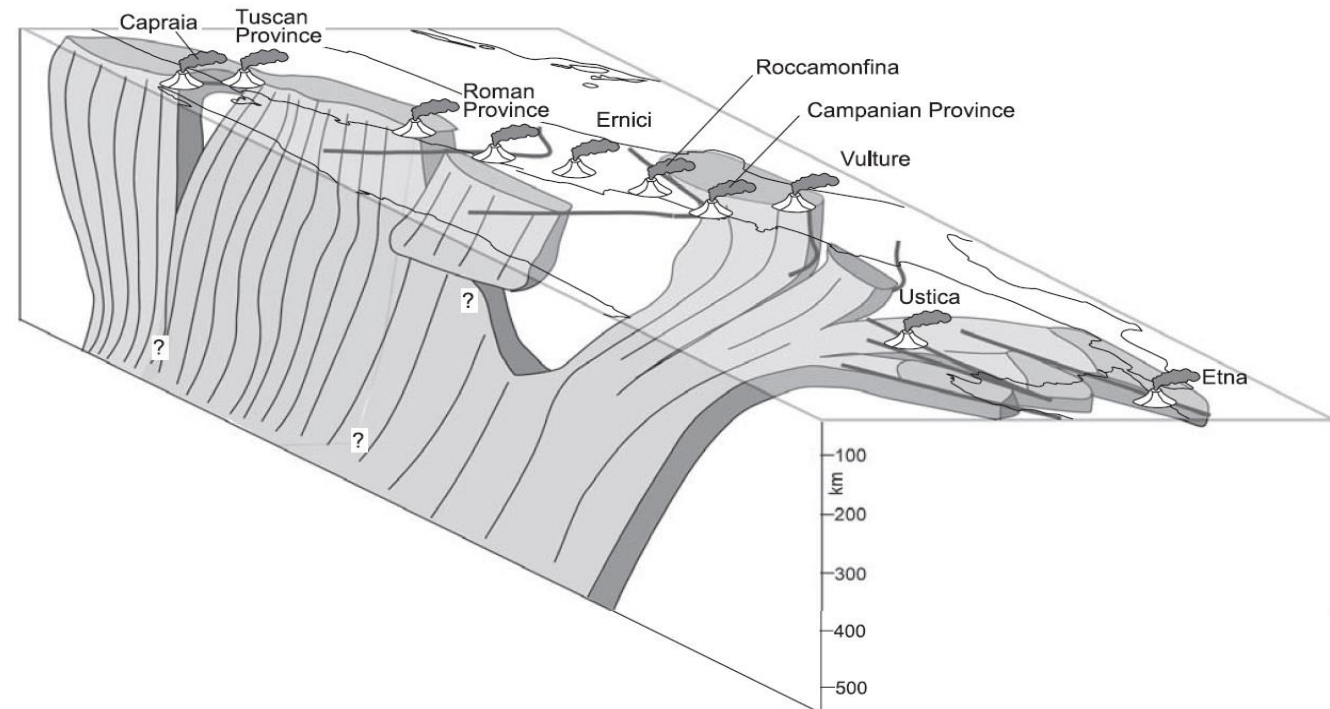
Koulakov et al., 2009, GJI

- The seismic velocity distribution shows evidence for the absence of high velocity slab material, and hence for slab detachment, below the north African margin and the central Apennines in the ~100–300 km depth range.

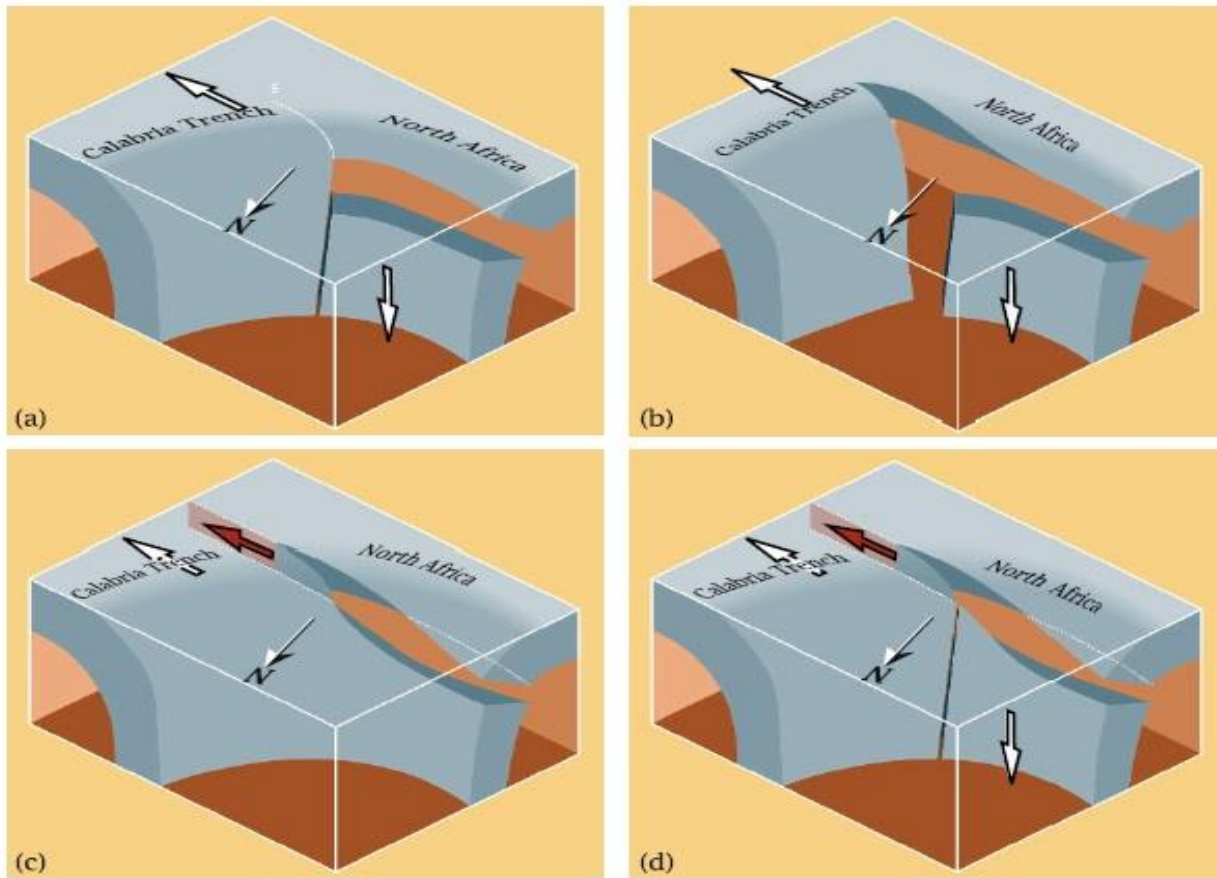
Slab Geometry in 3D



- Seismic tomography results show gaps within the subducting lithosphere, which are interpreted as deep subvertical tear faults.
- The development of such tear faults is consistent with proposed kinematic reconstructions, in which different rates of subduction rollback affected different parts of the subduction zone.
- There is a possible link between the development of tear faults and the occurrence of regional magmatic activity with transitional geochemical signatures between arc type and intraplate oceanic island basalts (OIB) type, associated with slab tearing and slab breakoff.



Slab geometry interpretation: formation of a Subduction-Transform-Edge-Propagator (STEP) fault



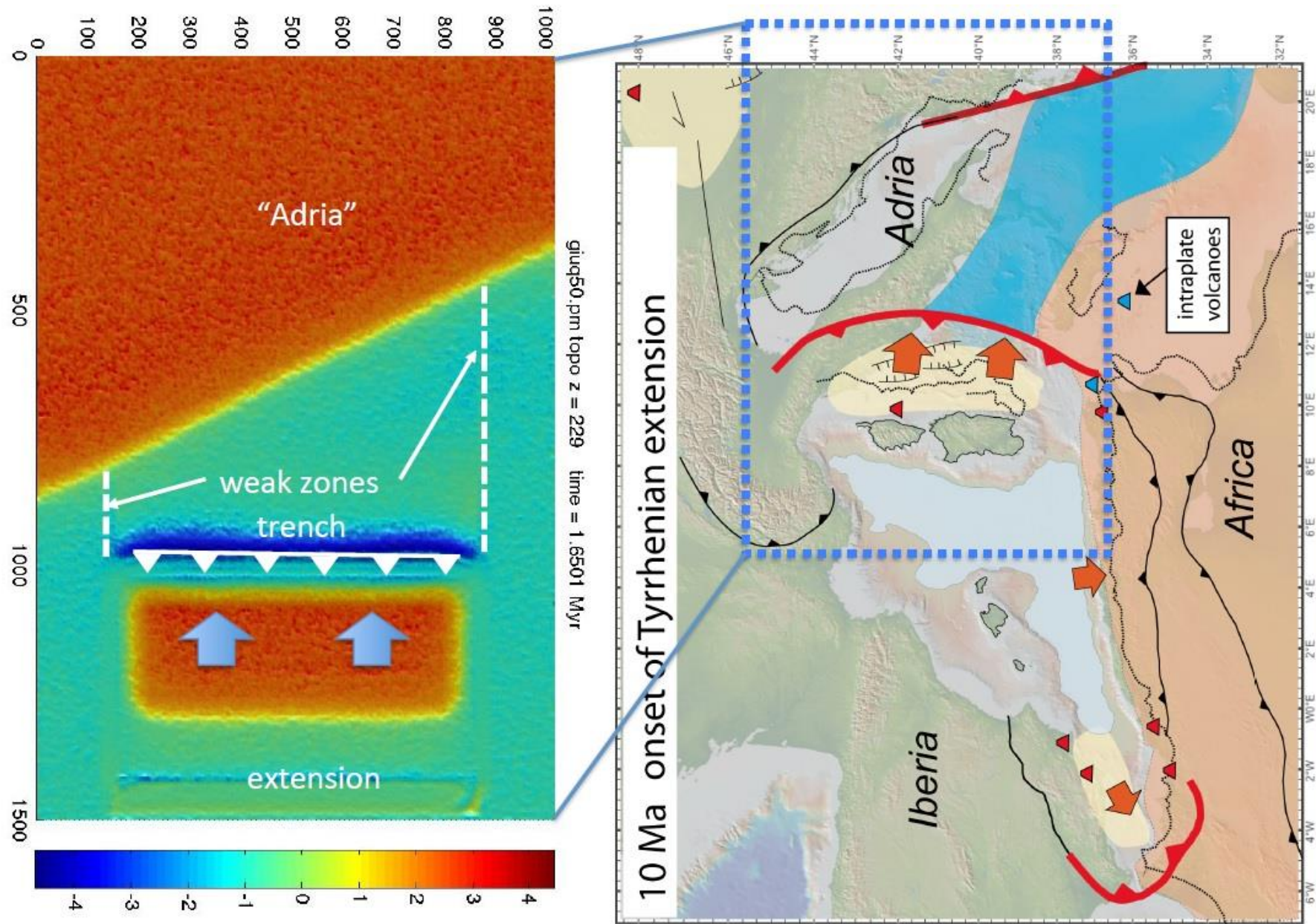
Wortel et al., 2009

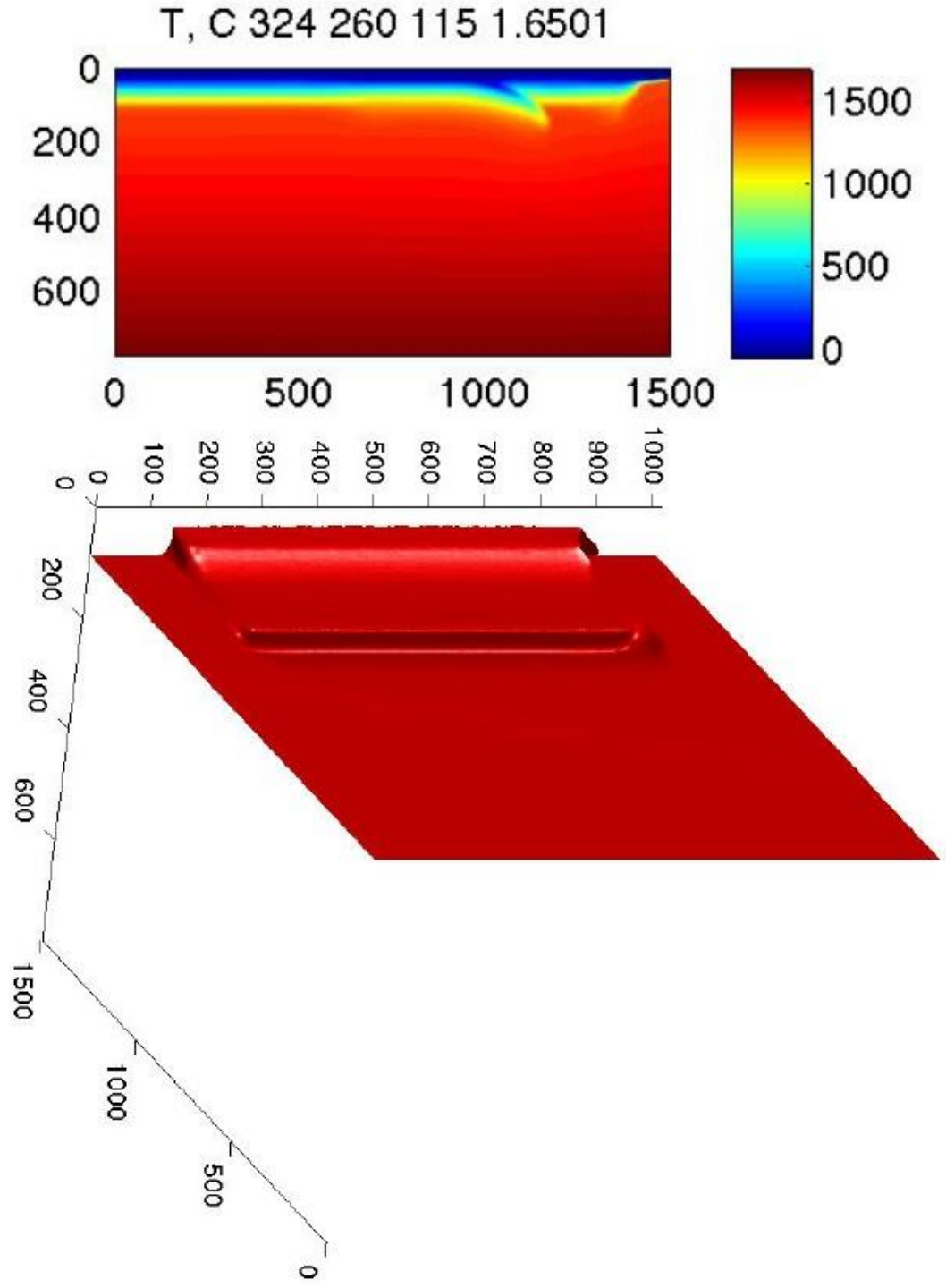
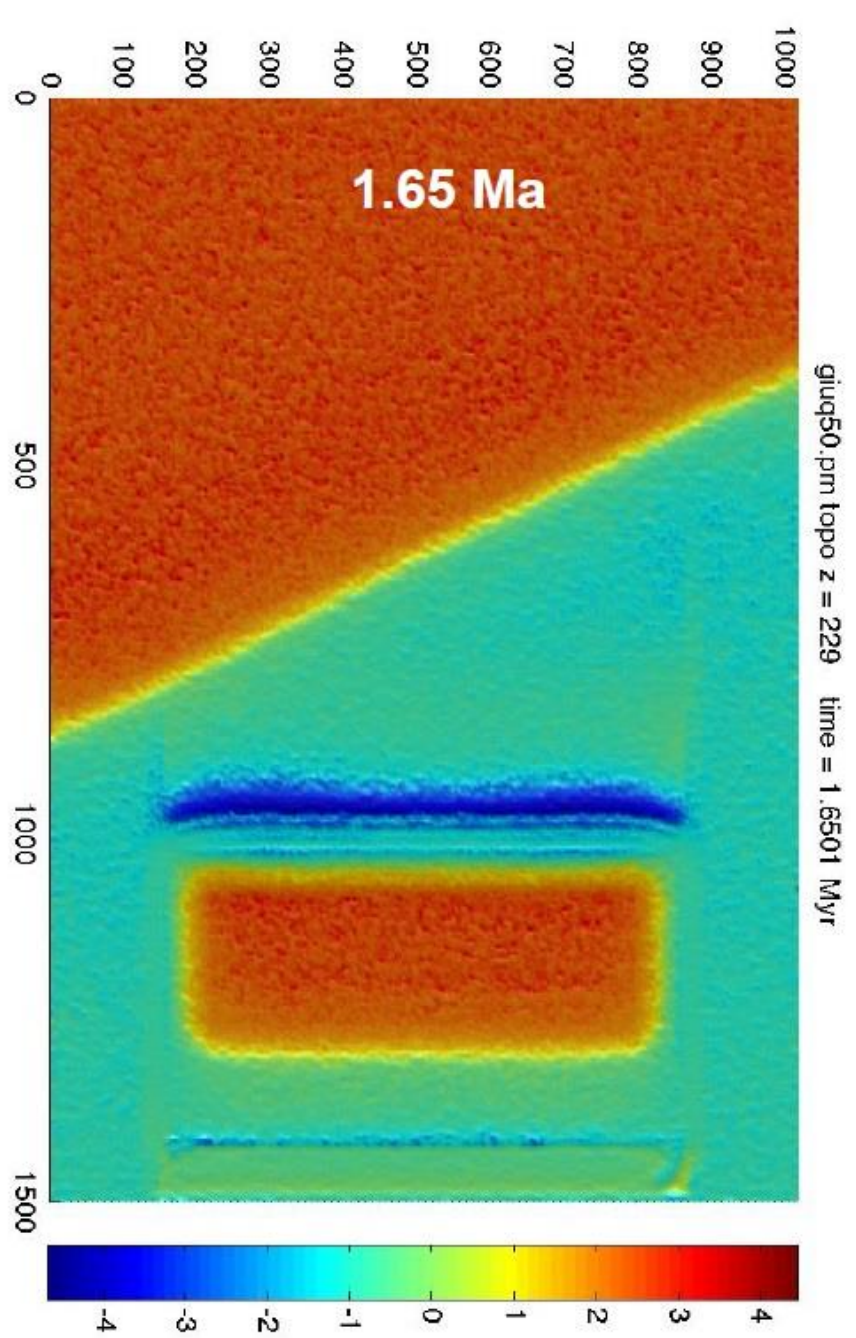
Plate boundary evolved through:

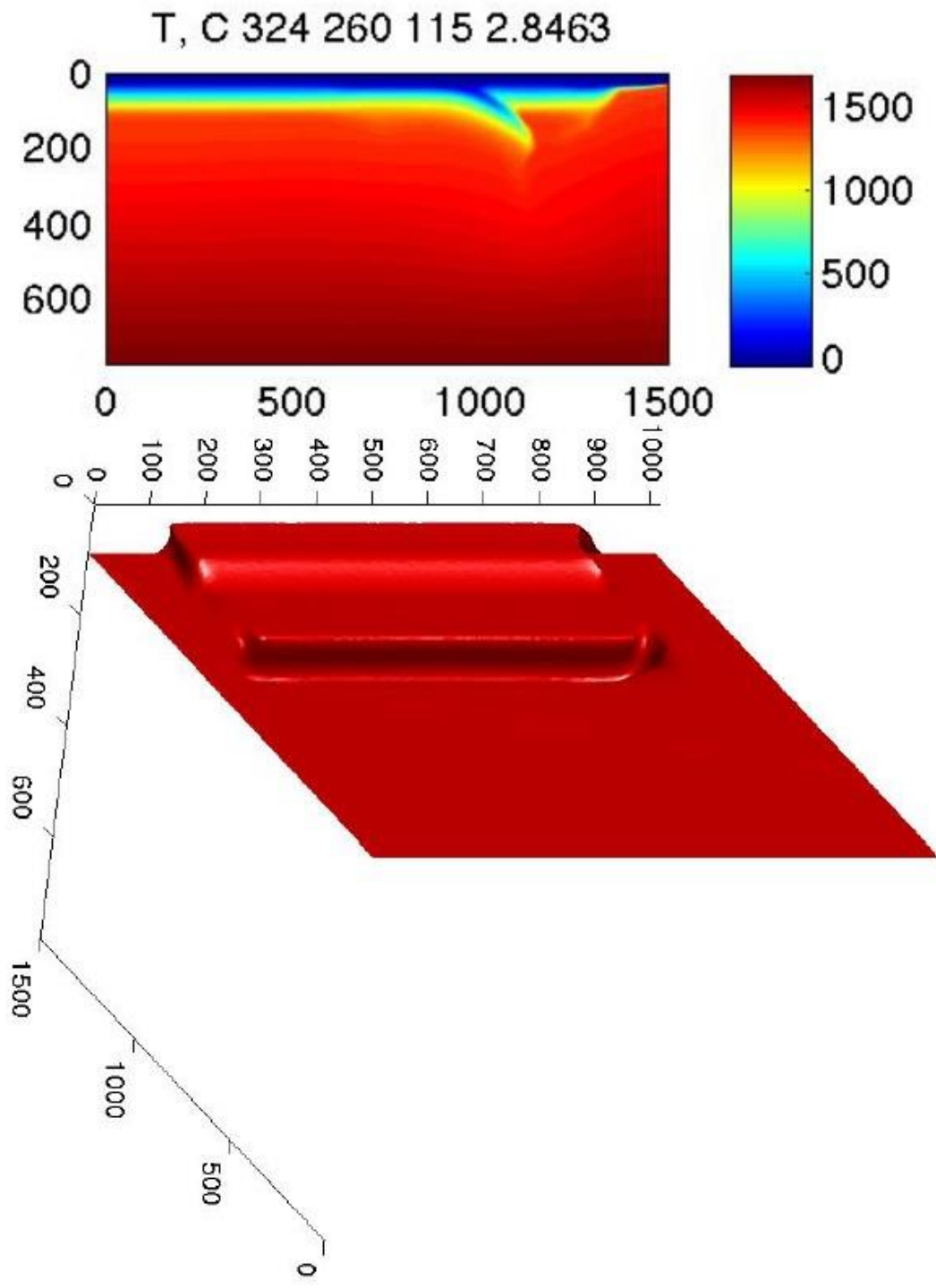
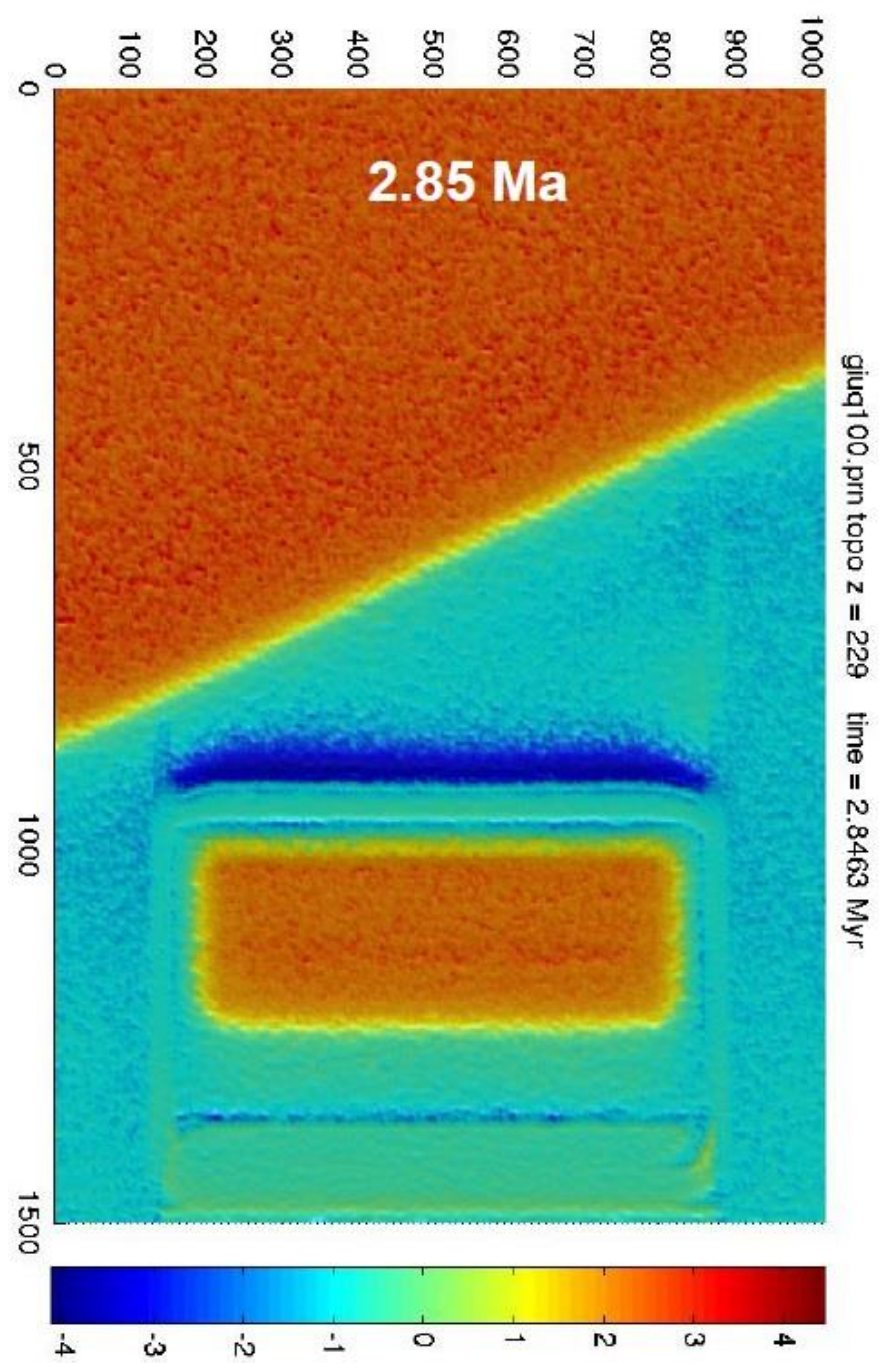
(1) Continental collision ("soft", in the north African case); (2) Slab detachment; (3) Formation of a vertical tear, which laterally separates the detached part of the slab from the adjacent still continuous part of the subducted slab; (4) Formation of a STEP fault and retreat of the continuous segment of the slab; (5) Back-arc extension.

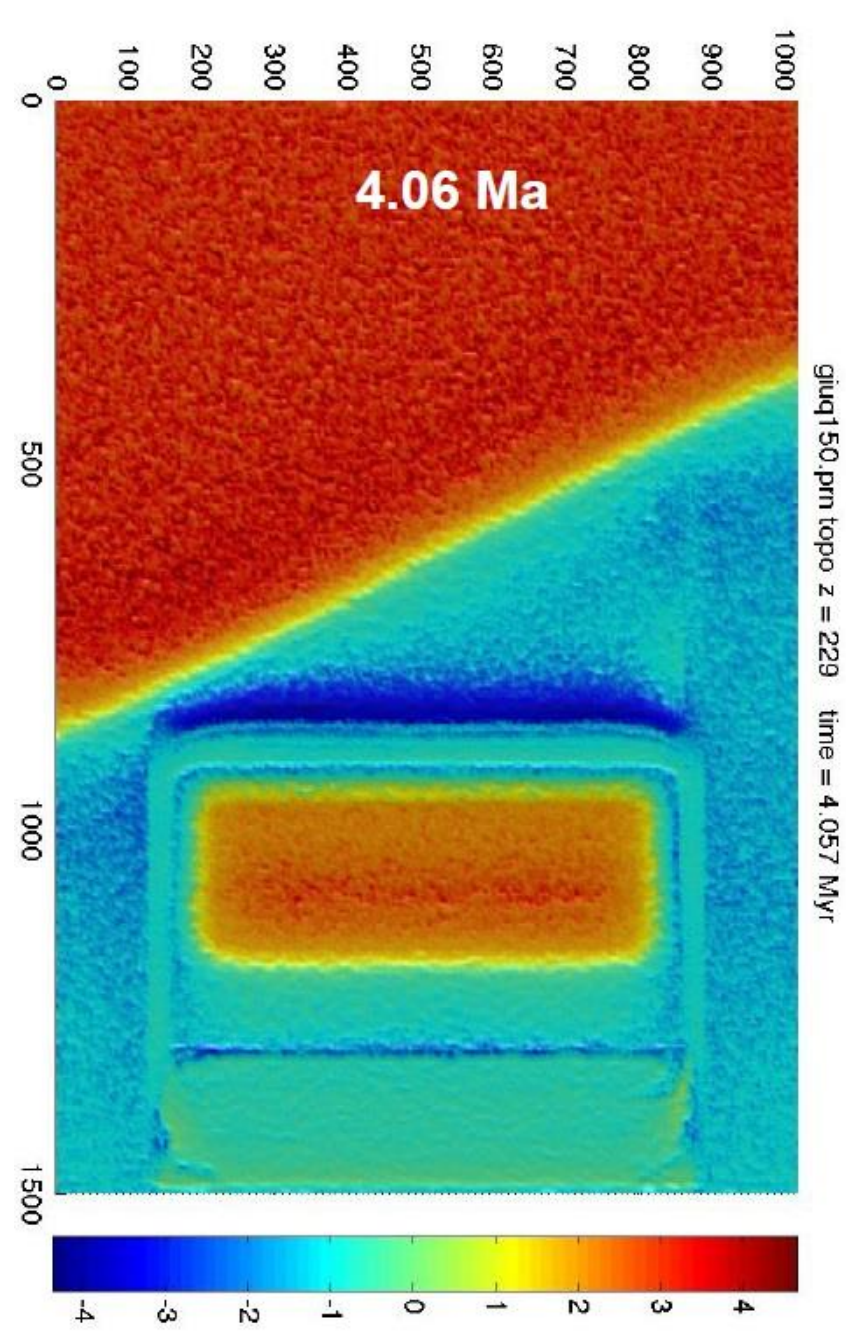
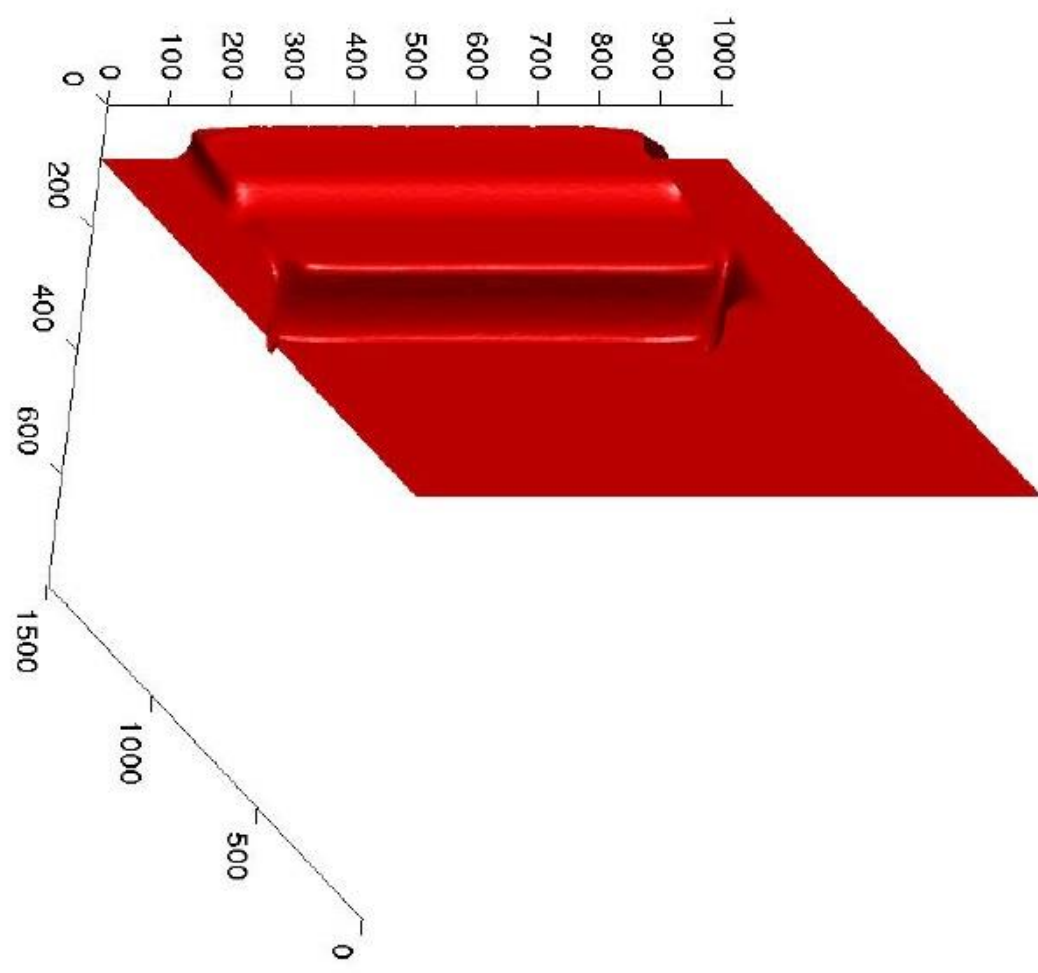
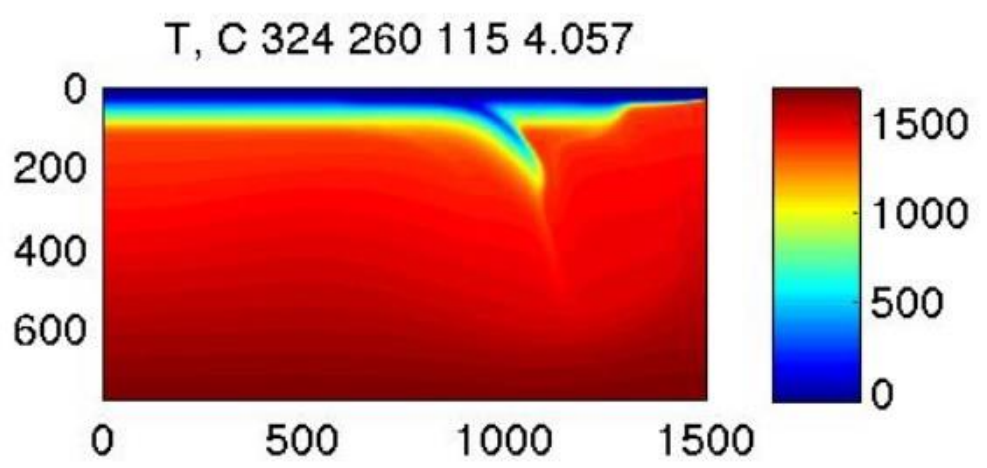
- The STEP is formed by the action of the slab pull acting on the continuous slab, around the edge of which the mantle material flows and accommodates the roll back.
- Another possibility for the STEP formation is the rotation of the detachment fault in the subducted slab towards an approximately vertical orientation (case c-d)

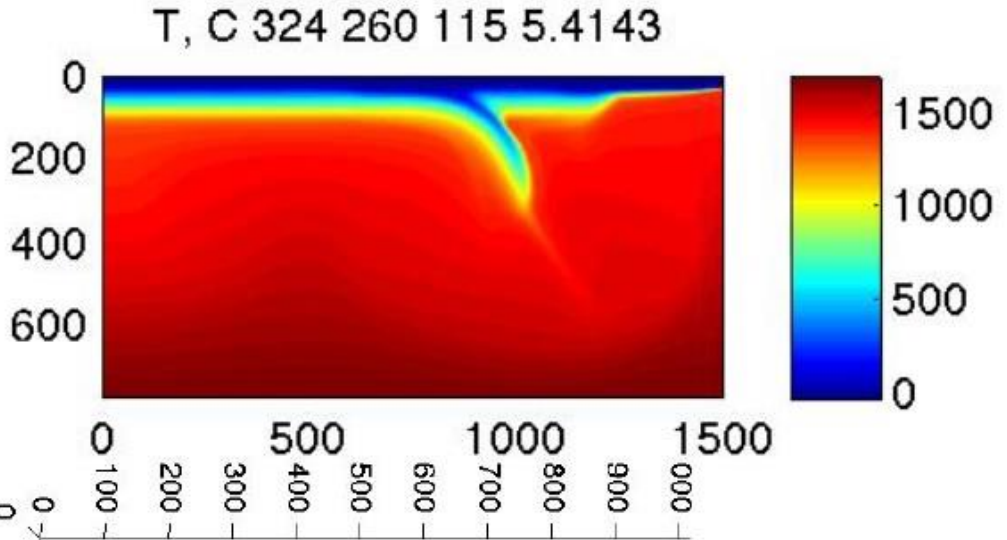
Numerical models simulate the slab tearing



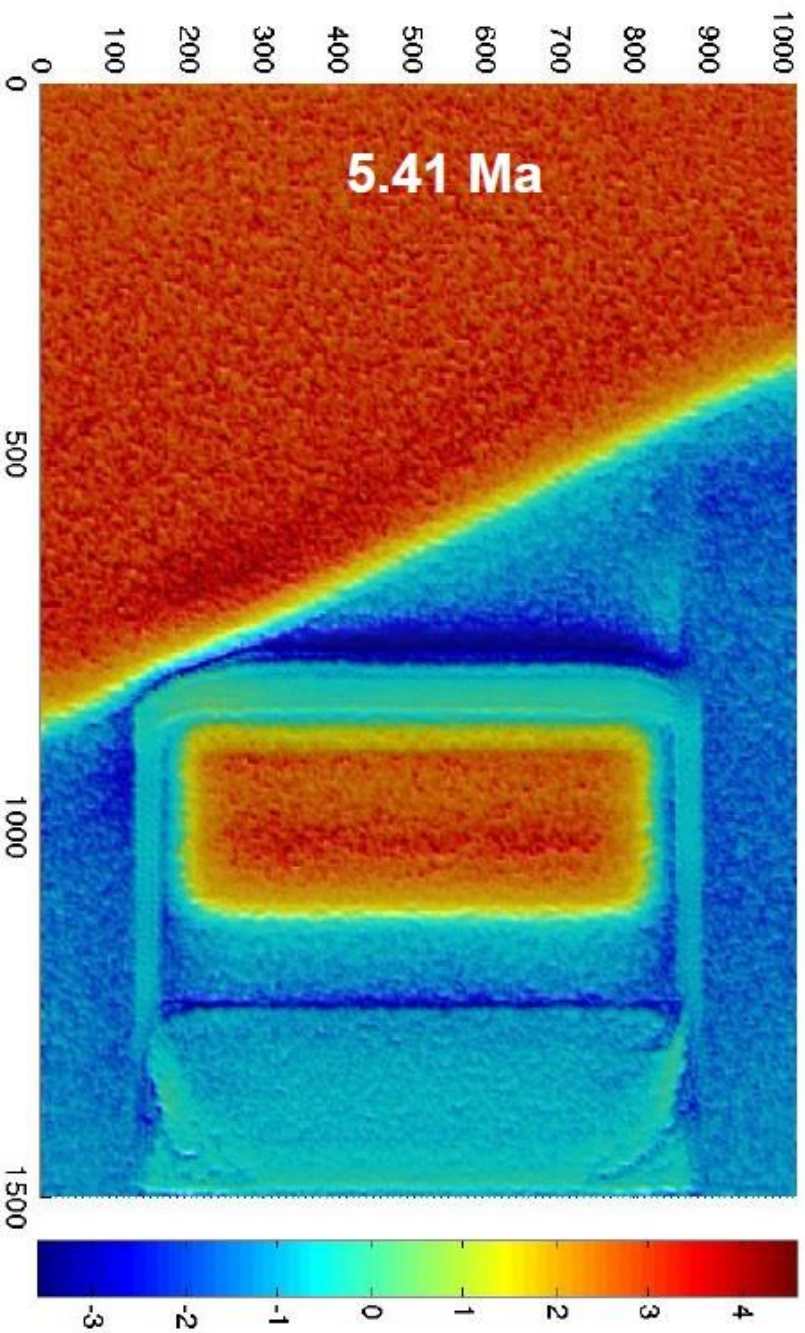


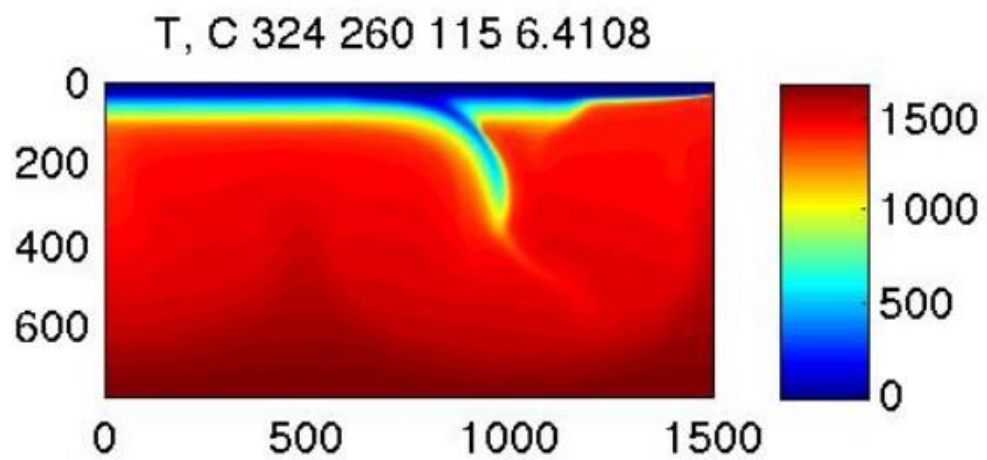




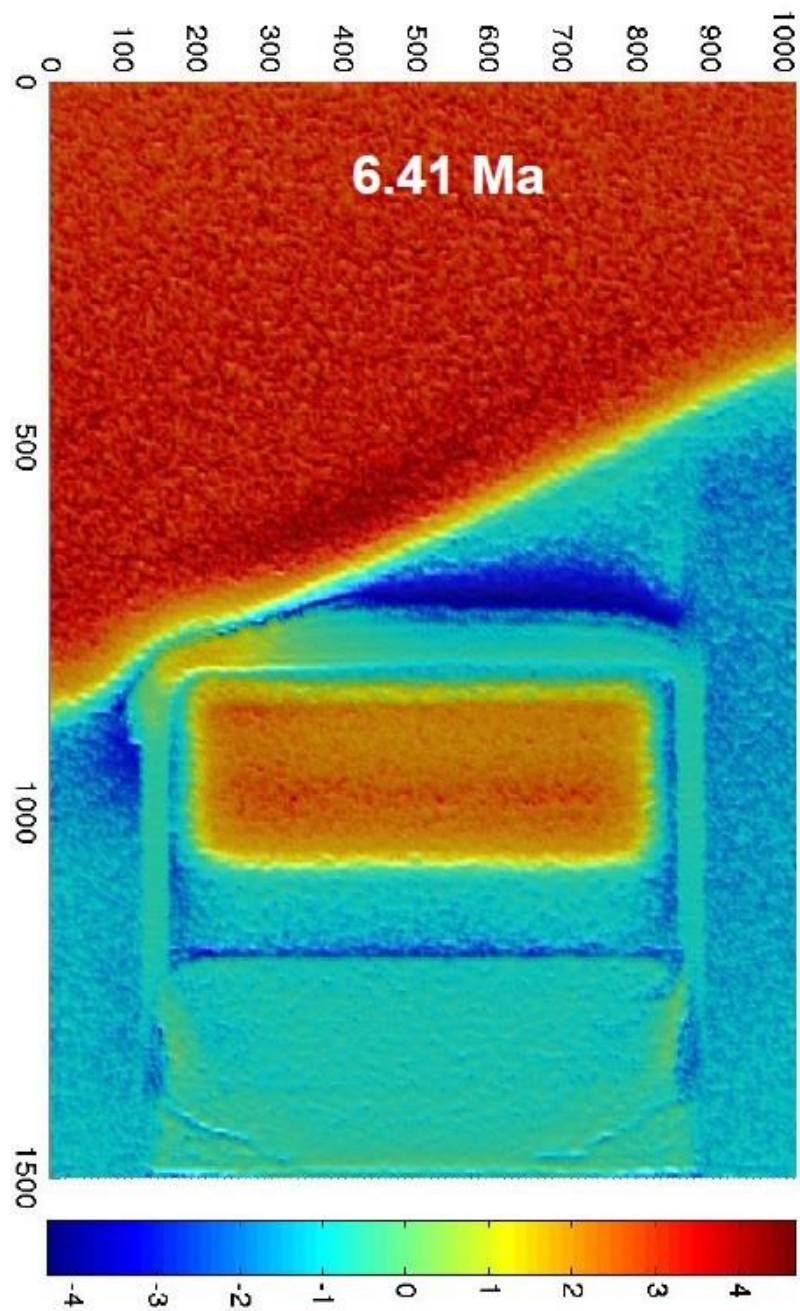
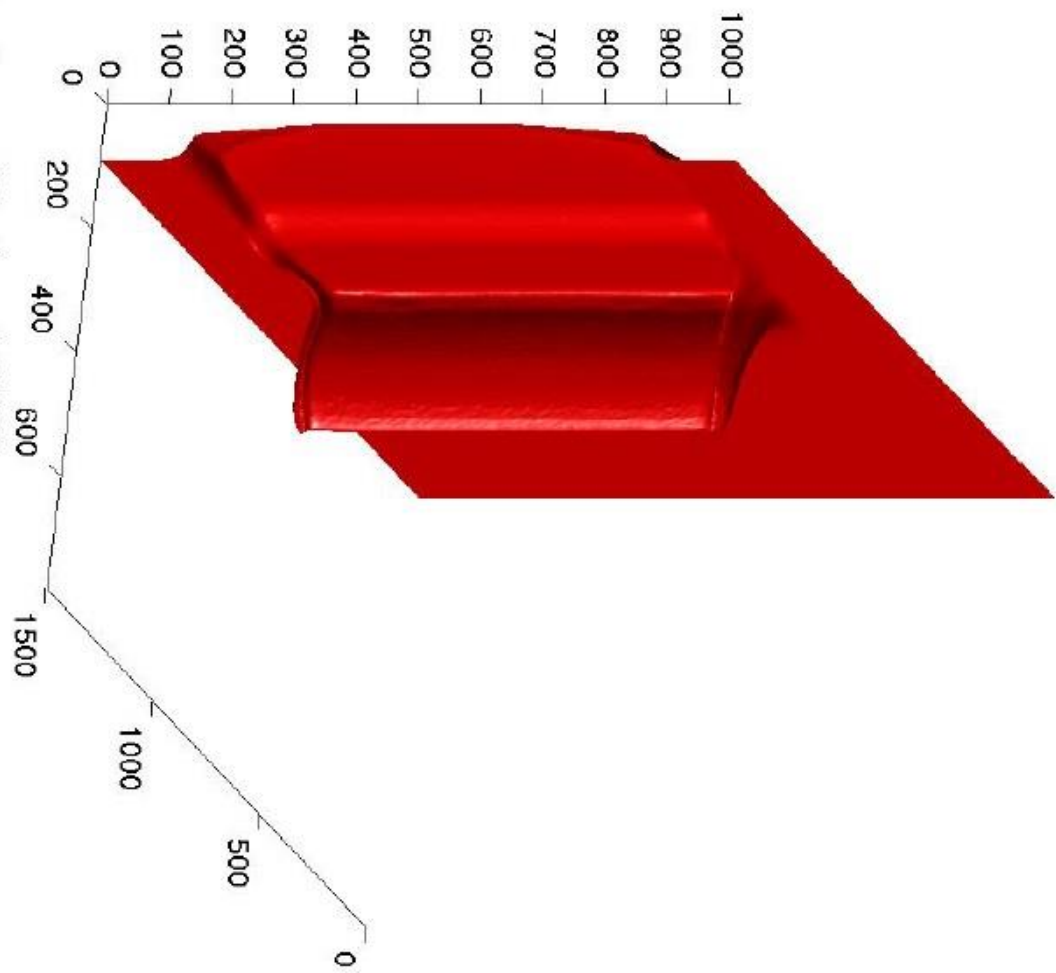


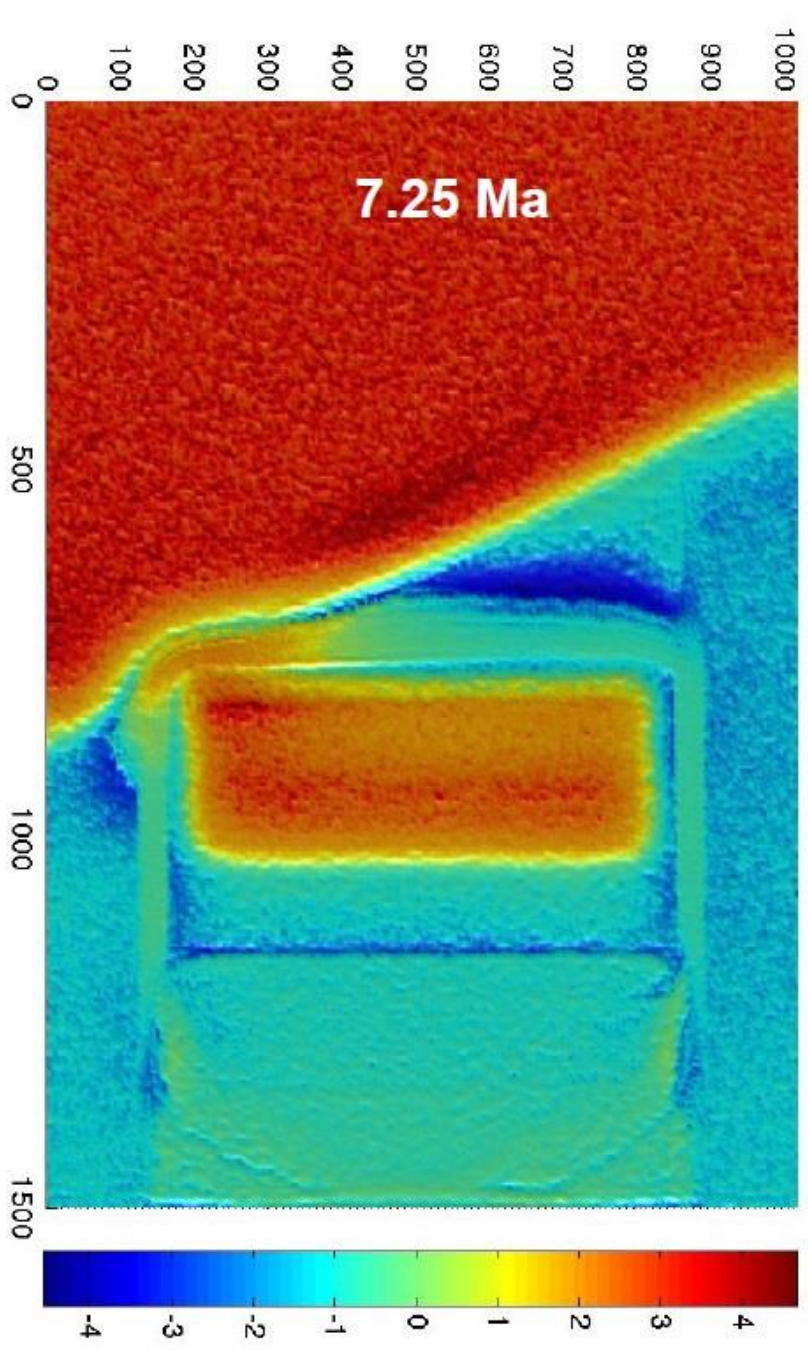
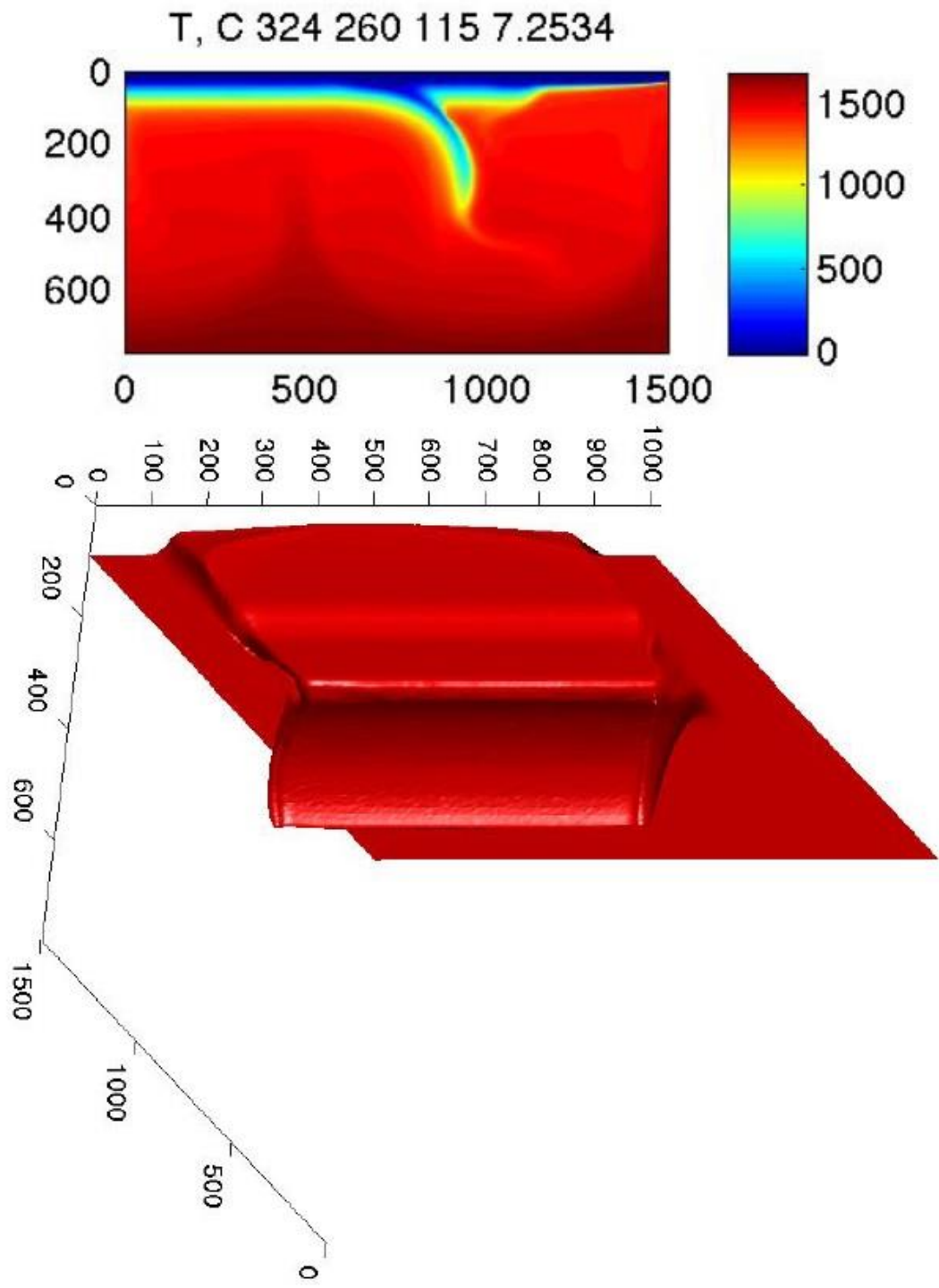
giuga50.prm topo z = 229 time = 5.4143 Myr

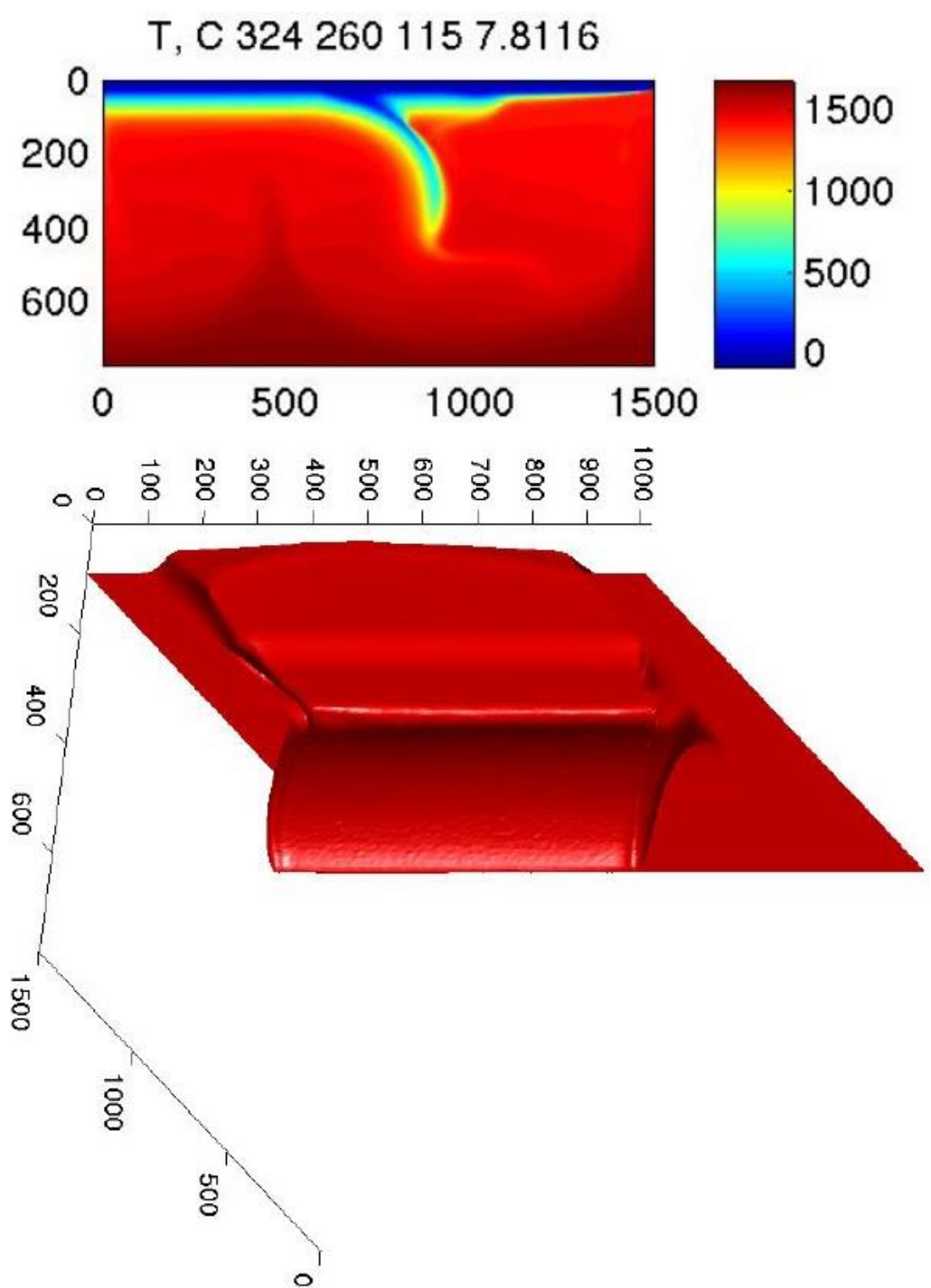
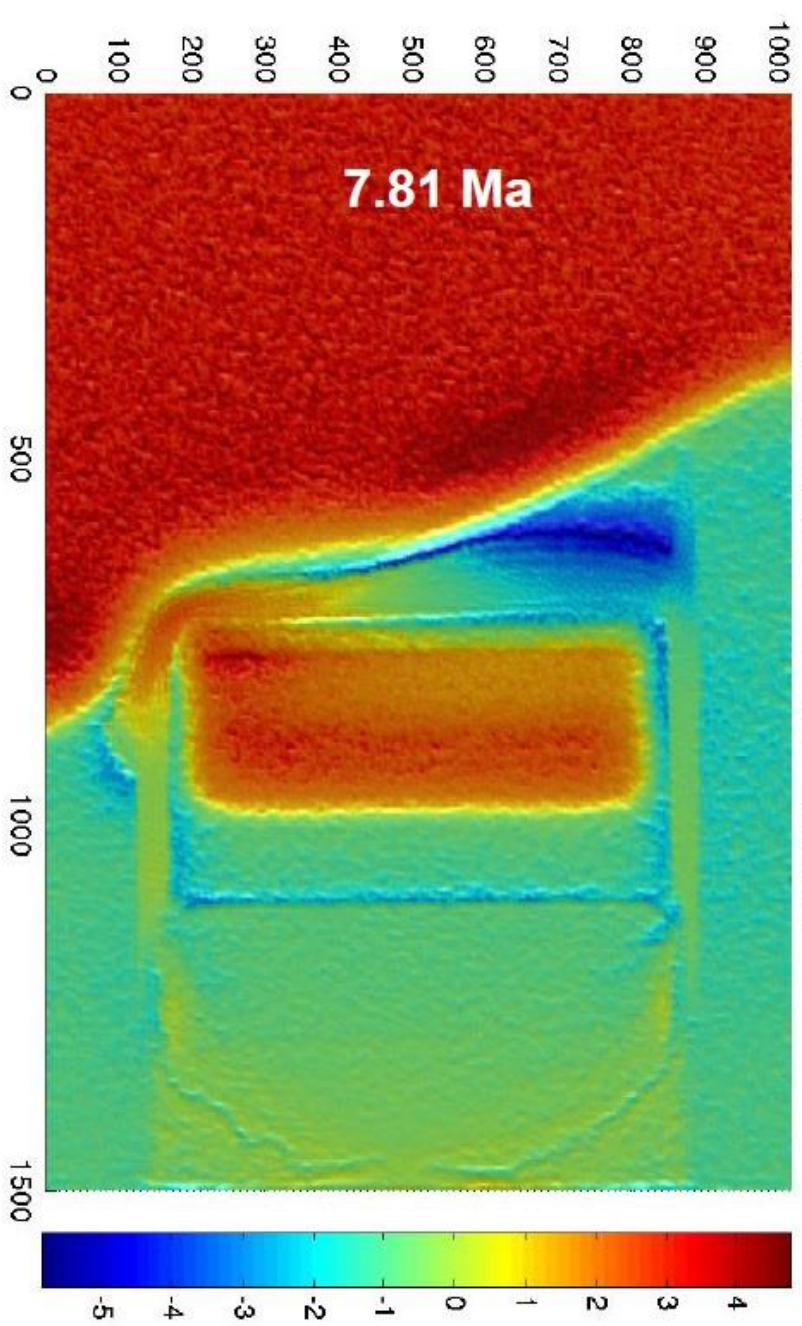


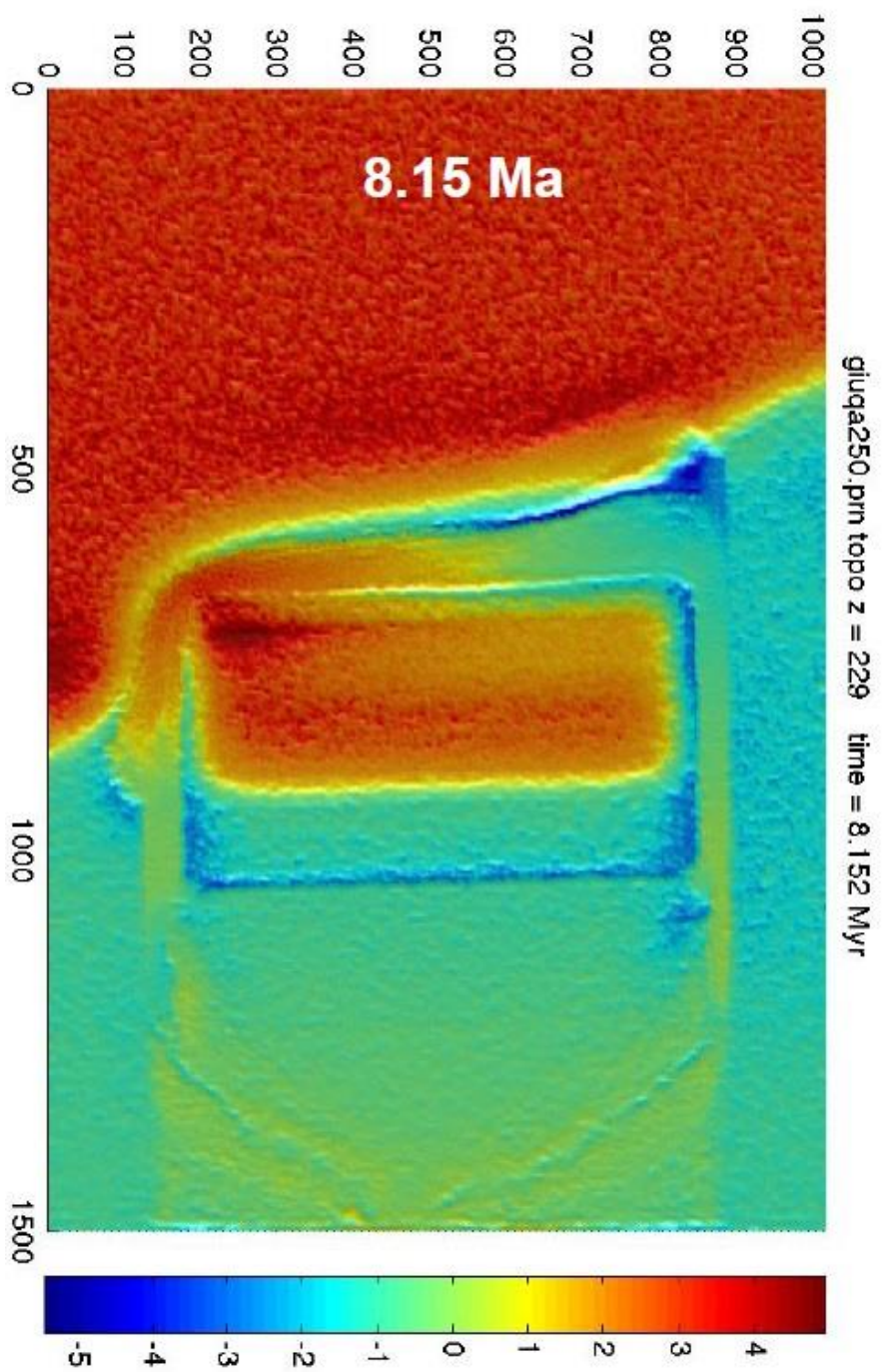
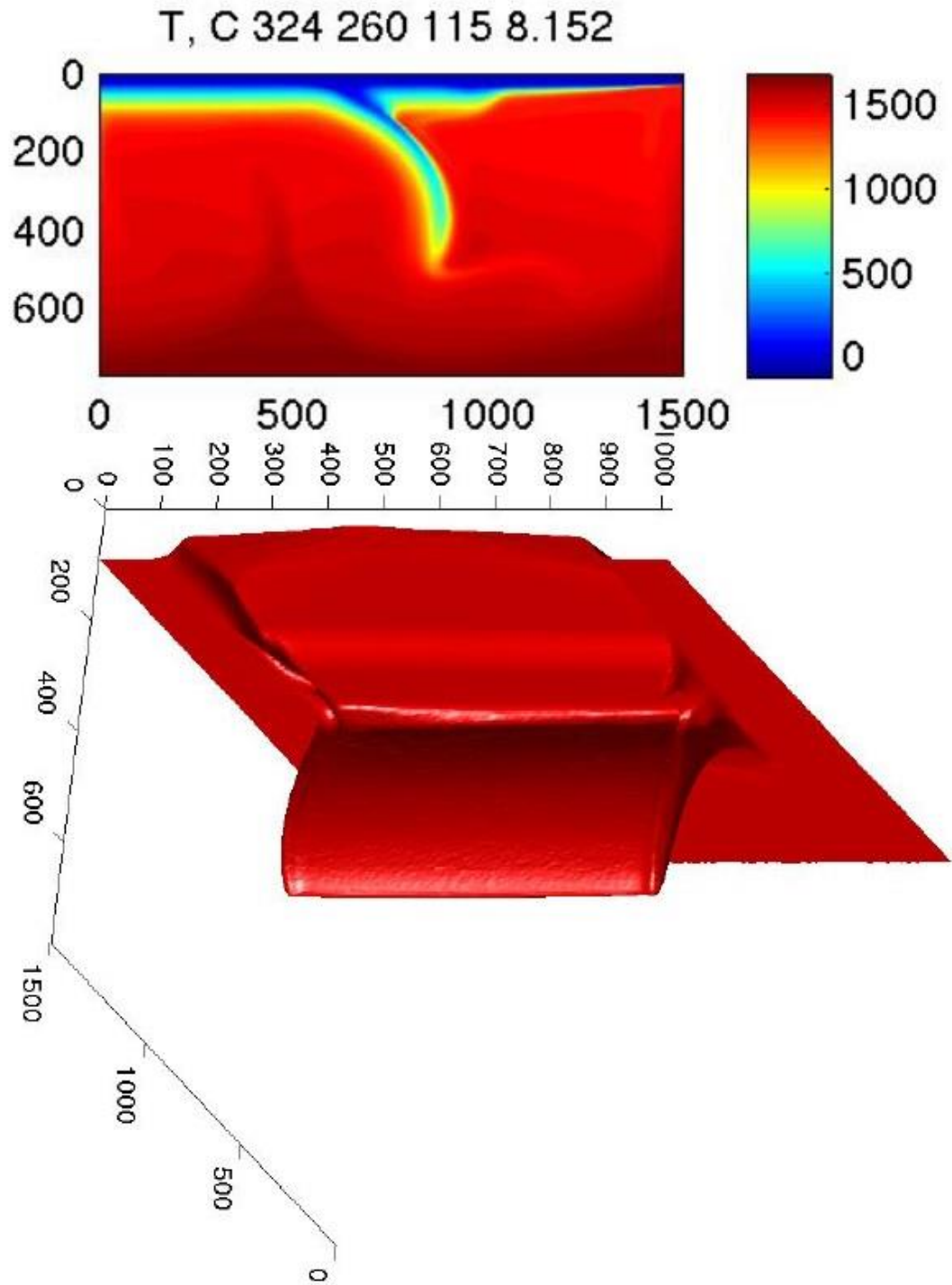


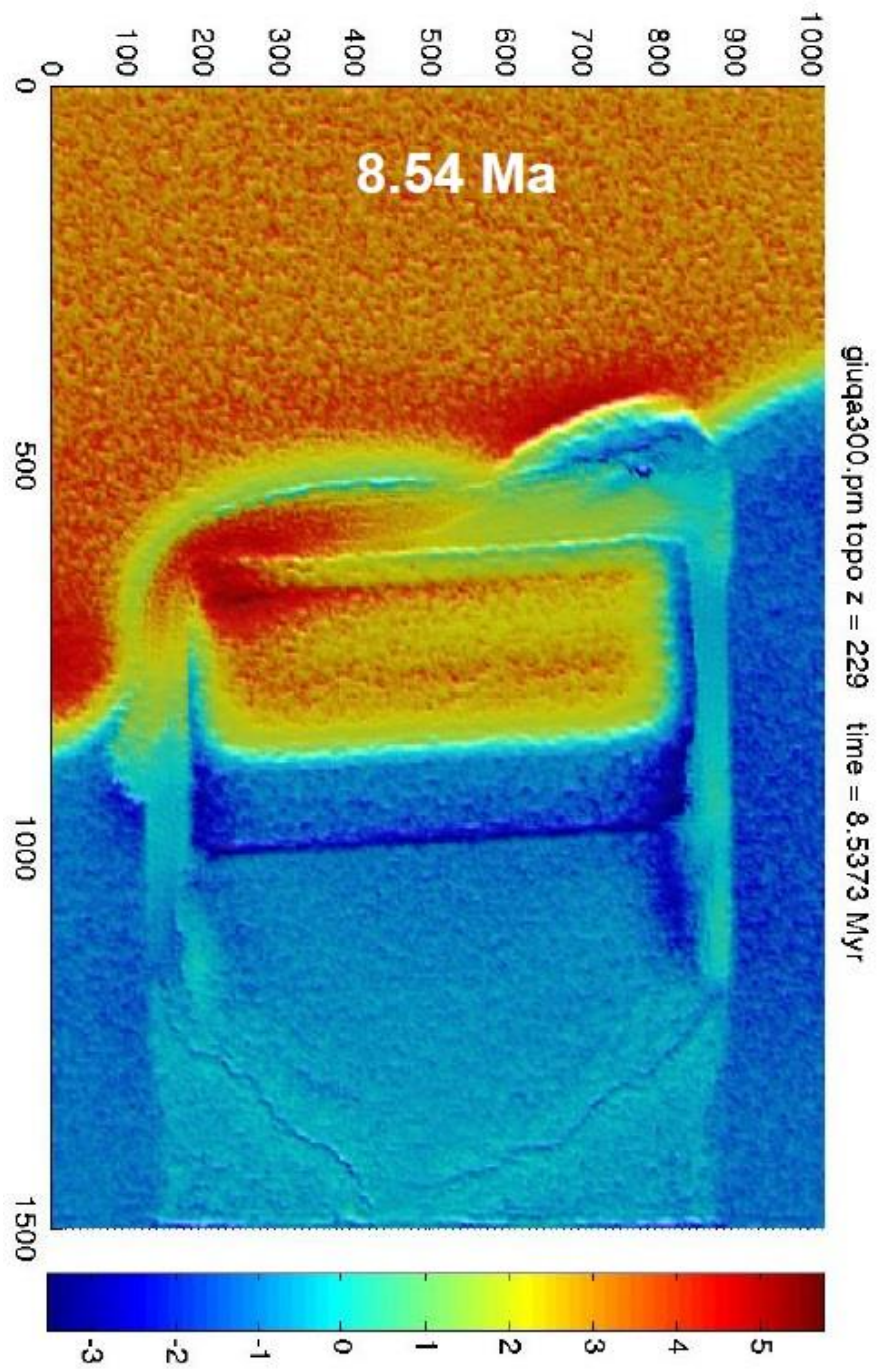
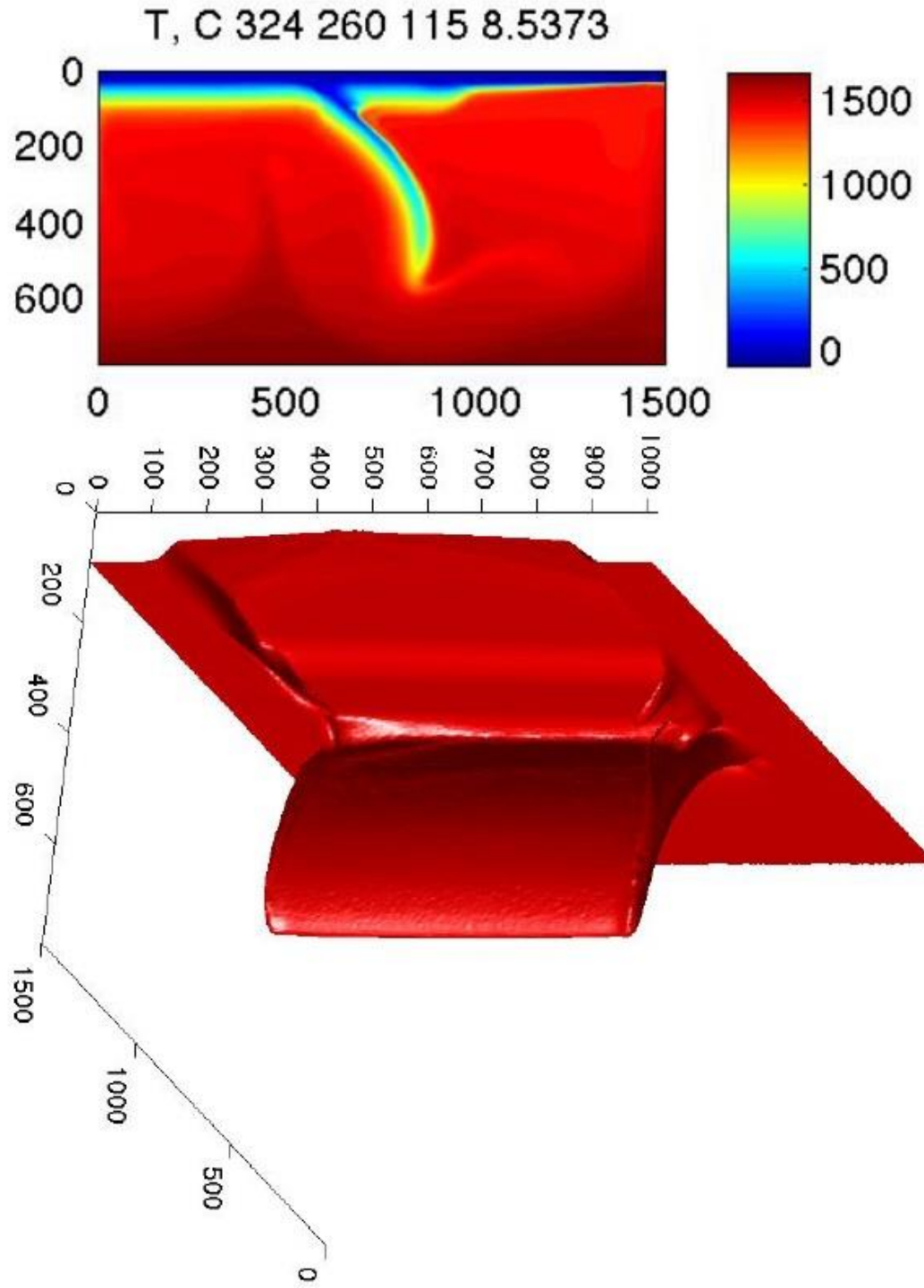
glua100.prm topo z = 229 time = 6.4108 Myr

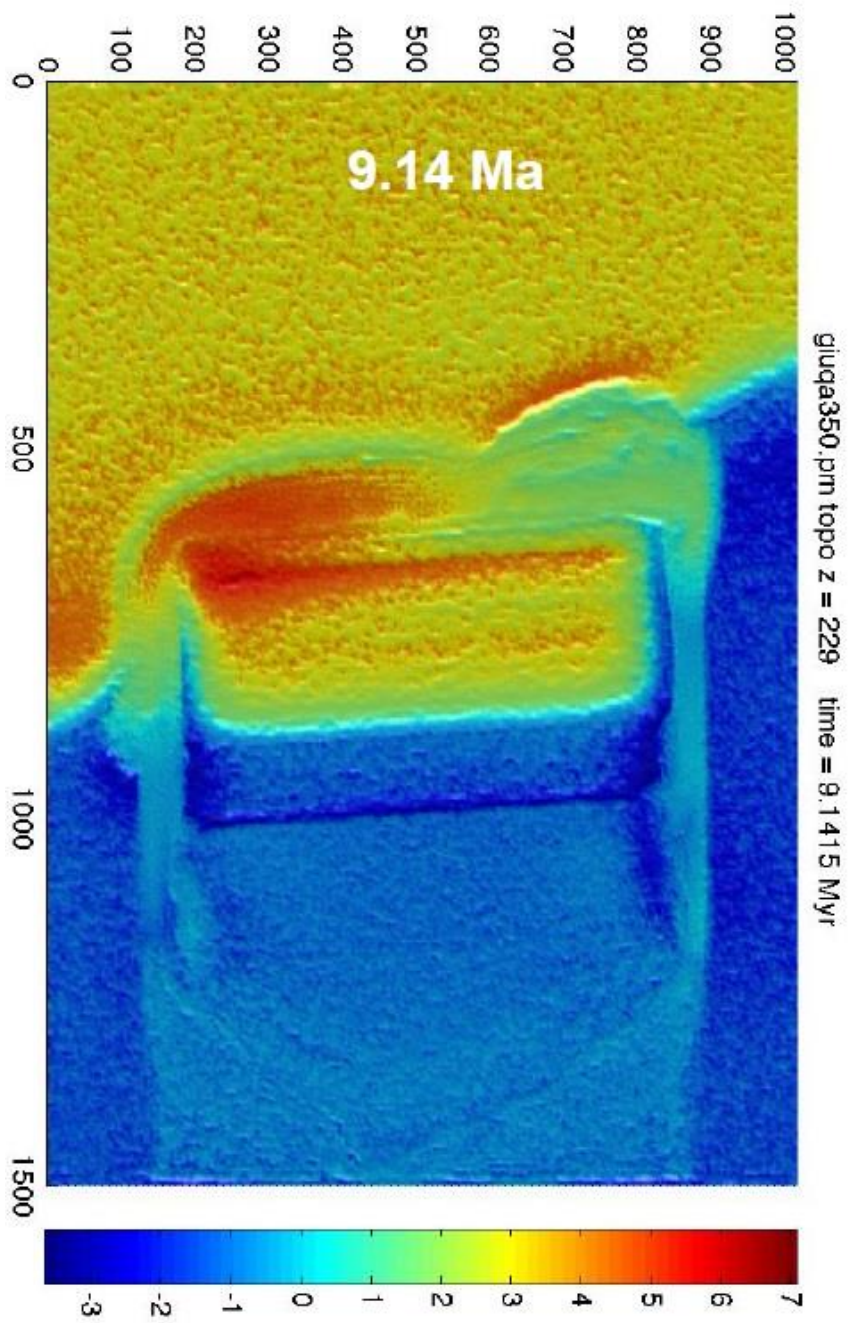
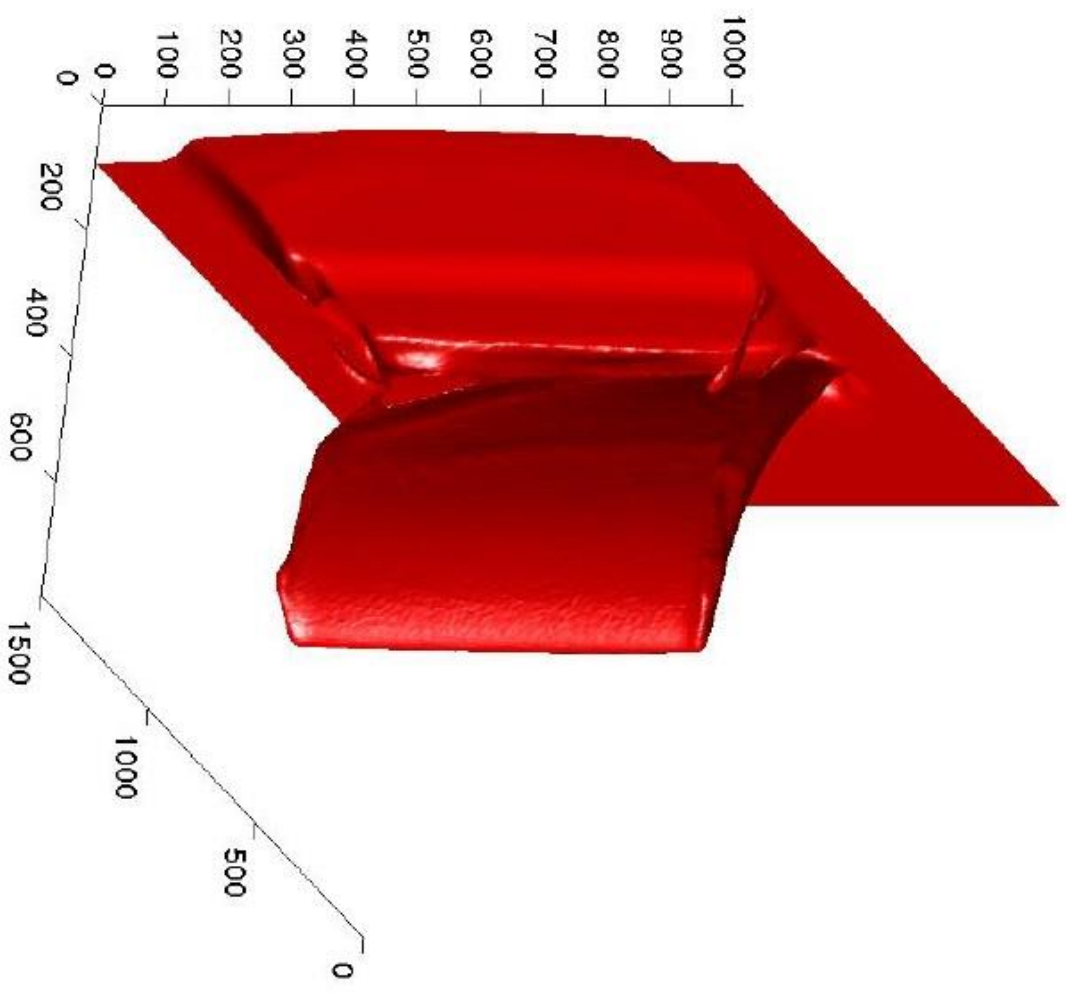
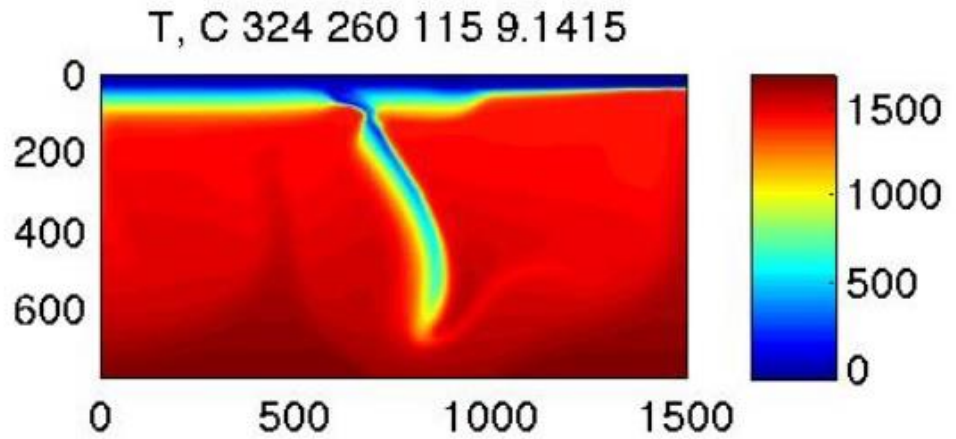


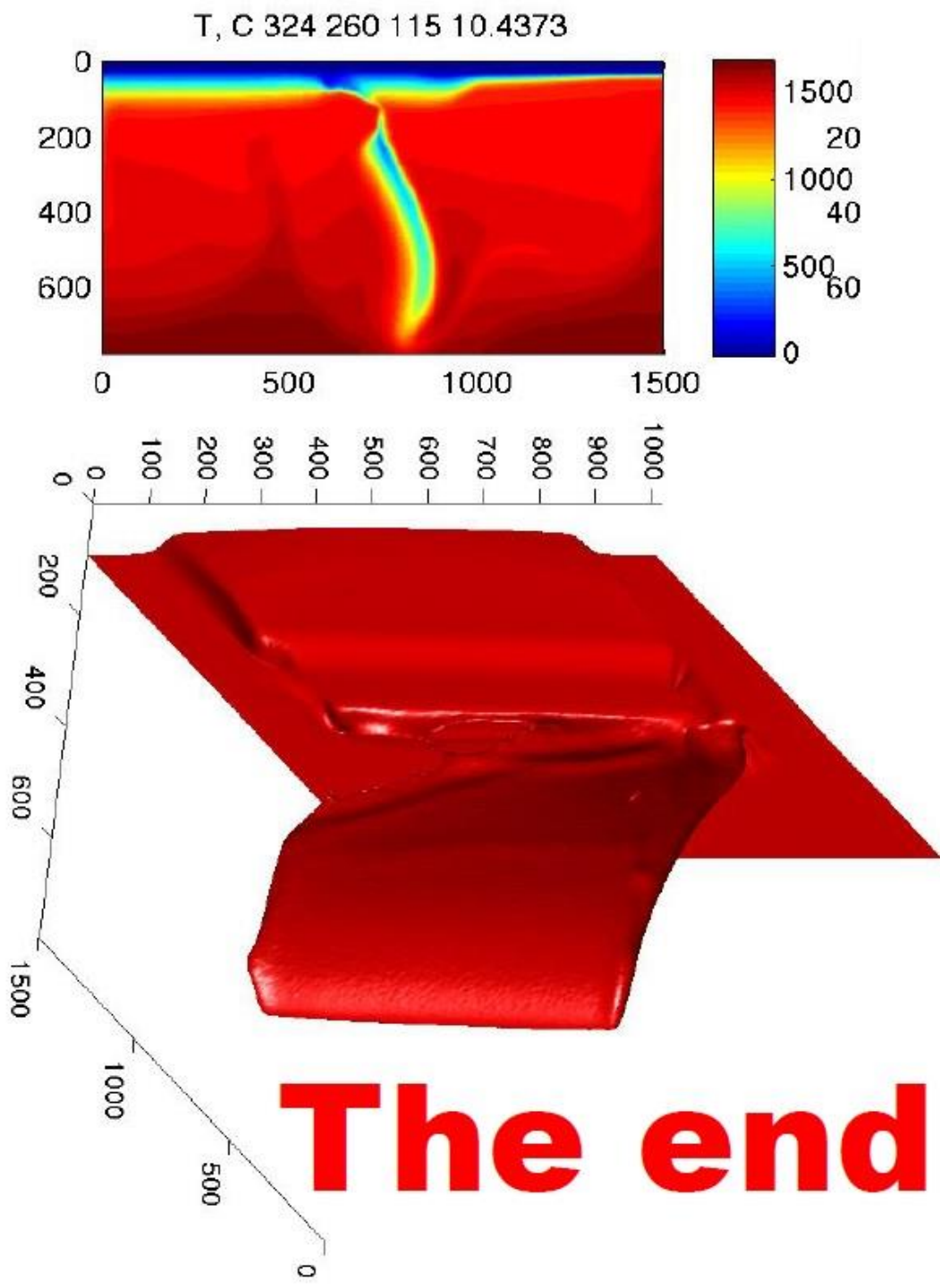
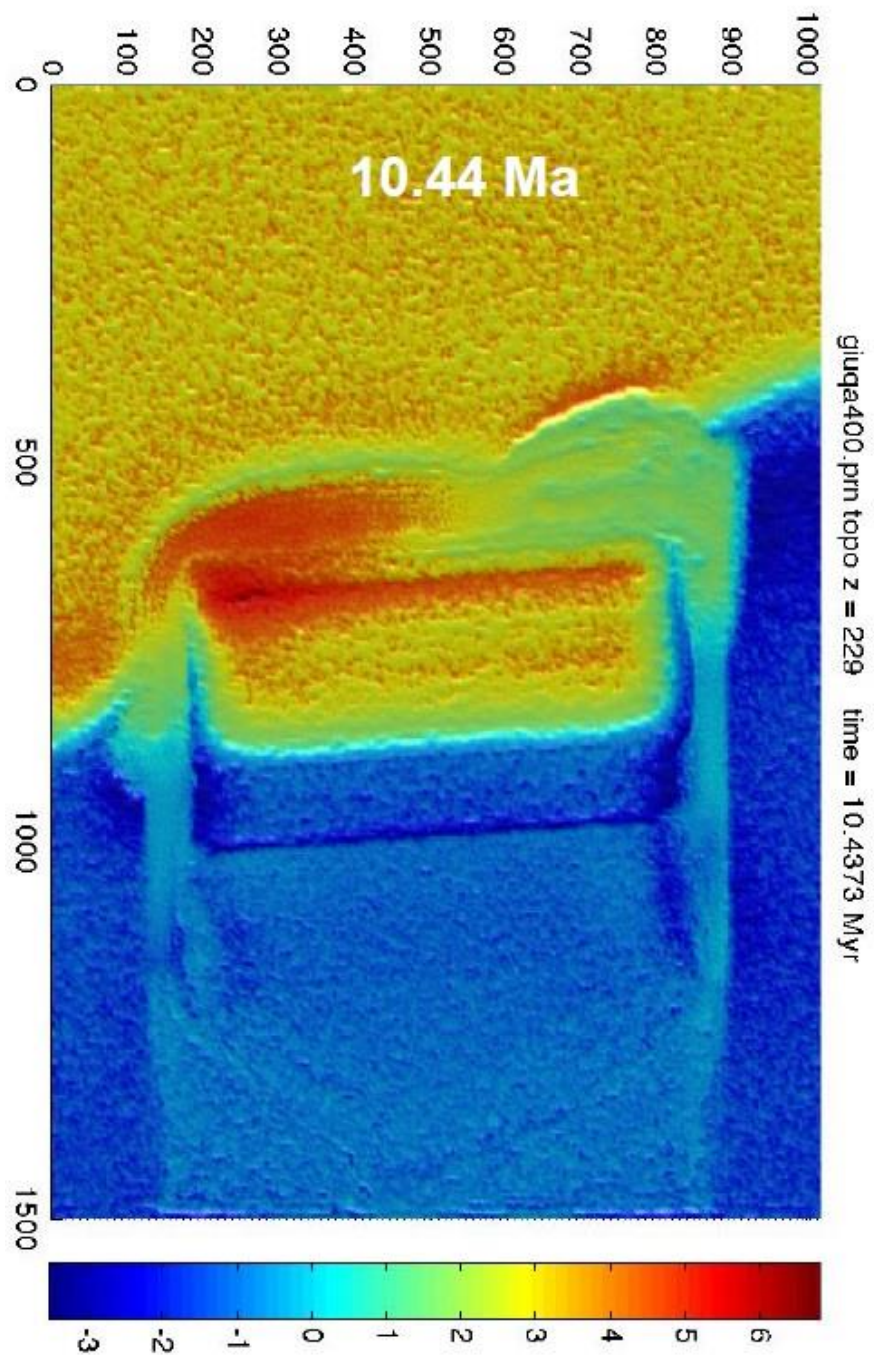


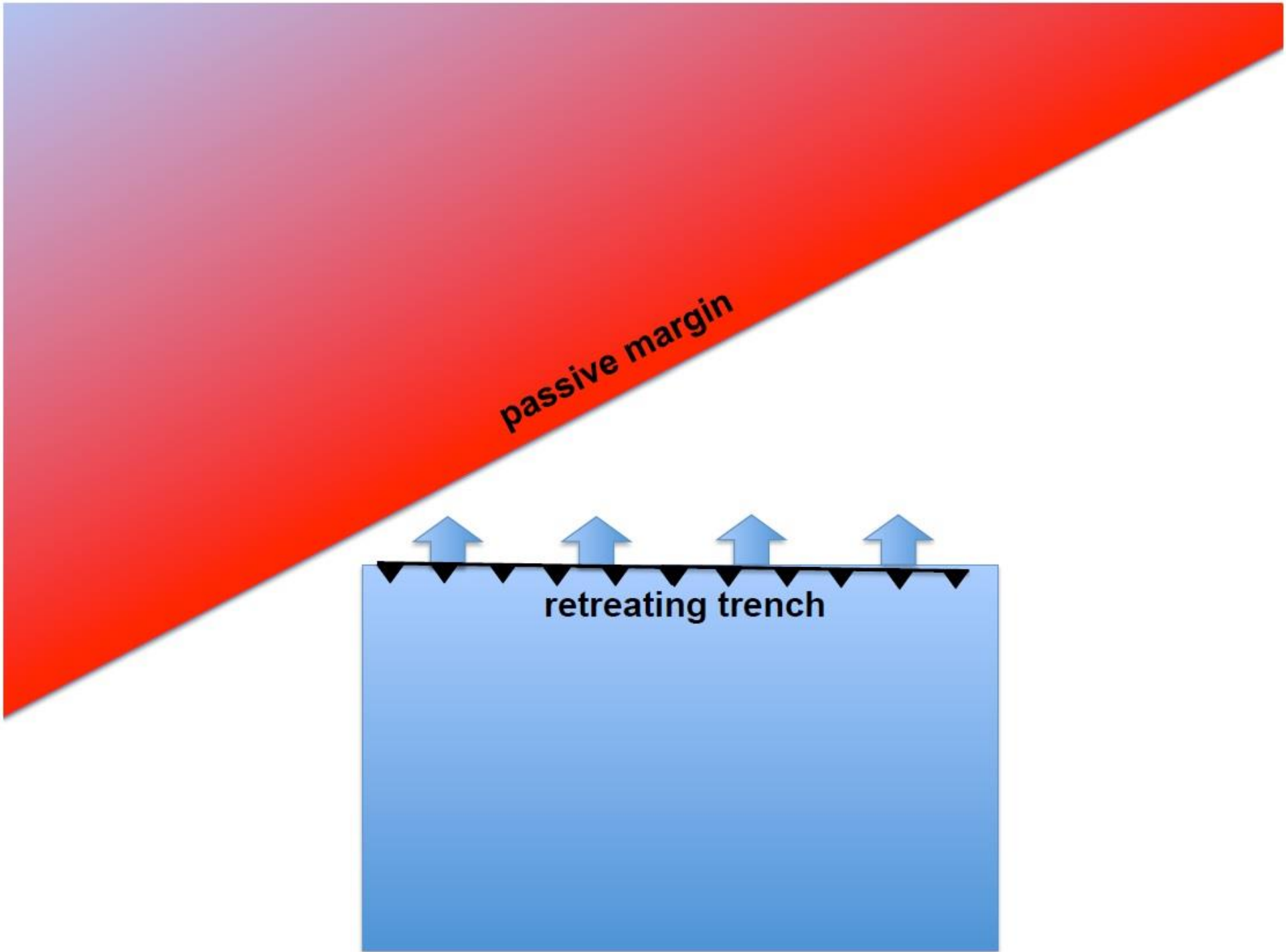


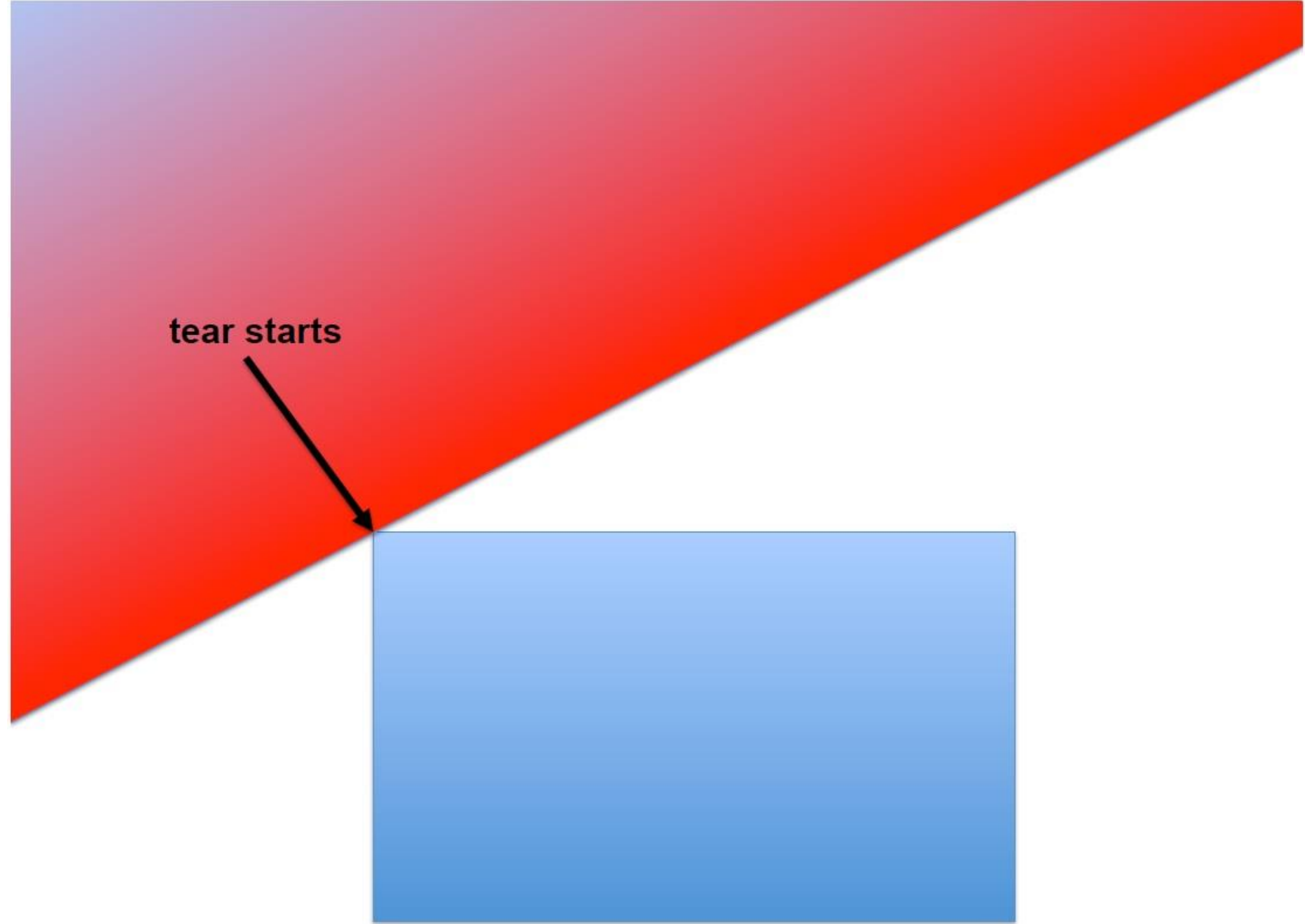




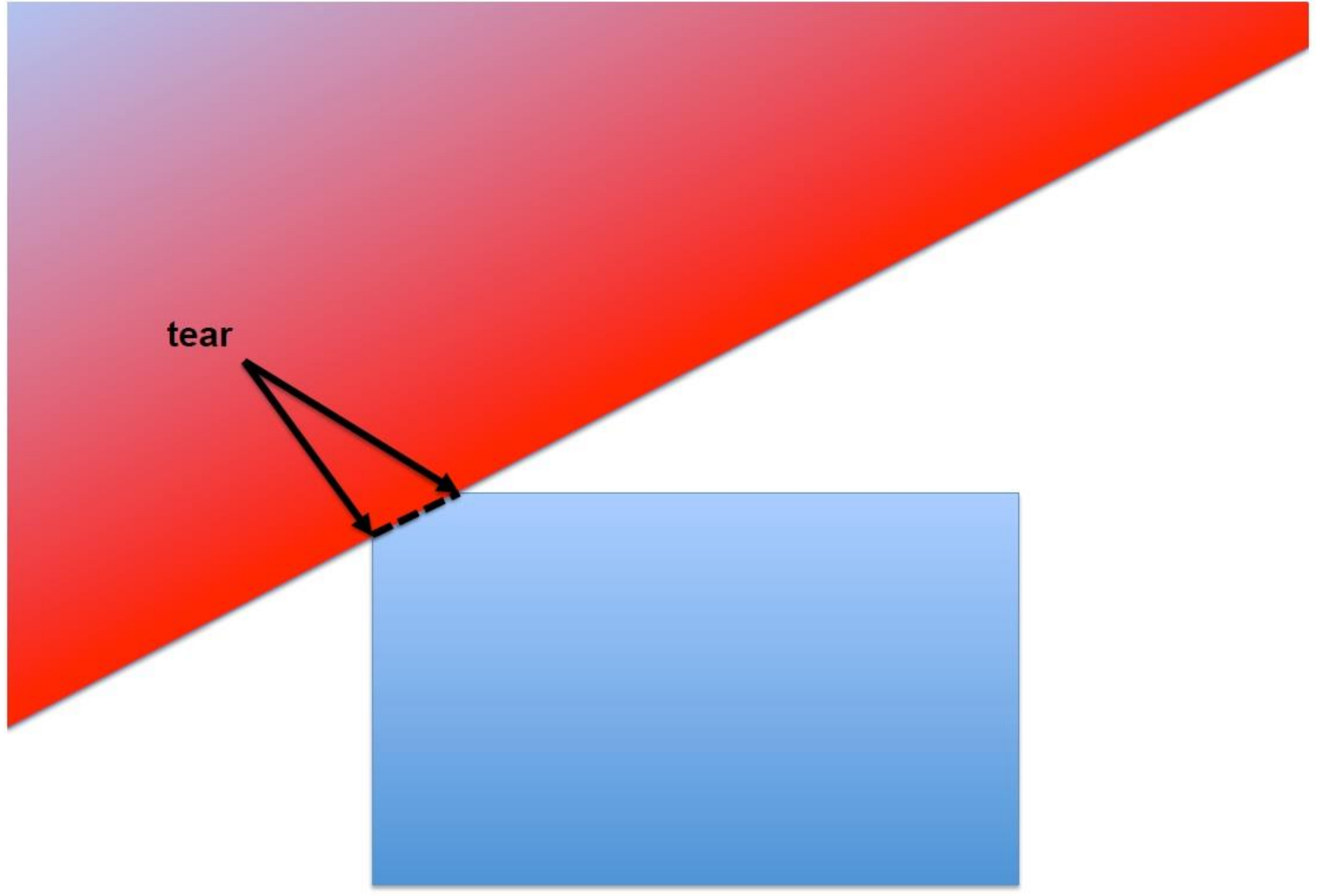


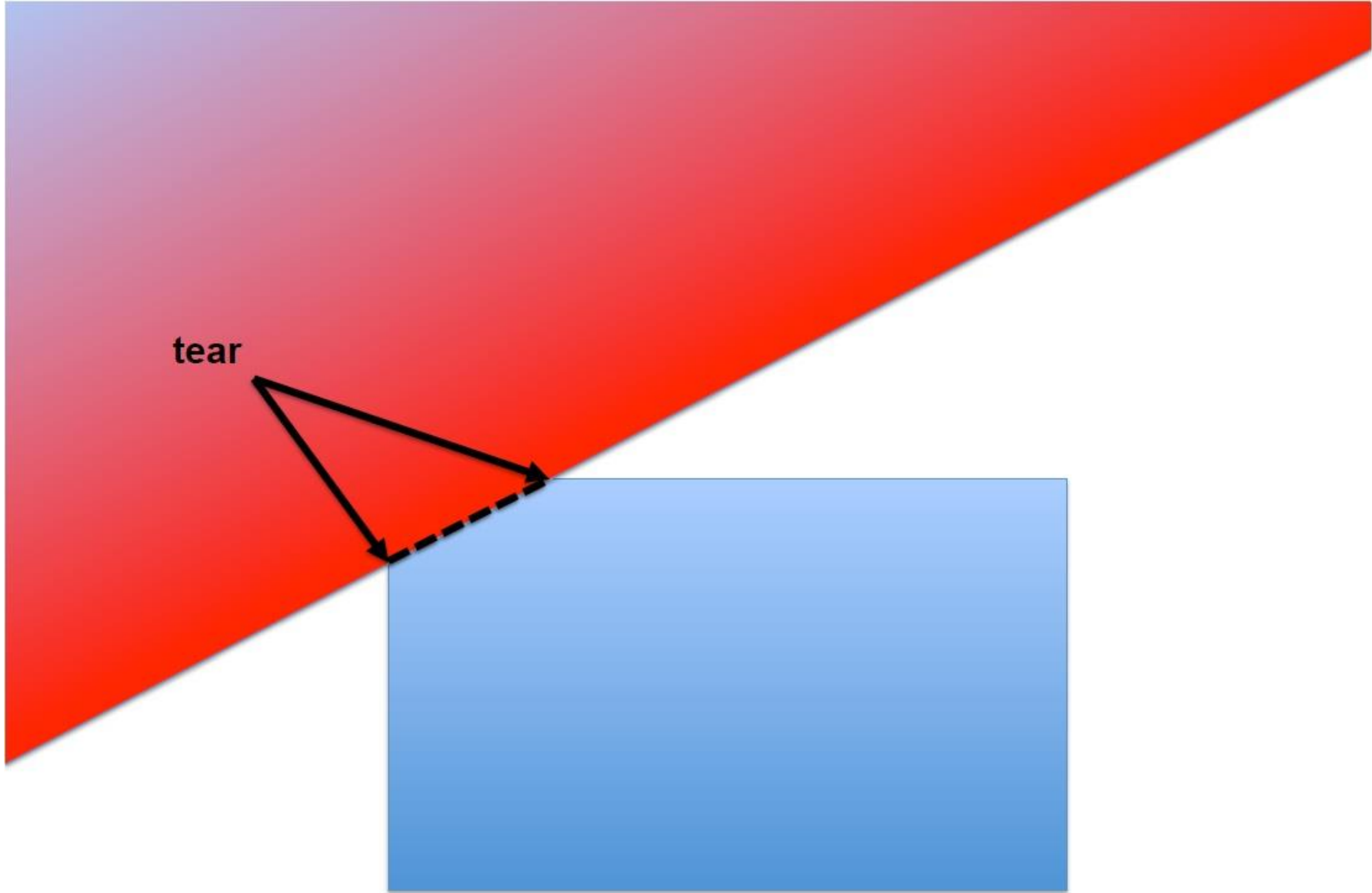


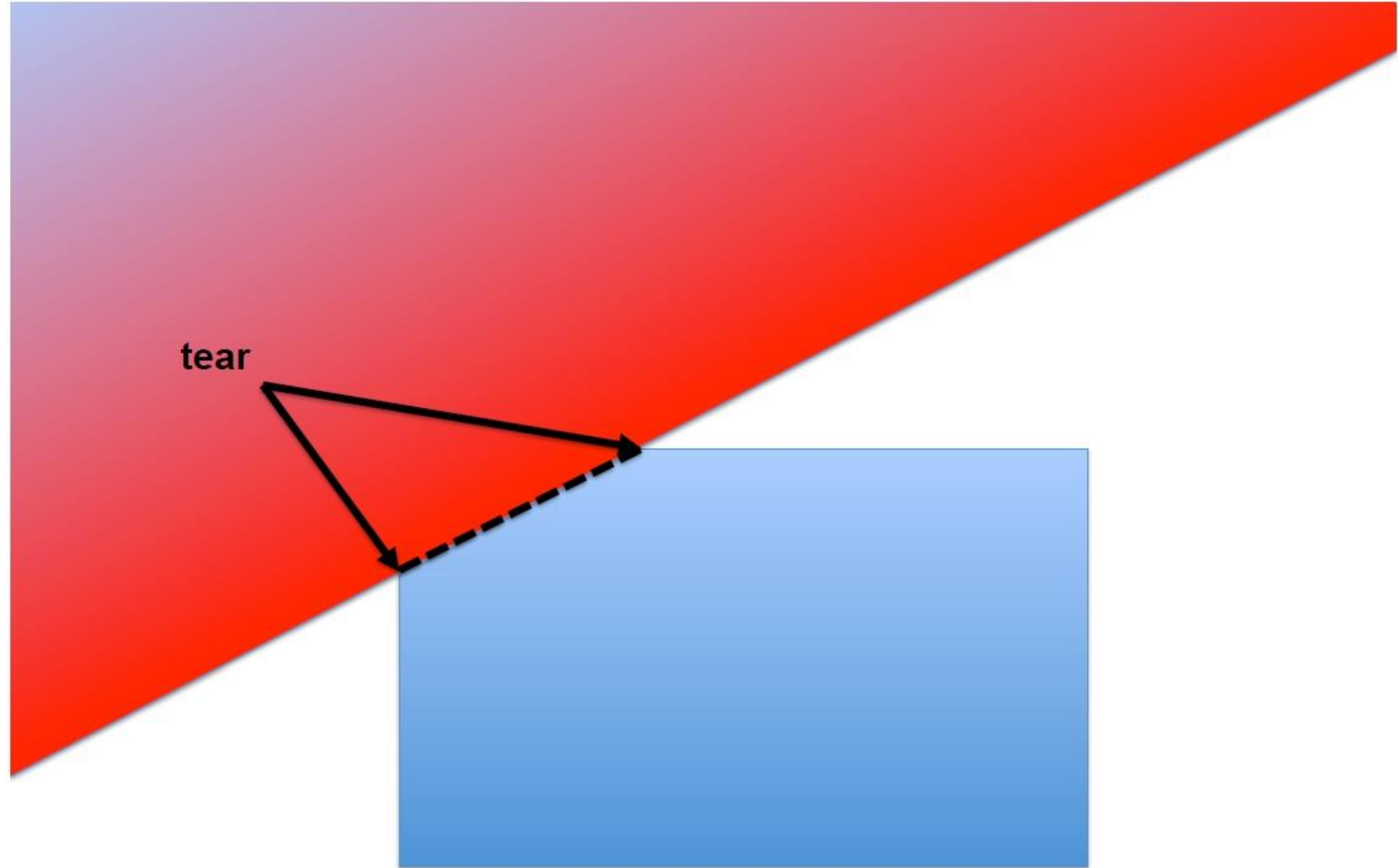


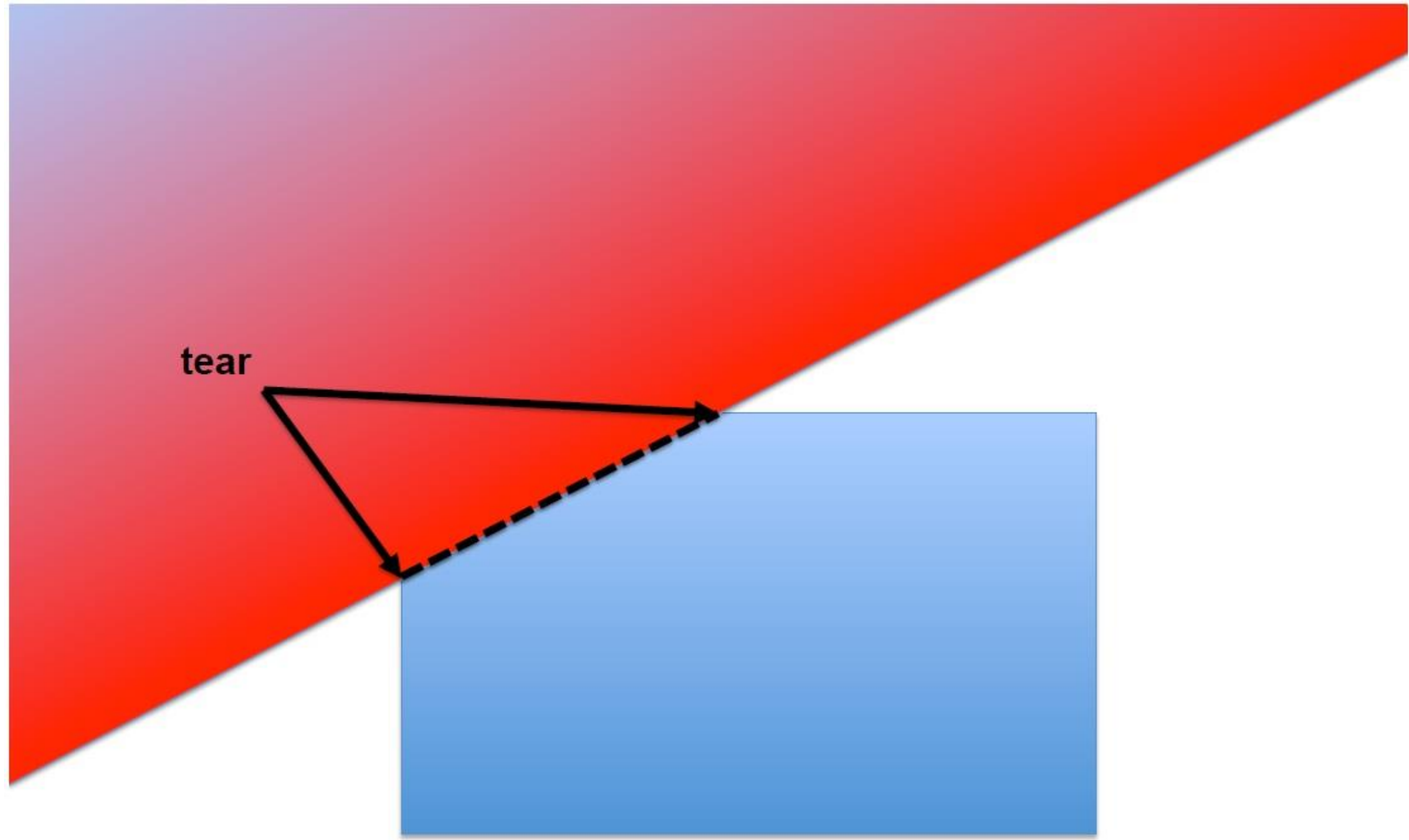


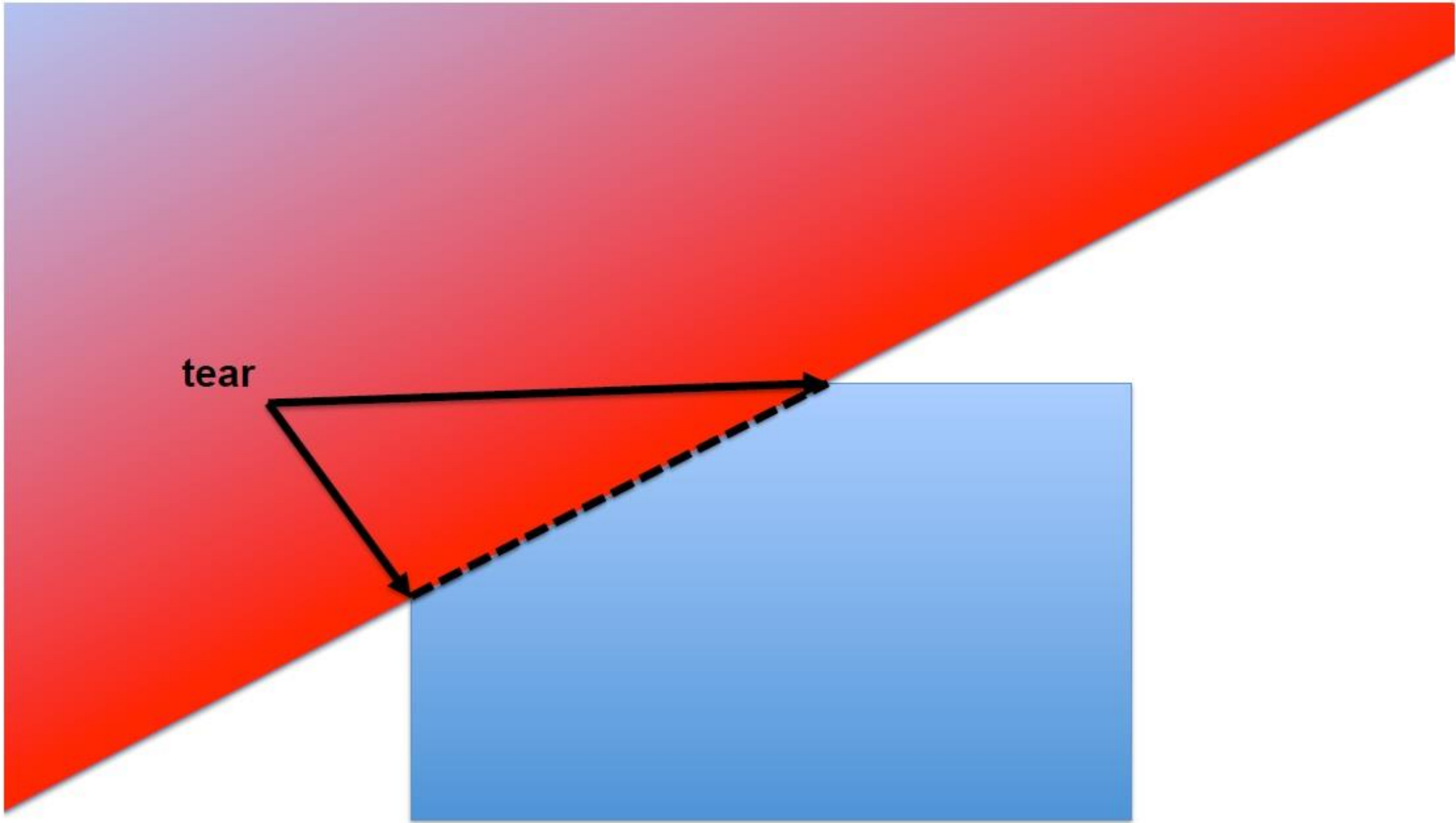
tear starts



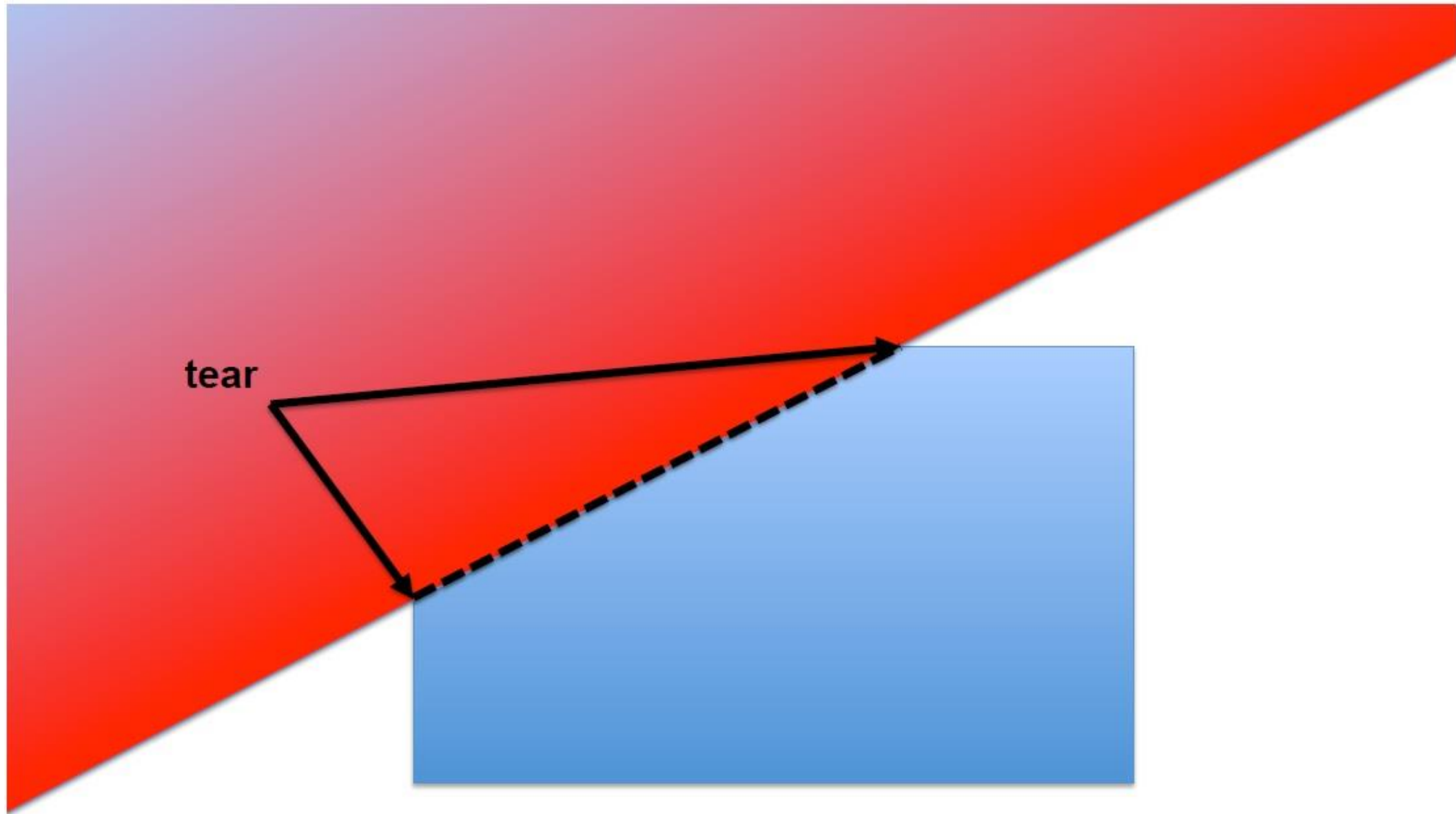


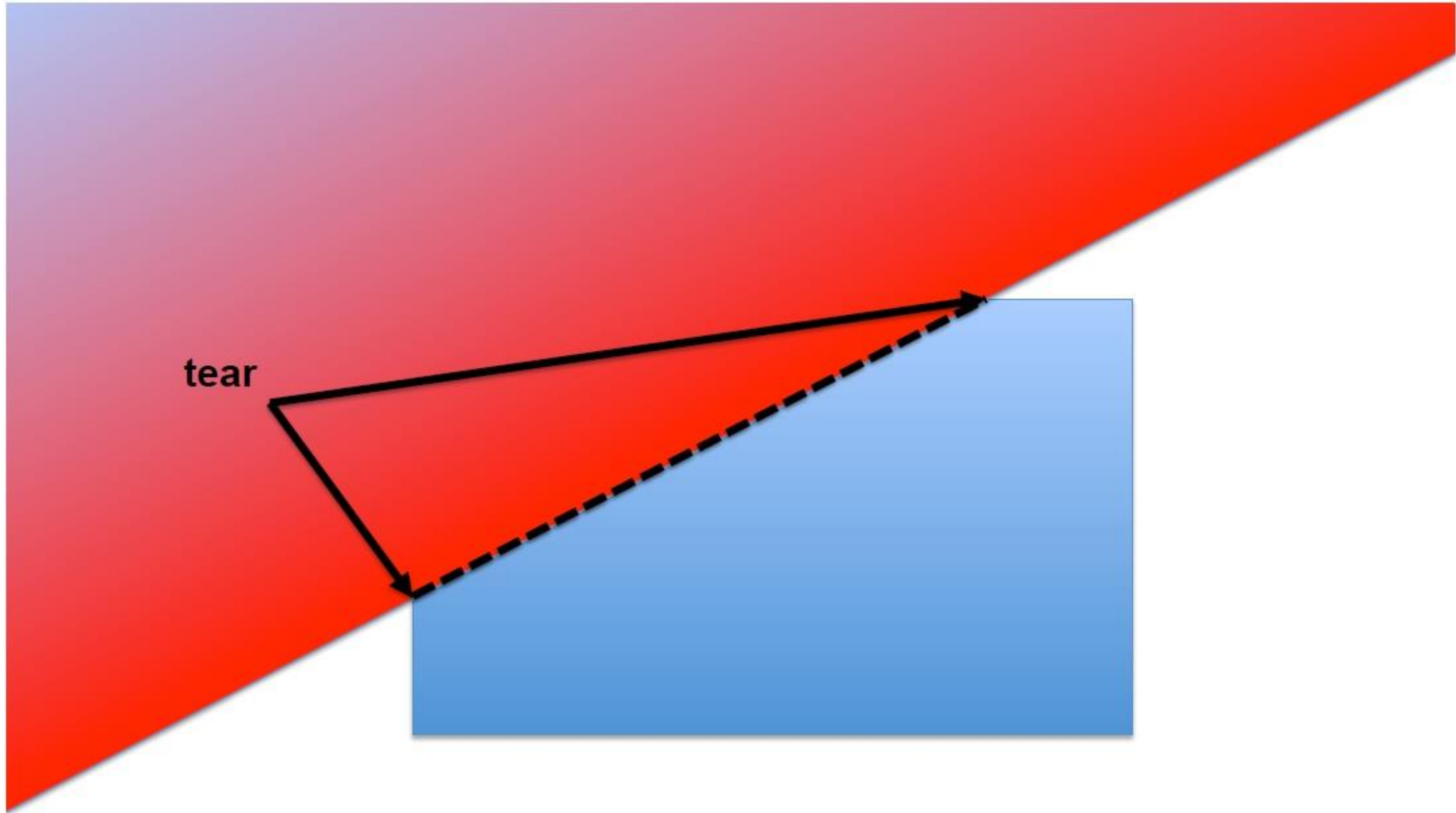


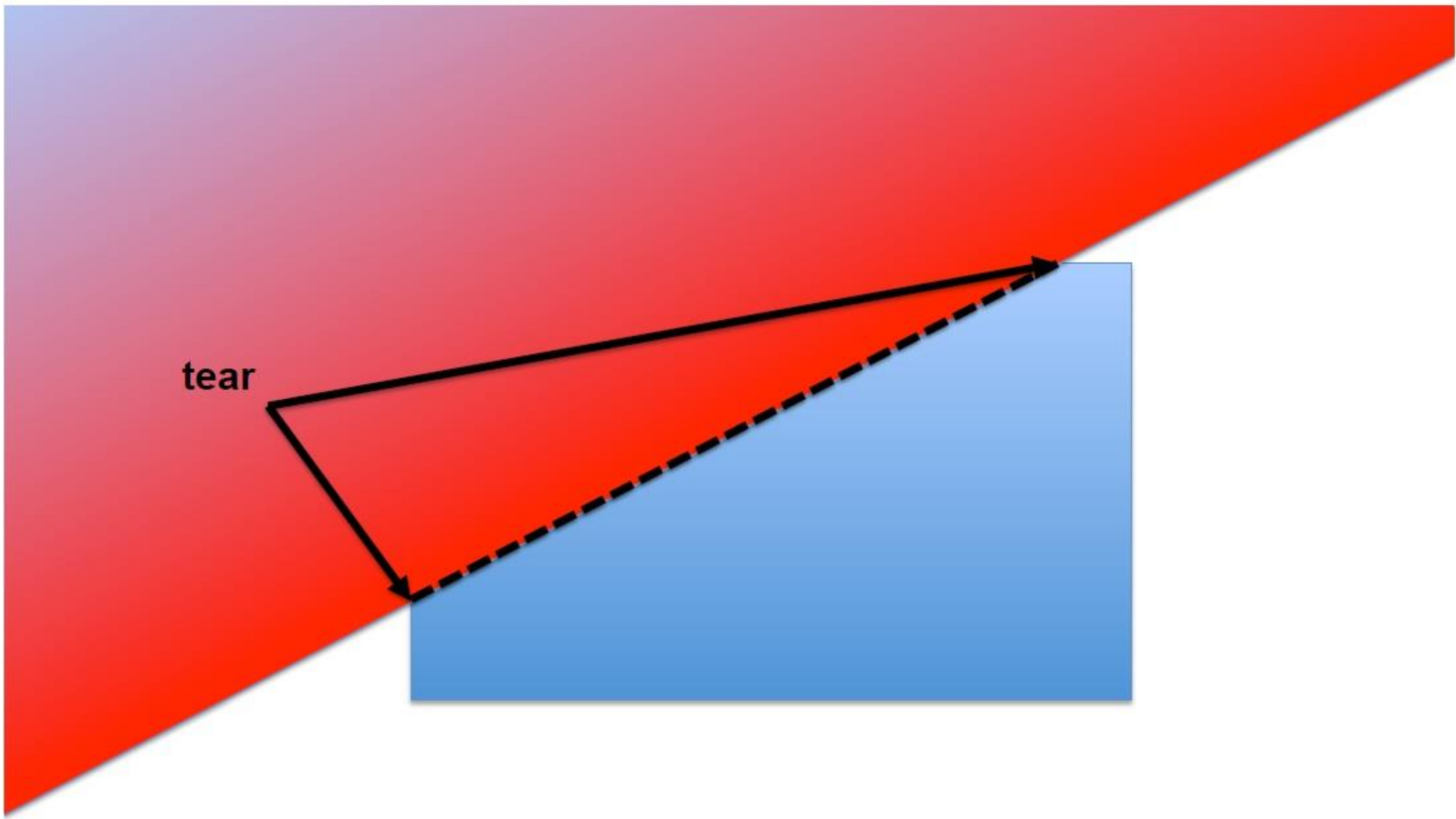


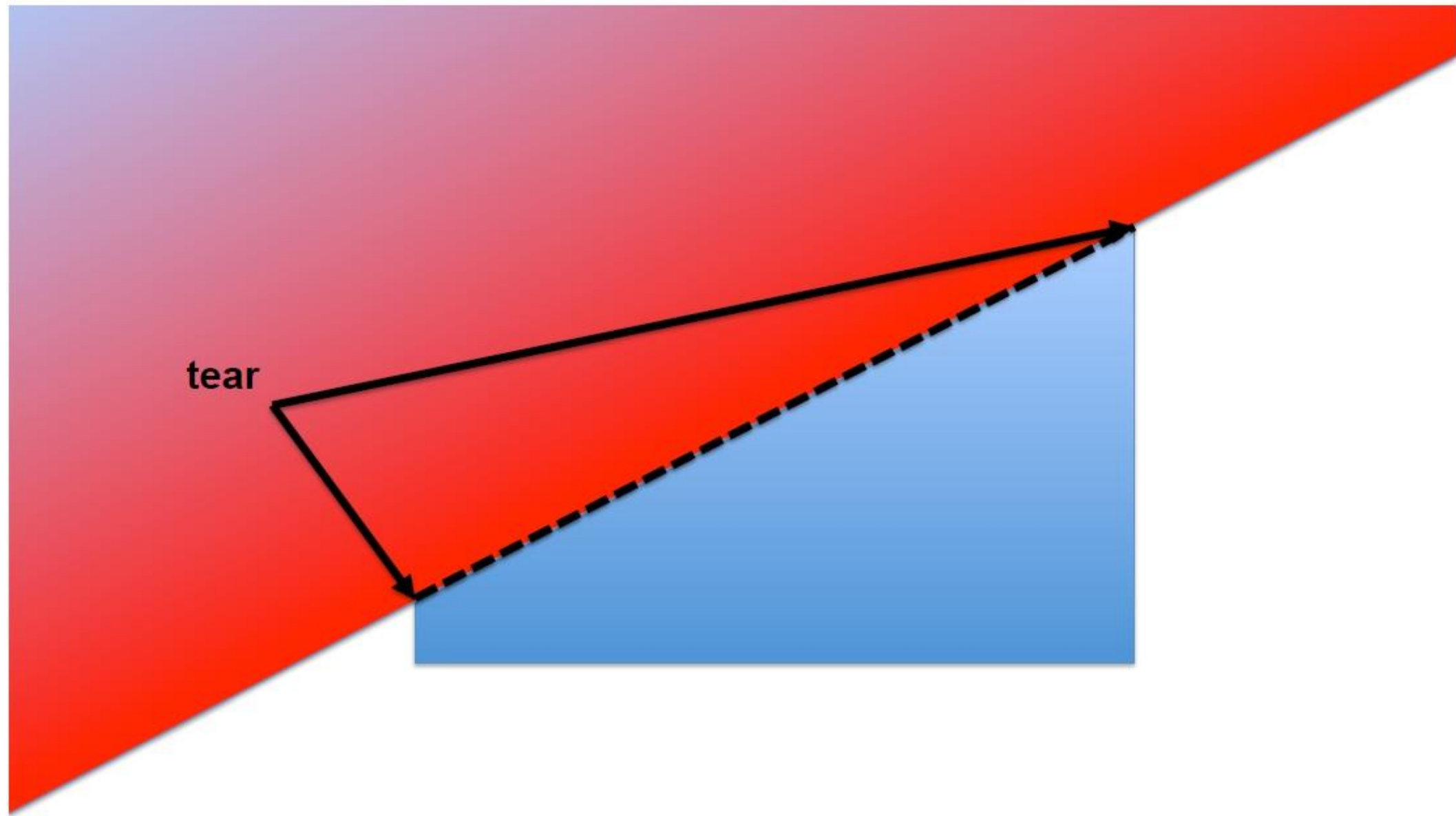


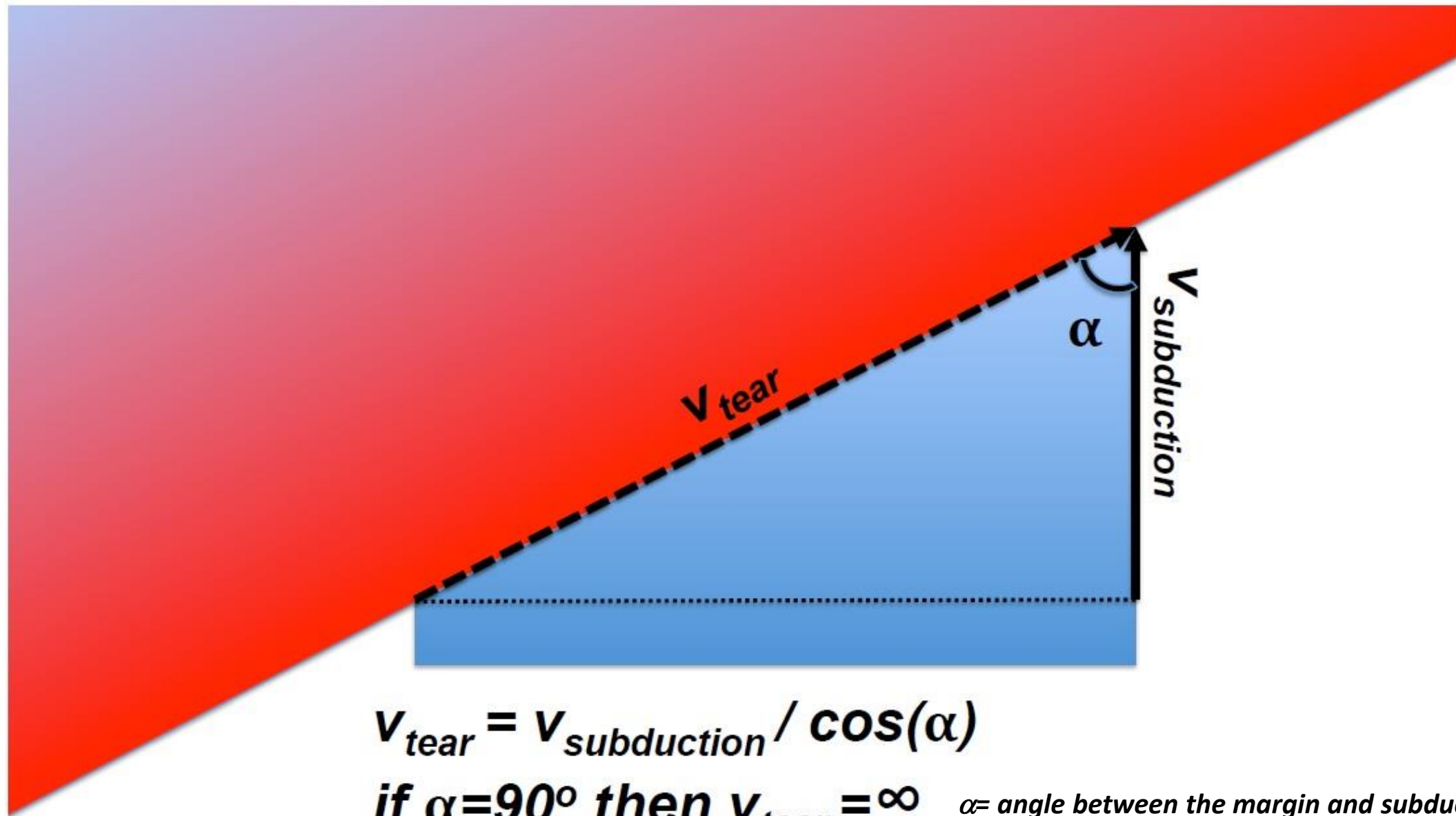
tear





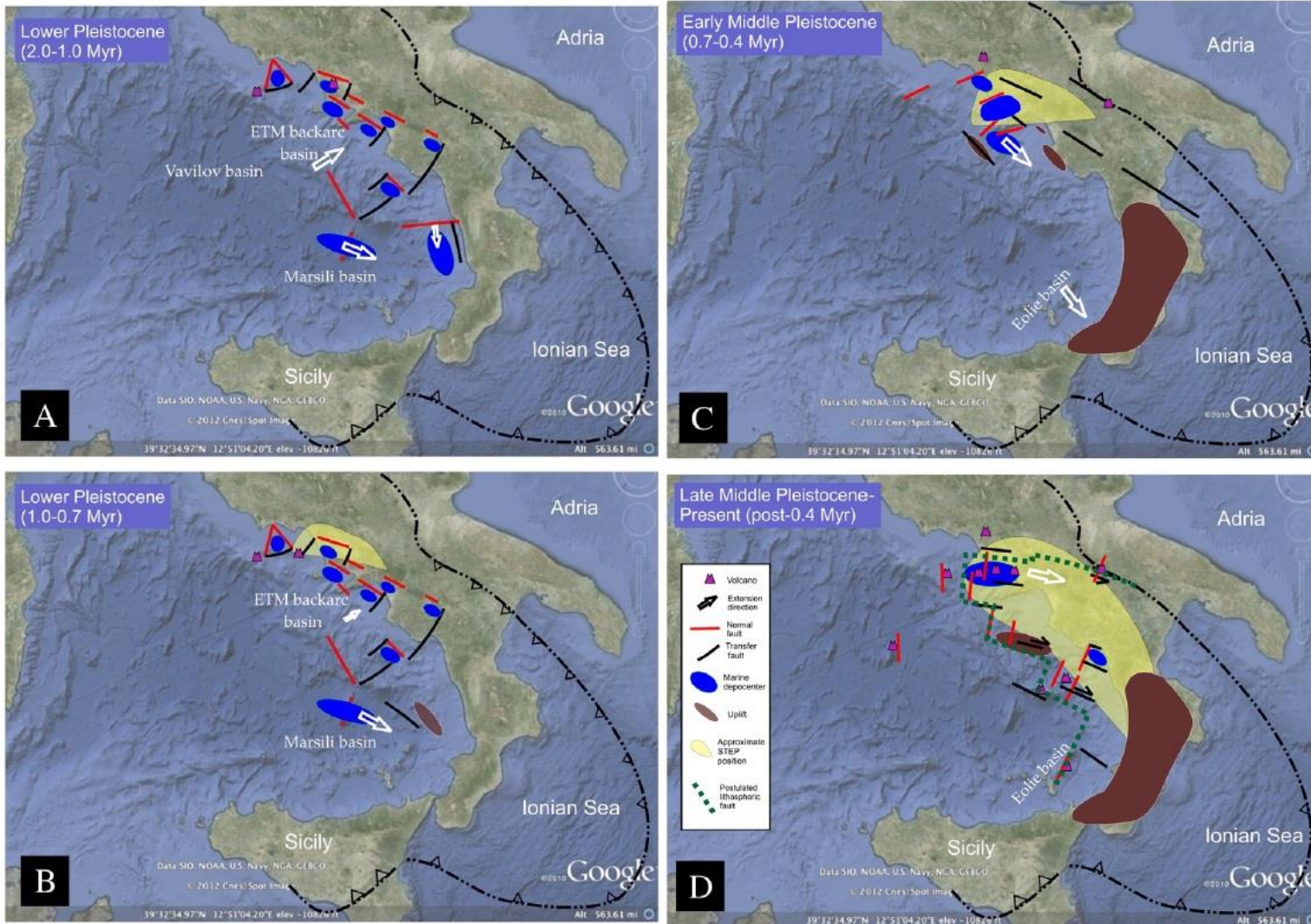






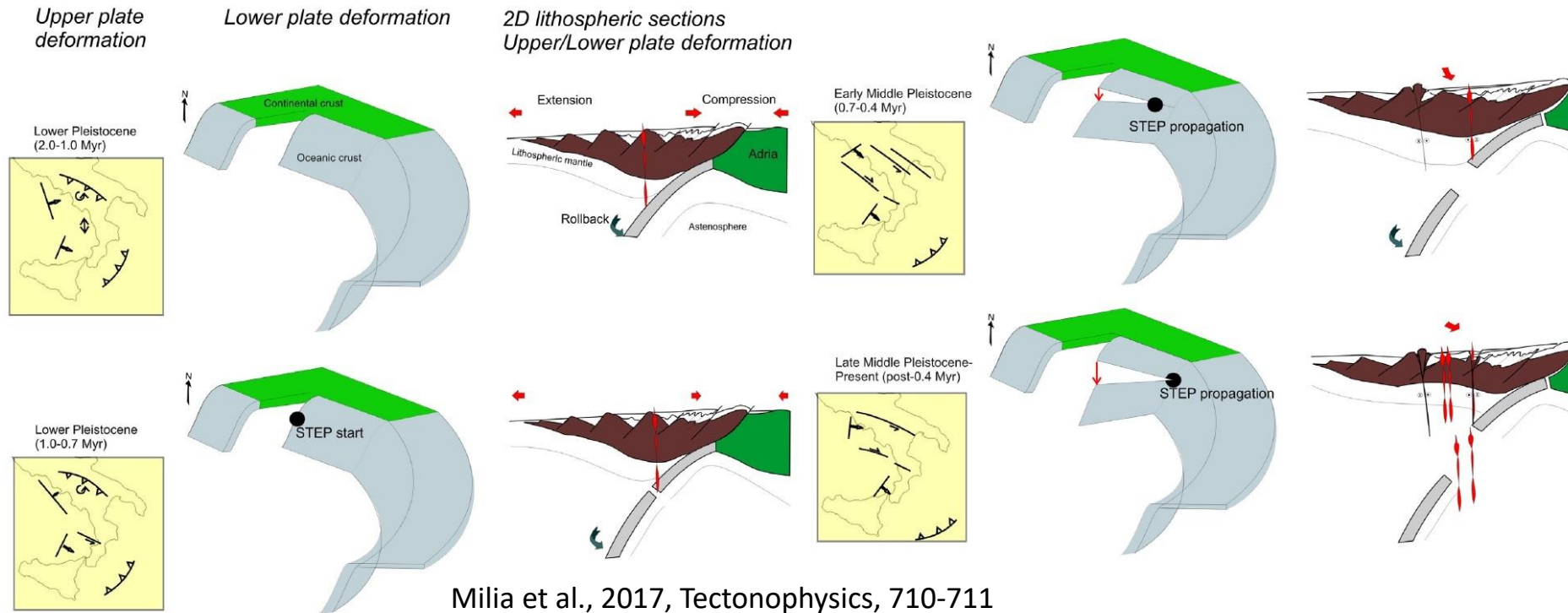
1. Retreating subduction is very efficient in causing slab tearing
2. Lateral tear propagation is controlled by the passive margin obliquity
3. Subduction may continue with different polarity after tearing

Kinematics of the Tyrrhenian



- During the Lower Pleistocene (2.0–1.0 Myr) extensional tectonics affected the entire Eastern Tyrrhenian Margin (ETM) and the western flank of the Apennines, creating several basins: three contemporaneous extension directions (NE–SW in the Campania margin, NW–SE in the Marsili basin and N–S in the Calabrian Margin) .
- In the late Lower Pleistocene (1.0–0.7 Myr), extensional faults continued their activity in the Campania Margin, Marsili basin, and western flank of the Apennines, with a higher speed of the Marsili basin opening compared to that of the ETM.
- In the Early Middle Pleistocene (0.7–0.4-Myr) an abrupt change of direction of extension (from NE-SW to NW-SE) in the ETM occurred, accompanied by uplift of Calabria and volcanic activity (tearing propagation).
- In the Late Middle Pleistocene to Present (>0.4 Myr) extensional basins (Southern Gaeta Bay, Campana Plain-Campi Flegrei and Sapri basins) formed, with intense volcanism and eastwards migration of the extension was recorded. NNE-trending normal faults developed in the ETM and Apennines.

Upper plate and slab features developed during the evolution of the STEP fault

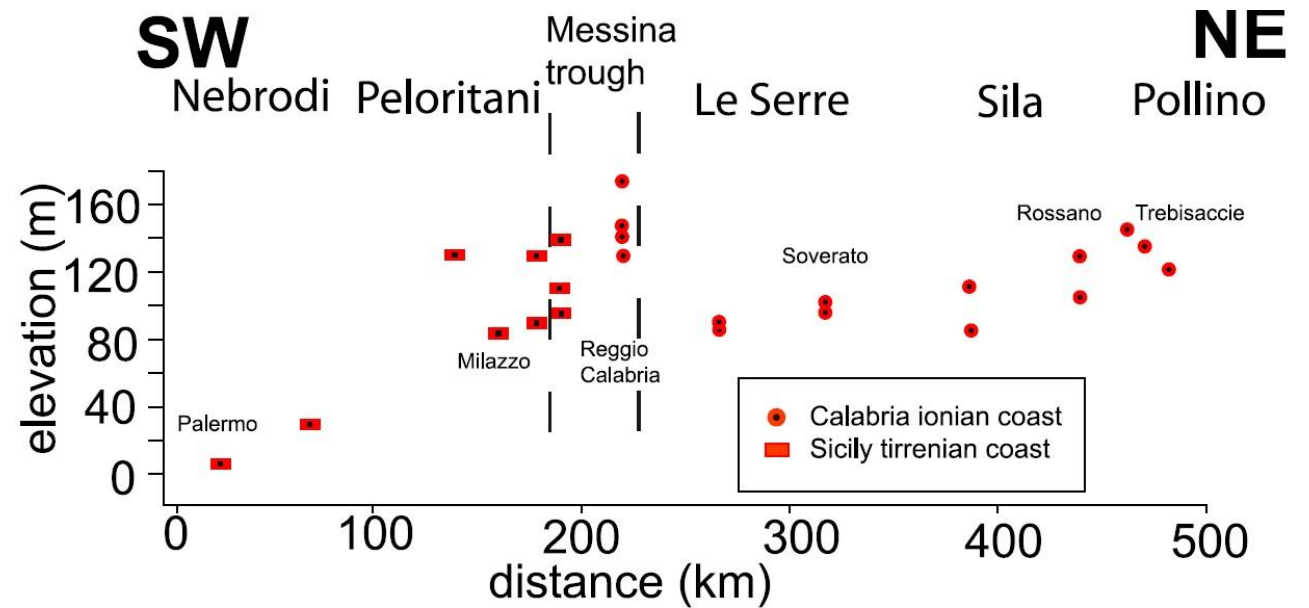
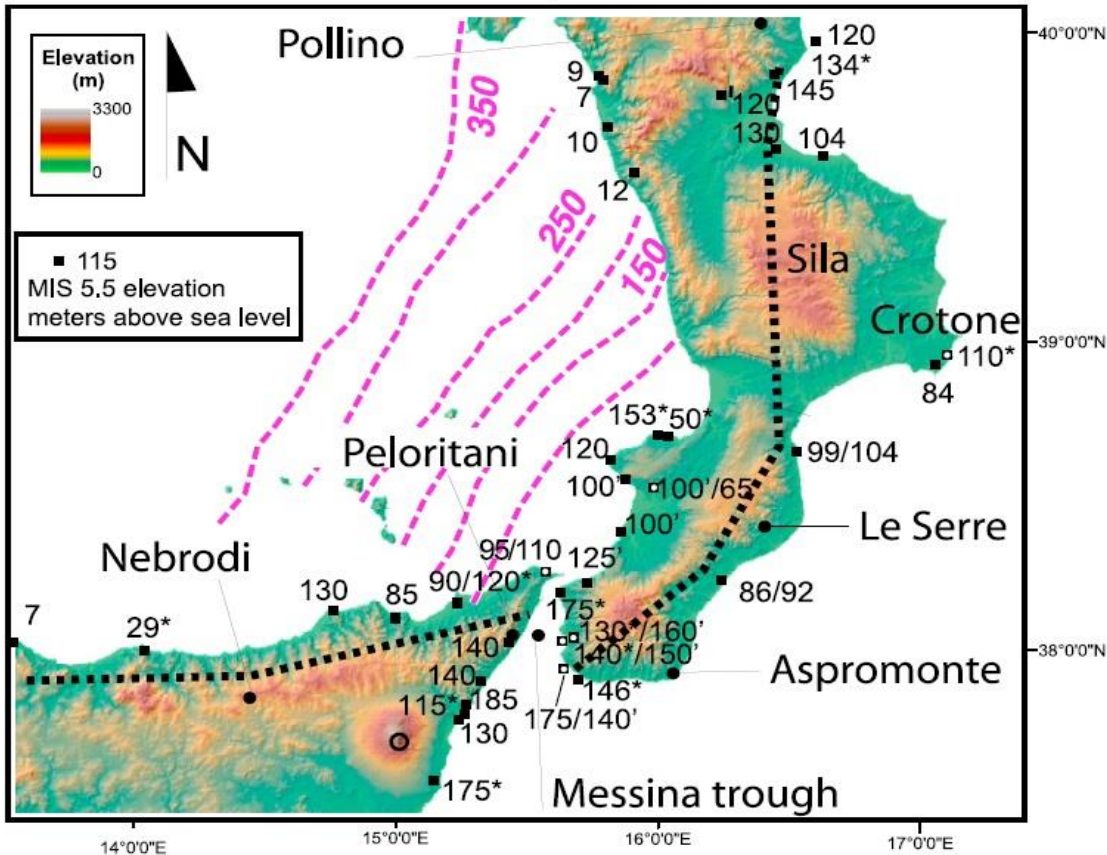


Milia et al., 2017, Tectonophysics, 710-711

- During the Lower Pleistocene (2.0–1.0 Myr) the upper plate extension is directed perpendicular to the Apenninic trench (ENE) contemporaneously, in the southern part, the extension is directed perpendicular to the Ionian trench (SE). The difference in the extension orientation may reflect the different velocity in the rollback of the continental and oceanic slab sectors.
- Through the late Lower Pleistocene (1.0–0.7 Myr) the reduction in the extension value along the Campania Margin and the increase in the extension value of the Marsili basin, induce the formation of a transfer fault zone in the Calabria Margin (maybe as a response in the upper plate of the STEP fault nucleation and rollback of the slab).
- The Early Middle Pleistocene phase (0.7–0.4 Myr) there was (1) an abrupt change in the extension direction (from NE to SE), associated to the formation of rapidly evolving half graben localized in the Northern Campania Margin; (2) end of the NE-directed thrust propagation in the Apennines and rapid uplift of Calabria (due to the toroidal flow around the Ionian slab).
- The Late Middle Pleistocene-Present (post-0.4 Myr) period records a minor reorientation (E-SE) of the direction of extension in the ETM (enlargement of the gap effect of the continuum propagation of the STEP fault).

Dynamic topography induced by subduction: the Calabrian Arc

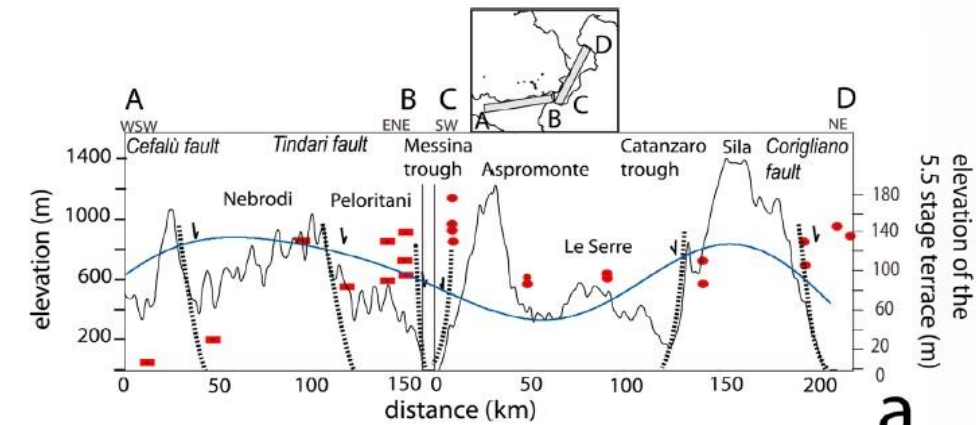
Elevation distribution of the marine terraces in northeastern Sicily and Calabria



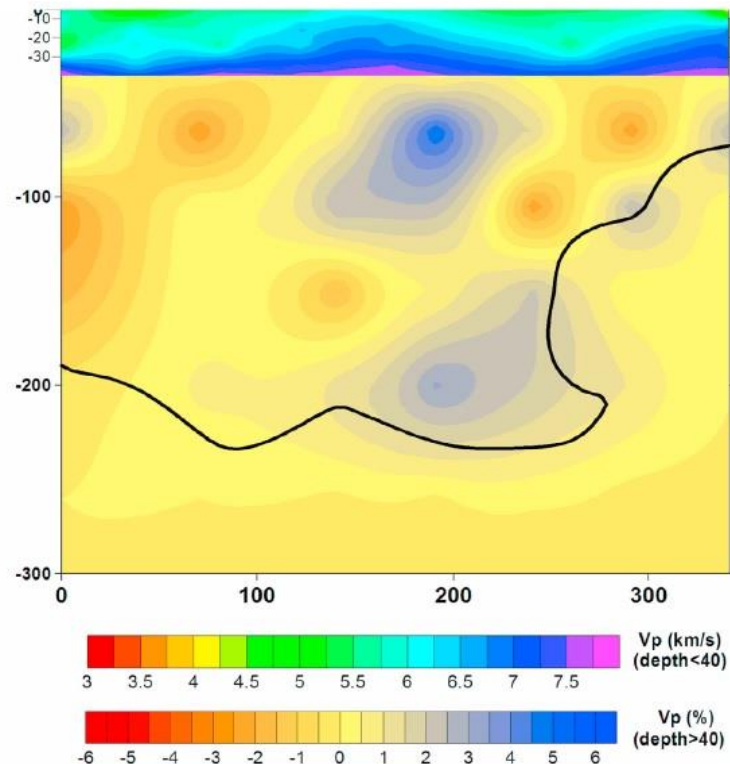
Faccenna et al., 2011, Tectonics, 30

- The Calabrian subducting slab presently consists of an approximately 200 km wide and ~600 km deep Wadati-Benioff zone dipping toward the northwest at about 70°.
- Minimum values of uplift correspond to the active portion of the slab, whereas maximum values of uplift correspond to the Messina region.

Dynamic topography induced by subduction: the Calabrian Arc



a



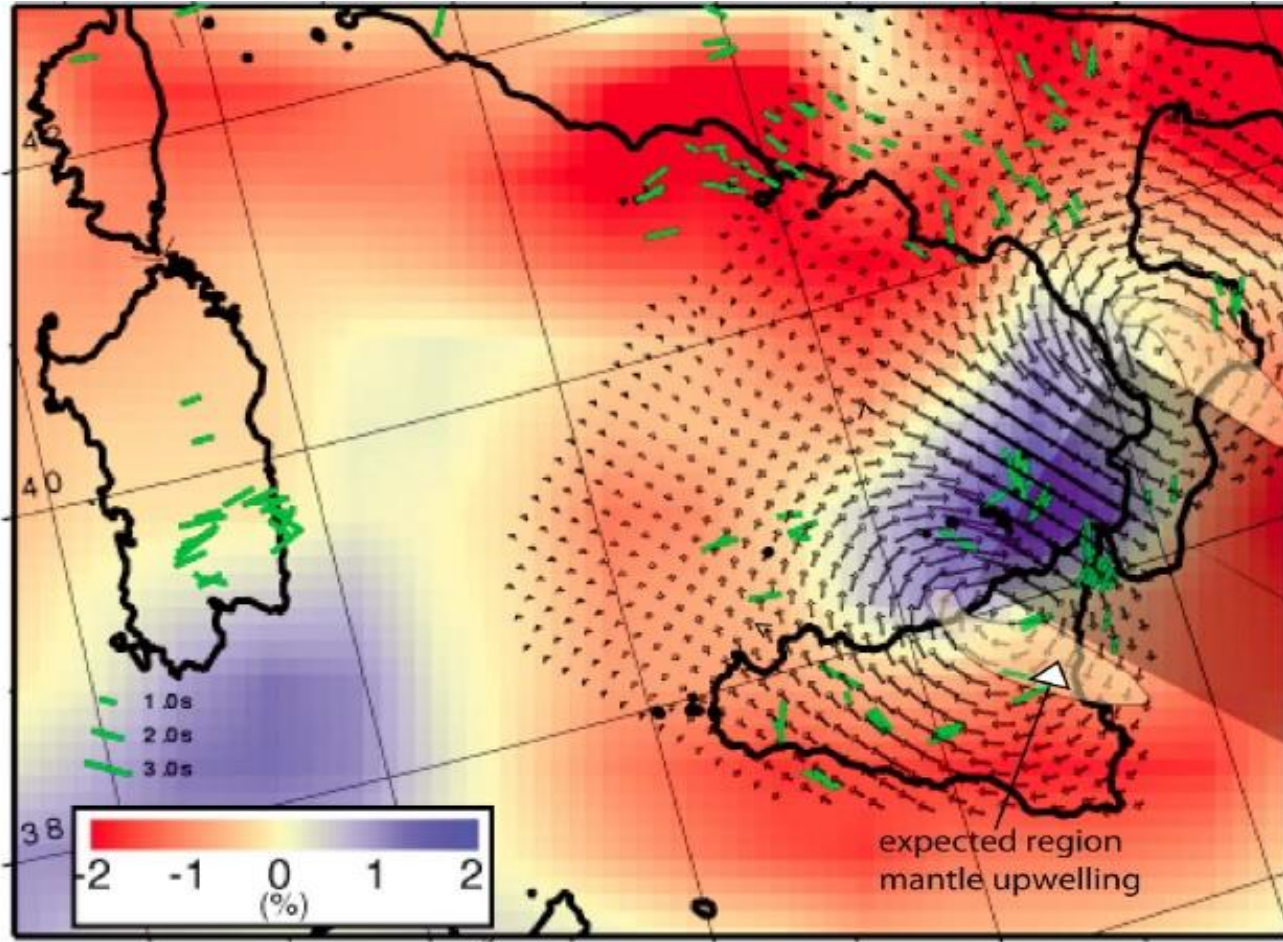
b

- The topography of the Calabrian Arc is dominated by the superposition of short-wavelength features, related to local faulting and regional-scale (≥ 100 km) wavelength features.
- Long-wavelength topography shows two maxima corresponding to the Nebrodi Mts. and the Sila-Pollino massif, which bound a relatively depressed region, corresponding to the area overlying the active Wadati-Benioff zone.
- Trench rollback is generally associated with topographic sinking of the upper plate, as retrograde slab motion pulls the upper plate down.
- Detachment or breaking of subducting slabs are efficient sources of rapid upper plate uplift, which would be related to the lithospheric response to unloading.
- The average differential elevation between the two flanking bulges and the central depressed region ranges between about 500 and 800 m.
- The uplift rate deduced from terraces elevation is of the order of 0.8–1 mm/yr and the onset of uplift is in the lower Pleistocene. The uplift is increased by about 30% to the north and southwest of Le Serre, at least during the last 125 kyr.
- Mount Etna volcanism is positioned on top of a highly uplifted and still uplifting region indicating, together with Etna's volcanism itself, upwelling on the slab's edge.

Dynamic topography induced by subduction: the Calabrian Arc

Instantaneous mantle flow generated by the subduction of an isolated slab adapted to the case of Calabria

P-wave velocities at a depth of 150 km



Faccenna et al., 2011, Tectonics, 30

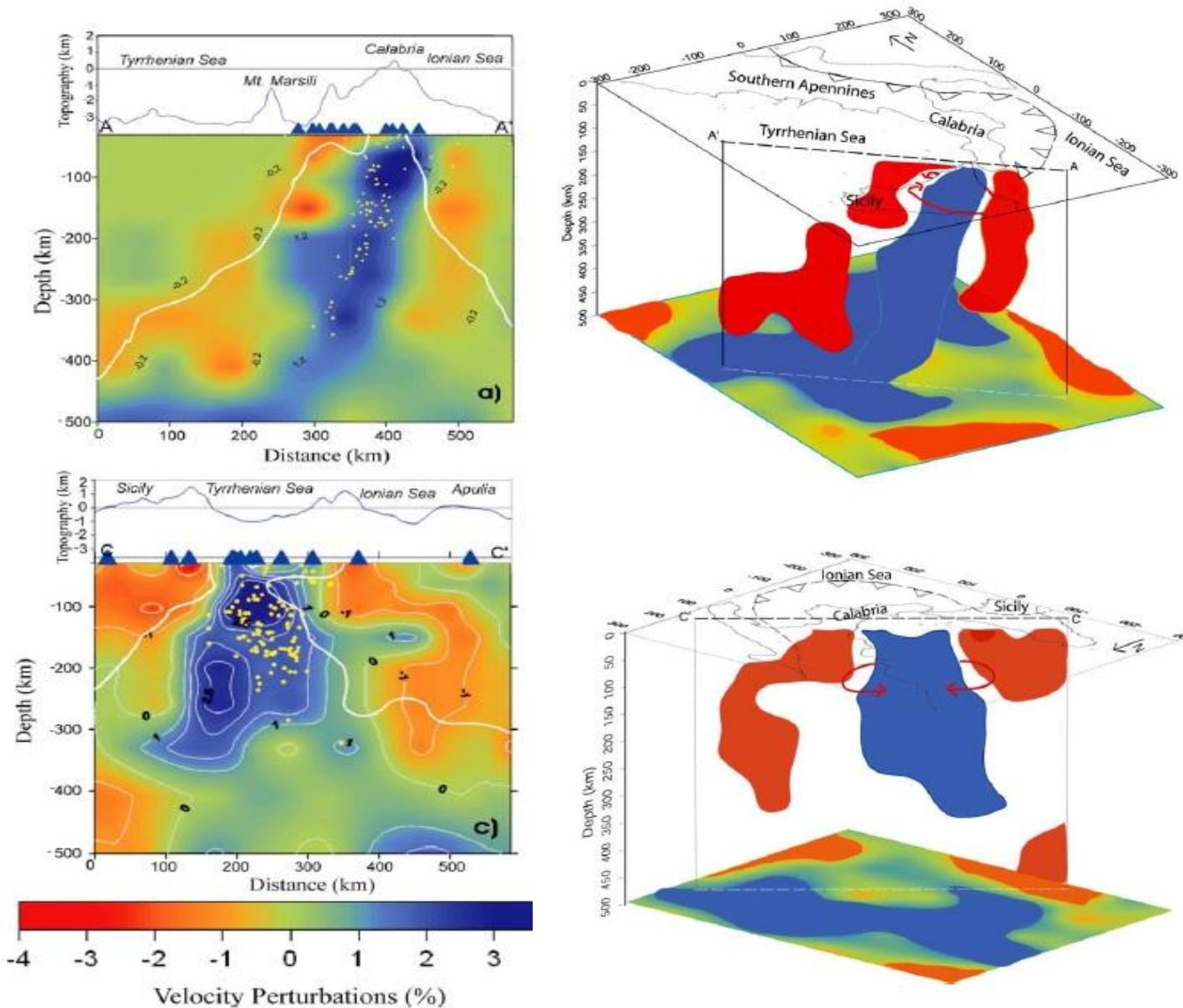
Different models have been proposed to explain uplift and deformation process in Calabria, among the others:

- (1) **Unloading due to slab break off.**
- (2) **Dynamic topography related to circulation around a narrow, retreating, subducting slab.**

- Rebound after unloading due to slab break-off could have indeed produced uplift of the upper plate. However, slab mantle viscous coupling is expected to produce subsidence rather than uplift during the fall of the detached portion of the slab.
- The deformation history of Calabria and the Etna's volcanism could have been originated dynamically by the action of a complex 3D mantle flow around the slab edge.

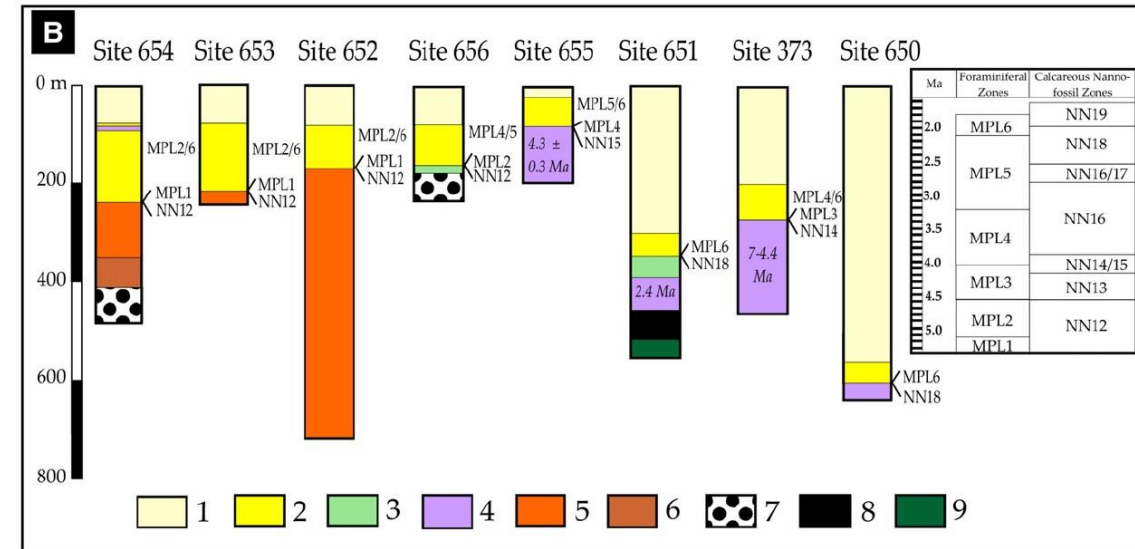
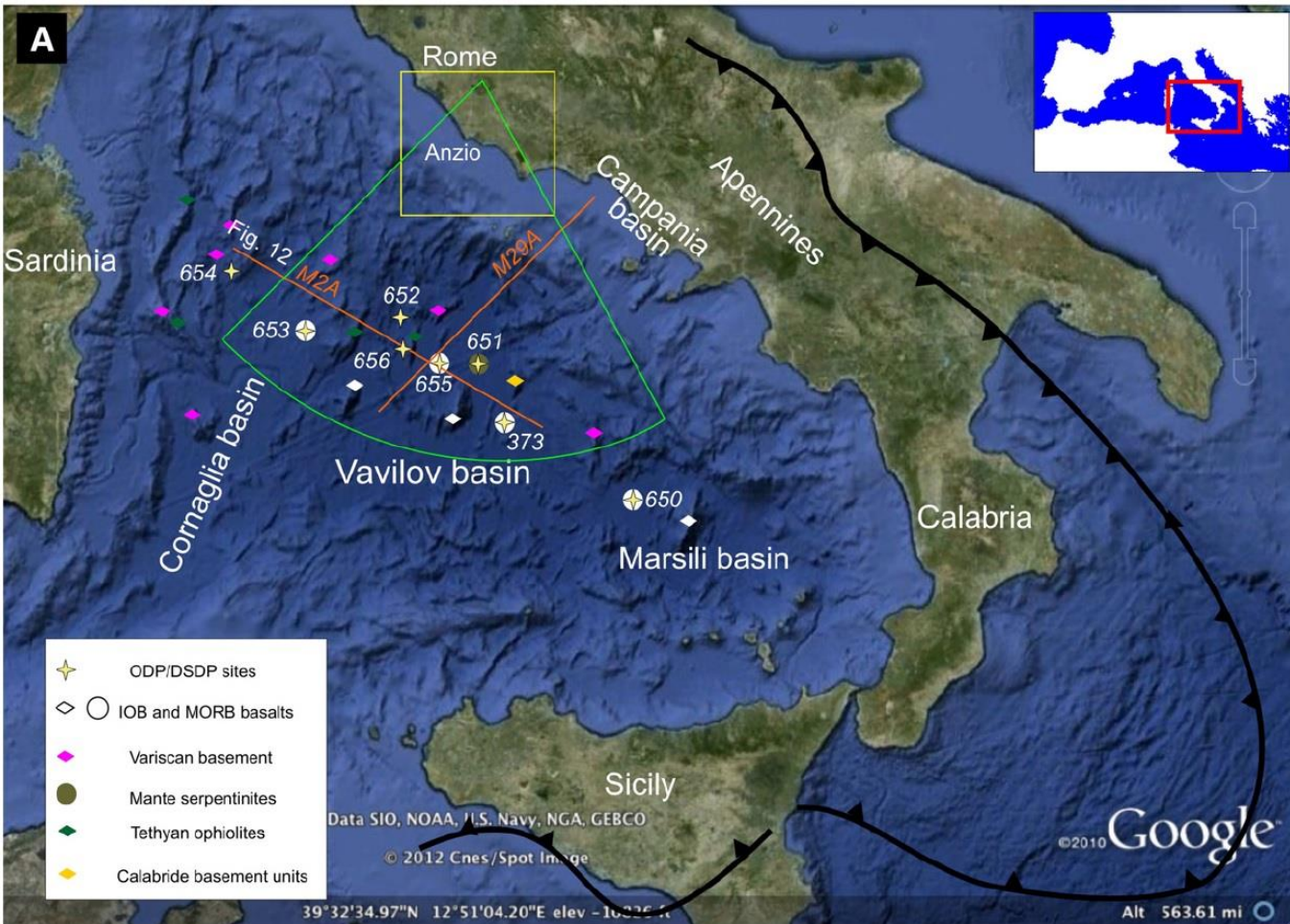
In green are shown the results from SKS splitting data

Toroidal flow around the Ionian slab caused by slab retreatment



- Toroidal motion is mostly enhanced during retrograde slab motion, or by its steepening as mantle material beneath the slab is displaced toward its front, flowing laterally around the edges and producing two symmetrical vortex-like structures.
- This induces a (1) pronounced upper mantle upwelling at the slab edges, resulting from the continuous interplay between poloidal and toroidal fluxes, and (2) uplift of the overriding plate and also volcanism induced by decompression melting.

From stretching to mantle exhumation: the Vavilov backarc basin



Stratigraphic logs of the DSDP and ODP sites. 1) Pleistocene deposits; 2) Pliocene deposits; 3) dolostones; 4) basalts; 5) Messinian deposits; 6) Tortonian deposits; 7) conglomerates; 8) breccias; 9) serpentinized peridotites.

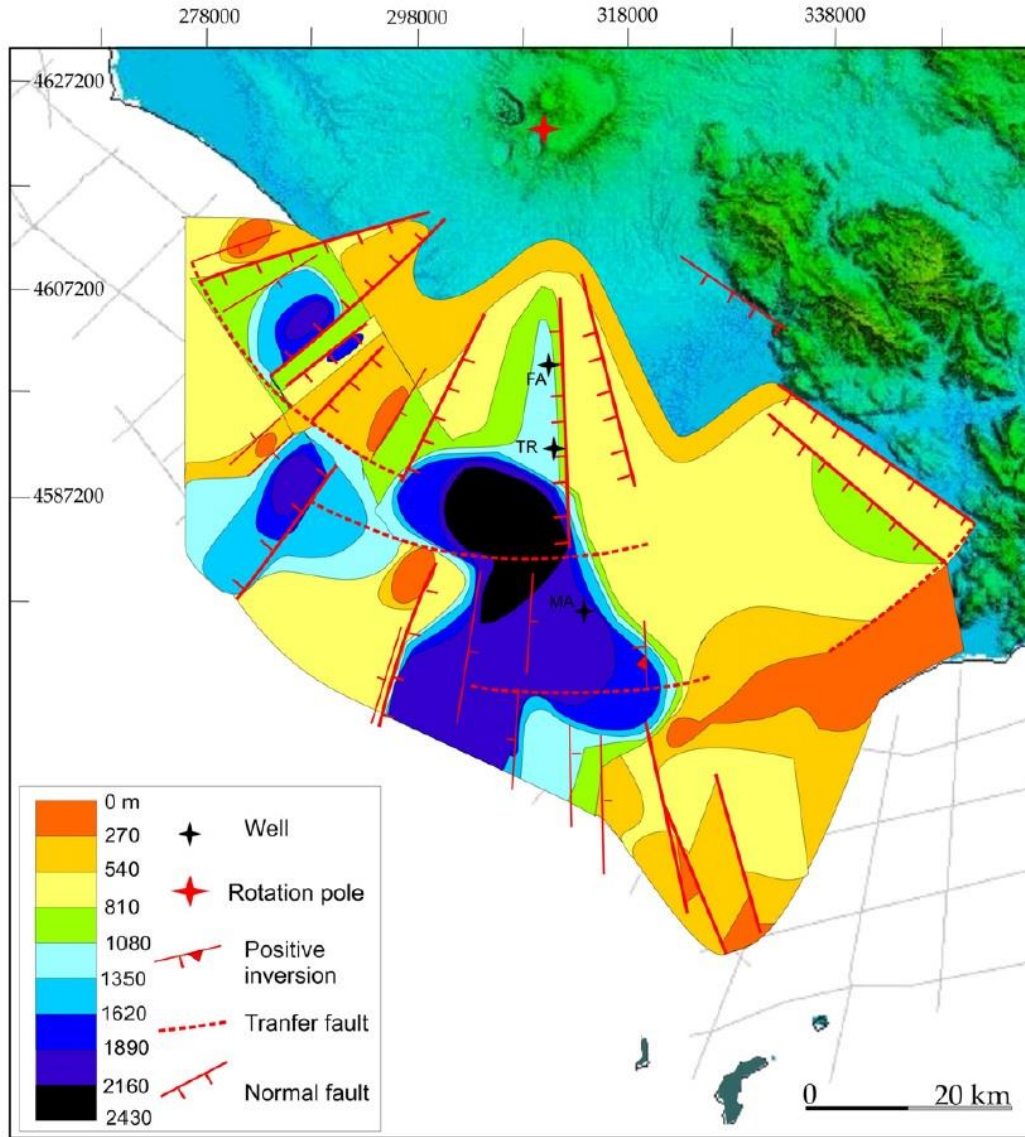
Milia et al., 2017, Tectonophysics, 710-711

The Tyrrhenian Basin can be divided into northern and southern sectors:

- The northern Tyrrhenian Sea started to form in the lower Miocene as a polyphase rift, displaying a trend of faults convergent toward the North and is characterized by a relatively low value of stretching (crustal thickness between 25 and 20 km).
- The Southern Tyrrhenian Sea is a middle Miocene–Quaternary polyphase rift with several fault trends, which includes the Vavilov basin and is characterized by thin crust (from 15 to 10 km) and lithosphere (~30 km), high heat flow values ($> 100 \text{ mWm}^{-2}$) and a large positive Bouguer gravity anomaly.

From stretching to mantle exhumation: the Vavilov backarc basin

Structural map of the Latium margin and thickness map of Pliocene-Quaternary deposits



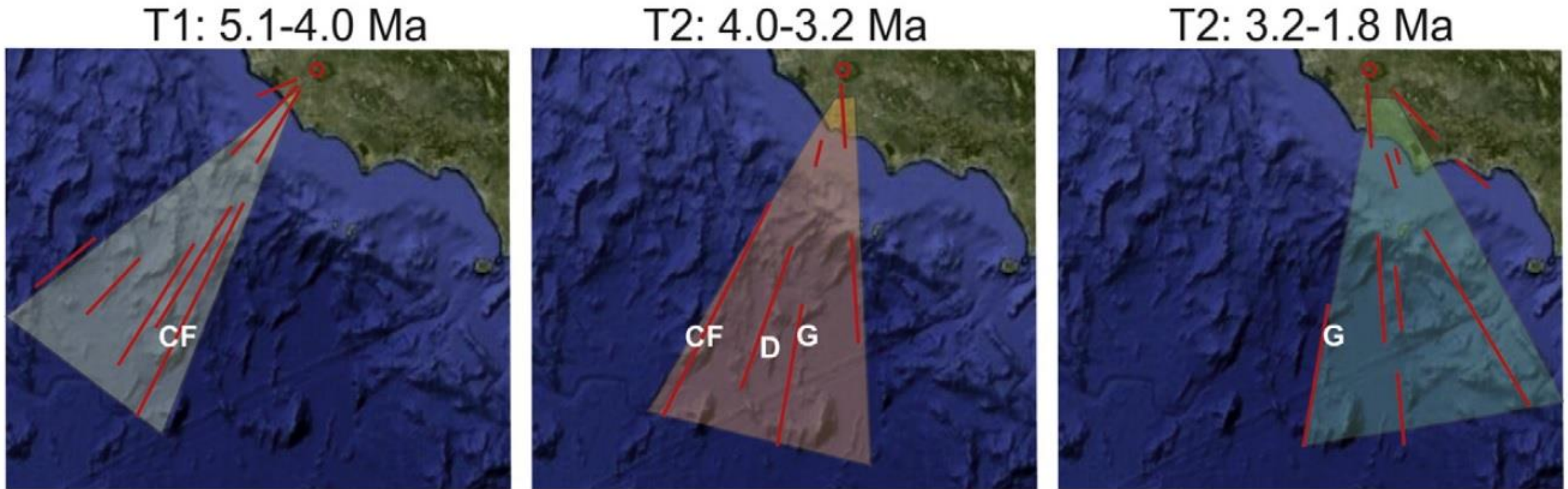
- Three main depocentres: a western basin (~10 km-wide and up to 2000 m thick), a central basin (~20 km-wide and up to 2400 m thick), and an eastern basin (Pontina Plain, up to 1000 m thick).
- The normal faults trend from ENE-WSW to N-S to NW-SE and converge toward a rotation pole located in correspondence of Alban Hills volcano.
- Positive inversion structures indicate that some of the pre-existing faults are successively inverted.

Milia et al., 2017, Tectonophysics, 710-711

FA= Fiume Astura, MA= Martina, TC = Tre Cancelli. Thickness values are estimated merging well and seismic reflection data.

From stretching to mantle exhumation: the Vavilov backarc basin

Eastwards time migration of extension in the Vavilov basin.

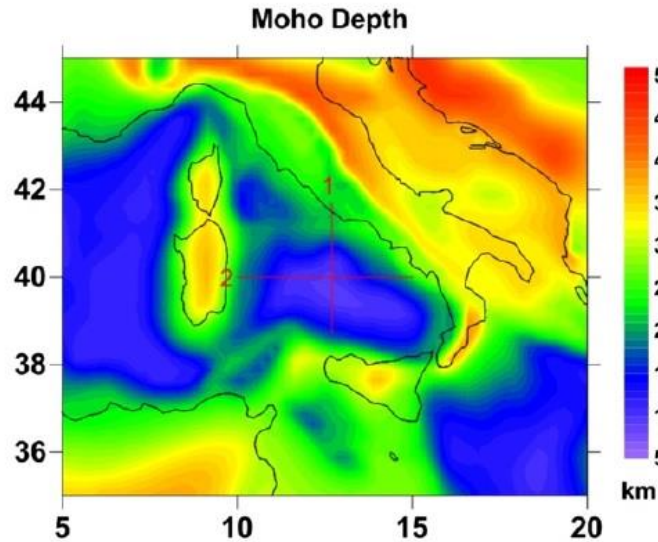


CF = Central Fault, D = De Marchi Seamount, G = Gortani Ridge

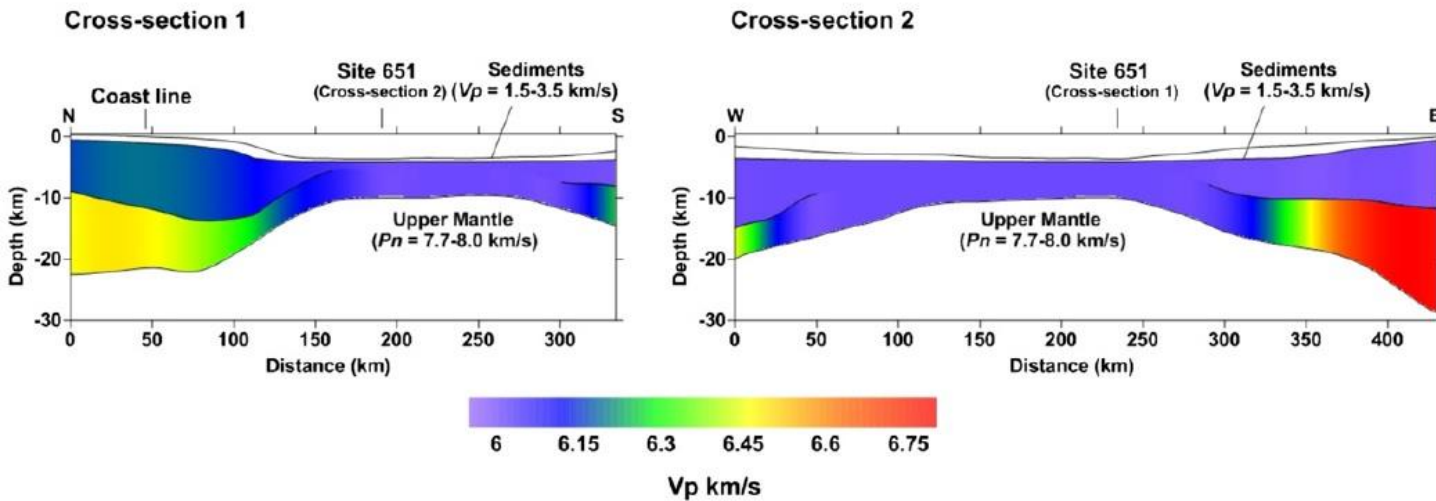
Milia et al., 2017, Tectonophysics, 710-711

- The Vavilov rift zone shows a converging pattern of normal faults bounding submarine ridges, from west to east.
- The convergent pattern of normal faults is coherent with a single Euler pole, located in Latium, during the entire basin history.

From stretching to mantle exhumation: the Vavilov backarc basin



- In the apex region of the Vavilov basin the crust has a thickness of 20–25 km and two crustal layers with distinct seismic velocities typical of extended continental crust.
- The crust thins and decreases its average velocity toward the bathyal part of the basin quite abruptly (decrease: ~ 10 km and ~ 0.3 km/s over a horizontal distance of less than 100 km).
- In the bathyal region, the crust of the basin is quite homogeneous, being characterized by a uniform thickness of ~ 7 km and low seismic velocities ($V_p \sim 6$ km/s) comparable to strong serpentinized peridotite.

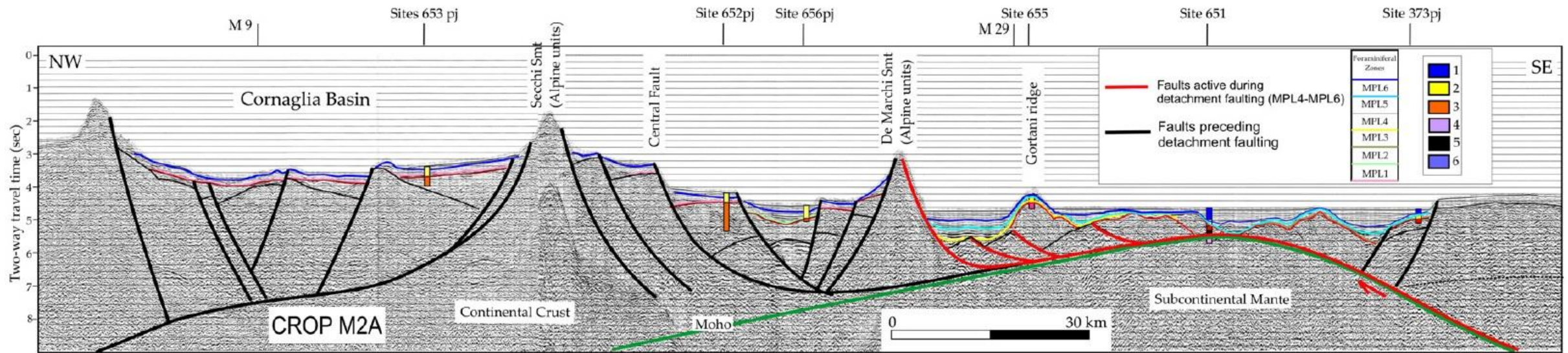


Difference in the crustal thickness variations between the distal (smooth) and apex (sharp) region can be due to a change in the crustal strength during the rifting:

- The higher extension rate in the central part of the basin has caused larger T in this area than in the apex during the opening phase. Consequently, the crustal brittle-ductile transition has migrated at shallower depth in the bathyal region.

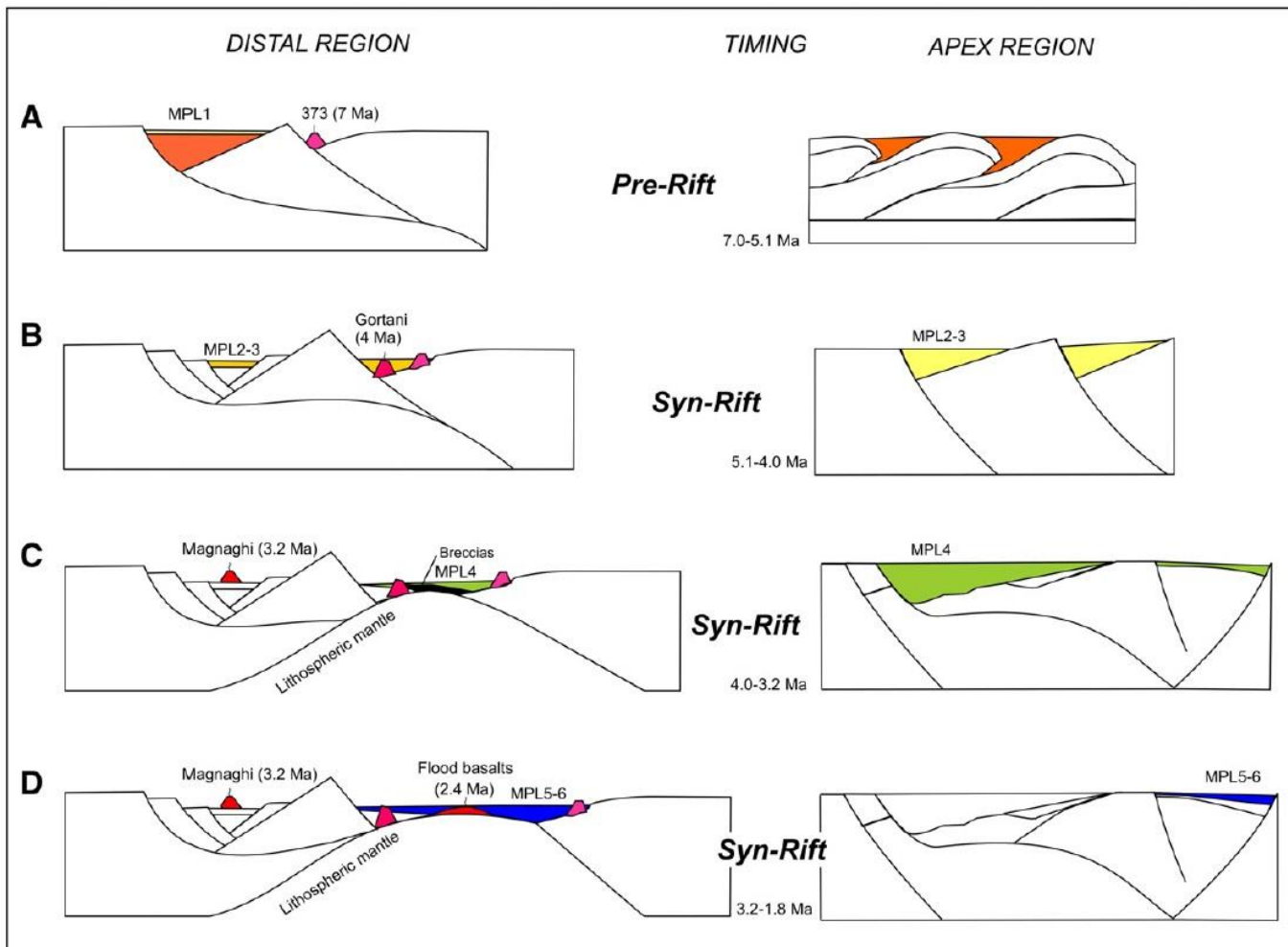
From stretching to mantle exhumation: the Vavilov backarc basin

Mantle rocks have been exhumed along a downward concave fault plane



CROP seismic profile M2A and interpretation. 1) Pleistocene deposits; 2) Pliocene deposits; 3) Messinian deposits; 4) basalts; 5) breccias; 6) serpentized peridotites. For profile location see Fig. 1. See text for explanation.

From stretching to mantle exhumation: the Vavilov backarc basin



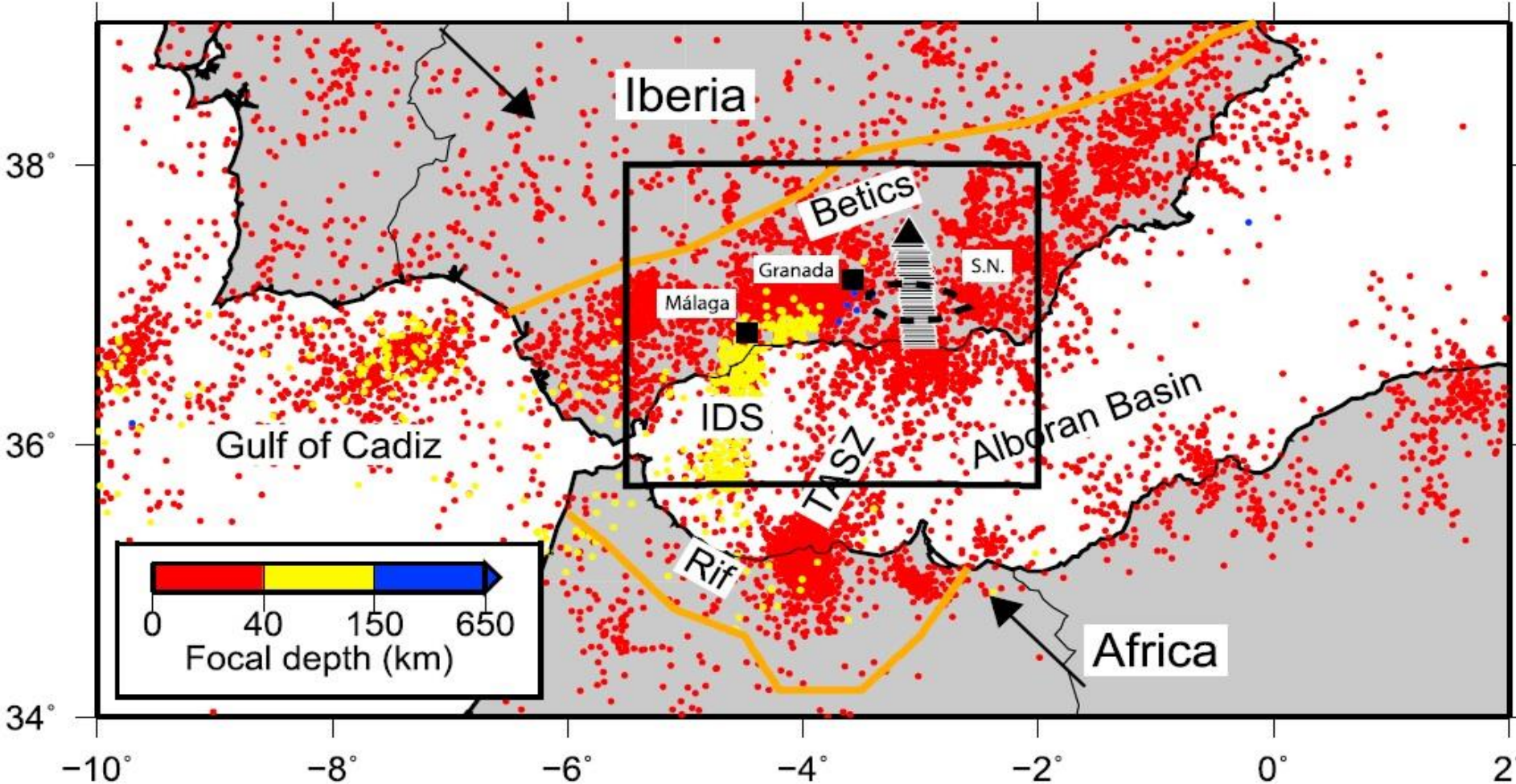
Downward concave fault geometry

Upward concave fault geometry

The kinematics of the Vavilov region records the complete evolution of a rift from stretching to mantle exhumation:

- The age of the sedimentary infill documents that the Vavilov basin started to open in the Lower Pliocene (5.1–4.0 Myr) coherently from the apex to distal regions by a pure shear mode, characterized by distributed high-angle normal faulting and asymmetric/symmetric rift basins.
- Rifting lasted 5.1–4 Myr and after a detachment basin evolved from 4 to 1.8 Myr. The extension switched during the upper Pliocene to a simple shear mode, associated to detachment faults.
- A supradetachment basin formed in the apex rift zone, which is characterized by strong subsidence and thick sub-horizontal deposits.
- In contrast, thin deposits are present in the distal zone, due to the increase of the distance from the sediment source area (Apennines).
- The final stage of opening of the Vavilov basin developed by a simple shear mode in the Upper Pliocene. The activity of detachments caused the maximum thinning and exhumation of serpentized peridotites of the mantle in the distal zone and metamorphic basement rocks in the proximal one.

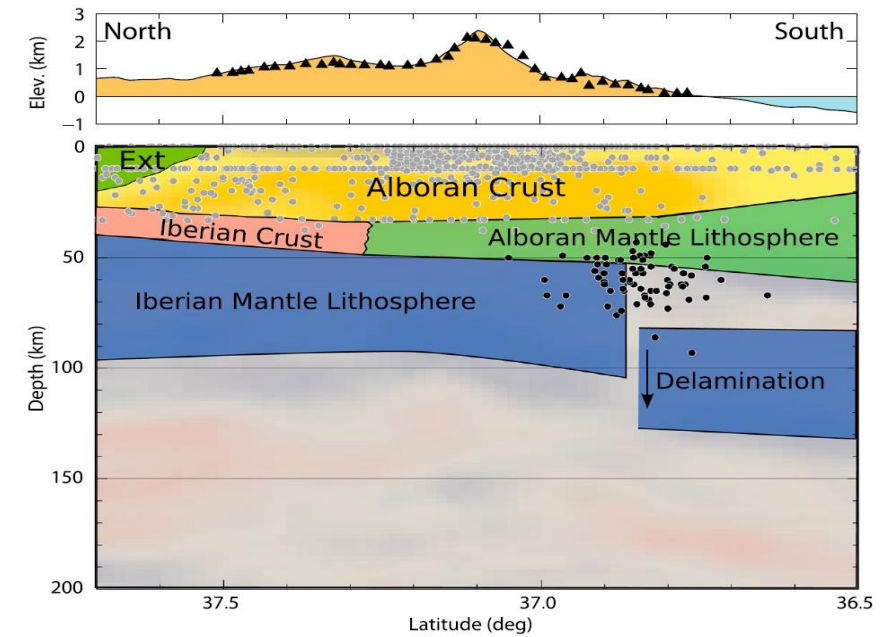
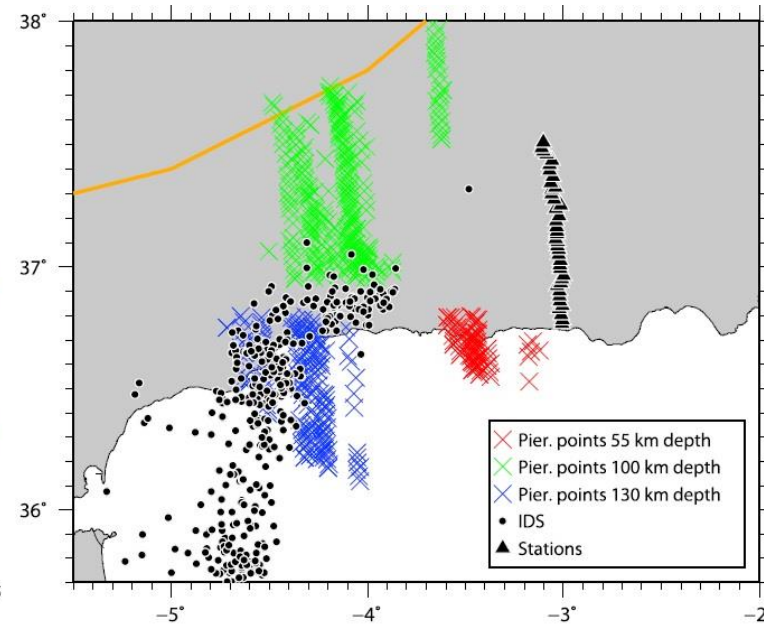
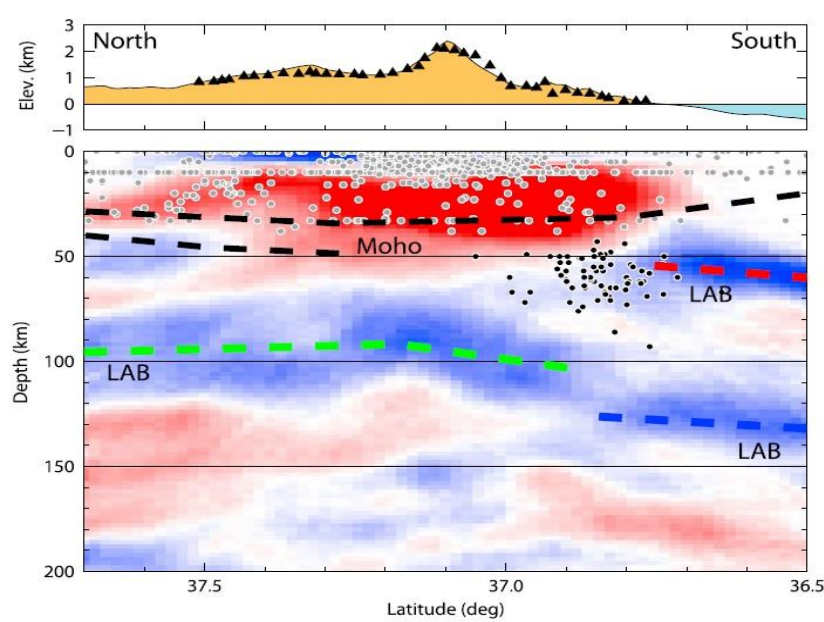
Gibraltar Arc



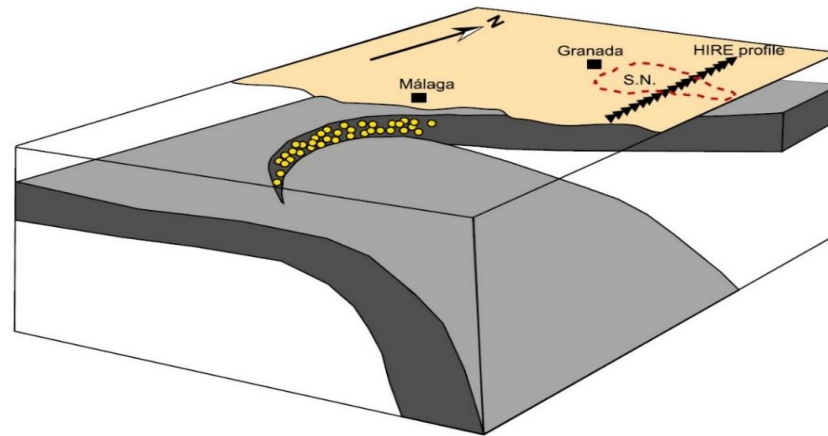
Heit et al., 2017 Geophys. Res. Lett., 44

Slab Subduction beneath Gibraltar Arc

S wave receiver functions (SRFs)



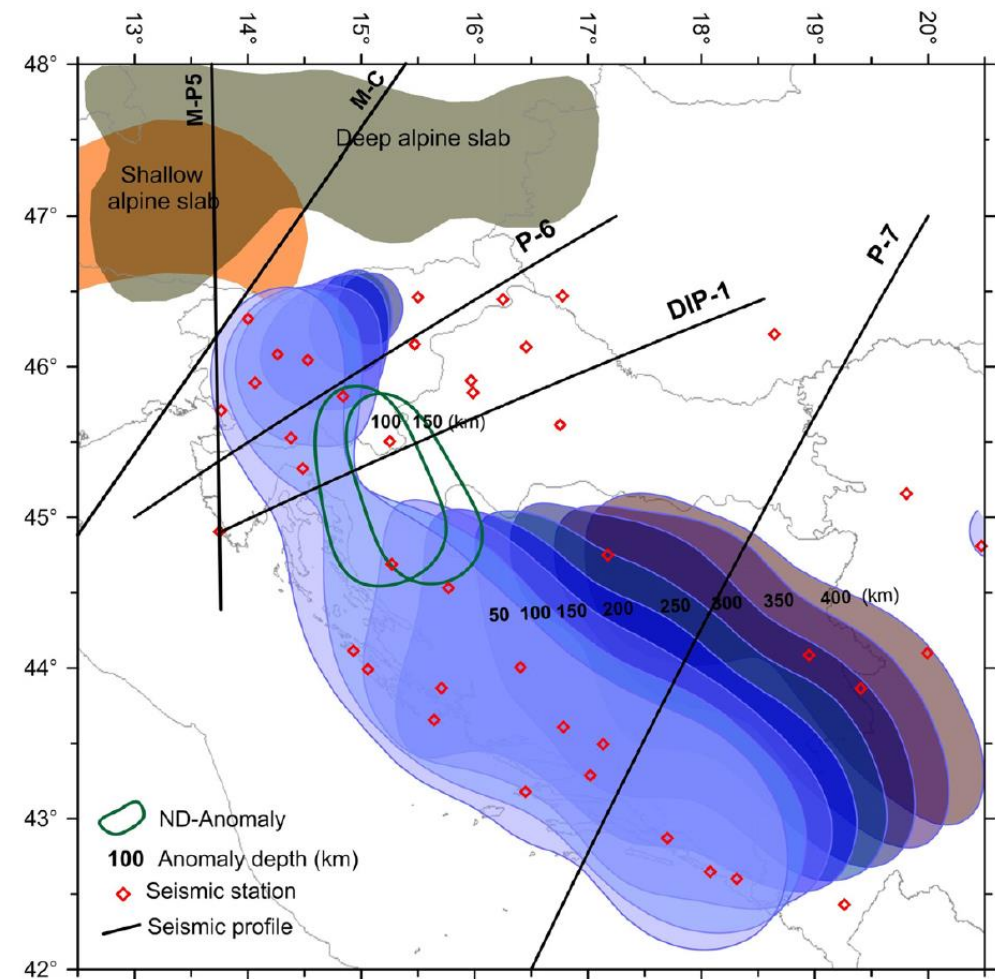
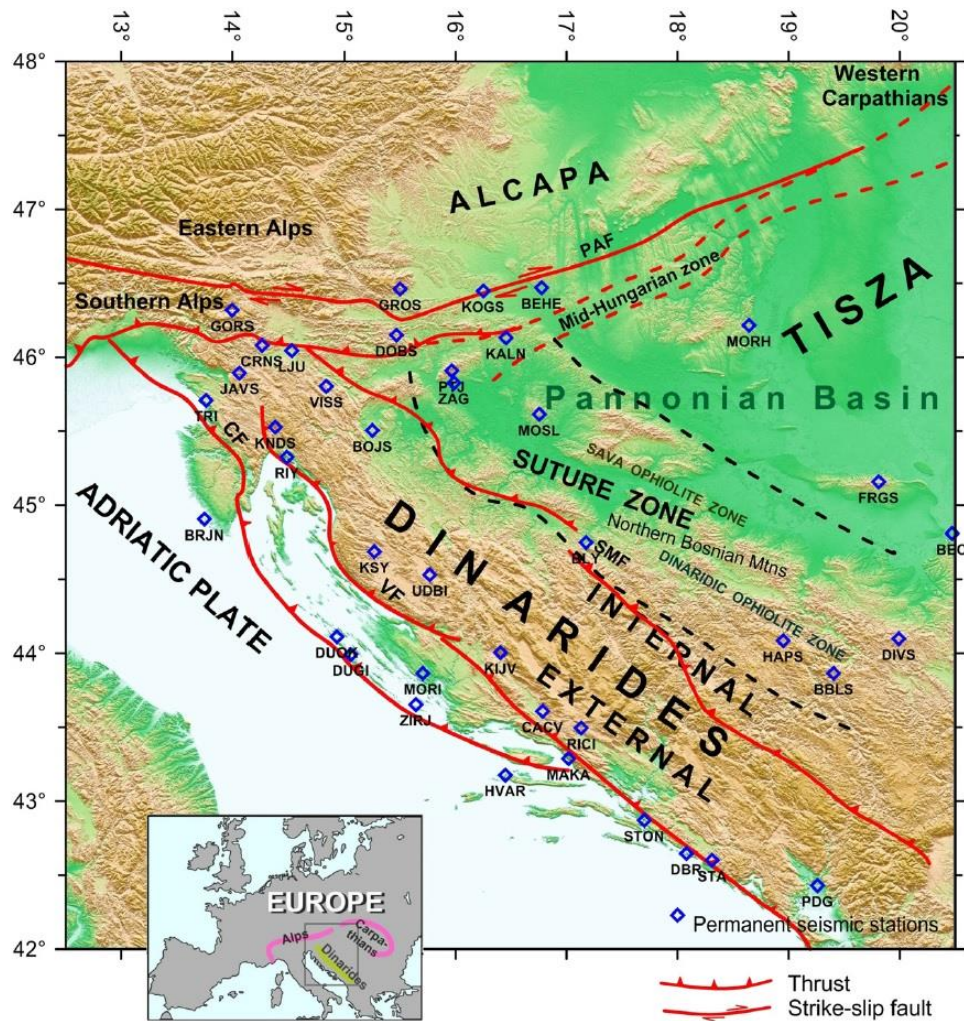
Heit et al., 2017 Geophys. Res. Lett., 44



IDS: Intermediate Depth Seismicity

- The rupture along the intermediate depth seismicity marks the onset of the lithospheric delamination, which is the result of slab pull and rollback.

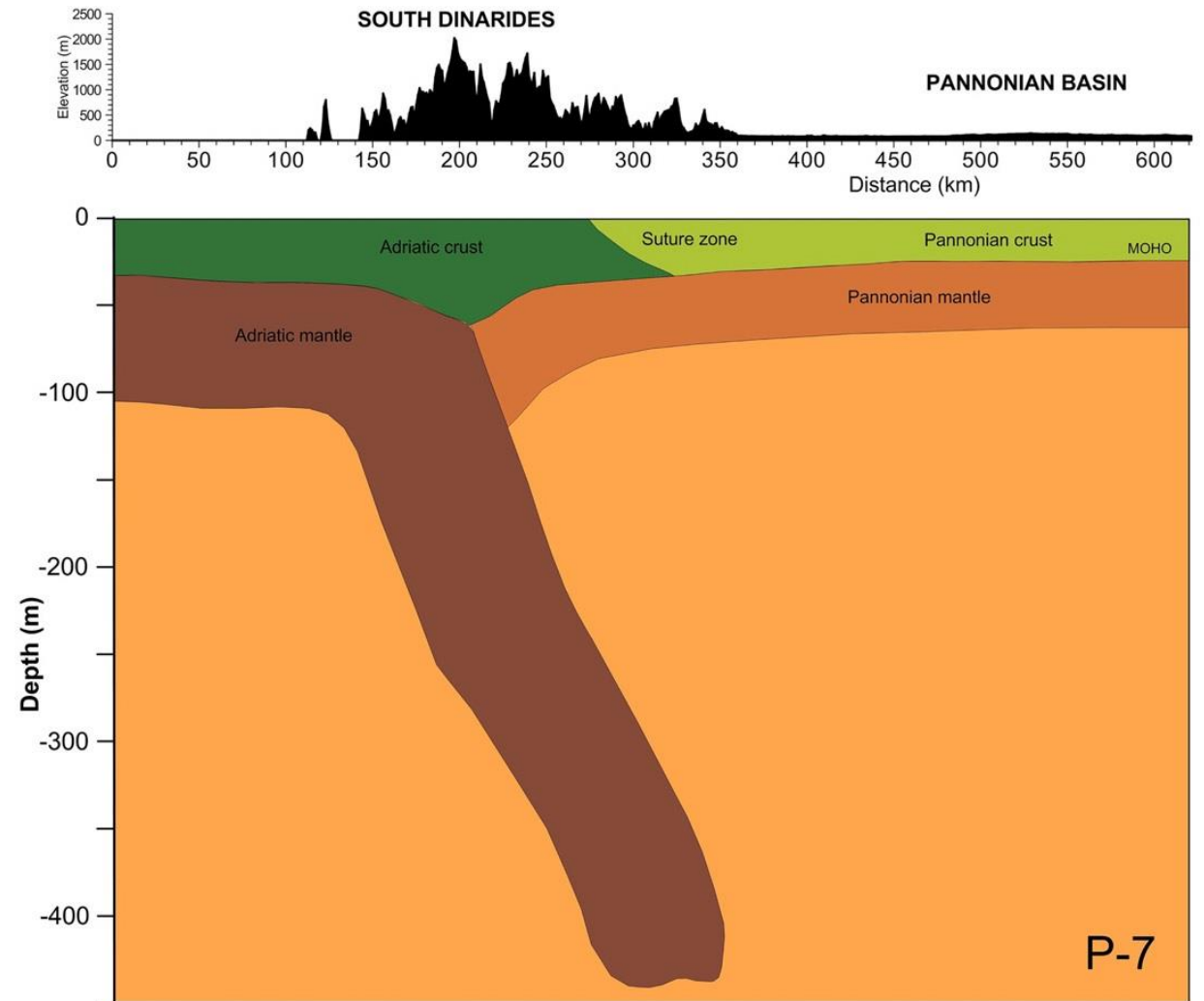
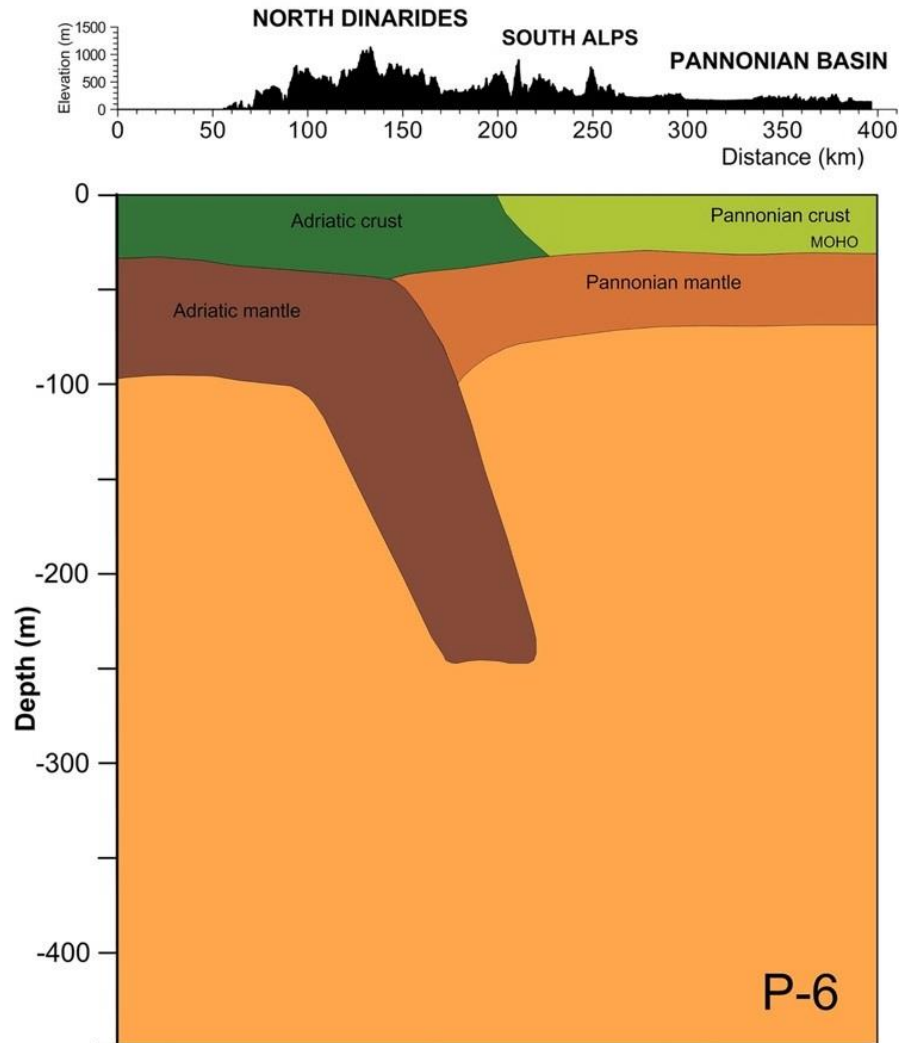
Slab Subduction beneath Dinarides



Šumanovac et al., 2017, Tectonophysics, 712-713

- The Dinarides are divided into External Dinarides spread along the Adriatic coast, and Internal Dinarides as narrow belt in the inland. This complex orogenic system formed because of the collision of the African and Eurasian plate.
- A fast velocity anomaly extending underneath the entire Dinarides mountain belt indicates cold, rigid materials.
- In the Northern Dinarides the anomaly, steeply sloping towards the northeast (due to the sinking of the Adria microplate underneath the Pannonian tectonic segment) extends to the depth of 250 km, whereas in the Southern Dinarides it reaches greater depths (up to 450 km).

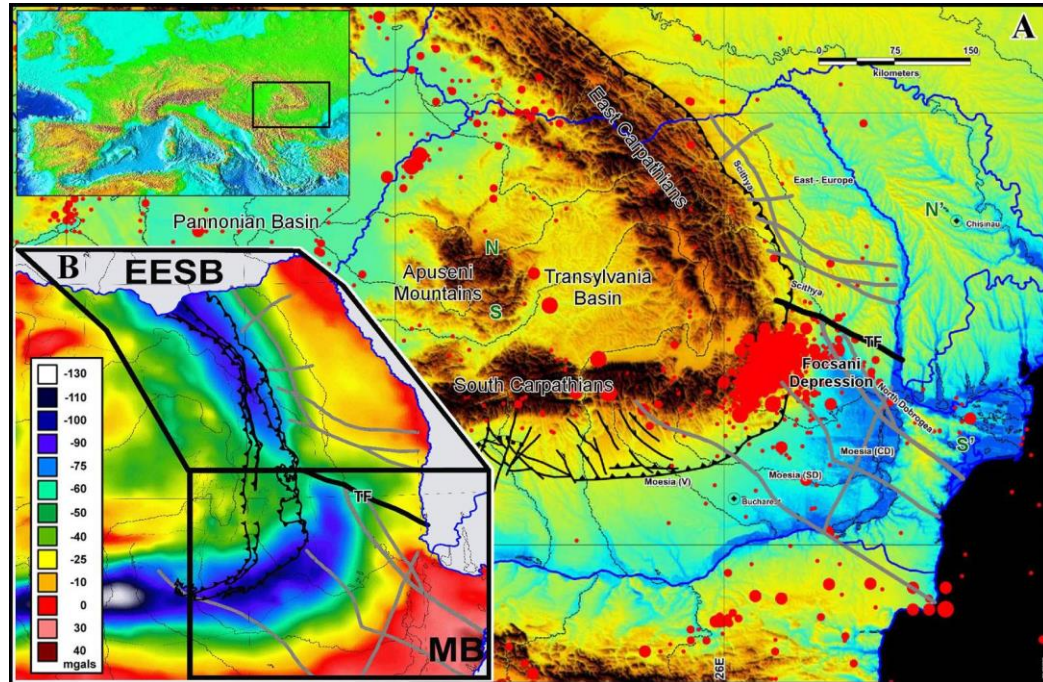
Slab Subduction beneath Dinarides



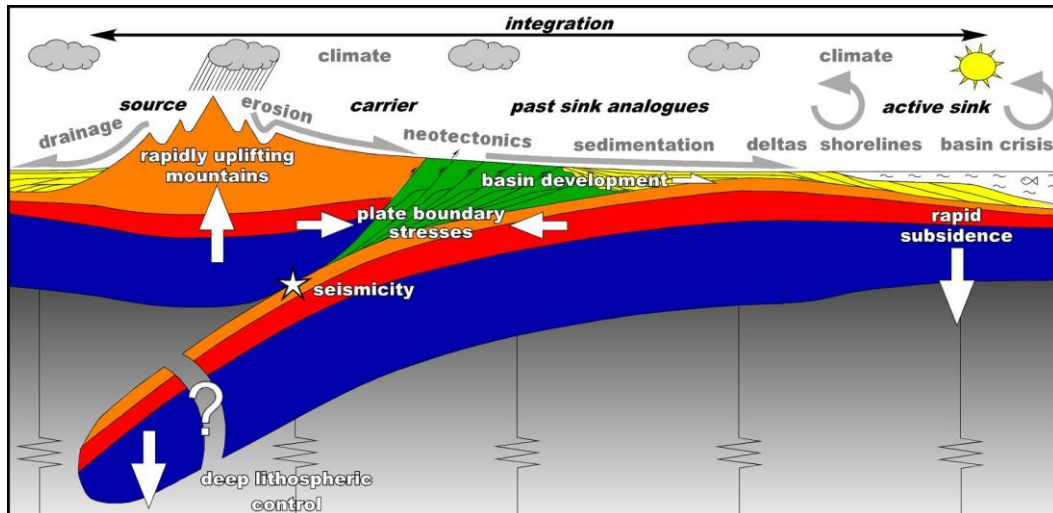
Šumanovac et al., 2017, Tectonophysics, 712-713

- Different slab depths are interpreted as the faster convergence of the plate in the southern Dinarides than in the northern, or the convergence of the plates had started in the southern part and systematically developed to the north.

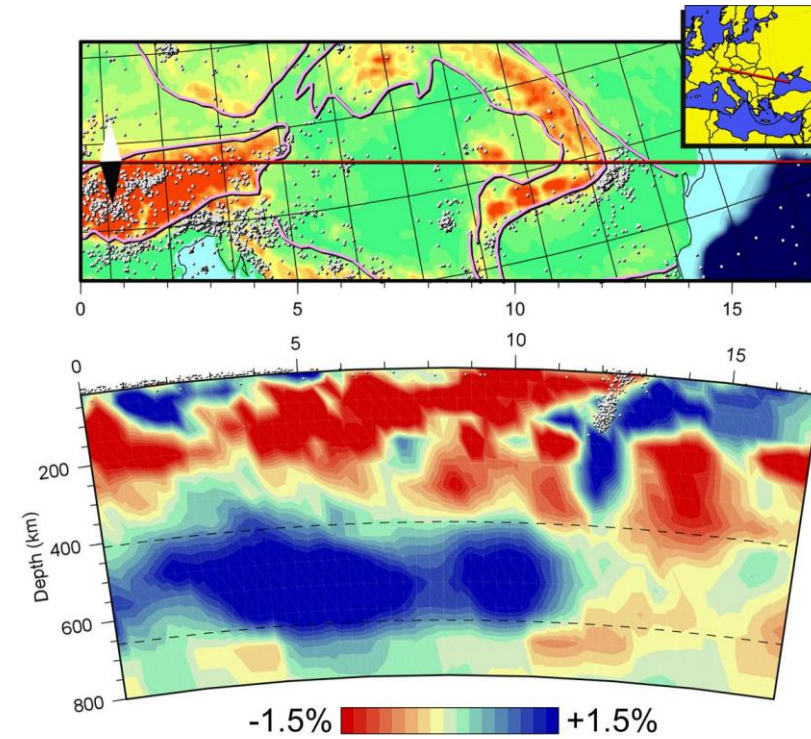
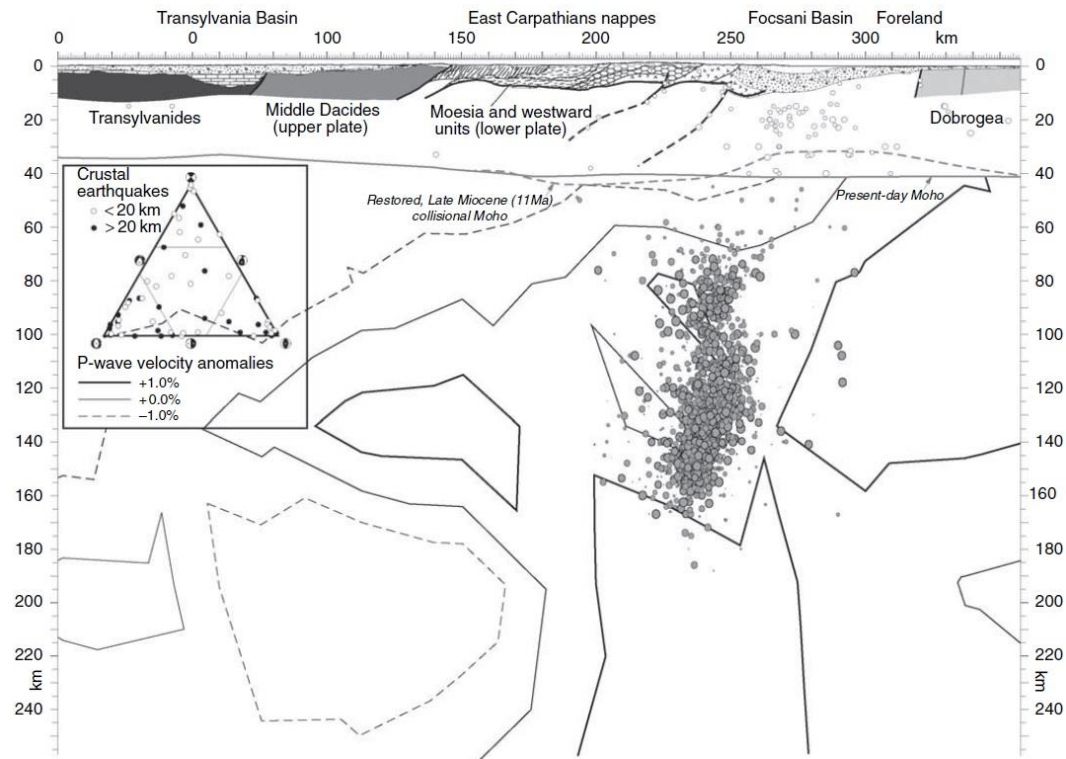
The Alps-Carpathians-Pannonian Basin System: Vrancea Area (Romania)



- The tectonic development of the Carpathian-Alpine system began in the Jurassic and is mostly controlled by the collision of three large continental plates: the Eurasian, African, and Arabian.
- The southeastern Carpathian Arc bend is located at the confluence of three main tectonic units (east European plate, Intra Alpine subplate and Moesian subplate) in the Vrancea region of Romania.
- The collision of this segment of the Alpine belt began in the Cenozoic as a result of the lateral eastward extrusion caused by the continuous convergence in the Alps.
- In the Vrancea region, an oceanic basin, floored by an oceanic crust, lays in the area of the present-day Carpathians which was consumed by subduction during Tertiary times.
- A complex active processes still take place beneath Vrancea in a very confined area, manifested in a cluster of intermediate seismicity beneath Vrancea in a narrow nearly vertical volume at depths below 60 km.



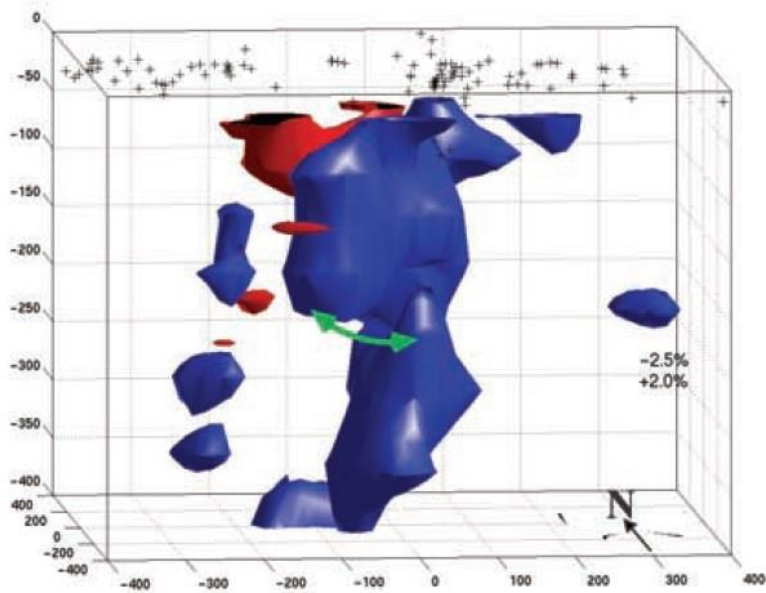
The Alps-Carpathians-Pannonian Basin System: Vrancea Area (Romania)



Bijwaard and Spakman, Geoph.J.Int, 2000

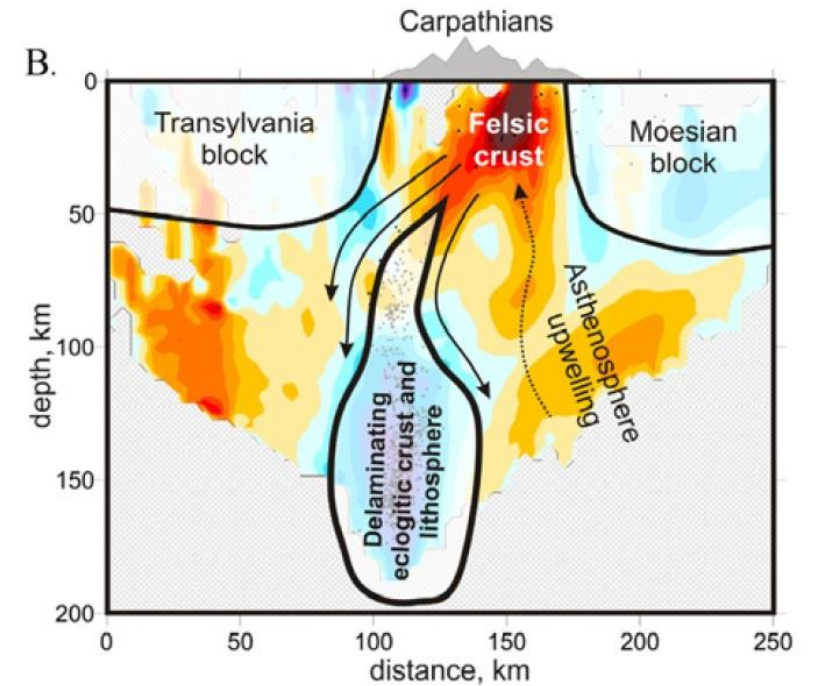
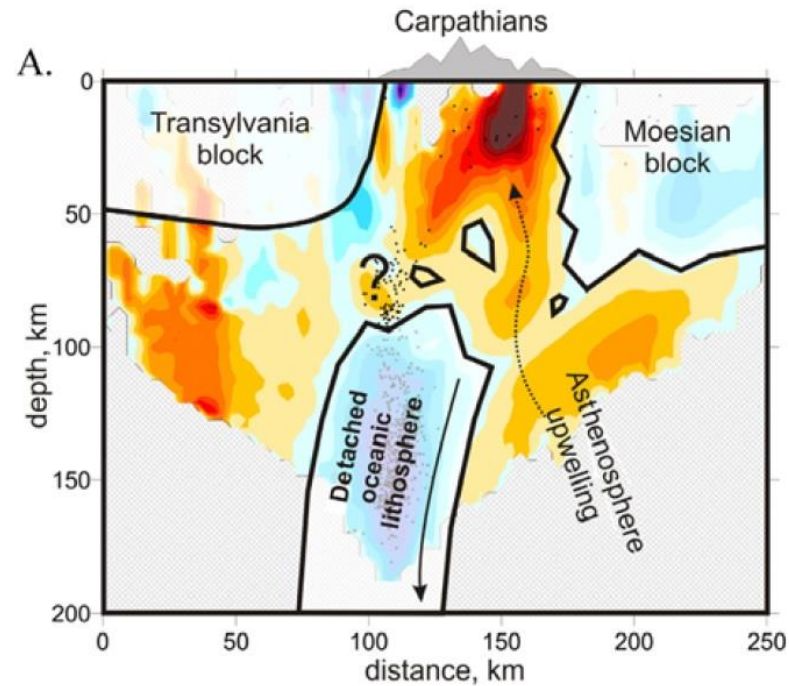
Wortel and Spakman, Science, 2000

The Alps-Carpathians-Pannonian Basin System: Vrancea Area (Romania)



Martin et al., 2006, Geophys. J. Int., 164

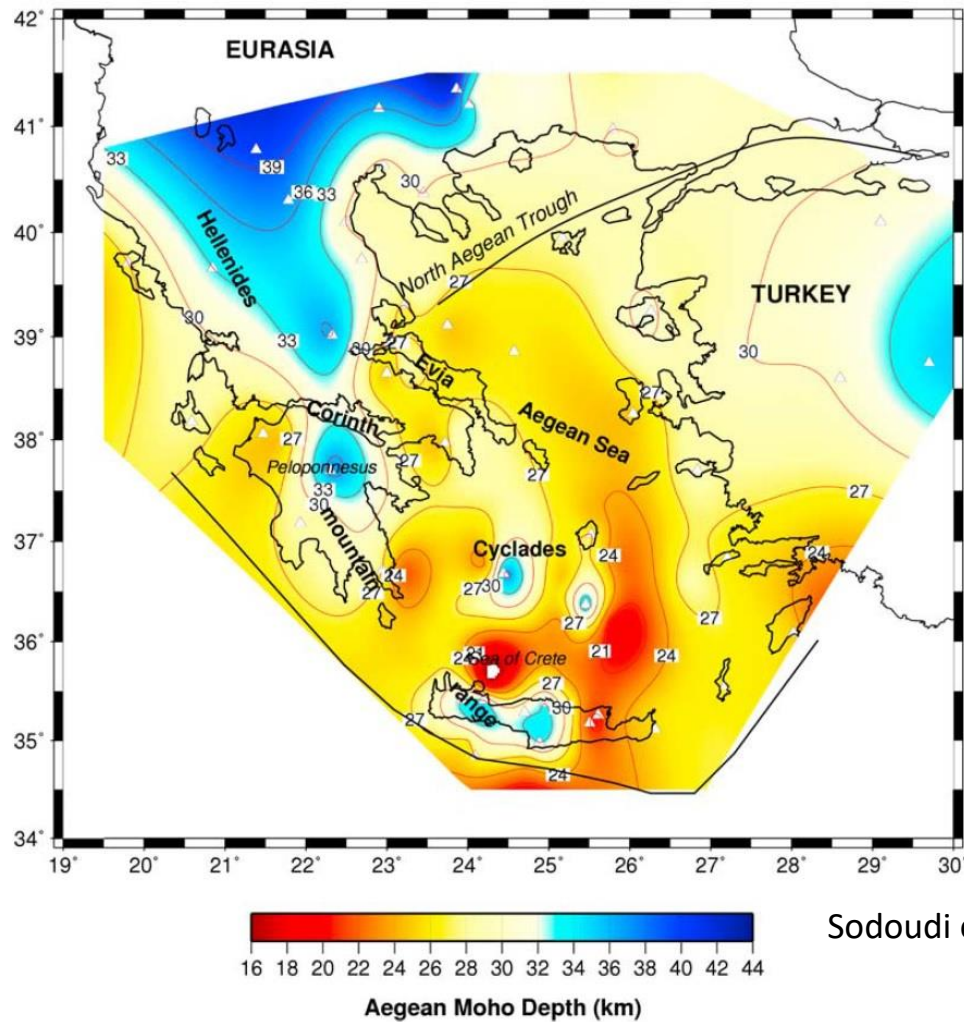
- The tearing of the slab at 200 km depth accompanied by the rotation of the slab from NE-SW towards N-S orientation (green arrow)



Koulakov et al., 2010, G3

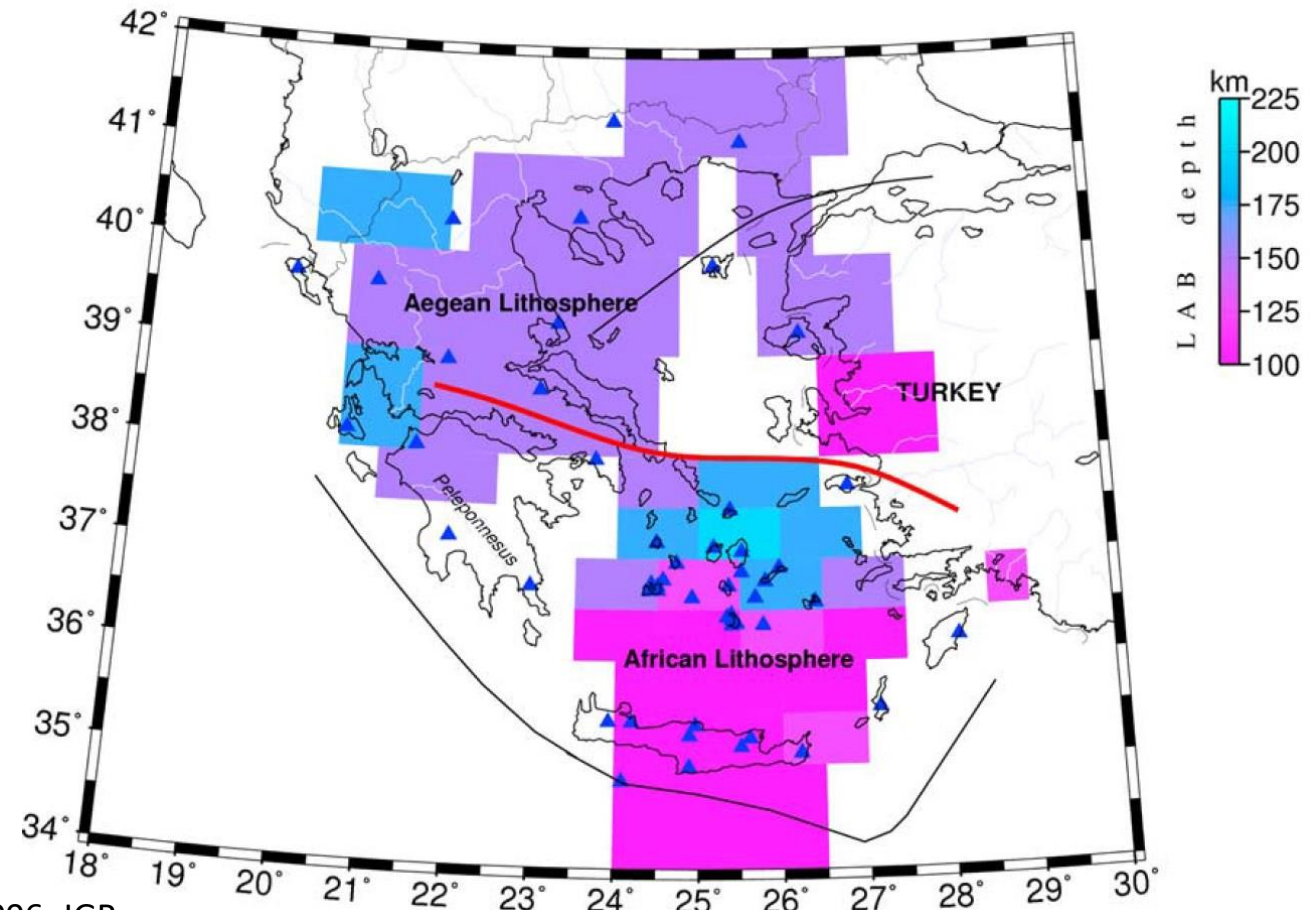
- It is observed a falling “drop” consisting of eclogitic lower crust material, result of phase transition in the mafic layer due to the thickening of the crust, surrounded by untrained lithosphere material. This delamination occurs after a long stage of accumulation of denser eclogitic material in the bottom of the crust.

Eastern Mediterranean



Sodoudi et al., 2006, JGR

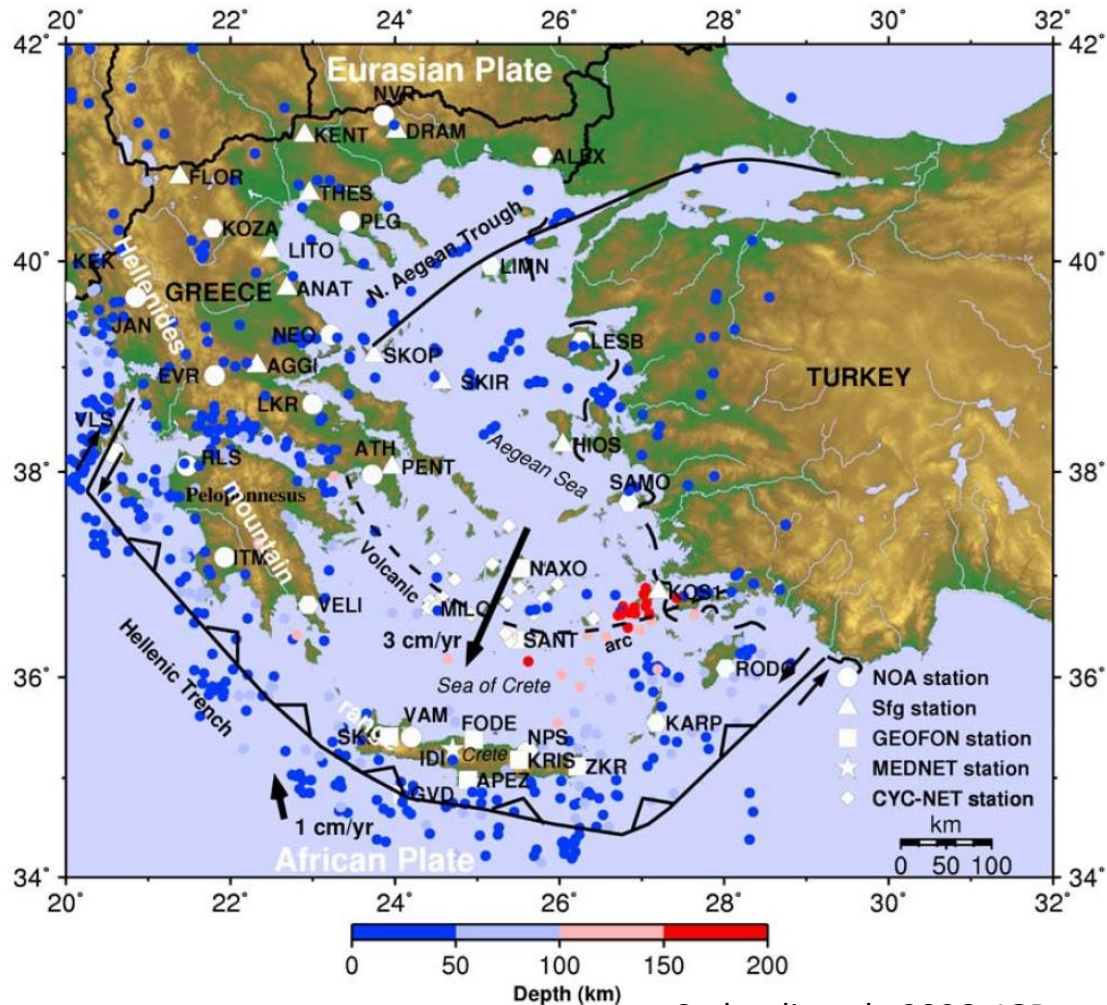
Aegean Moho depth map (in km) obtained from P and S receiver functions.



Red line indicates the boundary separating the observed continental Aegean lithosphere from the oceanic African lithosphere.

- The crustal structure of Aegean Sea and its surroundings is thinned and formed as an extensional backarc basin due to subduction of the African lithosphere beneath the Hellenic trench.

Eastern Mediterranean



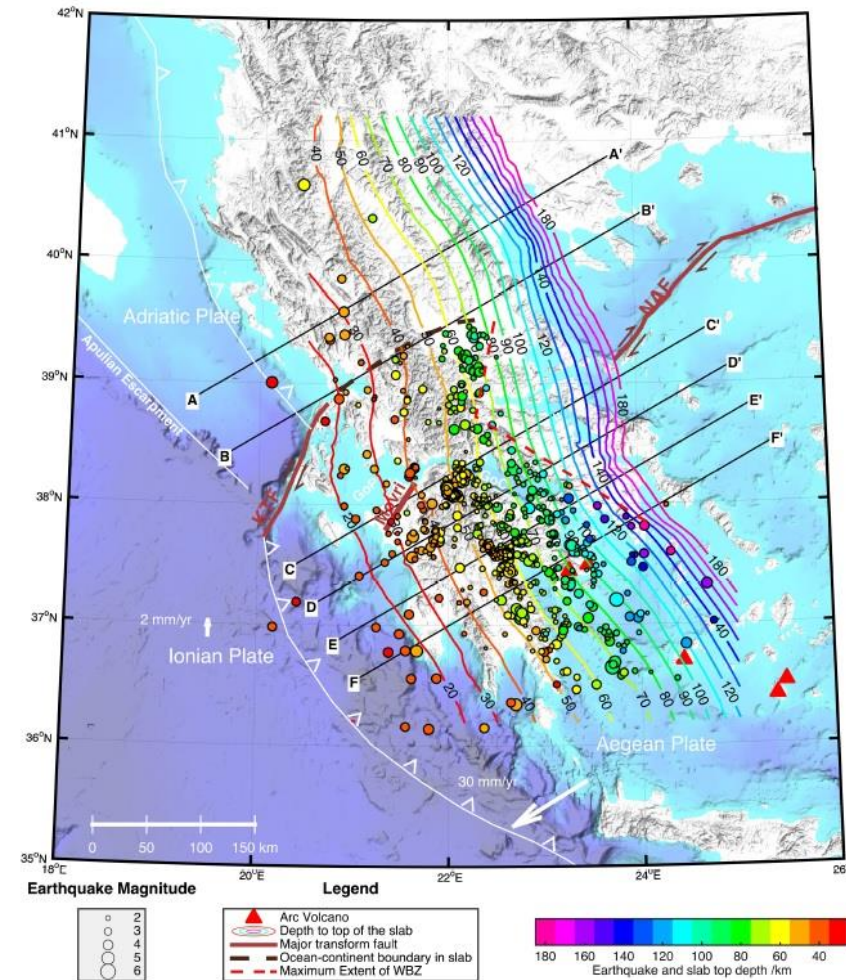
Sodoudi et al., 2006, JGR

Black solid lines = locations of the Hellenic trench and the North Aegean Trough.

Dashed line = location of the volcanic arc.

Black arrows = direction of the motion relative to Eurasia

Blue circles = earthquakes with $M_s > 4.5$

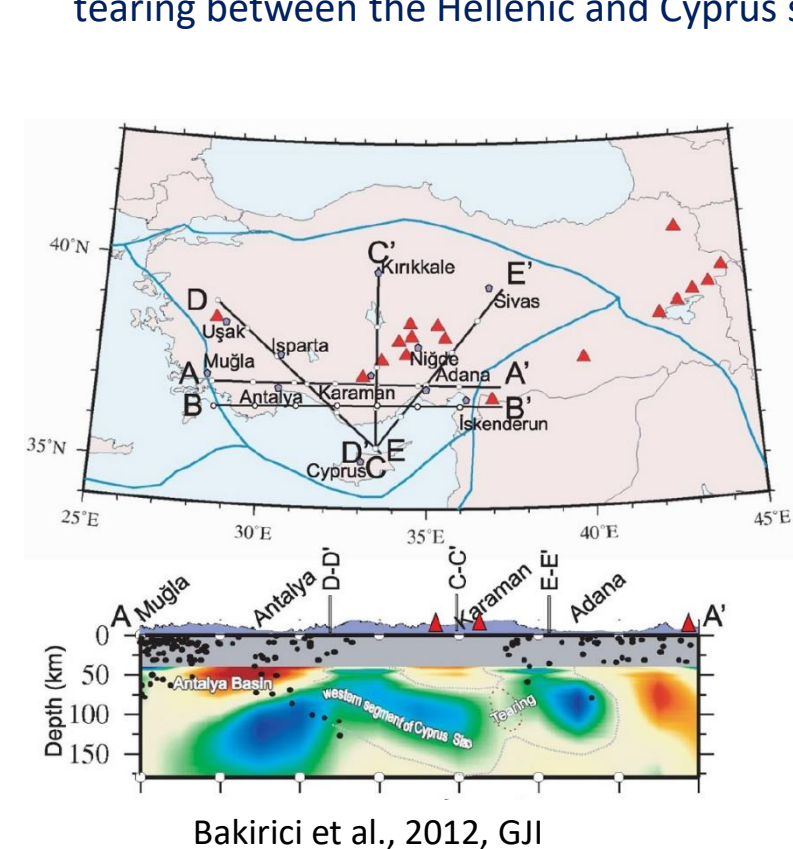


Halpaap et al., 2018, JGR

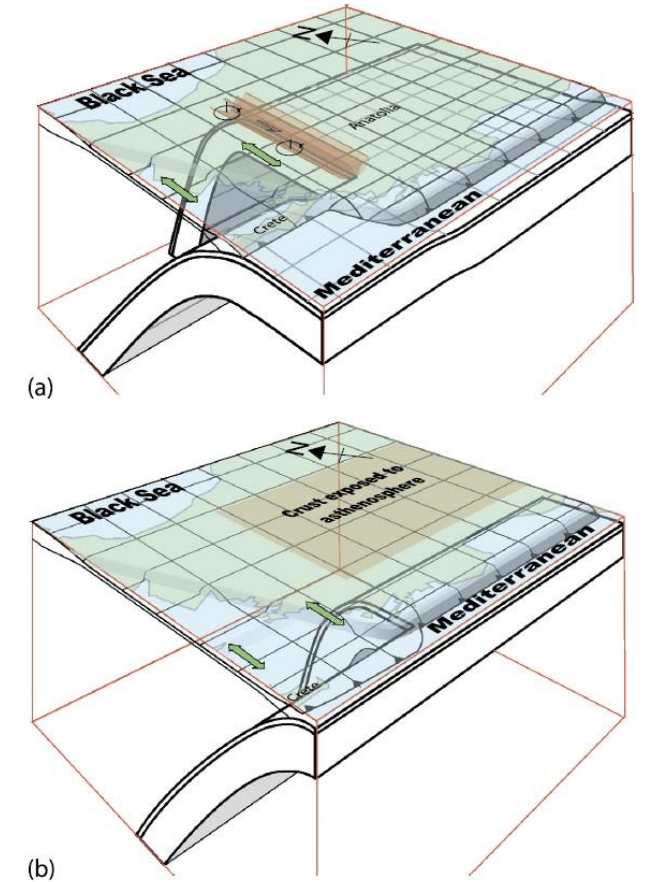
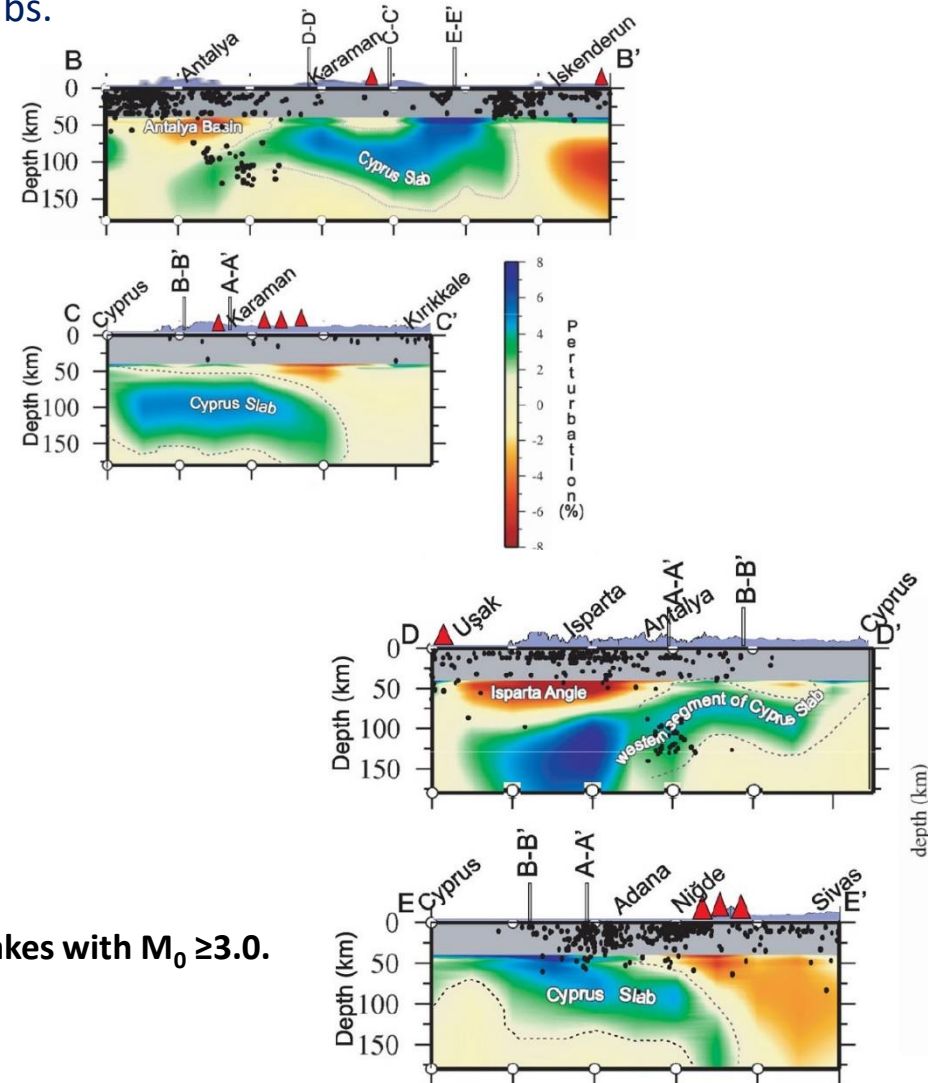
- The transition between oceanic subduction with more rollback in the south to continental subduction with less rollback in the north occurs in correspondence of Kefalonia fault and is reflected by a smoothly deformed slab, accompanied by a gap in deep intraslab seismicity (>60 km depth), probably indicative of a change in thermal regime between south and north.

Eastern Mediterranean

- The Eastern part of the Cyprus slab is extending beneath Nigde and Karaman cities and terminates beneath the quaternary volcanoes, while the western part of the Cyprus slab is extending under the Isparta Angle (IA) and Antalya Basin and is probably closed to the Hellenic slab.
- The Hellenic and Cyprus slab, divided by a tear, may simply be merged south of the Isparta Angle.
- The slow anomalies under the IA and Antalya Basin are likely to be associated with rising hot materials from asthenosphere due to major tearing between the Hellenic and Cyprus slabs.



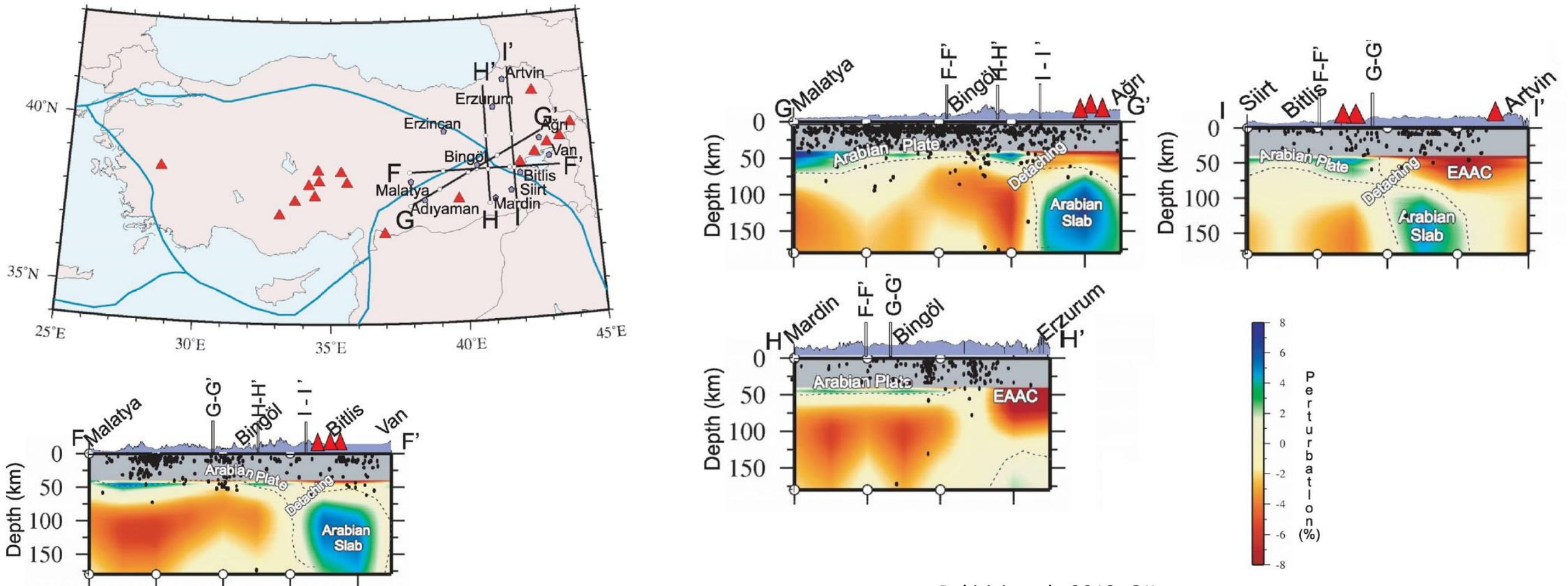
Black circles on the slices are focal depth of earthquakes with $M_0 \geq 3.0$.



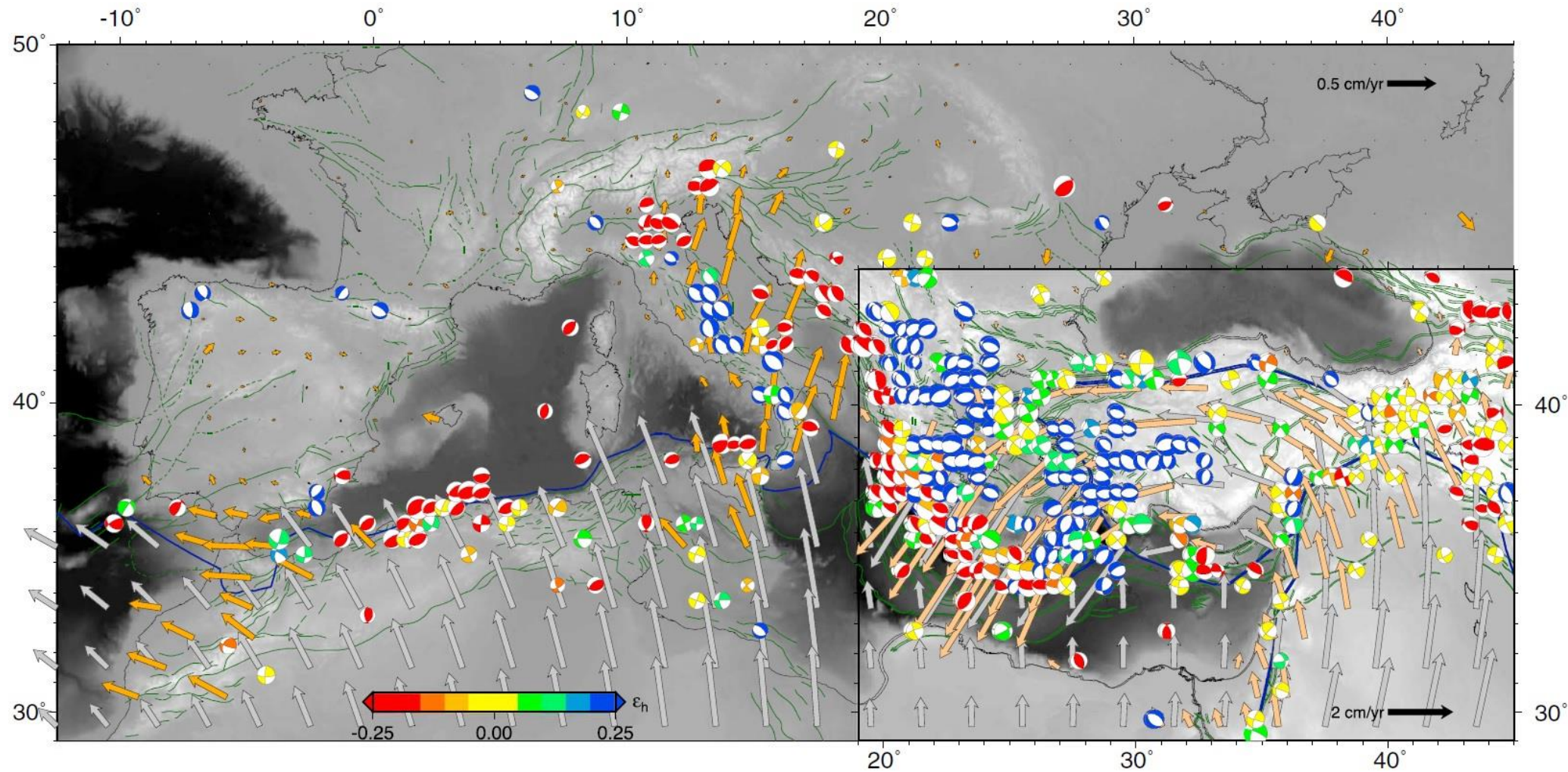
Govers and Fichtner, 2016, EPSL, 450

Eastern Mediterranean

- The Arabian slab appears to be broken-off under the Eastern Anatolia, which may cause the widespread volcanism and uplift in the Eastern Anatolia.



Mediterranean Tectonics

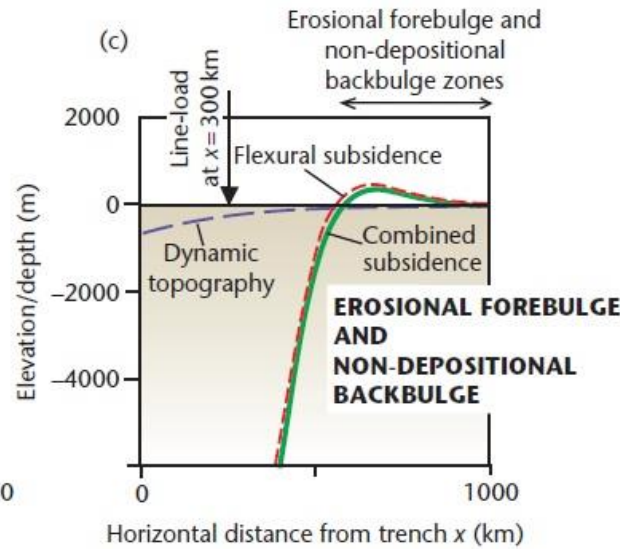
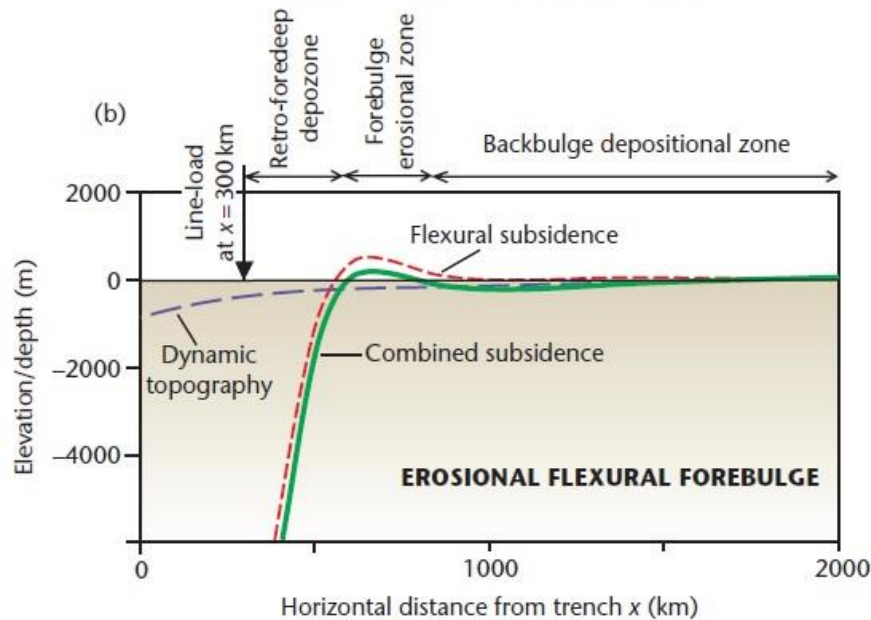
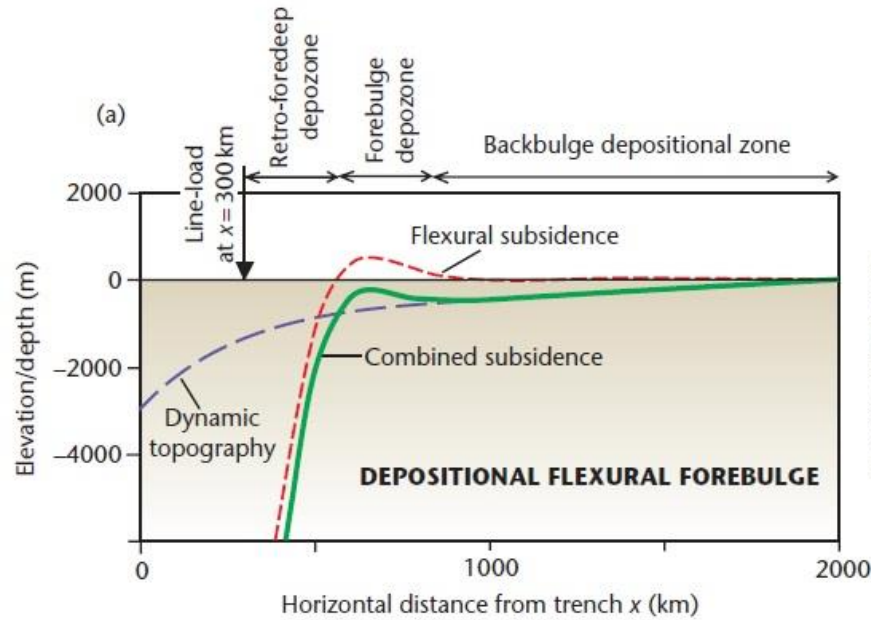


Faccenna et al., 2014, Rev. Geophys., 52

Interpolated GPS velocities (orange vectors obtained by first averaging velocities weighted by their uncertainties on a $1^\circ \times 1^\circ$ grid, and then using spline-in-tension interpolation) long-term plate velocities (gray vectors, both in Eurasia-fixed reference frame). Blue, red, and green indicate extensional, compressional, and strike-slip types of deformation state.

Dynamic topography

(due to subducting slabs)



An expression for the geometric form of the dynamic topography is obtained by assuming that it is made of two components:

- an exponential component with an exponent λ and maximum deflection f_m .
- a linear tilt with a maximum gradient α in m km^{-1} and a maximum distance from the trench at which tilting occurs η .

$$f(x) = f_m(e^{-x/\lambda}) + \alpha(\eta - x)$$

x = horizontal orthogonal distance from the trench

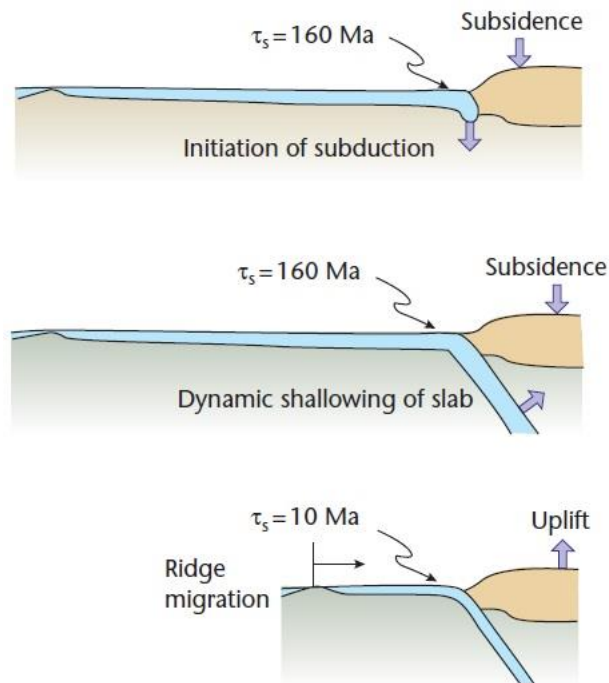
- for $\lambda=200$ km, $f_m = 2000$ m, $\alpha = 0.5$ m/km, and $\eta = 2000$ km
Dynamic topography exceeds the effects of flexural forebulge uplift.
- for $\lambda=200$ km, $f_m = 500$ m, $\alpha = 0.2$ m/km, and $\eta = 2000$ km
Dynamic topography is insufficient to exceed the magnitude of forebulge uplift.
- for $\lambda=200$ km, $f_m = 500$ m, $\alpha = 0.2$ m/km, and $\eta = 1000$ km (due to steepening of slab dip):
Dynamic topography is reduced, then back-bulge region is a non-depositional zone.

Dynamic topography

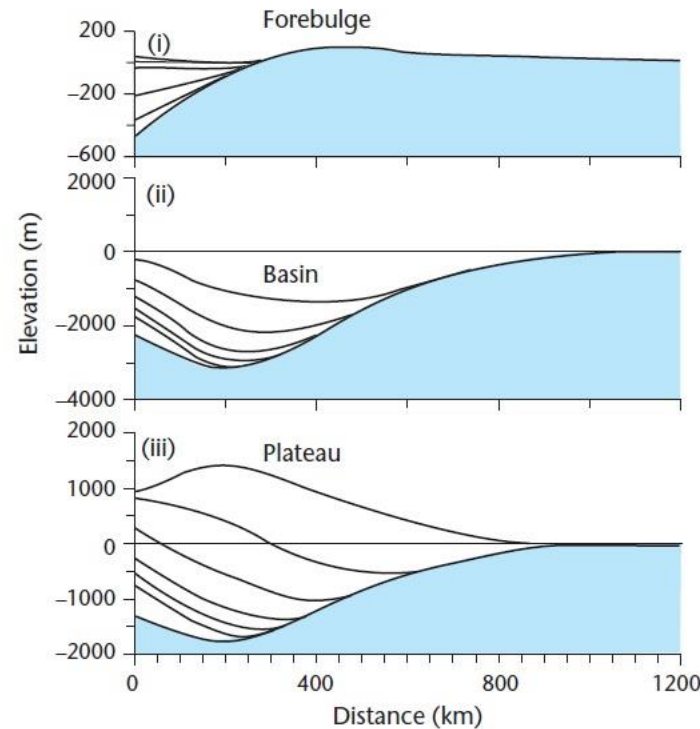
(due to subducting slabs)

- Horizontal distance into the upper plate affected by dynamic topography is likely related to the dip of the subducting slab.
- Subduction angle $< 45^\circ$ and a ΔT between slab and surrounding mantle of -200 K to -800 K produce deflections of the continental plate > 500 km from the trench.
- Factors influencing dynamic subsidence/uplift, besides subduction angle, are plate age, rate of subduction, flexural rigidity, and viscosity of the upper mantle.

(a) EVOLUTION OF OCEAN-CONTINENT CONVERGENCE

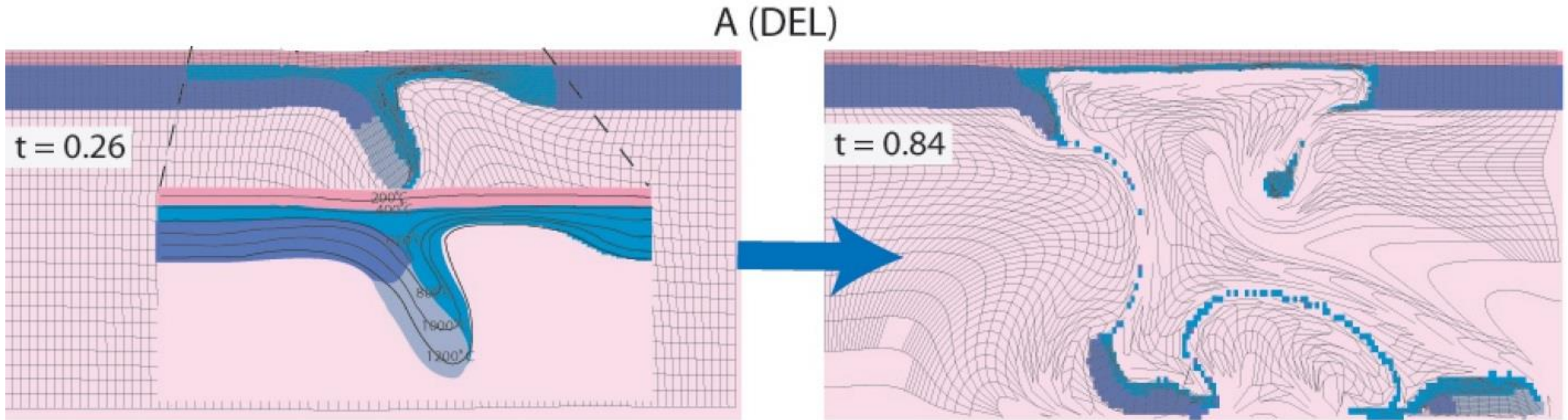


(b) DYNAMICALLY CONTROLLED STRATIGRAPHY



- Subduction of young oceanic lithosphere causes long-wavelength uplift (e.g., Farallon plate beneath North America caused uplift of the Colorado Plateau).
- The dip of the slab generally decreases with age or when it attempts to subduct positive buoyant region (e.g., mid-oceanic ridge).

Delamination of the subducting slab



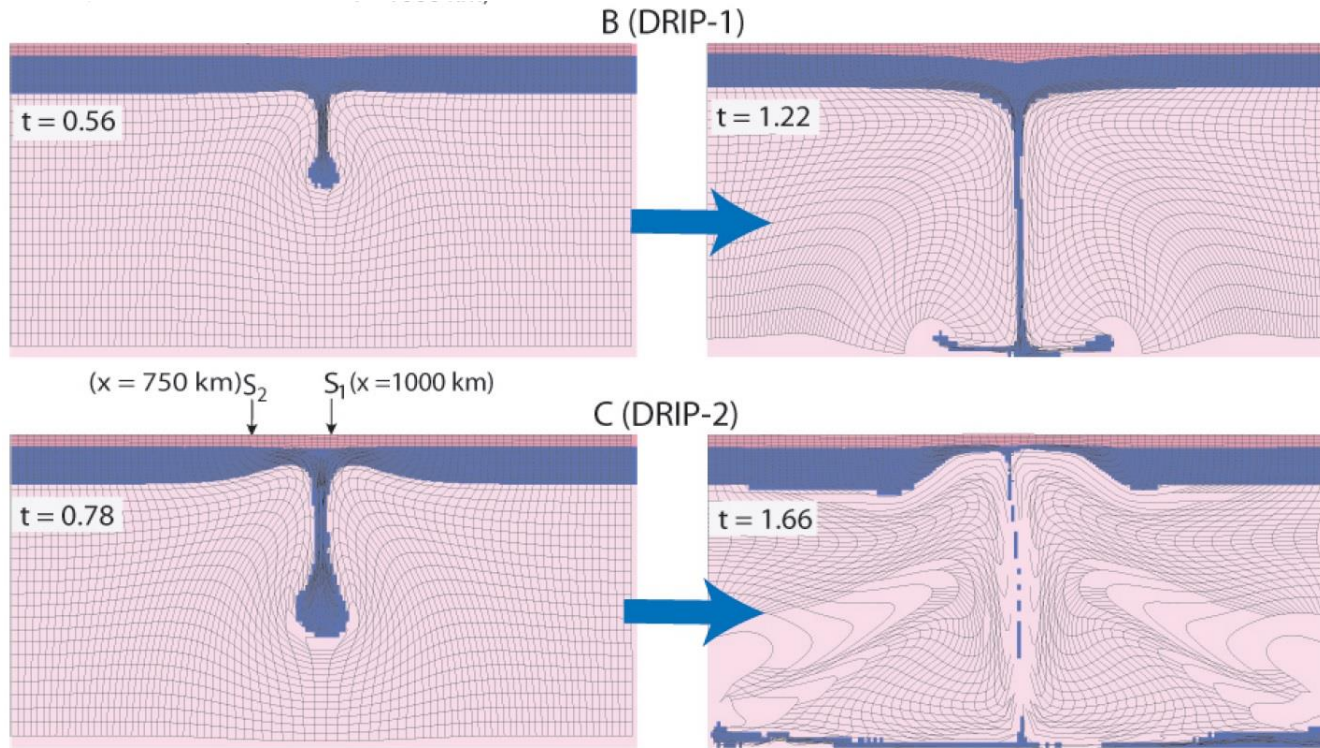
Gogus, 2010 (PhD thesis)

- As the mantle lithosphere starts to delaminate, it causes subsidence of the crust, while uplift occurs on the right side of the depression as hot mantle material is owing into the lithosphere breach vacated by the delaminating lithosphere.
- The signal of topography is becoming more asymmetrical as the delamination progresses in these very early stages.

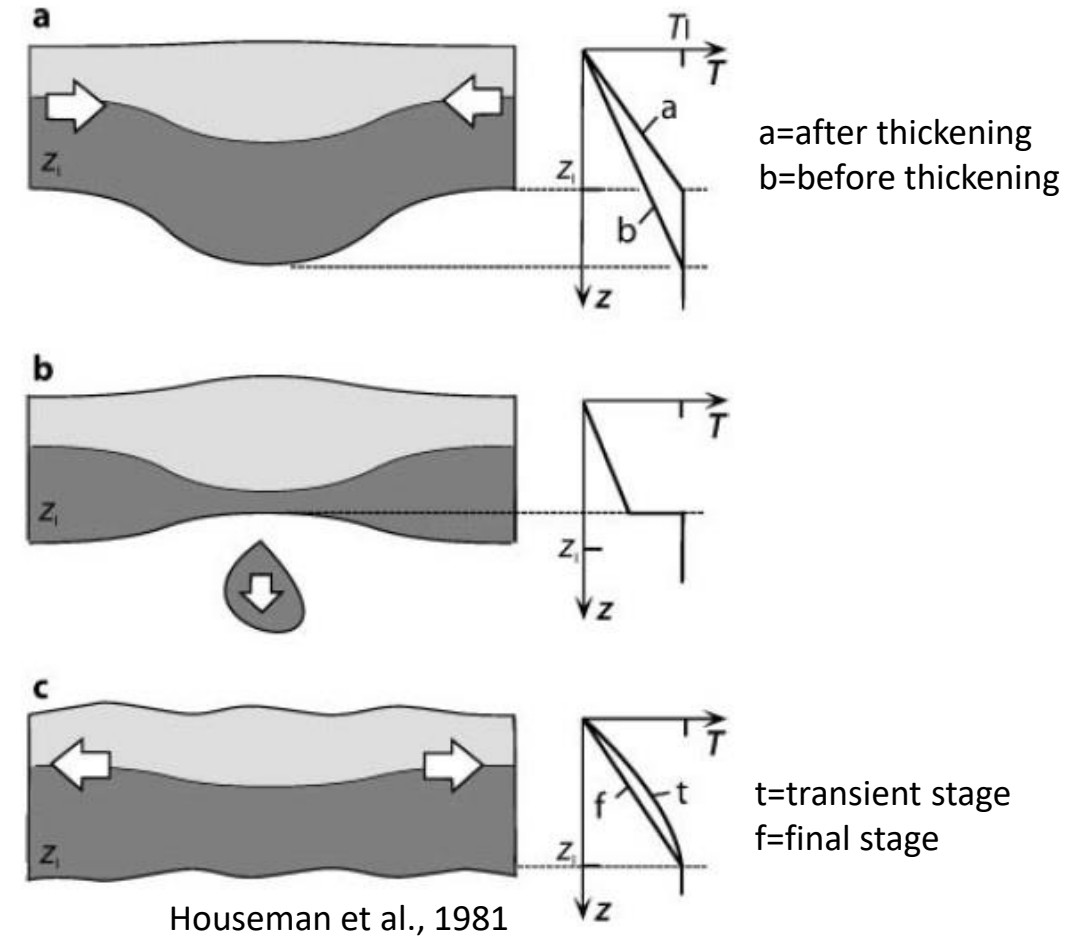
Dripping of the subducting slab

DRIP-1 viscous dripping with nonlinear, temperature dependent rheology

DRIP-2 viscous dripping with non-linear, temperature independent rheology



Gogus, 2010 (PhD thesis)



- A negative topography initially develops when the above the descending Raileigh-Taylor (*RT*) instability reaches a maximum depression.
- This symmetric topography is supported by the actively descending/dripping mantle lithosphere.
- The subsidence inverts to uplift as a result of the decrease in the downwelling forces as the descending mantle lithosphere is necking and narrowing, and reaches the bottom of the box.
- The topography is now dominated by isostatic uplift associated with the flow induced by crustal contraction and thickening.
- The drip models show clearly symmetrical topography signals that remain fixed in location above the downwelling mantle lithosphere (no migration of the *RT* instability).

References

Main Readings

Books:

- Kearey, Klepeis, and Vine, 2015, Subduction zones (Chapter 9), Global Tectonics.
- Frisch, Meschede, Blakey, 2011, Subduction zones, island arcs and active continental margins (Chapter 7), Plate Tectonics.
- Wortel et al., 2009, Continental collision and the STEP-wise evolution of convergent plate boundaries: from structure to dynamics, 47-59, Subduction Zone Geodynamics, Lallemand and F. Funiciello, eds.
- Royden and Husson, 2009, Subduction with variations in Slab Buoyancy: Models and Application to the Banda and Apennine Systems, 35-45, Subduction Zone Geodynamics, Lallemand and F. Funiciello, eds.

Articles:

- Milia et al., 2017, From stretching to mantle exhumation in a triangular backarc basin (Vavilov basin, Tyrrhenian Sea, Western Mediterranean), Tectonophysics, 710-711, 108-126.
- Faccenna and Becker, 2010, Shaping mobile belts by small-scale convection, Nature, 465.
- Faccenna et al., 2011, Topography of the Calabria subduction zone (southern Italy): Clues for the origin of Mt. Etna, Tectonics, 30, TC1003.
- Goes et al., 2017, Subduction-transition zone interaction: A review, Geosphere, 13, 3, 1-21.

References

Further Readings:

- Aretusini et al., 2019, Fluid pressurisation and earthquake propagation in the Hikurangi subduction zone.
- Barnes et al., 2020, Slow slip source characterized by lithological and geometric heterogeneity. Sci. Adv. 6.
- Dal Zilio et al., 2018, The role of deep subduction in supercontinent breakup, Tectonophysics, 746, 312-324.
- Faccenna et al., 2007, Slab disruption, mantle circulation, and the opening of the Tyrrhenian basin, Geological Society of America.
- Fagereng et al., 2019, Mixed deformation styles observed on a shallow subduction thrust, Hikurangi margin, New Zealand Geology, 47, 872–876.
- Rupke et al., 2004, Serpentine and the subduction zone water cycle, EPSL, 223, 17-34.
- Hyndman and Peacock, 2013, Serpentinization of the forearc mantle EPSL, 212, 417-432.
- Bostock et al., 2002, An inverted continental Moho and serpentinization of the forearc mantle, Nature, 417.
- Becker and Faccenna, 2009, A Review of the Role of Subduction Dynamics for Regional and Global Plate Motions, Subduction Zone Geodynamics, Lallemand and F. Funiciello, eds.
- Jadamec, M.A., 2016. Insights on slab-driven mantle flow from advances in three-dimensional modelling. J. of Geodyn., 100, 51–70.
- Schellart et al., 2011, Influence of lateral slab edge distance on plate velocity, trench velocity, and subduction partitioning, JGR, 116, B10408.
- Schellart, 2010, Evolution of Subduction Zone Curvature and its Dependence on the Trench Velocity and the Slab to Upper Mantle Viscosity Ratio, JGR, 115, B11406.
- Šumanovac et al., 2017, Shallow and deep lithosphere slabs beneath the Dinarides from teleseismic tomography as the result of the Adriatic lithosphere downwelling Tectonophysics, 712-713, 523–541.
- Zhang and Leng, 2021, Subduction Polarity Reversal: Induced or Spontaneous? Geophysical Research Letters, 48, e2021GL093201.